OPTICAL WAVEGUIDE ANALYSIS USING TRANSMISSION LINES

Xin Qian

A thesis submitted in partial fulfillment of the requirements of
Bournemouth University for the degree of
Doctor of Philosophy

July 2005

Bournemouth University

OPTICAL WAVEGUIDE ANALYSIS USING TRANSMISSION LINES

ABSTRACT

OPTICAL WAVEGUIDE ANALYSIS USING TRANSMISSION LINES

Xin Qian
Bournemouth University

Optical fibres have been used as a key medium for telecommunication and networking for more than two decades because in principle they offer sufficient transmission capacity, reaching total rates as high as Tbits/s per fibre. Critical fibre properties such as mode field profiles, single-mode propagation conditions and dispersion characteristics can all be related to the optical fibre refractive index profiles. For this reason, it is of fundamental importance to be able to determine the optical fibre refractive index profiles.

In this thesis, a novel Transmission-Line technique has been studied and extended for both the forward and inverse solutions. In the forward solution of the Transmission-Line technique, it is shown that the technique is not only capable of determining exactly the propagation constants in optical fibres with real refractive index profiles, but also evaluating accurately the complex propagation constants in single-mode fibres with arbitrary complex refractive index profiles. To illustrate the effectiveness of this technique, it is applied to the evaluation and manipulation of the gain in a typical 980 *nm* pumped Erbium-Doped fibre as well as to the calculation of the attenuation of optical fibres when radial loss factors are presented. Moreover, based on the Transmission-Line equivalent circuit model, the exact analytical formulas are derived for a recursive algorithm which allows direct and efficient calculation of dispersion of arbitrary refractive index profile optical fibres. The proposed algorithm computes dispersion directly from the propagation constants without the need for curve fitting and successive subsequent numerical differentiation. The algorithm results in savings for both storage memory and computation time.

In the inverse solution using the Transmission-Line technique, the optical fibre refractive index profile synthesis from the given mode electric field distribution is developed and demonstrated. The application of the Transmission-Line principles in the study of optical fibre properties was developed for the first time in the early 80's. However, until now the potential of using Transmission-Line technique for the design of optical fibres based on the given electric field pattern had not been examined. From Maxwell's equations, the Transmission-Line equivalent circuits are derived for a homogeneous symmetric optical fibre. This work demonstrates how to use the Transmission-Line model to reconstruct the exact refractive index profile from the electric field data. The accuracy of the reconstructed optical fibre refractive index profile is examined numerically.

DEDICATION

I dedicate the thesis to my parents for their love.

PUBLICATIONS RESULTING FROM THESIS

Journals

1. "Synthesis and Analysis of Symmetric and Asymmetric Planar Optical Waveguides" *Submitted to IEE Proc.-Optoelectronics.*
2. "Mode Dispersion and Delay Characteristics of Optical Waveguides Using Equivalent T-Circuits" *IEEE Journal of Quantum Electronics*, vol.41, No.7, pp.951-957, July 2005.
3. "Analysis of Bragg Fibers by the Transmission Line Technique" *IEEE Photonics Technology Letters*, vol.17, No.5, pp.1031-1033, May 2005.
4. "Propagation Characteristics of Single-Mode Optical Fibers with Arbitrary Complex Index Profiles" *IEEE Journal of Quantum Electronics*, vol.40, No.6, pp.771-777, June 2004.

International Conference Presentations

5. "Planar Optical Waveguide Refractive Index Profile Synthesis From Higher Order Mode Near Field" *PREP 2005*, Lancaster University, UK, pp.252-253, March 2005.
6. "Optical Fibre Refractive Index Reconstruction from Mode Near Field" *CSNDSP 2004*, Newcastle, UK, pp.164-167, July 2004.
7. "Analysis of Single-Mode Optical Fibres with Arbitrary Complex Index Profiles" *Future Challenges and Opportunities for DWDM and CWDM in Photonic Networks 2004*, University of Warwick, UK, June 2004.
8. "Accurate Optical Fibre Refractive Index Profile Synthesis from Higher Order Modes Near Field" *PREP 2004*, University of Hertfordshire, UK, pp.278-279, April 2004.
9. "Optical Fiber Refractive Index Profile Synthesis from Near Field" *IEEE GLOBECOM 2003 - Optical Networking and Systems*, San Francisco, CA, pp.2669-2673, November 2003.

ACKNOWLEDGEMENTS

This thesis would have not existed without the efforts of many kind individuals. It gives me a great pleasure to acknowledge their contribution here.

First and foremost, I would like to thank my supervisor, Professor Anthony Boucouvalas, for his advice, support and encouragement during my studies at Bournemouth. His understanding and personal attention to each student were found to be most valuable, especially at moments of frustration.

I would also like to express my gratitude to all my colleagues, Periklis Chatzimisios, Crispin Geoghegan, Glyn Hadley , Jacqui Holmes, Pi Huang, David John, John Kanyaru, Zulfiqar Khan, Piotr Stepien, Tom Teng, Petr Voles, Ying Wang, Zhe Xu, Wei Dong Zhang, Ping Zhao, for their friendship, support, assistance and the excellent working environment they have provided over the years.

I also wish to express special thanks to Professor Richard Wynne and Professor Jim Roach and the rest of the management team of the School of Design, Engineering & Computing who have provided generous support throughout my studies.

Financial support provided during my PhD study by the School of Design, Engineering & Computing is gratefully acknowledged.

Last but not least, I am grateful to my parents for their continuing support and encouragement in my pursuit of the scientific career over these years, which makes all my efforts worthwhile.

CONTENTS

LIST OF FIGURES AND TABLES

GLOSSARY OF SYMBOLS AND ABBREVIATIONS

c	velocity of light in vacuum
h	Planck's constant
J	Bessel function
K	Boltzmann's constant, modified Bessel function
l	azimuthal mode number
U	the core modal parameter
V	the normalised frequency
W	the cladding modal parameter
β	wave propagation constant
$\overline{\beta}$	normalised wave propagation constant
Δ	relative refractive index difference between the core and cladding
ε	electric permittivity
λ	optical wavelength
λ_c	cut-off wavelength for single mode fibre
λ_o	wavelength at which first order dispersion is zero
μ	relative permeability (μ_r) , permeability of free space (μ_o)
τ	time period (lifetime)
ϕ_c	critical angle
ω	angular frequency
ASE	amplified spontaneous emission
dB	decibel
DWDM	dense wavelength division multiplexing
EDF	erbium doped fibre
EDFA	erbium doped fibre amplifier
EH/HE	traditional mode designation
FDTD	finite difference time domain
H/L	high and low index
IR	infrared

LED	light emitting diode
LP	linearly polarized (mode)
LPFG	long period fibre grating
NA	numerical aperture
NAG	numerical algorithms group
nm	nanometre
rms	root mean square
S/N	signal to noise ratio
TE	transverse electric
TEM	transverse electromagnetic
TL	transmission line
T-Circuit	transmission line circuit
TM	transverse magnetic
WDM	wavelength division multiplexing
WKB	Wentzel-Kramers-Brillouin

CHAPTER 1

Introduction

1.1 Motivation

Optical fibres have become the backbone of telecommunication systems due to their enormous capacity to transmit simultaneously data, voice and video. Advantages of optical fibres include high data transmission rates and bandwidth, low losses, small cable size and weight, electrical safety and data security. Because of these advantages, the fibres are suitable for carrying high bit rate optical signals whilst being impervious to the disturbances which afflict electrical wires and wireless communication links.

The refractive index profiles of optical fibres play an important role in characterizing the properties of optical fibres. The profile allows the determination of the numerical aperture (*NA*) of an optical fibre and the theoretical number of propagating modes. At the same time the *NA* and profile defines intermodal dispersion. Also, since the information-carrying capacity of optical fibres is refractive index profile-dependent, it is essential for optical fibre manufacturers to produce controlled optical fibre index profiles with great accuracy. In a similar manner, the characterization of the refractive index profiles of planar waveguides has a fundamental importance for the determination of their optical properties. Features such as bandwidth, single-mode condition, fibre-to-guide and guide-to-guide coupling efficiency are related to the refractive index profiles. Refractive index profiling is essential for optical waveguide fabrication processes, as the profile can give valuable information about the physics of the fabrication process. Therefore the profiling permits the development of analytical process models useful in the fabrication process of optical waveguides.

It is important to establish an efficient and accurate method for determining the refractive index profile. Accurate knowledge of the refractive index profile allows designers to reduce optical waveguide device manufacturing costs through tight

control of the optical waveguide fabrication processes. Recently, the inverse techniques applied to the refractive index reconstruction from the mode electric field have been the topic of much research. Boucouvalas and Papageorgiou (1982) have shown that Transmission-Line (*TL*) techniques can be applied to optical fibres and can determine exactly the mode propagation constants and cut-off wavelengths of waveguide modes. In general, from knowledge of the refractive index, a complete waveguide characterization including the mode field plots can be achieved by using this technique. Furthermore, the inverse solution of the *TL* technique has the potential for the design of optical fibres based on a set of properties such as a given mode electric field.

Significant advances in optical fibre technology have resulted in the production of low loss, high bandwidth optical fibres for communication purposes. Single-mode optical fibres offer an excellent data transmission medium ranging in length from metres to hundreds of kilometres. For long distance high capacity transmission applications, an important concern of optical fibres is the dispersion, measured in the unit of *ps/nm/km*. Understanding and controlling the variation of dispersion against wavelength is essential for the design of optical fibres. Dispersion characteristics such as dispersion shifted and dispersion flattened fibres have been extensively studied and investigated in the optical communication systems. Numerical techniques for fast calculation of total dispersion from the mode propagation constant ideally should be as direct as possible. The methods must be theoretically accurate so that even a small value of dispersion can still be predicted and the dispersion must include a material dispersion component. Direct analytical techniques are preferred in order to avoid high order curve fitting and subsequent numerical differentiation of data.

The Erbium Doped Fibre Amplifier (*EDFA*) has now replaced optoelectronic repeaters as the primary design option for extending the range and capacity of the fibre optic telecommunication systems. The standard single-mode fibre deployed today is manufactured to optimize transmission at 1310 *nm* by effectively reducing dispersion to the minimum at that wavelength. The dispersion in the 1550 *nm* window far exceeds that of 1310 *nm* on standard fibre and hence is a limiting factor in single channel or Dense Wavelength Division Multiplexing (*DWDM*) systems

operating in that window. The advent of *EDFA* technology allowing the amplification of multiple optical carriers in the 1550 *nm* window has provided sufficient motivation for the development of optical fibres that will give minimal dispersion at 1550 *nm*, an example of which is dispersion shifted fibre.

In multimode optical fibres, the light confinement is achieved through total internal reflection in the high index centre core. A completely different confinement mechanism, Bragg reflection, provides an alternative way of guiding light. Since Bragg fibres and conventional multimode optical fibres utilize different guiding mechanisms, it is not unexpected that Bragg fibres offer many possibilities that are difficult to achieve in multimode fibres. One such example is the possibility of guiding light in air, which has attracted much recent interest. A Bragg fibre can also be designed to support a single guided mode without azimuthal dependence (i.e. the *TE* or *TM* mode). In contrast to the fundamental mode in conventional fibres, which is always doubly degenerate, these guided Bragg fibre modes are truly single-moded. Consequently, many undesirable polarization dependent effects can be completely eliminated in Bragg fibres.

1.2 Statement of The Problem

The reconstruction of the optical fibre refractive index profile from mode electric fields is generally difficult due to small dimensions and low refractive index differences. Therefore an efficient inverse algorithm is needed. The inverse *TL* technique as an efficient alternative algorithm to refractive index profiling is developed. The author can optimise the number of cylindrical layers and avoid prior exact knowledge of the mode propagation constant. The more cylindrical layers are used, the more accurate the results can be achieved. However, too many cylindrical layers will consume more computation time and memory.

Another challenge in this research work is the dispersion calculation. The definition of dispersion involves the use of first (delay) and second (dispersion) derivatives of mode propagation constant with respect to wavelength, thus theoretical evaluation of dispersion requires the determination of such derivatives in the first

instance. However, direct numerical calculation of the first and second derivatives from data points of mode propagation constant versus wavelength based on simple finite differences can result in errors due to approximations. It is an aim to obtain dispersion directly from the mode propagation constant without the use of first and second derivatives.

1.3 Outline of The Research Work

This research work is concerned with the development of efficient and novel algorithms based on *TL* principles for the design of optical waveguides. The following issues are addressed:

a) Forward Solution of The *TL* Technique

- An optical fibre can be represented as a cascade of Transmission-Line circuits (*T*-circuits), the impedances of the circuit represent a function of the waveguide physical and optical properties. The mode propagation constant can be determined when the optical energy is trapped inside the optical waveguide, and this is equivalent to the resonance condition of the equivalent *T*-circuits. The mode propagation constant can be obtained from the fibre refractive index profile by using the root searching method on the basis of the resonance technique. By using exact propagation constants, both the fundamental mode electric field distribution and the higher order mode electric fields can be plotted out.
- A new analysis leading to an exact and efficient algorithm is presented for calculating directly the dispersion characteristics of arbitrary refractive index profile optical fibres. Based on the *T*-circuit model the exact analytic formulas can be derived for a recursive algorithm which allows direct calculation of mode delay and dispersion. This technique has been demonstrated by calculating the fundamental mode dispersion for step, triangular and linear chirp refractive index profile optical fibres. The accuracy of the numerical results is examined. The proposed algorithm computes

dispersion directly from the propagation constant without the need for curve fitting and subsequent successive numerical differentiation. It is exact, rapidly convergent and it results in savings for both storage memory and computation time.

- The gain or loss in optical fibres is described by the imaginary component of the complex propagation constant, which is critically dependent on the imaginary component of the complex refractive index profile. A rapidly converging numerical procedure for evaluating mode characteristics of the optical fibre with an arbitrary complex refractive index profile is studied. This method is also based on *TL* principles. To illustrate the effectiveness of this procedure, it has been applied to optical fibres with complex step, parabolic, and segmented refractive index profiles. This method has also been used to evaluate and manipulate the gain in a typical 980 *nm* pumped Erbium-Doped fibre as well as to calculate the attenuation of optical fibres when radial loss factors are presented.
- The *TL* technique has been extended to calculate the effective index of leaky modes by using the model of Bragg fibres. From Maxwell's equations, the transmission line equivalent circuits for leaky waveguides, such as Bragg fibres, are derived to demonstrate how to determine the mode effective index using the root searching method on the basis of the resonance technique. As a result, the Bragg fibre *TM* mode band-gap structures can be obtained and analyzed using the *TL* method.

b) Inverse Solution of The *TL* Technique from Mode Electric Field

- A novel and accurate refractive index profile synthesis method for optical waveguides is demonstrated using the transmitted electric field data. This method is based on an inverse *TL* technique. The method of using the *T*-circuit model to carry out the inverse problem and synthesize the exact refractive index profile numerically from homogeneous symmetric optical fibre electric field has been demonstrated. Based on knowledge of the electric field, the numerical reconstruction results of step, parabolic and segmented

optical fibre refractive index profiles have been obtained. The accuracy of the reconstructed waveguide profiles is examined numerically.

- The *T*-circuit model has been used to synthesize the exact Bragg fibre refractive index profile when the desired Bragg fibre electric field is available. The accuracy of the reconstructed Bragg fibre refractive index profiles is also examined numerically.

1.4 Thesis Outline

The main scope of this thesis is to develop algorithms for both forward and inverse solutions of the *TL* technique. It focuses on the optical waveguide refractive index profiles that determine the performance of optical waveguides. The thesis has four parts; chapter 2 discusses existing alternative algorithms on the design of optical waveguides, chapters 3 and 4 consider the forward and inverse *TL* theories with the modelling of symmetric cylindrical optical waveguides, chapter 5 studies the forward and inverse *TL* solutions for isotropic symmetric and asymmetric planar optical waveguides, and chapter 6 presents the conclusions and suggestions for further research work.

Chapter 2 introduces an overview of optical fibres, followed by a general discussion of optimisation methods and their importance to optical fibres. This chapter presents the real and complex propagation constants in the design of optical fibres. Chapter 2 also presents a number of numerical methods used in calculating the dispersion of optical fibres. Finally, the current research on Bragg fibres and planar optical waveguides is critically reviewed.

Chapter 3 presents the forward *TL* theory and numerical methods associated with the modelling of optical fibres, followed by a detailed exploration of the strategy algorithm, along with its computational implementation. This chapter examines the performance of the forward *TL* method by comparing it with existing algorithms in the literature. The performance of the forward *TL* method shows that it is an effective and accurate method.

Chapter 4 examines the refractive index profile reconstruction results from the mode electric fields for step, graded index and Bragg fibres. The chapter then concludes with a discussion on the potential of such algorithms and related computational issues. The reconstructed refractive indices from electric fields are obtained not only for the fundamental mode but also for higher order modes. A high level of accuracy is achieved.

Chapter 5 presents the forward and inverse electric field solutions of Maxwell's equations for planar optical waveguides. The same simulation algorithm and analysis method used in optical fibres are also applied to isotropic symmetric and asymmetric planar optical waveguides.

Chapter 6 presents the conclusions of this thesis and proposes the direction for further research work.

CHAPTER 2

Background and Literature Review

Optical fibres are waveguides which normally guide light in the core region of the fibre, and they are generally made of silica. Takagi et al.(1992) point out that the design of fibres with particular characteristics in mind is an important issue, as general rules of thumb are known to apply to simple fibres, but not to more complex structures. Also, the problem here is not to attempt to discover the relationship between the fibre structure and its corresponding characteristics, but rather to arrive at a fibre structure that gives desired characteristics. Appendix A shows the basic background of optical fibres.

In order to appreciate the transmission mechanism of optical fibres, it is necessary to consider how light is guided by a cylindrical glass fibre. The guiding properties of optical fibres can be explained using the simple ray theory of light, and the wave theory of light. Ray theory considers light as narrow rays. This approach is also called geometrical optics (Adams 1981).

Experiments have shown that the wave theory of light is most successful for explaining propagating phenomena and fibre optic components, especially when the dimensions of the fibre are very small. The wave theory is used to describe the properties of light that ray theory is unable to explain. Light in this case is considered to be an electromagnetic wave, and has an optical wavelength λ. A set of guided electromagnetic waves are referred to as the modes of the optical fibre. This approach is discussed in more details by Schar (1999). When light is considered as an electromagnetic radiation which oscillates at frequency f, it has an electric field E and an orthogonal magnetic field of H. These fields travel in wavelike fashion along a propagation direction z, as shown in Fig.2.1.

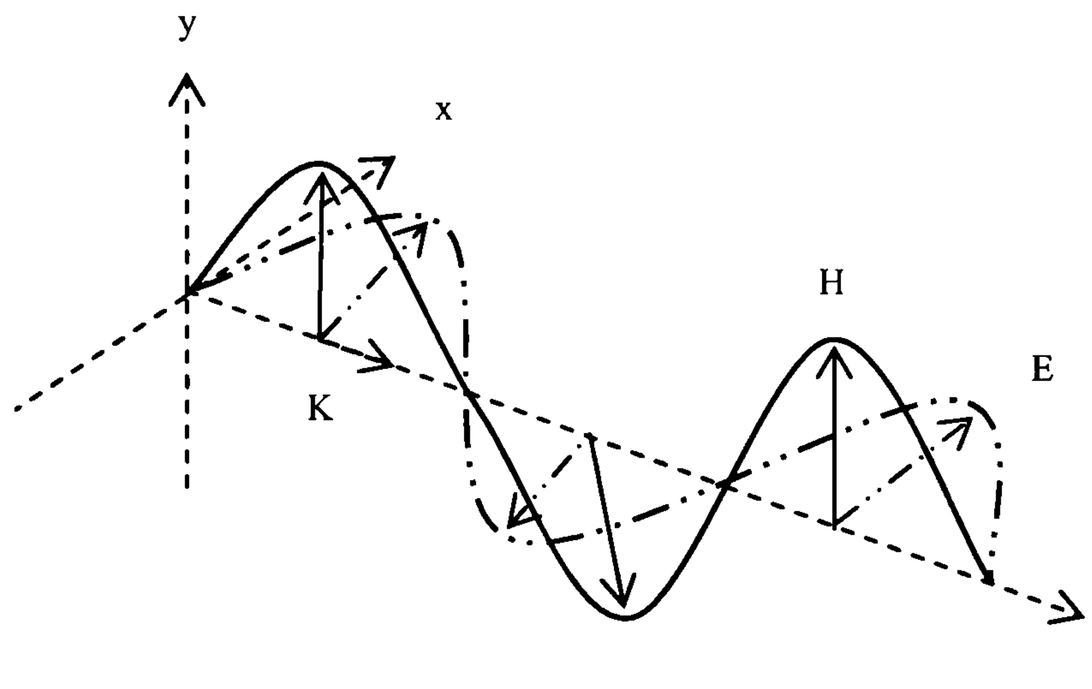

Figure 2.1 Electric and magnetic field distributions in a train of plane electromagnetic waves at a given instant in time

2.1 Real Propagation Constant

Determination of the optical properties of fibres is a very important issue due to the rapid development of optical fibre telecommunication. Advanced systems, such as *DWDM*, use fibres with specially designed refractive index profiles. Sensors use optical fibres whose refractive indices are significantly modified in order to meet the required applications. Thus, the refractive index is a crucial measure that is used to explore the optical properties of fibres and their parameters. One of the important optical fibre parameters is the propagation constant. It is the measure of signal phase difference and also of power loss during transmission of optical signals inside the fibre. The relation describing the correlation between the propagation constant β, the power loss or the attenuation constant α and the signal phase constant γ is given as $\beta = \alpha + i\gamma$ (Adams 1981).

The propagation constant depends on the constituents of the core. Other factors that may contribute to it are bending and the core–cladding index difference (Agraweal 1995). The most popular method for determining the propagation constant of optical waveguides appears to be the effective index method (Krijnen, Hoekstra et al. 1994). By applying separation of variables to the dominant field component, the complete problem is subdivided into two scalar problems in the lateral and transverse directions. Making use of the strong transverse confinement, as observed in most real

waveguide structures, the nonlinear index changes of the various transverse sections can be lumped into nonlinear effective indices of the equivalent layered planar structures. By using a slab solver (e.g., making use of transfer matrices and solving for the propagation constants), the effective indices of the mode in the transverse sections can be found. Since the effective index method can significantly reduce the amount of computational effort, it is widely used for the calculation of the propagation constant.

Lahart (1998), for a doubly clad fibre, has shown the dependence of the propagation constant on the radius of the core–inner-cladding and inner–outer-cladding layers for a constant set of refractive indices in the three regions. The variation of the optical fibre refractive index profile via index difference changes is reported by Hattori and Safaai-Jazi (1998) as the primary design tool for producing a class of depressed-core, low-nonlinearity, dispersion shifted fibres for very long-distance communications at 1.5 μm. Hou et al. (2003) use the end-etched fibre technique to separate all guided modes into individual rings. The propagation constant as a function of propagation angle and fibre parameters is measured for a single-mode fibre.

A quasi-optical technique for characterizing micromachined waveguides is demonstrated with wideband time resolved terahertz spectroscopy (Hadjiloucas, Galvao et al. 2003). In the quasi-optical technique, a transfer function representation is adopted for the description of the relation between the signals in the input and output port of the waveguides. The propagation constant for the multimode propagation can be calculated by measuring the attenuated energy which passes twice through a waveguide section of unit length. In (Themistos, Rahman et al. 1995), finite element analysis employing the vector magnetic field formulation, with the aid of the perturbation technique, is used to calculate the complex propagation constant for several different types of optical waveguides.

It is also possible to define the constant b for a step index optical fibre in terms of the parameters of $V = (U^2 + W^2)^{\frac{1}{2}} = ka(n_1^2 - n_2^2)^{\frac{1}{2}}$ so that $b = 1 - \frac{U^2}{V^2} = \frac{(\beta/k)^2 - n_2^2}{n_1^2 - n_2^2} = \frac{(\beta/k)^2 - n_2^2}{n_1^2 \Delta}$, where Δ is the relative refractive index difference, which is merely the difference in the index of refraction between the core

n_1 and the cladding n_2, $\Delta=(n_1-n_2)/n_1$. V is the normalized frequency, U is the core modal parameter and W is the cladding modal parameter. Referring to the expression for the guided modes given by $n_2k<\beta<n_1k$, the limits of β are n_2k and n_1k, hence b must lie between 0 and 1.

Most fibres of practical interest in optical communication systems are weakly guiding ($\Delta<<1$), and support nearly transverse electromagnetic modes. In the weak guidance approximation the field matching conditions at the boundary require continuity of the transverse and tangential electrical field components at the core-cladding interface (at $r = a$). Therefore, using the Bessel function relations, an eigenvalue equation for the LP modes may be written in the following form $U\frac{J_l\pm_1(U)}{J_l(U)}=\pm W\frac{K_l\pm_1(W)}{K_l(W)}$. Solving this equation with $U=a(n_1^2k^2-\beta^2)^{\frac{1}{2}}$ and $W=a(\beta^2-n_2^2k^2)^{\frac{1}{2}}$ allows the eigenvalue U and hence β to be calculated as a function of the normalized frequency. In this way the propagation characteristics of the various modes, and their dependence on the optical wavelength and the fibre parameters may be determined. However, this technique is only applicable for step index optical fibres (Jeunhomme 1983).

Considering the limit of mode propagation when $\beta=n_2k$, then the mode phase velocity is equal to the velocity of light in the cladding and the mode is no longer properly guided. In this case the mode is said to be cut-off and the eigenvalue W=0 (Murakami and H.Tsuchiya 1978; Marcuse 1993). The single-mode operation only occurs above a theoretical cut-off wavelength λ_c given by $\lambda_c=\frac{2\pi an_1}{V_c}(2\Delta)^{\frac{1}{2}}$, where V_c is the cut-off normalised frequency for the LP_{11} mode. Dividing $\lambda_c=\frac{2\pi an_1}{V_c}(2\Delta)^{\frac{1}{2}}$ by $V=\frac{2\pi an_1}{\lambda}(2\Delta)^{\frac{1}{2}}$ for the same fibre the inverse relationship $\frac{\lambda_c}{\lambda}=\frac{V}{V_c}$ can be obtained. Thus for a step index fibre where V_c=2.405, the cut-off wavelength is given by $\lambda_c=\frac{V\lambda}{2.405}$ (Jeunhomme 1983). For the operating wavelength $\lambda>\lambda_c$, the fibre is single-moded, and at $\lambda<\lambda_c$ the fibre is multi-moded. In practice,

the cut-off wavelength of the second order LP_{11} mode is used for this definition. The standard method of determining the cut-off wavelength is to calculate the effective index $\overline{\beta} = \beta/k$ of the LP_{11} mode at a particular wavelength, and vary the wavelength until $\overline{\beta} = n_2$ is obtained. Boucouvalas and Papageorgiou (1982) have developed the resonance technique to obtain the cut-off wavelength for arbitrary refractive index profile optical fibres. The cut-off wavelength is also achieved by Bourillot *et al.* (1995) for planar optical waveguides. Officially, an effective cut-off wavelength is defined by the International Telephone and Telegraph Consultative Committee (1985) which is obtained from a 2m length of fibre containing a single 14cm radius loop. This definition is produced because the first order LP_{01} mode is strongly affected by fibre length and curvature near cut-off. Recommended cut-off wavelength values range from 1100 to 1280 *nm* for single-mode fibres designed for operation in the 1300 *nm* wavelength region in order to avoid modal noise and dispersion problems. Moreover, practical transmission systems are generally operated close to the effective cut-off wavelength in order to enhance the fundamental mode confinement, but sufficiently distant from cut-off so that no power is transmitted in the second order LP_{11} mode (Martynkien, Harris et al. 2000).

Unguided or radiation modes have frequencies below cut-off when $\beta < n_2 k$, and hence W is imaginary. Nevertheless, wave propagation does not cease abruptly below cut-off. Modes exist when $\beta < n_2 k$ but the difference is very small, such that some of the energy loss due to radiation is prevented by an angular momentum barrier formed near the core-cladding interface. Solutions of the wave equation giving these states are called leaky modes, and often behave as very lossy guided modes rather than radiation modes. However, leaky modes can be relatively low-loss, therefore they can carry a large amount of power in short fibres (Issa and Poladian 2003). Alternatively, as β is increased above $n_2 k$, less power is propagated in the cladding. As indicated previously, the range of $n_2 k < \beta < n_1 k$ signifies the guided modes of the fibre.

The propagation of particular modes within a fibre may also be confirmed through visual analysis. The electric field distributions of different modes give similar distributions of light intensity within the fibre core. These waveguide patterns (often

called mode patterns) may give an indication of the predominant modes propagating in the fibre. The order of each mode is indicated by the number of field maxima within the core of the fibre. The electric field is at its maximum inside the core of the waveguide and diminishes toward the core-cladding boundary. HE_{11} is considered as the fundamental mode or the lowest order standing wave. As the number of field maxima increases, the order of the mode is higher. Generally, modes with more than a few (5-10) field maxima are referred to as high-order modes. The field intensity distributions for the three low-order *LP* modes are shown in Fig.2.2. In Fig.2.3, the mode patterns of two high-order *LP* modes are illustrated.

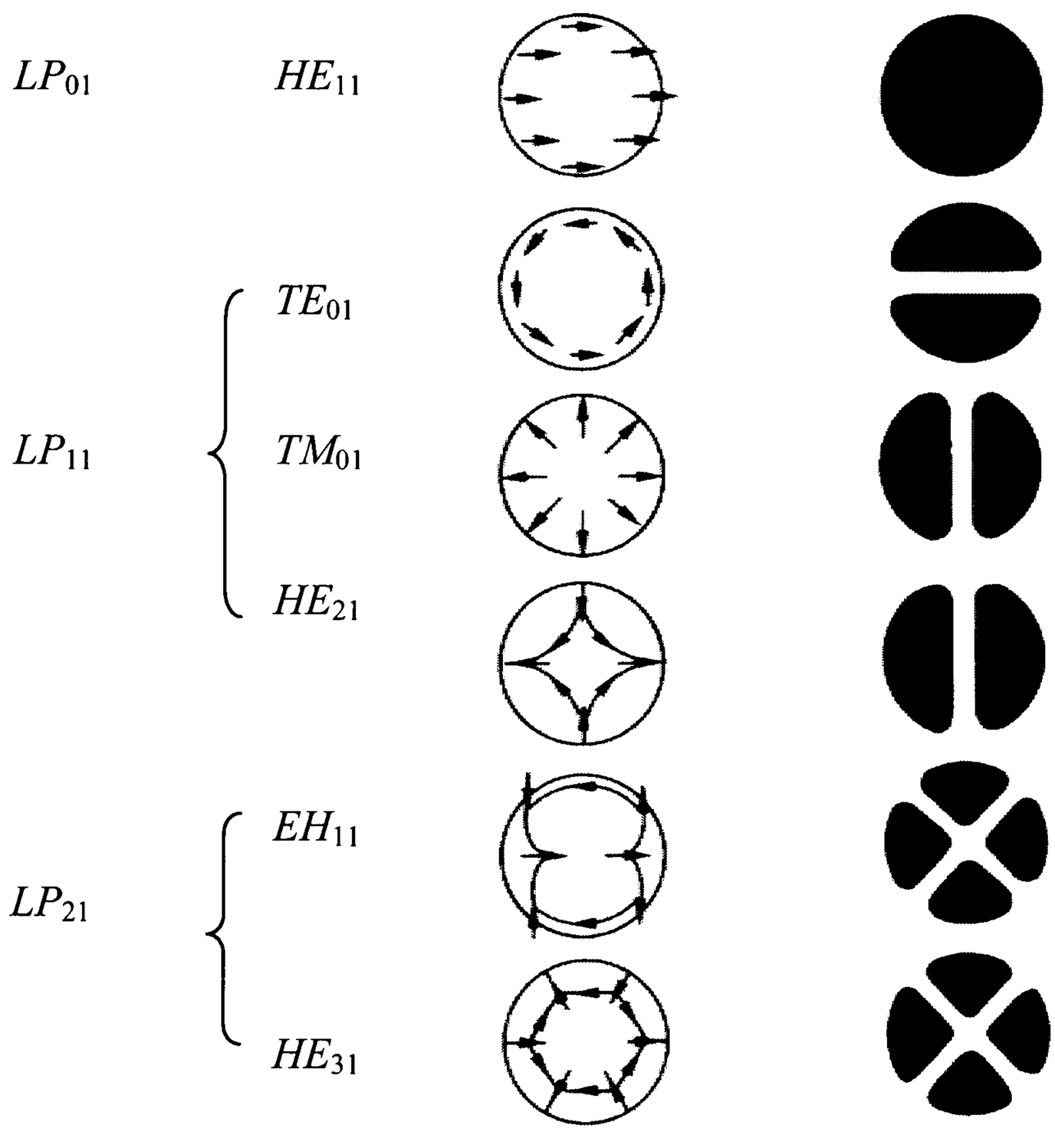

Figure 2.2 The electric field configurations for the three lowest *LP* modes illustrated in terms of their constituent exact modes: **(a)** *LP* mode designations, **(b)** exact mode designations, **(c)** electric field distributions of the exact modes, **(d)** intensity distributions of E_x for the exact modes indicating the electric field intensity profile for the corresponding *LP* modes.

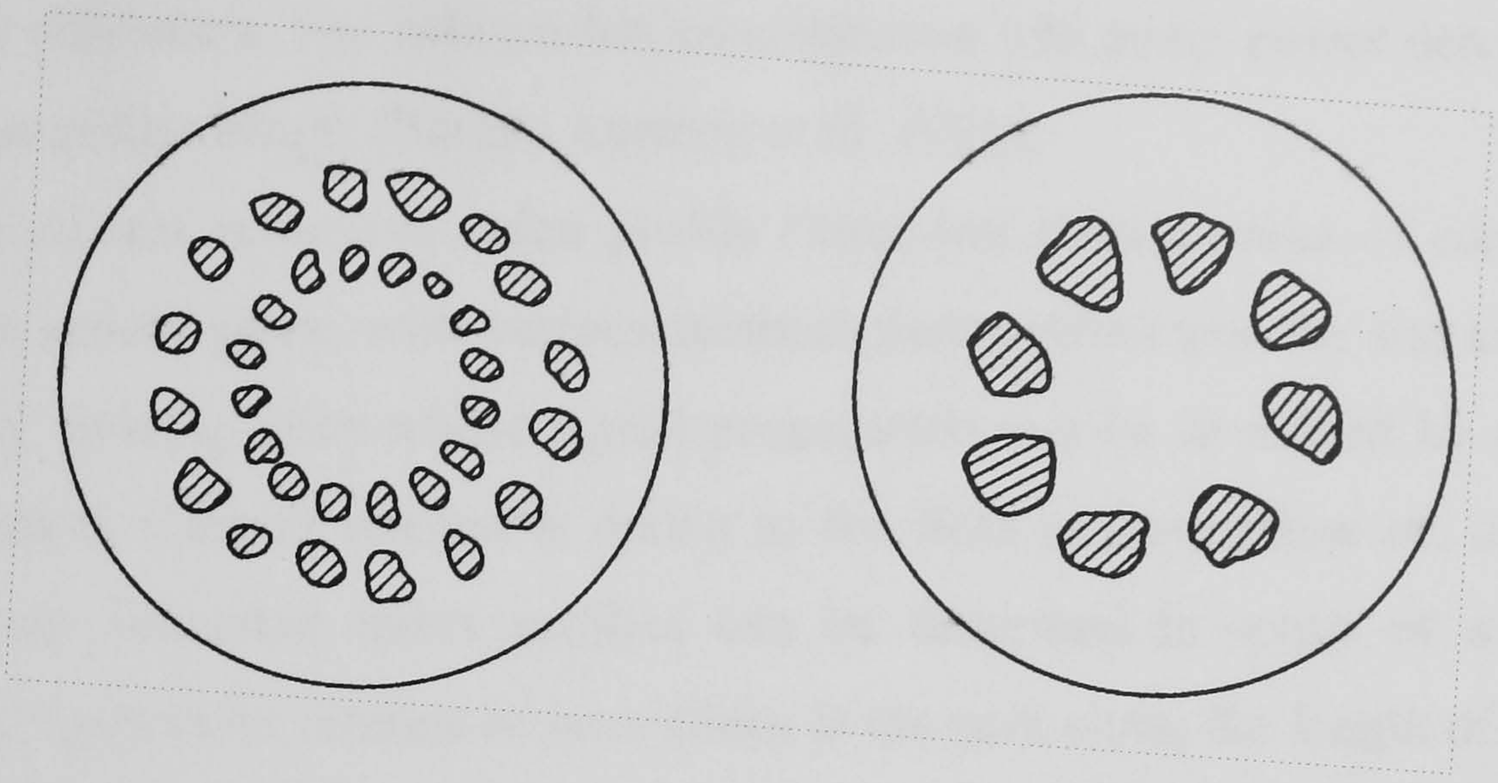

LP_{82} LP_{41}

Figure 2.3 Sketches of fibre cross sections illustrating the distinctive light intensity distributions (mode patterns) generated by propagation of individual linearly polarized modes.

2.2 Complex Propagation Constant

Recently, the *EDFA* has been shown to be a potential alternative to the semiconductor laser amplifier, operating in the third communication window for optical fibre systems (Yamada, Shimizu et al. 1990; Giles and Desurvire 1991; Von-der-Weid, Passy et al. 1998). As compared to the semiconductor laser amplifier, the advantages of using an *EDFA* include high gain (Von-der-Weid, Passy et al. 1998), high saturation output power (Desurvire, Zyskind et al. 1990), polarization independent gain, no crosstalk, low noise figure, and low insertion loss (Giles and Desurvire 1991). The *EDFA* can be pumped by semiconductor laser diodes. The most interesting pump wavelengths are at 810, 980, and 1480 *nm* (Lidgard, Digiovanni et al. 1992). The state absorption in the 810 *nm* pump band implies a high pump power to achieve a high gain. However, a high pump power results in a low operating life for the pump laser. The latest reports of high gain achieved with low pump power in the 980 and 1480 *nm* pump bands have stimulated the interest in these two pump bands (Shimizu, Yamada et al. 1990).

Erbium-Doped fibre structure and its dopant profile are important factors which determine the pumping efficiency. It has been shown that confinement of the Erbium-Ions near the centre of the fibre core where pump intensity is highest results

in the best efficiency. The Erbium-Ion concentration and pump power determine the optimum amplifier length (Barnes, Laming et al. 1991).

Analysis of real refractive index profile fibres has been an area of considerable research in recent years, with various methods being developed for the analysis of any weakly guiding fibre whose signal propagation can be described by the scalar wave equation. Current interest is drawn to the field of laser fibres or, in general, fibres whose refractive index profiles can be described in terms of a complex function. Of particular interest in laser fibres is the gain along the length of fibres. In order that this may be evaluated, the imaginary component β_i of the complex propagation coefficient β^* must be found. β_i is critically dependent on the imaginary component of the complex refractive index profile. Hence it would be of great use to be able to evaluate β_i for arbitrary complex refractive index profile fibres.

Some approximate or numerically cumbersome methods have been reported in the literature (Reisinger 1973; Sader 1990; Sunanda and Sharma 1999) for evaluation of the propagation characteristics of such fibres. The approximate method (Sader 1990) attempts to separate the real and imaginary parts of the complex scalar wave equation to obtain two real scalar wave equations. Under the assumption that the imaginary part of the field is much smaller than the real part, the imaginary part of the field is neglected. Thus, this method is accurate only for profiles in which the imaginary part of the refractive index is small. Another method for the analysis of such profiles has been the standard method of perturbation (Reisinger 1973), in which the restraining assumption is that the loss or gain exhibited by the fibre does not significantly alter the field and is also valid for profiles with low values of the imaginary part of the refractive index. In order to overcome this restraint, a numerical procedure (Sunanda and Sharma 1999) is developed, in which the Rayleigh–Ritz procedure, involving expansion of the field in terms of appropriate basis functions, has been extended to complex profiles by choosing the expansion coefficients as complex. This converts the problem to a complex matrix eigenvalue equation. Although this procedure does not neglect the imaginary part of the field, the number of basis functions required in the expansion, for sufficient accuracy, can often be as large as 50. Hence, the procedure requires evaluation of the complex eigenvalues of a matrix with complex

elements. This requires a cumbersome algorithm and the use of an optimized numerical algorithms group (*NAG*) library routine to attain the desired accuracy rapidly, taking a few seconds for one eigenvalue. Moreover, for any of the procedures to find direct application to *EDFA* gain calculations, the refractive index profile of the pumped Erbium-Doped fibre has to be defined.

In (Qian and Boucouvalas 2004), the author first defines the complex refractive index profile at signal and pump wavelengths in an Erbium-Doped fibre pumped at 980 *nm* and uses the *TL* procedure reported earlier for optical fibres with gain to obtain the modal gain or loss for both the signal and pump powers propagating in the *EDFA*. The complex refractive index profile depends on radial distance, pump and signal power levels, wavelength, and dopant profiles. A novel method that can easily be applied to fibres with arbitrary indices and dopant profiles is provided for looking at the gain characteristics of Erbium-Doped fibres. The *TL* method can be further extended to estimate the signal gain and pump loss for a given length of fibre by a beam-propagation type of procedure, in which the total length is divided into small segments and propagation is considered in terms of the local normal modes through each segment.

2.2.1 Gain in Optical Fibres

The two main approaches to optical amplification to date have concentrated on semiconductor laser amplifiers which utilize stimulated emission from injected carriers and fibre amplifiers in which gain is provided by either stimulated Raman or Brillouin scattering, or by rare earth dopants. Both amplifier types (i.e. semiconductor and fibre; specifically rare earth and Raman) have the ability to provide high gain over wide spectral bandwidths, making them eminently suitable for future optical fibre system applications.

The gain flattening of *EDFA* has been a research issue in recent years, with the development of high capacity *WDM* optical communication systems. For single channel systems, the gain variation with wavelength is not a problem. However, as the number of channels increases, the transmission problem arises because a conventional *EDFA* has intrinsic non-uniform gain. *EDFAs* typically present gain peaking at about 1530 *nm* and the useful gain bandwidth may be reduced to less than

10 *nm*. The gain in *EDFA*s depends on a large number of device parameters such as Erbium-Ion concentration, amplifier length, core radius and pump power. To increase the gain bandwidth of an amplified lightwave system several methods can be used.

These methods include the use of a waveguide Mach–Zehnder optical filter (Inoue, Kominato et al. 1991), an acousto-optic tuneable filter (Yun, Lee et al. 1999), gain-clamping in *EDFA* (Zhao, Bryce et al. 1997), long and short-period fibre Bragg gratings in *EDFA* (Rochette, Larochelle et al. 1999). However, many of these techniques involve the use of expensive components and complicated designs. The use of twin-core fibre, in which both cores are identically doped with Erbium, is also an obvious choice. This technique has been suggested by Laming, Minelly et al. (1993) and it involves the concatenation of a length of single core Erbium-Doped Fibre (*EDF*) with a length of twin-core *EDF*. The purpose of the twin-core *EDF* here is to introduce spatial hole burning which equalizes the output power at certain wavelengths. Wu and Chu (1994) have also suggested the use of twin-core *EDF* for power equalisation by launching pump power into both cores. The ratio of these powers has to be predetermined. However, this technique is not practical as it is difficult to have simultaneous access to the two input cores.

Gain flattening filters, amplified spontaneous emission (*ASE*) filters in EDFAs, and band rejection filters are some examples where long period fibre gratings (*LPFG*s) can be applied with success. *LPFG*s are produced using the electric arc technique (Rego, Frazao et al. 2001). This method of fabrication has several advantages over others, namely, it does not require that the fibre be photosensitive and the arc-induced gratings possess high thermal stability. However, the writing of gratings at short wavelengths puts forward several problems. Usually, fibres are multimode for those wavelengths and therefore the filters on them are very sensitive to bending (even to micro-bends during their inscription) making the control of background loss difficult. Moreover, the well-known process of increasing the tension or the current to widen a spectrum or to have a deeper peak-loss also results in an increased background loss. Therefore, transposing what is known about the writing of *LPFG*s in the third telecommunication window to this particular issue is not straightforward.

Generally, the gain flatness is improved for smaller bandwidths. Further developments that implement advanced techniques for high performance *WDM* applications are being carried out.

2.2.2 Loss in Optical Fibres

The traditional way of compensating for optical loss in lightwave communication systems has been the rather cumbersome procedure of regeneration. Regeneration includes photon-electron conversion, electrical amplification, retiming, pulse shaping and finally electro-photon conversion (Desurvire 1994). In many applications, direct optical amplification of the light signal would be advantageous. Optical amplifiers can be used in any system that is loss limited, i.e. dispersion effects are not the limiting factor (Fleming and Whitley 1996). This is the case for most systems operating beneath the dispersion minimum at 1310 *nm* and for coherent lightwave systems. The use of optical fibre amplifiers as a booster for 1550 *nm* optical systems operating over 400km at 2.56Tbit/s has been demonstrated (Kaman, Zheng et al. 2005), and reveals the potential of fibre amplifiers for upgrading optical systems.

The spectrum of optical power loss in an optical fibre is a complicated function of absorption and scattering phenomena that are introduced during the drawing of the fibre, either because of impurities introduced during the drawing or because scattering centres increase or decrease according to the level of dopant used. The review in (Garrett 1983) gives a thorough account of single-mode fibre loss contributors, including:

1) Scattering and absorption that is intrinsic to the glass compound used in the fibre.
2) Impurity absorption, including the transition-metal contaminants and residual hydroxyl groups.
3) Absorption and scattering centres that are introduced during the drawing process.

The drawing-induced losses depend on drawing speed and temperature, and the resulting loss profile is thought to be approximately exponential in the core. Raleigh scattering is the important intrinsic loss mechanism in doped silica fibres and it is generally assumed that the scattering centres depend on the dopant, and hence will

probably have a profile that approximately replicates the refractive index profile. Raleigh scattering is caused by microscopic inhomogeneities of the refractive index of glass (Strohhofer and Polman 2001). These inhomogeneities are due to thermal fluctuations when the fibre is in the molten state. As the fibre solidifies, these fluctuations cause refractive index variations. Raleigh scattering is proportional to λ^{-4}, where λ is the wavelength of the light. The same phenomenon is responsible for the colour of the sky, the stronger scattering of light at shorter wavelengths gives the sky its blue colour. Raleigh scattering represents by far the strongest attenuation mechanism in silica fibres. It is responsible for 90% of the total attenuation. Fig.2.4 shows the attenuation characteristics of typical modern fibres in the infrared range (Heitmann and Klein 2004). Little reduction of Raleigh scattering can be achieved by improving fibre manufacturing techniques. Zervas and Laming (1995) have considered the Raleigh scattering effect on the gain efficiency and noise of *EDFA* in detail. Their analysis is based on an empirical relation between Raleigh backscattering coefficient and optical fibre *NA* obtained by fitting data from different sources and hence varying drawing conditions. Hartog and Gold (1984) have developed a comprehensive theory of backscattering in single-mode fibres that allows an arbitrary scattering loss distribution in giving results, but allows the average value in the core to differ from that of the cladding.

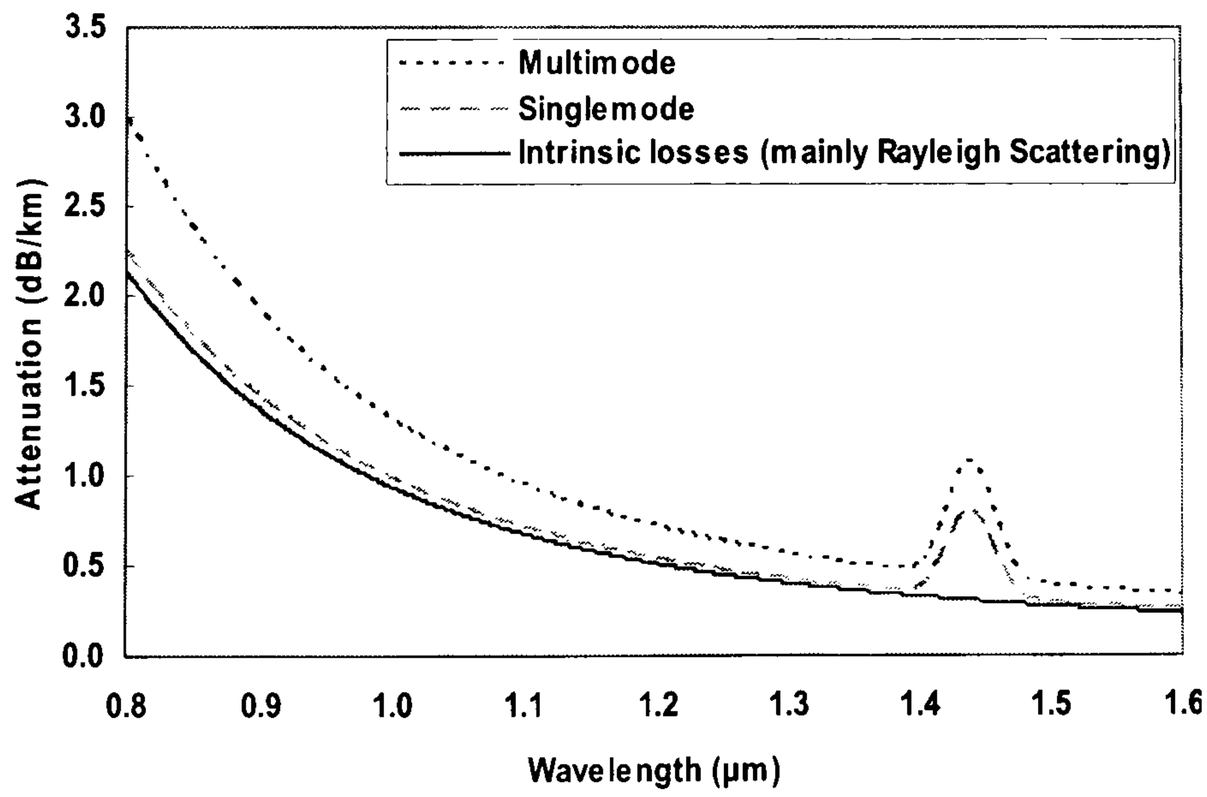

Figure 2.4 Typical fibre infrared absorption spectrum. The lower curve shows the characteristics of a single-mode fibre made from a glass containing about 4% of GeO_2 dopant in the core. The upper curve is for graded index multimode fibre. Attenuation in multimode fibre is higher than in single-mode because higher levels of dopant are used. The peak at around 1400 *nm* is due to the effects of traces of water in the glass.

The recently proposed methods of loss prediction include a perturbation method that works well when exact solutions of Maxwell's equations are available (Sabadash and Chaika 1991) and a variational method based on the optimization of a variational parameter (Oksanen and Lindell 1990). In the latter case, there are two parameters to be adjusted, a detail that renders the method cumbersome. Several loss profiles have been tried with a step-index fibre. Good results are obtained for some of the profiles but for certain other loss profiles results are less convincing (Oksanen and Lindell 1990). In (Sabadash and Chaika 1991), the authors have assumed that only the cladding contributes to the loss because:

a) The cladding is much thicker than the core.

b) The core is usually formed at higher temperature than the cladding, inhibiting the formation of the hydroxyl groups in the core.

They have assumed that the imaginary part of the index is constant in the cladding. Their methods can be used when the core contributes to the loss, even though the authors did not consider that case.

In this thesis, a simple direct numerical procedure has been developed to evaluate the exact propagation characteristics of an optical fibre with an arbitrary complex refractive index profile. The direct method is especially useful for calculations in high gain (or loss) fibres where the earlier reported approximate methods are inaccurate. Furthermore, its practical application to evaluate gain in a typical 980-*nm* pumped *EDF* has been shown and the results have been compared with those obtained earlier.

2.3 Bragg Fibres

Telecommunication has continued to push optical fibres towards ever more demanding applications, such as high bit rates, *DWDM* and long distance, and in response there has been renewed interest in alternative fibre designs to lift fundamental limitations of silica fibres. A particularly exciting departure from traditional fibres is fibres based on photonic band-gaps, forbidden frequency ranges in periodic dielectric structures that can confine light even in low-index or hollow regions. Recently all-dielectric waveguides have been introduced that confine light by means of one-dimensional (1-D), 2-D and 3-D photonic band-gaps (Joannopoulos, Meade et al. 1995). These new designs have the potential advantage that light propagates mainly through the empty core of a hollow waveguide, thus minimizing effects associated with material nonlinearities and absorption losses (Argyros and Bassett 2002). Moreover, because confinement is provided by the presence of at least a partial photonic band-gap, this ensures that light should be able to be transmitted around a bend with a smaller radius of curvature than is possible with the optical fibre. Two main classes of fibres have emerged using photonic band-gaps: photonic crystal holey fibres that use a two-dimensional transverse periodicity (Cregan, Mangan et al. 1999), and Bragg fibres that use a one-dimensional periodicity of concentric rings (Yeh, Yariv et al. 1978; Doran and Blow 1983; Fink, Ripin et al. 1999).

The Bragg fibre combines some of the best features of metallic coaxial cables and dielectric waveguides. The metallic coaxial cables and dielectric waveguides are the backbone of modern optoelectronics and telecommunication systems, which are used in two separate regimes of the electromagnetic spectrum. For radio frequencies, the metallic coaxial cables are of greatest prominence (Waldron 1969). At optical wavelengths, the optical waveguides are done with the traditional index-guiding (that is, total internal reflection) mechanism, as exemplified by silica and chalcogenide optical fibres. Such dielectric waveguides can achieve very low losses (Saleh and Teich 1991). Although highly successful, silica waveguides have fundamental limitations in their attenuation and nonlinearities that result from the interaction of light with a dense, material-filled core. Prior to the emergence of silica fibres, hollow

metallic waveguides were seriously considered as candidate media for long-distance telecommunications. A weakness of metallic waveguides is that they become lossy at high frequencies due to the finite conductivity of metals. Thus, their use is restricted to low frequencies. This severely limits the ultimate bandwidth that they can transmit. By adding a dielectric coating on the inside of the metallic waveguides, their properties can be improved. Such metallodielectric waveguides have been developed for infrared wavelengths, in particular, for laser power delivery (Miyagi and Kawakami 1984). The limitations that exist in both the silica fibres and the hollow metal waveguides can be systematically reduced in the Bragg fibre due to its hollow core and the use of dielectric materials which are transparent at high frequencies.

Bragg fibres are composed of a low index core (possibly air) surrounded by alternating annular layers with different dielectric constants. Bragg fibres are first proposed by Yeh, Yariv et al. (1978), while Doran (1983) points out that cylindrical Bragg fibres would not only be extremely difficult to fabricate but also give the ideal structure the losses would be larger than for the high index core case. Because Doran (1983) believes that loss due to radiation is only small for silica core structures. The hope of achieving very small losses by confining the field in a hollow core is unreasonable. However, the possibility of guiding light in air by Bragg fibres or photonic crystal fibres has recently attracted a lot of attention. Omni-fibres, which are Bragg fibres with very large cladding indices contrast, have been experimentally demonstrated (Fink, Ripin et al. 1999; Johnson, Ibanescu et al. 2001).

It is also necessary to know that one variant of the original Bragg fibre, which has a uniform low-index core, is the so-called coaxial Bragg fibre (Ibanescu, Fink et al. 2000). Coaxial Bragg fibres also guide light through Bragg reflection, except now that a smaller high index column is embedded in the centre of the low index core. In practice, in order to provide structural support it may be replaced by some dielectric material with a high index of refraction without greatly affecting the main observation of theoretical work.

Several numerical approaches have been used to analyze the modal properties of Bragg fibres with air core and periodic claddings. In (Yeh, Yariv et al. 1978), Bragg fibres have been successfully analyzed using the transfer matrix method, where the

Bragg modes are considered as quasi-modes with minimum radiation loss. In (Xu, Ouyang et al. 2002), the photonic band-gap concept is used in the transfer matrix method. Photonic band-gap is an energy range (and corresponding wavelength range) for which a material neither absorbs light nor allows light propagation. Photonic band-gap materials are similar to semiconductors, where the electrons are replaced by photons (also known as light). By creating periodic structures out of materials with contrast in their dielectric constants, it becomes possible to guide the flow of light through the Photonic band-gap material in a way similar to how electrons are directed through doped regions of semiconductors. The period of the structure is related to the wavelength of light for which a Photonic band-gap will exist, for instance a few hundred nanometers for visible light.

The authors have obtained the band-gap by searching for the fast increasing solutions. The increasing numerical errors make the field calculation very sensitive to the propagation constants. In (Ouyang, Xu et al. 2001; Xu, Yariv et al. 2003), periodic alternate cladding layers are approximated by planar Bragg stacks (Mizrahi and Schachter 2004) using the asymptotic approximation of Bessel functions; therefore, the Bloch theorem can be used to obtain an analytical eigen-equation. The drawback is that this simple asymptotic analysis may fail if the Bragg fibre core becomes too small and it is difficult to estimate the accuracy of the asymptotic results. In (Ibanescu, Fink et al. 2000), plane wave expansion for photonic crystal calculation is used along with the super-cell concept. Since a Bragg fibre is not strictly a photonic crystal, a plane wave method is not quite suitable nor efficient. The multipole method is a potential approach to calculate the modal properties of microstructured optical fibres (White, Kuhlmey et al. 2002), however it is at present limited to designs composed of nonintersecting circular inclusions. The Galerkin method makes use of a set of orthogonal associated Laguerre-Gauss functions to approximate the guided modes, and it has been used to calculate *LP* modes in conventional fibres (Sharma and Banerjee 1989). One advantage of this method is its versatility in treating circular fibres with arbitrary index profiles, and it is not limited to treating the step index profile.

The transfer matrix method is the most accurate method, but it has no explicit form for obtaining the propagation constants. In order to obtain the field distribution of

Bragg fibre modes, highly accurate propagation constants may be needed. The transfer matrix technique may be quite demanding in terms of memory space and computation time if highly accurate results are required. The asymptotic method provides an explicit form for the propagation constants, and is generally stable if the asymptotic condition is satisfied. The transfer matrix method can be modified to calculate the leakage loss in Bragg fibres (Themistos, Rahman et al. 1995; Johnson, Ibanescu et al. 2001; Argyros 2002; Issa, Argyros et al. 2003) due to a finite number of high and low index (*H/L*) layers, which is more straightforward than the commonly used Chew's method (Chew 1999). The Galerkin method (Sharma and Banerjee 1989) is generally stable and gives good results when the mode is away from the cut-off region. Further, the method allows one to analyze fibres with arbitrary index profiles.

Two of the most important parameters of Bragg fibres are the modal dispersion and the propagation loss. Fleming *et al.* (2002) have developed an asymptotic formalism that greatly simplifies the analysis of Bragg fibres. Xu, Yariv *et al.* (2003) have incorporated a leaky mode method into the asymptotic formalism. The extended asymptotic approach developed in (Fleming, Lin et al. 2002) is capable of fully characterizing the dispersion and loss in Bragg fibres, while retaining the simplicity and physical transparency of the original asymptotic approach. Fleming *et al.* (2002) have applied the asymptotic approach to analyze the guiding behaviour of a miniature Bragg fibre reported in (Cregan, Mangan et al. 1999) as a function of the absorption in the cladding layers, the geometries of the Bragg cladding, and the core radius. They find that only four Si/Si_3N_4 cladding pairs are required to achieve propagation loss below $1dB$/cm. From asymptotic analysis results, they have established that the material absorption in the Si cladding layers has little influence on the propagation loss of the guided air core modes. Issa, Argyros *et al.* (2003) obtain a simple formula that characterizes the exponential reduction of the modal propagation loss as the number of cladding pairs increases. They find that the quarter-wave stack cladding geometry, which is commonly used in the literature, does not necessarily lead to optimal guiding. Due to the fabrication processes, it is difficult to realize the miniature Bragg fibres with perfect cylindrical symmetry. By using the finite difference time domain (*FDTD*) simulations (Ouyang, Xu et al.

2002), a deformed Bragg fibre is investigated and the Bragg fibre dispersion insensitive to the air core deformation is also demonstrated. However, the guided modes in the deformed Bragg fibre are no longer cylindrically symmetric, which may lead to a higher propagation loss.

Bragg fibres are becoming an attractive optical waveguide for the delivery of high power laser radiation as well as for important temperature and chemical fibre sensor applications. In general, these guides enjoy losses of a few tenths of a *dB*/m and are quite flexible. Because the energy is carried in the hollow core, there is no core material that might be easily damaged by high peak or average laser powers as there would be in a comparable solid core infrared (*IR*) fibre. In addition, there is no Fresnel loss; this is especially important in comparison to the chalcogenide glass fibres where Fresnel loss can be as high as 25%. When selecting a hollow guide, it is important to remember that the optical principles of a hollow core guide differ from those of a solid core fibre. The most important distinctions are that the hollow guides have a loss that varies as the reciprocal of the core radius cubed and that there is an additional loss on bending which varies as $1/R$, R is the core radius. These properties are not shared by conventional solid core fibres. However, most applications of *IR* fibres do not require tight bending radii and so the additional loss on bending is not prohibitive. The other potential advantage of hollow guides is important; these guides are nearly single-moded (Cregan, Mangan et al. 1999).

The wave vector β has an imaginary part that is proportional to the radiative loss of the modes. This imaginary part decreases exponentially with the number of layers in the cladding; in the limit of an infinite number of layers these resonant modes become truly guided modes. For the cladding with only five layers, the imaginary part is of the order of $10^{-4} \times 2\pi / d$, where d (μm) is the unit length of periodicity in the cladding. This means that light can be confined in the hollow core for a distance equals to several hundred of wavelengths before it radiates away. For a waveguide intended for transmission of light over longer distance, more layers need to be added to the cladding. Fortunately, the imaginary part of the wave vector decreases exponentially with the increase in the number of layers. Thus, for pure *TE* modes, only 20 layers are enough to give radiative decay lengths of more than 100 km while

for *TM* modes and mixed modes, 40 layers are enough (Johnson, Ibanescu et al. 2001).

Note that while the silica fibre has a very low loss only for wavelengths near λ=1.55μm, the Bragg fibre can be designed to have a very low loss in the vicinity of any desired wavelengths, from infrared to visible wavelengths.

In this thesis, from Maxwell's equations a *T*-circuit has been derived for the Bragg fibre cylindrical layer and it has been demonstrated how the *T*-circuit can be used to determine the mode effective index. *TM* modes of Bragg fibres, and mode band-gap structures can be analyzed using the *TL* method. Furthermore, the *T*-circuit model has been carried out to examine the inverse problem and synthesize the exact refractive index profile if the desired Bragg fibre electric field is available. The accuracy of the reconstructed Bragg fibre refractive index profile is examined numerically (Qian and Boucouvalas 2005).

2.4 Delay and Dispersion

2.4.1 Signal Distortion in Optical Fibres

Fibre dispersion becomes increasingly important as the overall capacity is increased and it constrains all aspects of the transmission strategy. The multimode step index optical fibres exhibit the greatest dispersion of a transmitted light pulse, while the multimode graded index fibres give a considerably improved performance. The single-mode fibres give the minimum pulse broadening and thus are capable of the greatest transmission bandwidths which are currently in the gigahertz range (Lu, Chen et al. 2001), whereas transmission via multimode step index fibres is usually limited to bandwidths of a few tens of megahertz. However the amount of pulse broadening is dependent upon the distance the pulse travels within the fibre, and hence for a given optical fibre link the restriction on usable bandwidth is dictated by the distance between regenerate repeaters. Thus the measurement of the dispersive properties of a particular fibre is usually stated as the pulse broadening in time over a unit length of the fibre. Hence, the number of optical signal pulses which may be transmitted in a given period, and therefore the information carrying capacity of the

fibre, are restricted by the amount of pulse dispersion per unit length (Matsuda, Naka et al. 1996).

The various dispersive mechanisms involved in the fibres are considered next. These are material dispersion, waveguide dispersion and intermodal dispersion.

Material Dispersion

Pulse broadening due to material dispersion results from the different group velocities of the various spectral components launched into the fibre from the optical source. A material is said to exhibit material dispersion when the refractive index variation with wavelength is non-linear. In general the second derivative of the refractive index with wavelength is non-zero ($d^2n/d\lambda^2 \neq 0$).

The material dispersion for optical fibres is sometimes quoted as the material dispersion parameter D_M defined as $D_M = \frac{\lambda}{c}\left|\frac{d^2 n_1}{d\lambda^2}\right|$, which is expressed in units of *ps/nm/km*.

The material dispersion parameter D_M varies with wavelength for pure silica, and tends towards zero in the linear wavelength region around 1300 *nm* (Mazzali, Grosz et al. 1999). This provides an incentive (other than low attenuation) for operation at longer wavelengths where the material dispersion is minimised. Furthermore, the use of lasers of narrow optical spectrum rather than light emitting diodes (*LED*s) as optical sources leads to substantial reduction in the pulse broadening due to material dispersion, even in the shorter wavelength region.

Waveguide Dispersion

The waveguiding of optical fibres may also create waveguide dispersion. This results from the variation in group velocity with wavelength for a particular mode. Considering the ray theory approach, the waveguide dispersion is equivalent to the angle between the ray and the fibre axis varying with wavelength which subsequently leads to a variation in the transmission times for the rays. For a single-mode fibre, having a mode of propagation constant β, the fibre exhibits waveguide

dispersion when $(d^2\beta/d\lambda^2) \neq 0$. The waveguide dispersion is given by $D_W = -\left(\frac{n_1 - n_2}{\lambda_c}\right) V \frac{d^2(Vb)}{dV^2}$ and for a single-mode fibre it is always negative.

In designing optical fibres for the 1550 *nm* zero dispersion region, designers make use of the fact that waveguide and material dispersions are of opposite sign and as a result shifts the zero dispersion for longer wavelengths (Frenkel, Heritage et al. 1989). The waveguide dispersion value is affected by the refractive index profile of the optical fibre. A triangular core refractive index profile shifts the zero dispersion towards 1550 *nm* (Yabre 2000). Multimode fibres, where the majority of modes propagate far from cut-off, are almost free of waveguide dispersion and it is generally negligible in comparison with material dispersion.

Intermodal Dispersion

Pulse broadening due to intermodal dispersion (also called mode dispersion) results from propagation delay differences between modes within a multimode waveguide. As the different modes which carry the optical pulse power in a multimode fibre travel along the channel at different group velocities, the pulse width at the output is dependent upon the transmission times of the slowest and the fastest modes (Liu and De 2003). The step index multimode fibres have the largest intermodal dispersion. Parabolic index fibres have significantly reduced intermodal dispersion since the parabolic index profile equalises the group velocities of the modes. Single-mode fibres have no intermodal dispersion since only a single mode propagates.

Dispersion in Multimode Step Index Fibres

Using the ray theory model, the fastest and slowest modes propagating in the step index fibre may be represented by the axial ray and the extreme meridional ray (which is incident at the core-cladding interface at the critical angle ϕ_c) respectively. As both rays travel at the same velocity within the constant refractive index fibre core, the delay difference is directly related to their respective path lengths within the fibre. Hence the time taken for the axial ray to travel along a fibre of length L gives

the minimum delay time $T_{\min} = \frac{\text{distance}}{\text{velocity}} = \frac{L}{(c/n_1)} = \frac{Ln_1}{c}$. The extreme meridional ray exhibits the maximum delay time $T_{\max} = \frac{L/\cos\theta}{(c/n_1)} = \frac{Ln_1}{c\cos\theta}$.

The delay difference δT_s between the extreme rays may be obtained by $\delta T_s = T_{\max} - T_{\min}$. After some algebra, and replacing $\cos\theta$ with the sine of the critical angle, the delay difference is $\delta T_s \cong \frac{L(NA)^2}{2n_1 c} = \frac{Ln_1^2\Delta}{cn_2} = \frac{Ln_1\Delta}{c}$, where NA is the numerical aperture for the fibre. NA is an important parameter to describe the light gathering ability of an optical fibre. It is used to define the maximum angle at which incident rays on the optical fibre core. Incident rays will enter the fibre and propagate via internal reflection. The numerical aperture is given by $NA = \sin\theta_a = \sqrt{n_1^2 - n_2^2}$. Typical NA for single-mode fibre is 0.1. For multimode, NA is between 0.2 and 0.3 (usually closer to 0.2).

Dispersion in Multimode Graded Index Fibres

Intermodal dispersion in multimode fibres is minimised with the use of graded index fibres. The optimum profile is very nearly parabolic, and a dramatic improvement in reducing dispersion is possible, hence greatly improving the bandwidth. For a parabolic index profile, the delay difference between the fastest and slowest rays is given by $\delta T_s = \frac{Ln_1\Delta^2}{8c}$ (Yabre 2000).

Dispersion in Single-mode Fibres

The pulse broadening in single-mode fibres results almost entirely from inframodal effects (Hakki 1996). Hence the bandwidth is limited by the finite spectral width of the source. The transit time or the group delay is $\tau_g = \frac{1}{c}\frac{d\beta}{d\lambda}$ where c is the speed of light in vacuum, β is the propagation constant of the mode in vacuum. The total dispersion of a single-mode fibre, D_T, is given by the derivative of the specific group delay with respect to the wavelength, as $D_T = \frac{d\tau_g}{d\lambda}$.

The *rms* pulse broadening caused by waveguide dispersion over a fibre length L is given by (total *rms* pulse broadening) $\sigma_\lambda = L\left|\frac{d\tau_g}{d\lambda}\right|$.

Detailed calculation of the above derivatives, gives rise to two composite dispersion components (Lin, Wu et al. 1992). They are:

1. The material dispersion parameter D_M defined by $D_M = \frac{\lambda}{c}\left|\frac{d^2 n_1}{d\lambda^2}\right|$,, where n is either the core or cladding refractive index.
2. The waveguide dispersion parameter D_W, which may be obtained by $D_W = -\left(\frac{n_1 - n_2}{\lambda c}\right) V \frac{d^2(Vb)}{dV^2}$, where V is the normalised frequency as defined earlier.

Note that the material dispersion is positive at wavelengths longer than the zero material dispersion point. The waveguide dispersion component is always negative and when added to the material dispersion component, it shifts the zero dispersion point to longer wavelengths.

2.4.2 Review of Dispersion Calculation Methods

Calculation of optical waveguide mode propagation constants as a function of wavelength for optical fibres is a well-established problem and many different solution methods have been proposed and developed. For long distance high capacity transmission applications, an important concern of optical fibres is the pulse dispersion, measured in the unit of *ps/nm/km*. Understanding and controlling the variation of dispersion against wavelength is essential for the design of optical fibres. The dispersion characteristics such as dispersion shifted and dispersion flattened fibres have been extensively studied and investigated in the optical communication systems (Ainslie and Day 1986). Dispersion shifted fibre differs from standard fibre in that the zero dispersion point is shifted from 1310 *nm* to 1550 *nm* (Badolo and Emplit 1997). A fibre in which the dispersion is low over a broad wavelength range is defined as the dispersion flattened fibre. A few refractive index profiles for an optical fibre have been proposed in the past to get dispersion zero or flattened

characteristics over a wavelength range of 1300 *nm* to 1550 *nm* (Frenkel, Heritage et al. 1989; Hinata, Furukawa et al. 1994; Lundin 1994; Survaiya and Shevgaonkar 1996). Dispersion can also be controlled using dispersion management (Ennser, Ibsen et al. 1998). Lengths of negative dispersion fibre are periodically placed in the network in order to cancel out the positive dispersion of the transmission fibre (Urquhart 2003).

Owing to low-loss and low-dispersion characteristics, single-mode fibres are the solution for the large capacity and long-haul transmission system. Silica-based single-mode fibres have two distinguishing features; one is zero material dispersion in the vicinity of 1300 *nm* [1] (Payne and Gambling 1975), the other is intrinsic minimum loss of 0.2*dB*/km in the 1500 *nm* wavelength region (Miya, Nakahara et al. 1983).

Dispersion in a single-mode fibre is composed of material and waveguide dispersions. Dopant concentration dependence of material dispersion is small and consequently waveguide-structure dependence is also small. Waveguide dispersion, on the other hand, depends on features of the waveguide structure, such as the core radius, the refractive index difference between the core and cladding and the shape of the refractive index profile, which are suitable parameters for controlling dispersion in single-mode fibres (Lundin 1993).

Dispersion describes the spreading of optical pulses as they travel through a fibre. The different optical frequencies that make up the pulses travel at different speeds due to the composition of the glass. In a long enough fibre span the dispersion can be sufficiently large so that the pulses will overlap, resulting in inter symbol interference at the receiver producing a high bit error rate. Dispersion limits the rate at which transmission can occur using an optical carrier. Thus, it is one of the major limitations placed on the speed of the optical communication systems (Matsuda, Naka et al. 1996). The standard single-mode fibre deployed today is manufactured to optimize transmission at 1310 *nm* by effectively eliminating dispersion at that wavelength. The dispersion in the 1550 *nm* window far exceeds that for 1310 *nm* on standard fibre and hence is a limiting factor in single channel or *DWDM* systems operating in that window. The advent of *EDFA* technology allowing for the

---

[1] In pure silica the material dispersion is zero at about 1300 *nm*, and the addition of germanium shifts the material dispersion curve to longer wavelengths. Other dopants available to the fibre fabricator have relatively less effect on the material dispersion.

amplification of multiple optical carriers in the 1550 *nm* window gives sufficient motivation for the development of fibres that have minimal dispersion at 1550 *nm*, one of which is dispersion shifted fibre. It is best suited for applications involving single channel transmission at 1550 *nm* providing the benefits of zero dispersion as well as taking advantage of the lower attenuation occurring at that wavelength.

Numerical techniques for fast calculation of total dispersion from the mode propagation constant ideally should be as direct as possible. The methods must be theoretically exact hence correct prediction of even small values of dispersion would be possible and they must allow for the inclusion of material dispersion component. Analytical direct techniques are preferred in order to avoid high order curve fitting and subsequent numerical differentiation of data.

The definition of dispersion involves the use of first (delay) and second (dispersion) derivatives of mode propagation constant with respect to wavelength, thus theoretical evaluation of dispersion requires the determination of such derivatives in the first instance. However, direct numerical calculation of the first and second derivatives from data points of mode propagation constant versus wavelength based on simple finite differences can result in errors due to approximations (Sammut 1979). Different improved procedures have then been proposed, aiming at obtaining good accuracy in calculation of the dispersion (Mammel and Cohen 1982; Sharma, Sharma et al. 1982; Sharma and Banerjee 1989). In (Mammel and Cohen 1982), the Rayleigh quotient is proposed to obtain the first derivative of the propagation constant, but the direct numerical differentiation is used in the calculation of the second derivative. E.K. Sharma *et al.* (1982) avoid numerical differentiations by solving three differential equations for the propagation constant and its first and second derivatives, respectively. Recently, A. Sharma and S. Banerjee (1989) have reported another method based on a matrix perturbation theory and showed that computational effort can be reduced compared to the method in (Sharma, Sharma et al. 1982).

In this thesis, a new analysis leading to an exact and efficient algorithm is presented for calculating directly and without numerical differentiation the dispersion characteristics of cylindrical dielectric waveguides of arbitrary refractive index profiles (Boucouvalas and Qian 2005). The new algorithm is based on the equivalent

T-circuit model. The exact analytic formulas are derived for a recursive algorithm which allows direct calculation of delay and dispersion. This technique has been demonstrated by calculating the fundamental mode dispersion for step, triangular, and linear chirp refractive index profile optical fibres. The accuracy of the numerical results is examined. The proposed algorithm computes dispersion directly from the propagation constant without the need for curve fitting and subsequent successive numerical differentiation. It is exact, rapidly convergent and it results in savings for both storage memory and computation time.

2.5 Refractive Index Profile Reconstruction

It is of fundamental importance to be able to determine the refractive index profile of optical waveguides, as their main characteristics, bandwidth, spot size, single-mode propagation conditions, and inter waveguide coupling coefficients can all be related to their refractive index profiles.

The conventional method of designing optical cylindrical waveguide structures is to assume a refractive index profile and solve the governing differential equations to find the various propagating modes and their propagation characteristics. If the results do not exhibit the expected behaviour, the propagation characteristics are again evaluated with the changed refractive index. This procedure is repeated until the expected propagation characteristics of the modes are obtained. Since the procedure is iterative, it is time consuming. Also, it is not possible to guess the correct initial refractive index profile to obtain a specific arbitrary transmission characteristic nor is it easy to determine the profile changes that are necessary to produce the required optical characteristics. In these cases, it is common to work with initial profiles that have a mathematically closed form, such as parabolic and secant hyperbolic forms. According to the disadvantages of the method mentioned above, the inverse techniques applied to the refractive index reconstruction from the measured field profiles have been the topic of research. Methods for reconstruction of the optical fibre refractive index profile, however, are generally mathematically

difficult. These methods are classified into three groups according to the types of measured data used:

a) The far-field radiation pattern (Hotate and Okoshi 1979).

b) The near-field radiation pattern (Morishita 1983).

c) The mode effective index, which can be measured by a prism coupler (Ulrich and Torge 1973) et al..

2.5.1 Refractive Index Reconstruction from the Far-Field Radiation Pattern

Several methods have been proposed to characterise single-mode step index optical fibres with circular core from the far-field radiation pattern (Gambling, Payne et al. 1976; Hotate and Okoshi 1979; Gauthier, Auge et al. 1981). The far-field radiation pattern technique requires a large detector dynamic range and time-consuming computer calculations. This technique is particularly sensitive to dust on the fibre end face which causes variation in the reflectivity, and has the intrinsic error caused by the geometric optic approximation and the finite beam size. It requires great care to ensure uniform illumination of the core and cleanliness of the fibre and optics, because the information on the refractive index profile is expressed as a variable light intensity. In (Hotate and Okoshi 1979), the refractive index profile is computed from the measured far-field radiation pattern of the fundamental mode at the end of the single-mode fibre under test. This method is applicable to a fibre with an arbitrary index profile. It is possible by a computer-oriented measuring set up. The spatial resolution limit is half the wavelength of the light used in the measurement. A similar method is proposed in (Gambling, Payne et al. 1976), but only the core radius and the index difference between the core and the cladding in a uniform core single-mode fibre are determined from the far-field radiation pattern.

The near-field is usually defined as the region within a^2/λ of the optical fibre end-face. The far-field applies at distances much greater than this, a is the radius of the fibre core and λ is the wavelength of the propagated mode in the optical fibre. In the far-field pattern technique presented by Hotate *et al.* (1979), the index profile is obtained from the near-field pattern which is given by the inverse Hankel transform of the far-field pattern measured. The inverse Hankel transform, however, requires time consuming calculation. In (Qian and Boucouvalas 2003), the refractive index

profile is determined from the electric field of a propagation mode, i.e., the light intensity distribution across the output face of an optical fibre, by virtue of a new equation derived from the scalar wave equation. In this method, the mode electric field is measured directly and obtained easily without the laborious calculations.

2.5.2 Refractive Index Reconstruction from the Near-Field Radiation Pattern

In (Gauthier, Auge et al. 1981), the authors discuss both far-field and near-field methods. The near-field method is easier to set up and gives direct information on the index profile. The measurement accuracy and sensitivity rely upon the spot size and can be slightly improved by reducing the spot size to its ultimate limit. A number of techniques have been proposed for determining the refractive index distribution of optical fibres from the propagation mode near field, and the most well known rely on the seminal theoretical work by Morishita (1983). The refractive index profile is determined from the measurement of the near-field pattern of a propagation mode by an equation derived from the scalar wave equation. In this method, the error in the computed profile is very sensitive to the accuracy of the measured light intensity distribution and smoothing. In (Dhar, Lee et al. 1996), the measurement of the near field intensity is improved using a scanning optical microscopy technique rather than conventional optics, which is based on the measurement of the transmitted beam intensity near the guide facet. Improvements from Morishita (1983), have been recently reported by Lin and Chen (2002), which is a robust no-iterative method for noise and errors, but it is reported only for planar waveguides. Helms *et al.* (1990) have reported a method to reconstruct refractive index profiles of diffused Gaussian profile optical waveguides by analyzing the near field pattern of the waveguide. In this method, a computer simulation of measurement errors due to noise, quantization, defocusing and nonlinearity of the camera system is presented by using data of a typical camera measurement system. However, it is necessary to correct the intensity profile by a function with an inverse exponent. The reason is because some significant errors might be associated with the use of a non-linear IR-Vidicon camera. Most recently, Lassen *et al.* (2005) have presented a new technique for determining the refractive index profiles of axially symmetric optical fibres based on imaging phase gradients introduced into a transmitted optical field by a fibre sample.

However, as it is the case with quantitative phase microscopy, the ultimate spatial resolution and phase (and hence refractive index) sensitivity obtainable with the phase gradient technique are influenced by the choice of defocus distance.

It has been shown that *TL* technique can be applied to optical fibres and can determine exactly the mode propagation constants (Papageorgiou and Boucouvalas 1982), and cut-off wavelengths of waveguide modes (Boucouvalas and Papageorgiou 1982). In general from knowledge of the refractive index, complete waveguide characterisation can be achieved, including mode field plots using this technique (Boucouvalas and Robertson 1985).

In contrast to the traditional approaches, the proposed inverse solution of the *TL* method for refractive index reconstruction from electric fields requires no prior information on the functional form of the unknown quantities, no iterations in the calculating process, and no intensity smoothing in advance (Qian and Boucouvalas 2003; Qian and Boucouvalas 2004). Furthermore, the advantages of this method are that the unknown quantities of the refractive index can be reconstructed directly and the inverse problem can be solved in a linear domain. It is different from the traditional methods using nonlinear least squares formulation, which require numerous iterations in the process or prior knowledge about the profiles to be determined, and which must perform the calculation in the nonlinear domain. This implies that the present model offers a great deal of flexibility.

In this section, various methods for optical fibre refractive index reconstruction both from far-field and near-field patterns have been discussed. It is worth noting that some methods using the far-field radiation pattern do not give the exact profile of optical fibres, they merely give an equivalent step index refractive index profile. The optical waveguide refractive index can also be reconstructed from the mode effective index. However, this technique is mostly used for planar optical waveguides. In the following section, the inverse problem for planar optical waveguides will be discussed.

2.6 Planar Optical Waveguides

Microwave electronics, integrated optics and laser technology are areas sharing a common interest in dielectric planar layered structures. Knowledge of the propagation constants and cut-off frequencies of the various modes in such waveguides is very important.

The characterization of the refractive index profiles of planar waveguides also has a fundamental importance for the determination of their optical properties. Features such as bandwidth, single-mode condition, fibre-to-guide and guide-to-guide coupling efficiency are related to the refractive index profiles. Refractive index profiling is also a useful means in the study of the waveguide fabrication processes, as the profile can give valuable information about the physics of the fabrication process. Therefore the profiling permits the development of adequate analytical process models useful in relating the process itself to the optical parameters.

A variety of well-established approaches have been developed in order to determine the planar waveguide refractive index profiles. Some of these approaches start with the required propagation characteristics of the planar waveguide to synthesize the refractive index profiles. Examples of these approaches are compositional measurements (Caccavale, Chakraborty et al. 1995), interferometric methods (Kaminow and Carruthers 1973; Ramadan, Fazio et al. 1996), the measure of effective indices ("m-lines") (Ulrich and Torge 1973; Mathey, Jullien et al. 1995; Caccavale, Gonella et al. 1996; Chiang, Wong et al. 1996). Recently, ellipsometry has also been successfully employed. However, a close agreement between refractive index profiles determined by the "m-lines" method and ellipsometry have been found only at depths above 0.5-0.6 μm (Tonova, Paneva et al. 1998). Among these approaches, compositional measurements require advanced knowledge of the relation between dopant concentration and refractive index variation in a given matrix, while interferometric methods are complicated because accurately polished surfaces are necessary. Very attractive features are obtained by "m-lines" measurement, together with a reconstruction algorithm based on the Inverse Wentzel-Kramers-Brillouin (IWKB) method. Examples of this are the Chiang and White-Heidrich methods (Chiang, Wong et al. 1996), (White and Heidrich 1976), the iterative Finite

Differences Method (Caccavale, Gonella et al. 1996) and the reflectivity method (Mathey, Jullien et al. 1995). However, the "m-lines" technique only gives best results when applied to multimode planar waveguides, while poor information can be extracted when the number of the modes is low (e.g., single mode waveguides). In order to overcome this limitation, new techniques making use of a combination of the effective indices measured for both mode types [transverse electric (TE) and transverse magnetic (TM)] and multiple wavelength methods have been proposed (Wang and Huang 1999; Wang and C.S.Hsiao 2001). Nevertheless, these methods have the disadvantage of requiring the knowledge of the dispersion properties of the waveguide substrate, as well as the dispersion properties of the coupling prism used to measure the effective indices (Chiang, Wong et al. 1996). Ulrich *et al.* (1973) have proposed a method for determining the thickness and refractive index difference of the guided layer of 2-D three-layer waveguides. Laser light is coupled into the epitaxial waveguide layer though the air gap between the prism base and the film. At certain angles the coupling is observed for the allowed modes of the waveguide. When the diffracted beam from the prism is viewed at those coupling angles, a decrease in the light intensity is observed as a vertical dark line in the middle of the laser spot. After measuring the coupling angles for all the available modes, the thickness and the index difference of the epitaxial layer may be obtained. In order to obtain these values, the thickness of the layer should be large enough to allow at least two modes in the waveguide. By using orthogonal polarizations for the laser light, ordinary and extraordinary refractive indices may be obtained for uniaxial crystals. However, their method is not applied to graded index waveguides. Bourillot *et al.* (1995) have also proposed a method for determining the parameters of the refractive index distribution function of graded index waveguides. However his method can not be applied where the number of parameters to be determined is not equal to the number of data, as his technique does not use the least squared method.

Apart from the previous methods, Boucouvalas (1983) extends the far-field radiation pattern method (Gambling, Payne et al. 1976) to characterise a step index symmetric planar waveguide. The core thickness and the refractive index difference can be unambiguously determined from the far-field radiation pattern of the fundamental *TE* mode. However, an alternative most useful and accurate approach

for the refractive index determination is the transmitted near-field profiling from knowledge of the mode field distribution (Brooks and Ruschin 1996; Caccavale, Segato et al. 1998). It has been the industrial standard for the refractive index reconstruction.

In this thesis, an inverse *TL* approach to the design of planar optical waveguides with propagation characteristics of *TM* modes has been presented. The refractive index profile of the planar waveguide is formulated as a solution to the electric field equation which is obtained from the application of Maxwell's equations. The only mathematics involved in this approach is the wave impedance transformation formulas, which have been widely used in the field of Microwaves. Because of its simplicity, the method can be implemented into short but effective computer codes. The method is exact and is shown to be very accurate in comparison to the exact analytical solutions when the refractive index profiles are of graded index shapes. This method can reconstruct smooth refractive index profiles for planar optical waveguides that support single-modes or multi-modes. The cases of both isotropic symmetric and asymmetric arbitrary refractive index profile planar optical waveguides are discussed. By using the inverse *TL* technique, the refractive index profiles of planar optical waveguides can be reconstructed from their electric field data without the disadvantages existing in the methods discussed above.

CHAPTER 3

Forward Solution of Maxwell's Equations for Cylindrical Waveguides

3.1 Propagation Constant

Solution of the wave equation is necessary in order to obtain the mode propagation constants of cylindrical dielectric structures. Unfortunately this is analytically possible for only a few refractive index profiles. When the index profiles are derived from those for which analytical solutions exist, numerical methods for solving the wave equation are necessary. Approximate techniques, such as the variational method (Sharma, Sharma et al. 1982) and *WKB* (Hartog and Adams 1977), to mention but a few, are extensively used.

The resonance technique which uses transmission line principles has been presented in this thesis. Equivalent circuits of optical cylindrical waveguides are derived for the *TE*, *TM*, *HE*, and *EH* modes from which the propagation constants are obtained from the resonance condition of the circuits. Results of this method are compared with methods using the characteristic equations. An optical waveguide can be divided into a large number of homogeneous cylindrical layers of thickness δr, permittivity ε, permeability μ and conductivity σ in Fig.3.1. It is assumed that the time z and azimuthal behaviour of the fields are of the form $\exp\{j(\omega t + \beta z + l\vartheta)\}$, where β is the propagation constant of a mode of azimuthal number l.

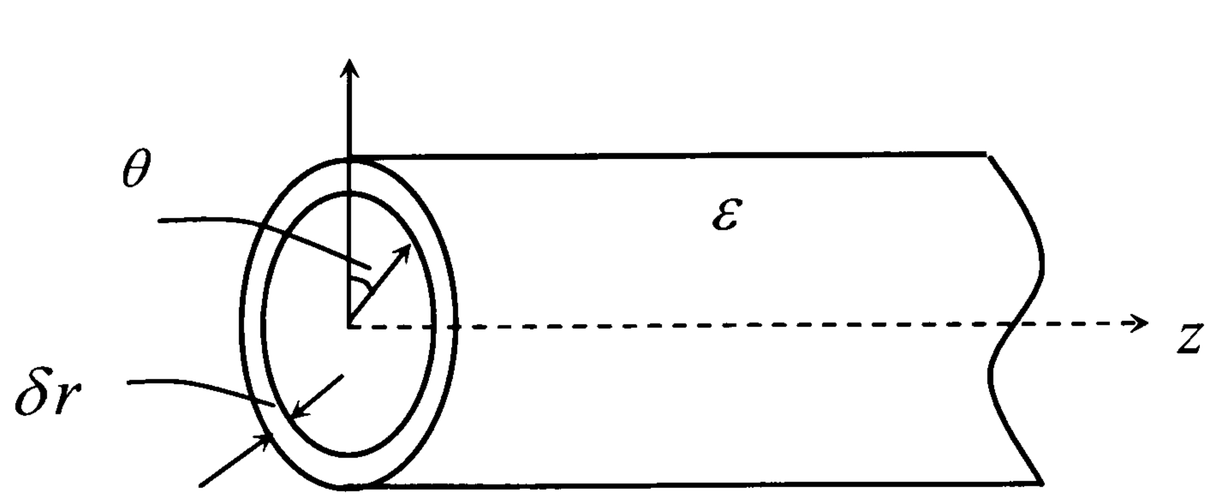

Figure 3.1 Homogeneous cylindrical layer

The E and H components of Maxwell's equations for any such layer can be written as:

$$\left.\begin{aligned} &\beta r E_\theta - l E_Z = \omega \mu r H_r \\ &l H_Z - \beta r H_\theta = (\omega\varepsilon - j\sigma) r E_r \\ &\frac{\partial(\omega \mu r H_r)}{\partial r} = -j\omega\mu(l H_\theta + \beta\, r H_Z) \end{aligned}\right\} \tag{3.1}$$

$$\left.\begin{aligned} &\frac{\partial[(\omega\varepsilon - j\sigma) r E_r]}{\partial r} = -(\sigma + j\omega\varepsilon)(l E_\theta + \beta r E_Z) \\ &\frac{\partial(l H_\theta + \beta r H_Z)}{\partial r} = -\frac{\gamma^2}{j\omega\mu}\omega\mu r H_r + \beta H_Z - \frac{l}{r} H_\theta \\ &\frac{\partial(l E_\theta + \beta\, r E_Z)}{\partial r} = -\frac{\gamma^2}{\sigma + j\omega\varepsilon}(\omega\varepsilon - j\sigma) r E_r + \beta\, \mathrm{E}_Z - \frac{l}{r} E_\theta \end{aligned}\right\} \tag{3.2}$$

where $\gamma^2 = \beta^2 + (\frac{l}{r})^2 - \omega^2\mu\varepsilon + j\omega\mu\sigma$, β is the propagation constant, l is the azimuthal mode number (integer), and ω is the mode frequency. The analysis is restricted to the case $\sigma = 0, \mu = \mu_0, \varepsilon = n^2\varepsilon_0$, where n is the refractive index of the layer at distance r from the axis.

The following variable voltages and currents are defined:

$$\left.\begin{aligned} V_s &= \frac{V_M}{\sqrt{n}} + V_E\sqrt{n} \qquad \text{(sum)} \\ V_d &= \frac{V_M}{\sqrt{n}} - V_E\sqrt{n} \qquad \text{(difference)} \\ I_s &= I_M\sqrt{n} + \frac{I_E}{\sqrt{n}} \qquad \text{(sum)} \\ I_d &= I_M\sqrt{n} - \frac{I_E}{\sqrt{n}} \qquad \text{(difference)} \end{aligned}\right\} \tag{3.3}$$

where

$$V_M = \frac{l H_\theta + \beta r H_Z}{jF} Z_0 \qquad \text{(magnetic voltage)}$$

$$I_M = \frac{\omega\mu r H_r}{jZ_0} \quad \text{(magnetic current)}$$

$$V_E = \frac{lE_\theta + \beta r E_Z}{F} Z_0 \qquad \text{(electric voltage)}$$

$$I_E = \omega \varepsilon_0 n^2 r E_r \qquad \text{(electric current)}$$

$Z_0 = 120\pi$ the free space impedance, $F = \dfrac{(\beta r)^2 + l^2}{r}$.

After algebraic derivatives, (3.1) and (3.2) can be transformed into:

$$\left.\begin{aligned} \frac{\partial V_s}{\partial r} &= \frac{-\gamma_s^2}{j\omega\varepsilon_0 nF} I_s \\ \frac{\partial I_s}{\partial r} &= -j\omega\varepsilon_0 nF V_s \end{aligned}\right\} \tag{3.4}$$

$$\left.\begin{aligned} \frac{\partial V_d}{\partial r} &= \frac{-\gamma_d^2}{j\omega\varepsilon_0 nF} I_d \\ \frac{\partial I_d}{\partial r} &= -j\omega\varepsilon_0 nF V_d \end{aligned}\right\} \tag{3.5}$$

where $\gamma_{s\atop d}^2 = \beta^2 + (\frac{l}{r})^2 - n^2 k_0^2 \mp \dfrac{2nk_0\beta l}{(\beta r)^2 + l^2}$ (- for HE, + for EH modes), and k_0 the free space propagation constant.

Equations (3.4) and (3.5) represent two independent transmission lines with voltages V_s, V_d and currents I_s, I_d. The corresponding characteristic impedances are:

$$\left.\begin{aligned} Z_s &= \frac{\gamma_s}{j\omega\varepsilon_0 nF} \\ Z_d &= \frac{\gamma_d}{j\omega\varepsilon_0 nF} \end{aligned}\right\} \tag{3.6}$$

The above equations are recognized as the well known transmission line equations with the solution represented by the following electric circuit Fig. 3.2.

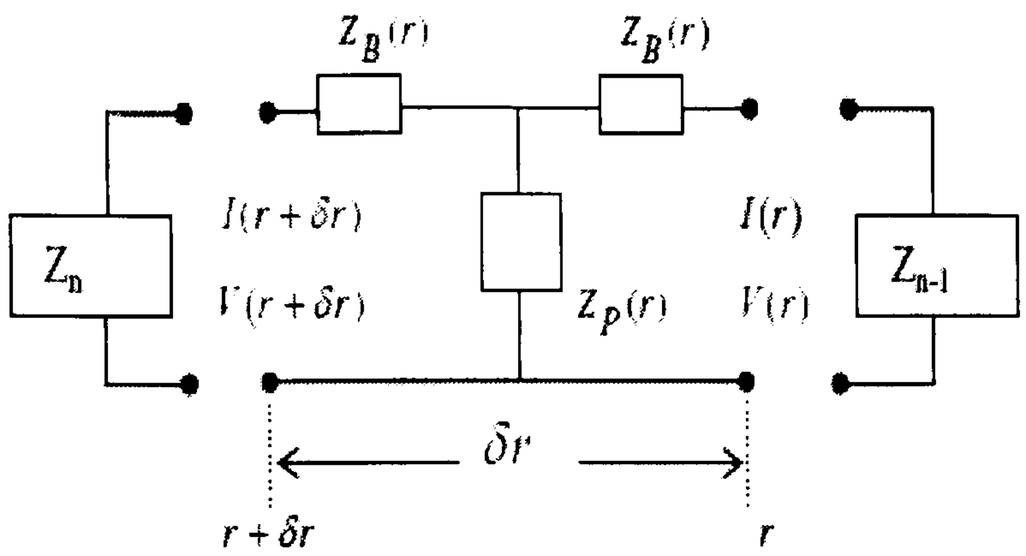

Figure 3.2 Equivalent circuit for an optical fibre cylindrical thin layer

$$\left.\begin{aligned} Z_B &= Z_{sd} \tanh\left(\gamma_{sd} \frac{\delta r}{2}\right) \\ Z_P &= \frac{Z_{sd}}{\sinh(\gamma_{sd} \delta r)} \end{aligned}\right\} \tag{3.7}$$

Where δr is the length of the transmission line. After combining (3.6) and (3.7), the following equations can be derived:

$$\left.\begin{aligned} Z_B &= \sinh(\gamma_{sd} \delta r) \tanh\left(\gamma_{sd} \frac{\delta r}{2}\right) Z_P \\ Z_P &= \frac{\gamma_{sd} Z_0}{jnrk_0\left(\beta^2 + \left(\frac{l}{r}\right)^2\right) \sinh(\gamma_{sd} \delta r)} \end{aligned}\right\} \tag{3.8}$$

Since δr is infinitesimal, $\left(\frac{\delta r}{r} << 1\right)$, hence:

$$\left.\begin{aligned} Z_B &= \frac{1}{2}(\delta r)^2 \gamma_{sd}^2 Z_P \\ Z_P &= \frac{Z_0}{jnr\,\delta r k_0\left(\beta^2 + \left(\frac{l}{r}\right)^2\right)} \end{aligned}\right\} \tag{3.9}$$

with $\gamma_{sd}^2 = \beta^2 + \left(\frac{l}{r}\right)^2 - n^2 k_0^2 \mp \frac{2nk_0\beta l}{(\beta r)^2 + l^2}$.

Normalizing (3.9) with respect to k_0 gives:

$$\left.\begin{aligned} \overline{Z}_B &= \frac{1}{2}(\delta \overline{r})^2 \overline{\gamma}_{sd}^2 \overline{Z}_P \\ \overline{Z}_P &= \frac{Z_0}{jn\overline{r}\,\overline{\delta r}\left(\overline{\beta}^2 + \left(\frac{l}{\overline{r}}\right)^2\right)} \end{aligned}\right\} \tag{3.10}$$

where $\bar{r} = rk_0, \delta\bar{r} = \delta rk_0, \bar{\beta} = \dfrac{\beta}{k_0}$, $\bar{\gamma}_{s_d}^2 = \gamma_{s_d}^2 / k_0^2 = \bar{\beta}^2 + (\dfrac{l}{\bar{r}})^2 - n^2 \mp \dfrac{2n\bar{\beta}l}{(\bar{\beta}\bar{r})^2 + l^2}$,

$\bar{Z}_p = Z_p \times K_0, \bar{Z}_B = Z_B \times K_0$.

We have come to the conclusion that the electromagnetic behaviour of a homogeneous cylindrical dielectric layer of thickness δr can be described from the analysis of independent *T*-circuits, (3.10). The first *T*-circuit (sum) corresponds to the *HE* modes, and the second to the *EH* modes (difference), $l \neq 0$. For the *TE* and *TM* modes, $l = 0$, from (3.10) $\bar{Z}_p = Z_0 / j\delta\bar{r}\bar{F}$ and $\bar{Z}_p = Z_0 / jn^2\delta\bar{r}\bar{F}$ can be obtained respectively, where $\bar{F} = F / K_0$.

The *T*-circuits representing the thin consecutive layers can be connected in tandem. The series of *T*-circuits are terminated by the characteristic impedance of the core medium at $r = 0$ and the characteristic impedance of the outer cladding medium at $r = \infty$, Fig.3.2. For *HE* and *EH* modes, the characteristic impedances become $Z(r = \infty) = 0$ and $Z(r = 0) = Z_0 / jn_1 l$, n_1 being the refractive index at $r = 0$. For *TE* and *TM* modes, $Z(r = 0) = \infty$ and $Z(r = \infty) = 0$ (Appendix B).

The total reactance up to the core-cladding interface, from infinity and from the centre of the fibre, can be found by varying β. The propagation constant of a mode can be determined when the total reactance is zero, i.e. the circuit resonates. Therefore a root searching technique is required to locate β at resonance. The convergence of the resonance method for a segmented index profile optical fibre with core radius a_1 =4583*nm*, inner cladding radius a_2 =8685*nm*, outer cladding radius a_3 =13150*nm*, $n_1 = 1.51508$, $n_2 = 1.508$, n_3=1.512, and V-value V=5, as a function of the number of layers, is illustrated in Table 3.1, where $b = ((\beta / K_0)^2 - n_2^2)/(n_1^2 - n_2^2)$. The accuracy level of the technique, using 600 homogeneous cylindrical layers and $\delta r / r = 0.02$, is illustrated with the aid of the graded index profiles. The speed of the method decreases with increase of the number of layers, and an efficient root searching technique would greatly reduce the computation time. As a final demonstration of this technique, Fig.3.3b shows b against V, where V=$k_0 a_3 (n_1^2 - n_2^2)^{1/2}$, for the segmented index profile optical fibre shown in Fig.3.3a.

In Fig.3.3b, we can see that the HE_{11} mode is the first mode that propagates in the optical fibre. Thus it has the highest propagation constant when a search is carried out at frequencies where higher order modes also propagate. The cut-off frequency is found from V = 2.825. Only the lowest *HE* mode, HE_{11}, has no cut-off frequency. For $0 < V < 2.825$, it is the only mode that propagates in the fibre. In a multimode fibre the different modes corresponding to the same V-value have different propagation constants. In addition, the propagation constant for each mode depends on the V-value. In a single-mode fibre the dependence of the propagation constant on V is the only cause of waveguide dispersion.

TABLE 3.1

Root-searching technique is a function of the number of layers

No. of layers	500	600	700	800	Exact (The asymptotic value)
b_{HE11}	0.83827	0.84062	0.84067	0.84067	0.84075
b_{HE12}	0.21032	0.21481	0.214909	0.21491	0.21490

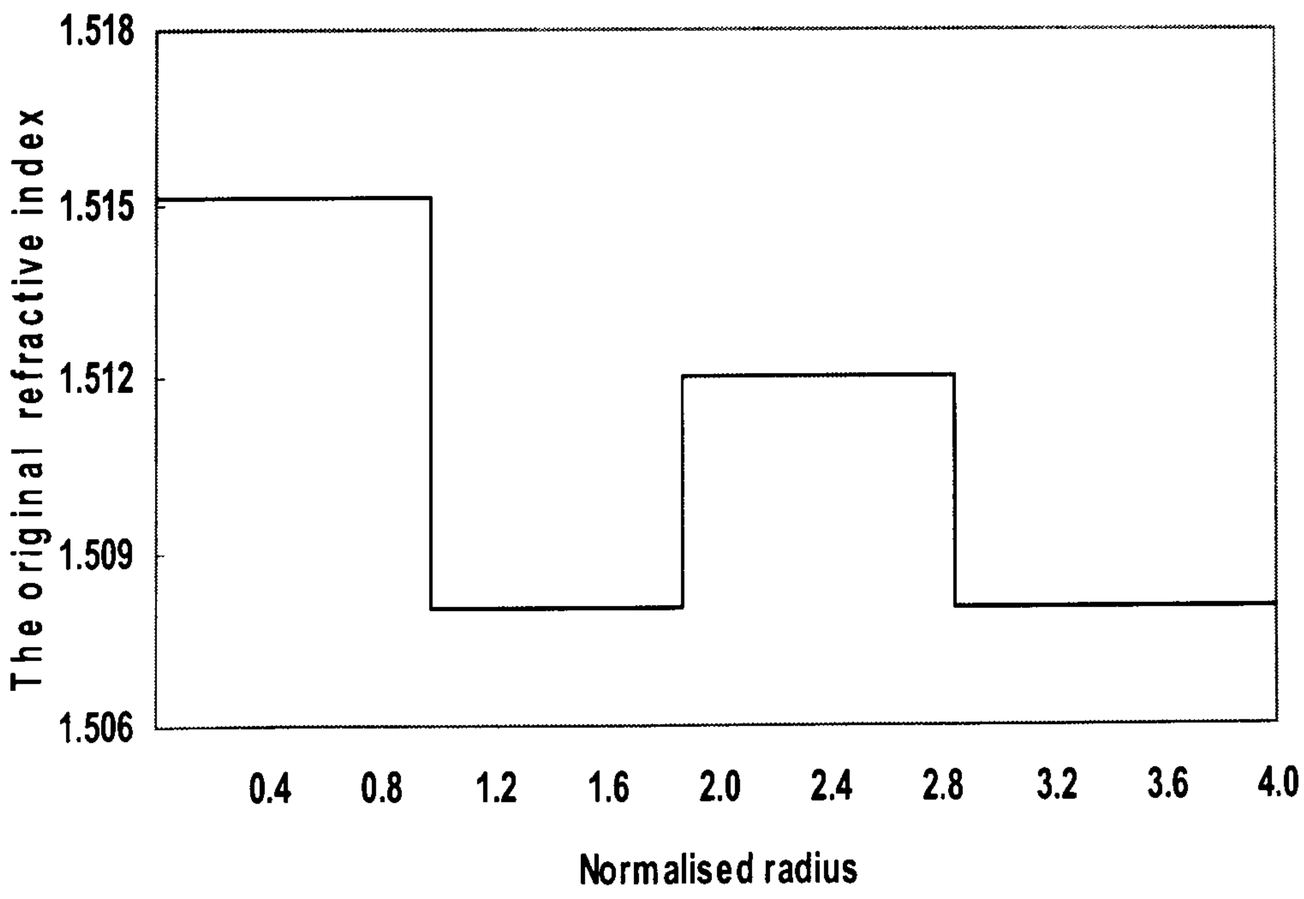

(a)

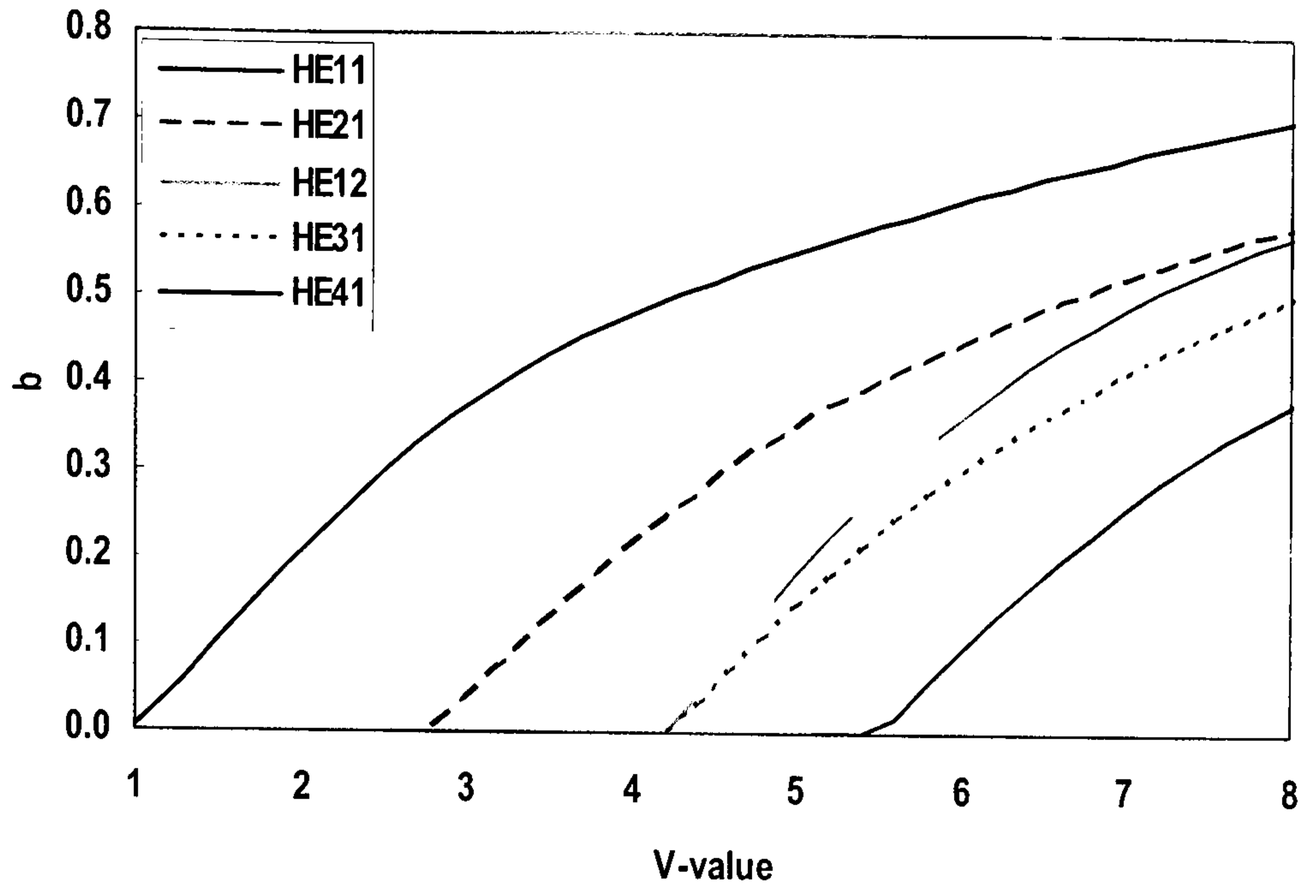

(b)

Figure 3.3 **(a)** Segmented index profile of the optical fibre with core radius a_1 =4583nm, inner cladding radius a_2 =8685nm, outer cladding radius a_3 =13150nm, core index n_1=1.51508, cladding index n_2 =1.508, n_3=1.512, and V=5

(b) b/V diagram for a segmented index profile optical fibre Fig.3.3a.

3.2 Field Plot

As mentioned previously, an optical fibre is envisaged as consisting of a large number of thin, homogeneous, consecutive cylindrical layers. The long series of layers can be described as a long series of equivalent T-circuits connected in tandem. The nth layer impedance can be expressed in terms of the (n-1) layer by the formula $Z_n = \frac{(Z_{n-1} + Z_{B,n})Z_{p,n}}{Z_{n-1} + Z_{B,n} + Z_{p,n}} + Z_{B,n}$ for n =1,2,3…,N, where $Z_{B,n}$, $Z_{p,n}$ are the series and parallel elements of the T-circuit representation of the nth layer. In order to achieve resonance, the total impedance of the circuit, the sum of Z_N and Z_{air} (the characteristic impedance of the surrounding air medium) must be determined. Z_N is computed starting with Z_{air} as Z_{n-1} and using $Z_n = \frac{(Z_{n-1} + Z_{B,n})Z_{p,n}}{Z_{n-1} + Z_{B,n} + Z_{p,n}} + Z_{B,n}$ for n =1,2,3…,N. The resonance condition is achieved when $Z_N + Z_{air} = 0$ is satisfied. Using a root searching technique the appropriate value of the propagation constant

β can be found. The series of the equivalent T-circuits are terminated with the characteristic impedance of the medium at the axis ($r = 0$), and the characteristic impedance of the outer cladding ($r = \infty$). Using an elementary circuit theory, starting from large r in the cladding, the total impedance Z_{out} up to the cladding-core boundary can be found and similarly, Z_{in} the total impedance from $r = 0$ to that boundary. When Z_{in} and Z_{out} are equal and opposite, the circuit resonates and therefore the appropriate value of β can be obtained.

Once β is obtained by root searching method on the basis of the resonance technique, the electric fields for different modes and different refractive index profile optical fibres can be plotted. From (3.10), the electric current I and electric field E_r can be derived:

$$\left.\begin{aligned} V_{HE} &= \frac{V_M}{\sqrt{n(r)}} + V_E\sqrt{n(r)} \\ V_{EH} &= \frac{V_M}{\sqrt{n(r)}} - V_E\sqrt{n(r)} \end{aligned}\right\} \tag{3.11}$$

$$\left.\begin{aligned} I_{HE} &= I_M\sqrt{n(r)} + \frac{I_E}{\sqrt{n(r)}} \\ I_{EH} &= I_M\sqrt{n(r)} - \frac{I_E}{\sqrt{n(r)}} \end{aligned}\right\} \tag{3.12}$$

The E/M field of the HE mode in terms of the variables I_{HE} and V_{HE} will be determined, $I_{EH} = V_{EH} = 0$ can be set when the HE modes are of interest. This implies that:

$$\left.\begin{aligned} I_M\sqrt{n(r)} &= \frac{I_E}{n(r)} \\ \frac{V_M}{\sqrt{n(r)}} &= V_E\sqrt{n(r)} \end{aligned}\right\} \tag{3.13}$$

Substituting into (3.11) and (3.12), the following equations can be derived:

$$\left.\begin{aligned} V_{HE} &= 2V_E\sqrt{n(r)},\ I_{HE} = 2I_M\sqrt{n(r)} \\ V_{HE} &= 2\frac{V_M}{\sqrt{n(r)}},\ I_{HE} = 2\frac{I_E}{\sqrt{n(r)}} \end{aligned}\right\} \tag{3.14}$$

Note that I_{HE} , V_{HE} are also referred to as I_s , V_s respectively.

Hence:

$$\left.\begin{aligned} V_E &= \frac{V_s}{2\sqrt{n(r)}},\ I_M = \frac{I_s}{2\sqrt{n(r)}} \\ V_M &= \frac{V_s\sqrt{n(r)}}{2},\ I_E = \frac{I_s\sqrt{n(r)}}{2} \\ I_E &= \omega\varepsilon_0 n^2(r) r E_r \end{aligned}\right\} \tag{3.15}$$

Hence:

$$E_r = \frac{I_E}{\omega\varepsilon_0 n^2 r} = \frac{Z_0 I_E}{k_0 n^2(r) r}$$

and:

$$E_{\bar{r}} = \frac{Z_0 I_E}{n^2(\bar{r})\bar{r}} \tag{3.16}$$

Therefore if the refractive index as a function of radius is known, the electric field $E_{\bar{r}}$ can be plotted out precisely by using (3.16) with knowledge of $n(\bar{r})$ and I_E which can be known at the initial condition and they can be calculated at every layer using circuit theory. Fig.3.4 shows the plotted electric fields of step, parabolic, triangular index profile single-mode optical fibres. As we see, in the step index single-mode optical fibre, most of the light travels in the high index core, while in the parabolic index single-mode optical fibre, a significant proportion (up to 20%) of the light actually travels in the cladding. This implies that the electric field distribution depends on the refractive index profiles of optical fibres. Fig.3.5(a) shows how different modes propagate in different propagation channels on a multimode optical fibre. For lower order mode HE_{11}, the electric field is concentrated near the centre of the optical fibre, as shown in Fig.3.5(b). The higher order modes HE_{12} and HE_{21} penetrate further into the cladding. For the HE_{12} and HE_{21} modes, the electric fields are distributed more toward the outer edge of the core, as shown in Fig.3.5(c) and Fig.3.5(d) respectively.

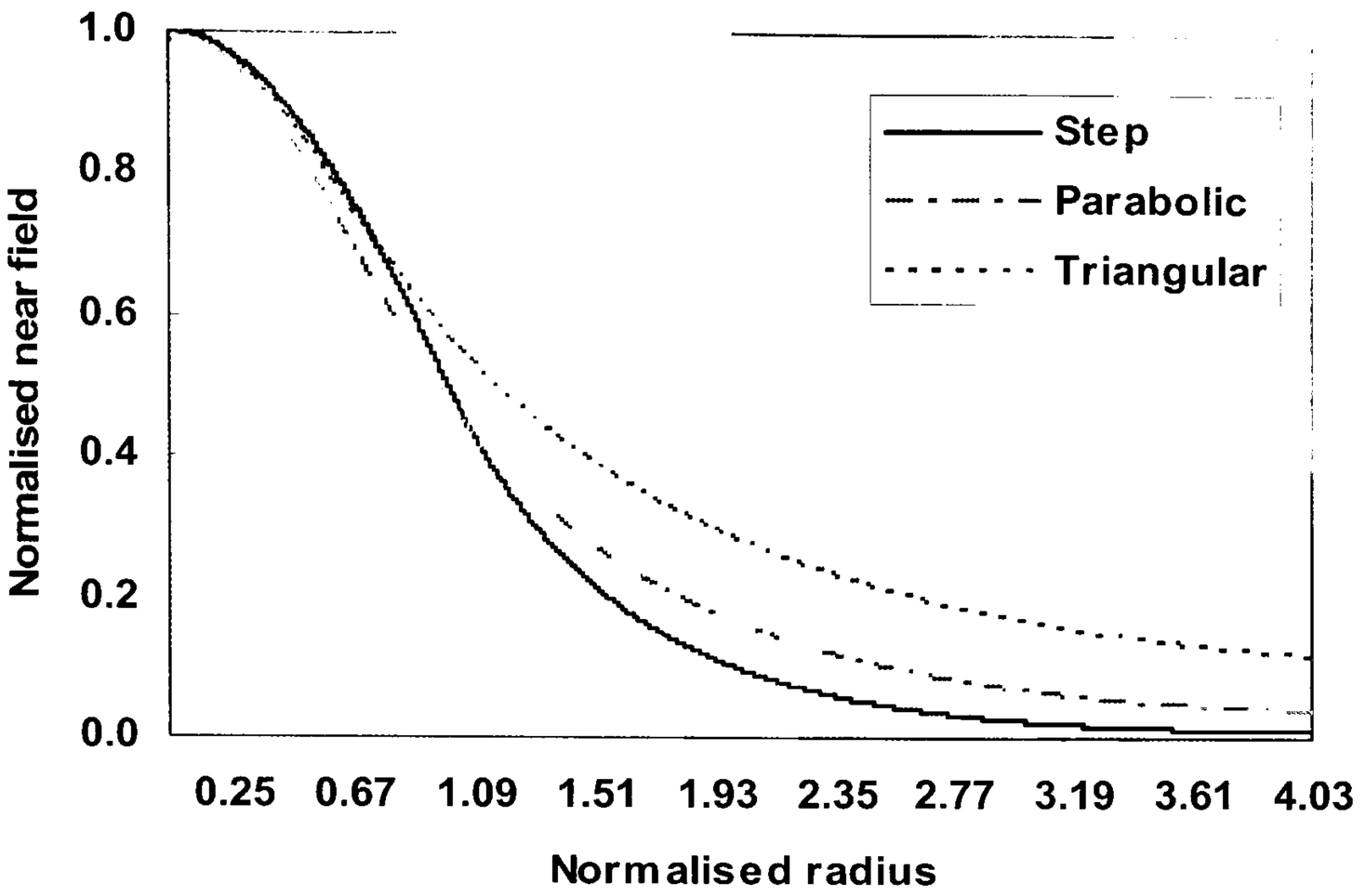

Figure 3.4 Electric field plot for step, parabolic and triangular index profiles single-mode optical fibres with core radius a=4583*nm*, core axis index n_1=1.51508, cladding index n_2=1.508, and V=5

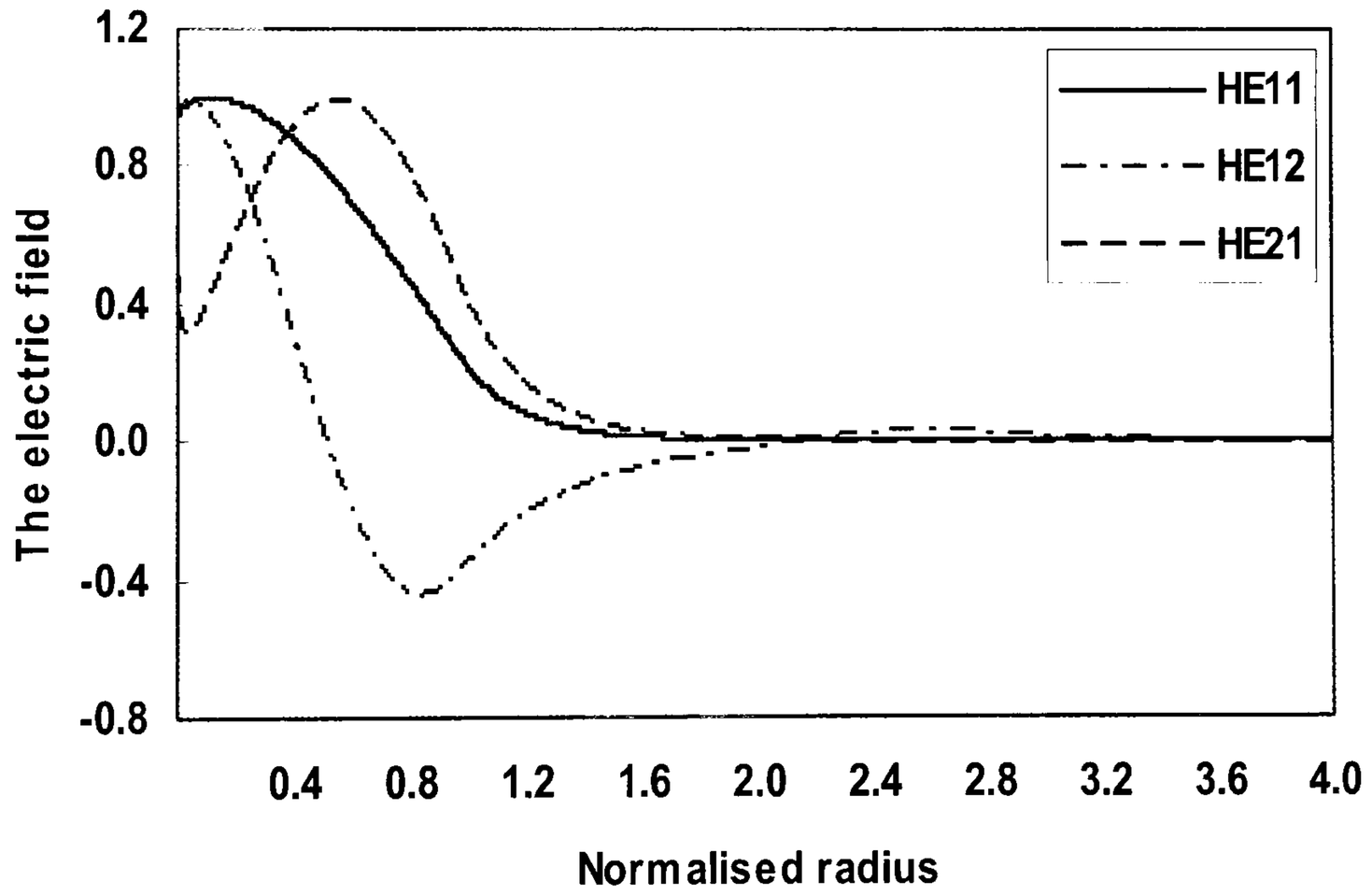

(a)

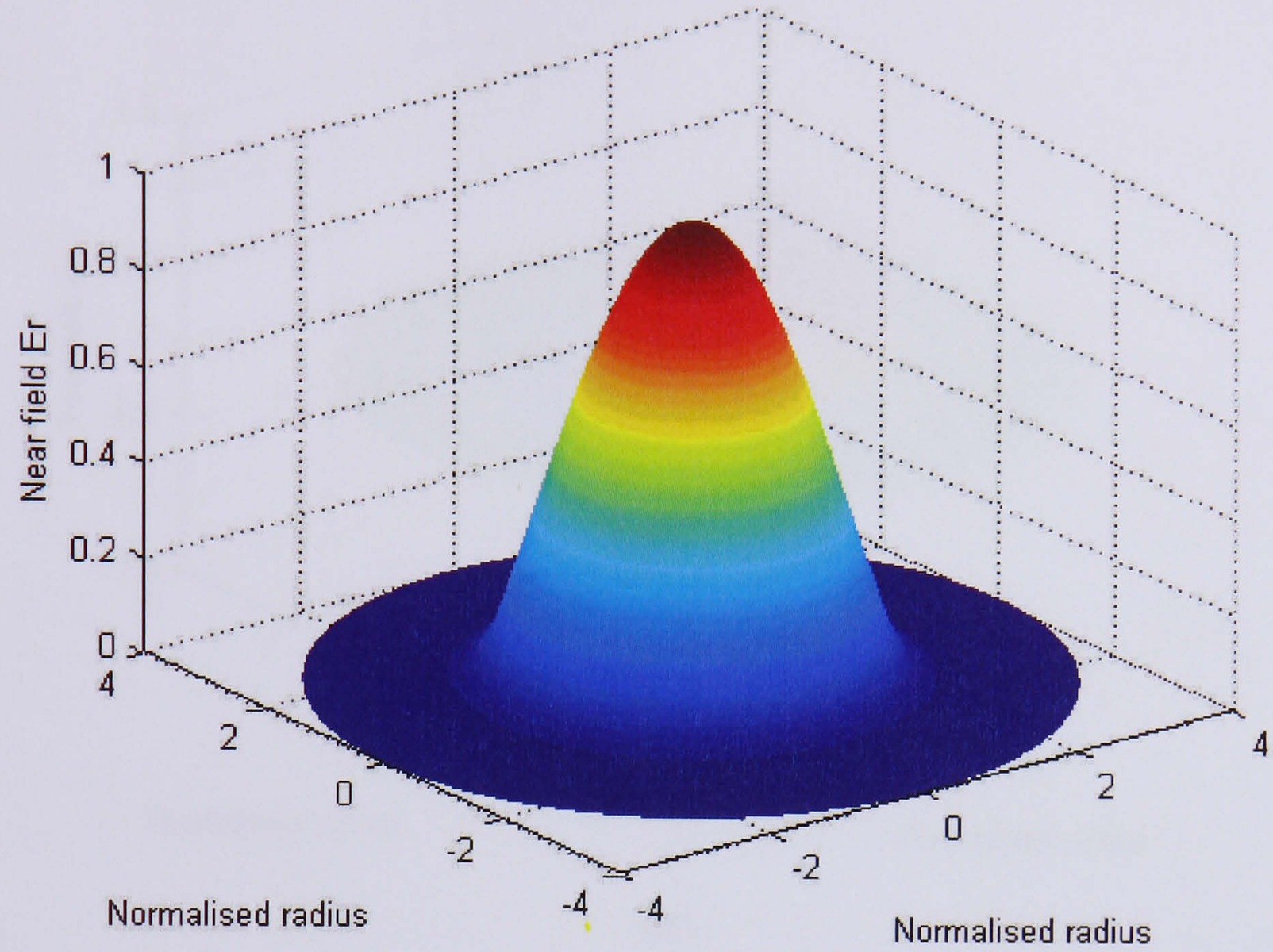
Near field Er
1
0.8
0.6
0.4
0.2
0
4
2
0
-2
-4
-4
-2
0
2
4
Normalised radius
Normalised radius

(b)

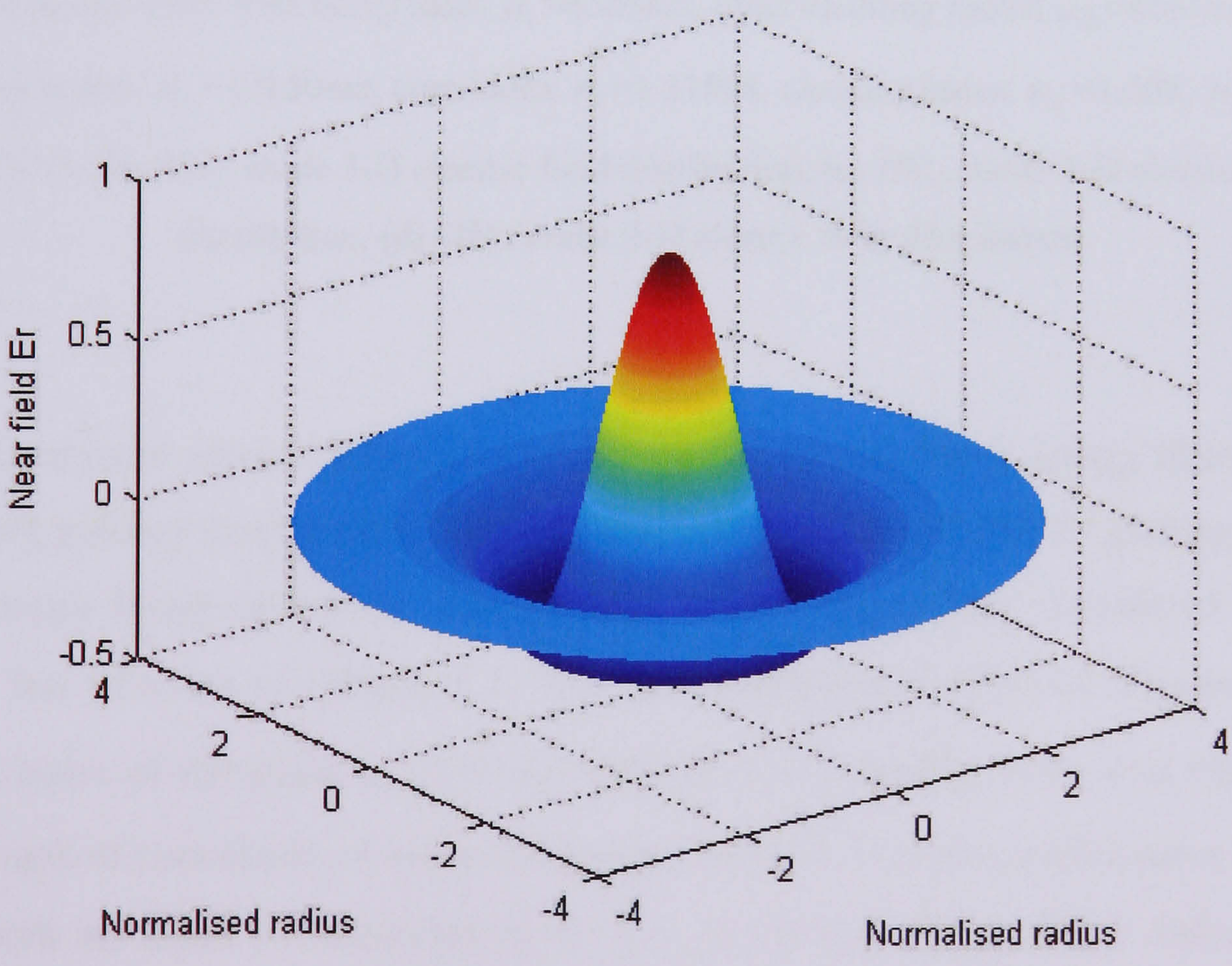
Near field Er
1
0.5
0
-0.5
4
2
0
-2
-4
-4
-2
0
2
4
Normalised radius
Normalised radius

(c)

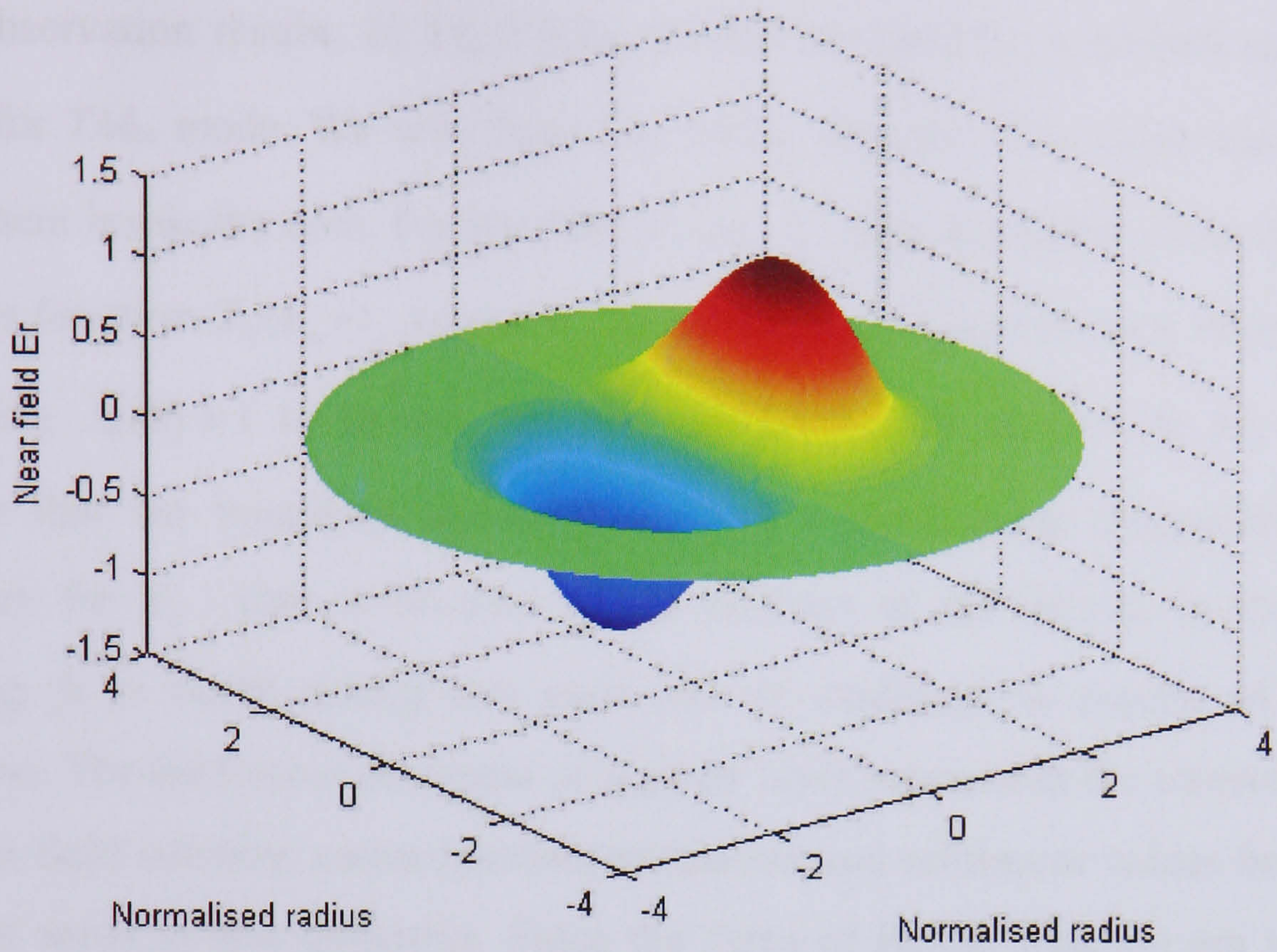

(d)

Figure 3.5 (a) Electric field plot for HE_{11}, HE_{12}, and HE_{21} modes on the segmented index profile optical fibre with core radius a_1 =4583*nm*, inner cladding radius a_2 =8685*nm*, outer cladding radius a_3 =13150*nm*, core index n_1=1.51508, cladding index n_2 =1.508, n_3=1.512, and V=5, **(b)** HE_{11} mode 3-D electric field distribution, **(c)** HE_{12} mode 3-D electric field distribution, **(d)** HE_{21} mode 3-D electric field distribution.

As mentioned above, compared to conventional optical fibres, Bragg fibres utilize different guiding mechanism. One such example is the possibility of guiding light in air through Bragg reflection. The structure of the Bragg fibre considered here is: layer1 has an index of refraction n_1=4.6 and a thickness d_1=0.333d, whereas layer2 has an index of refraction n_2 =1.6 and a thickness d_2 =0.667d. Here d=d_1+d_2 is the unit length of periodicity of the multilayered structure. The Bragg fibre has a uniform core with an index of refraction n_0 =1 (i.e. an air-core Bragg fibre) and a radius r_0 =1.4d. Fig.3.6(a) shows the Bragg fibre index profile. It is worth noting that in practice, in order to provide structural support the uniform core may be replaced by some dielectric material with a low index of refraction without greatly affecting the

main observation results. In Fig.3.6(b), the electric field $E_{\bar{r}}$ is plotted out by using (3.16) for TM_{01} mode. We note from Fig.3.6(b) that the TM_{01} mode has a large $E_{\bar{r}}$ component inside the core. For the TM_{01} mode, $E_{\bar{r}}$ is proportional to the zeroth order Bessel's function $J_0(k_{co}r)$, where k_{co} is the transverse wave-vector inside the core. Assuming $J_0(0)=1$ is known, we see that $E_{\bar{r}}$ would necessarily be large. We observe that the boundary matching imposes a small jump discontinuity at the boundary for $E_{\bar{r}}$. This is because of the contrast of the indices in the core and cladding. It is worth noting that each pair of claddings is exactly of half-wave thickness. The half-wave thickness of a given layer means that the transverse Bessel function field solution varies between maximum and minimum values between two adjacent zeros in that thickness. Since the zeros of Bessel function are not equally spaced, the cladding thicknesses are not identical. However, they tend to become similar as r becomes large. This is due to the asymptotic form of the Bessel functions which approaches that of sine and cosine functions.

In the forward solution of Maxwell's equations for cylindrical optical waveguides, the propagation constant of optical fibres can be worked out by using the root searching method on the basis of resonance technique. The mode electric field can be plotted for single-mode and multimode optical fibres and Bragg fibres using the obtained propagation constant. Also, the complex propagation constant of the complex refractive index profile optical fibres can be calculated out by using the same method. The solution to this problem will lead into working out the gain and loss in Erbium-doped optical fibres. It will be discussed in the next section.

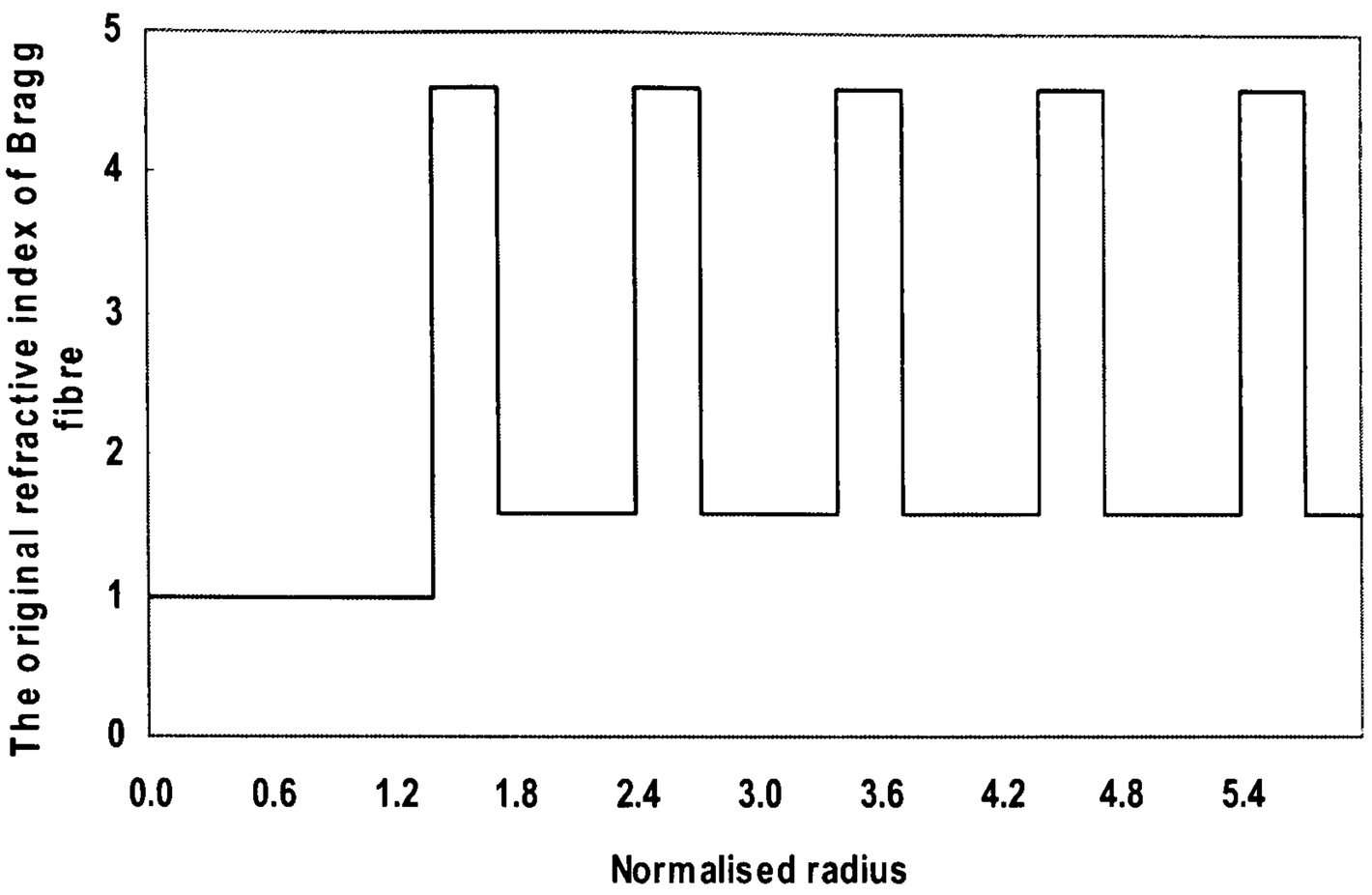

(a)

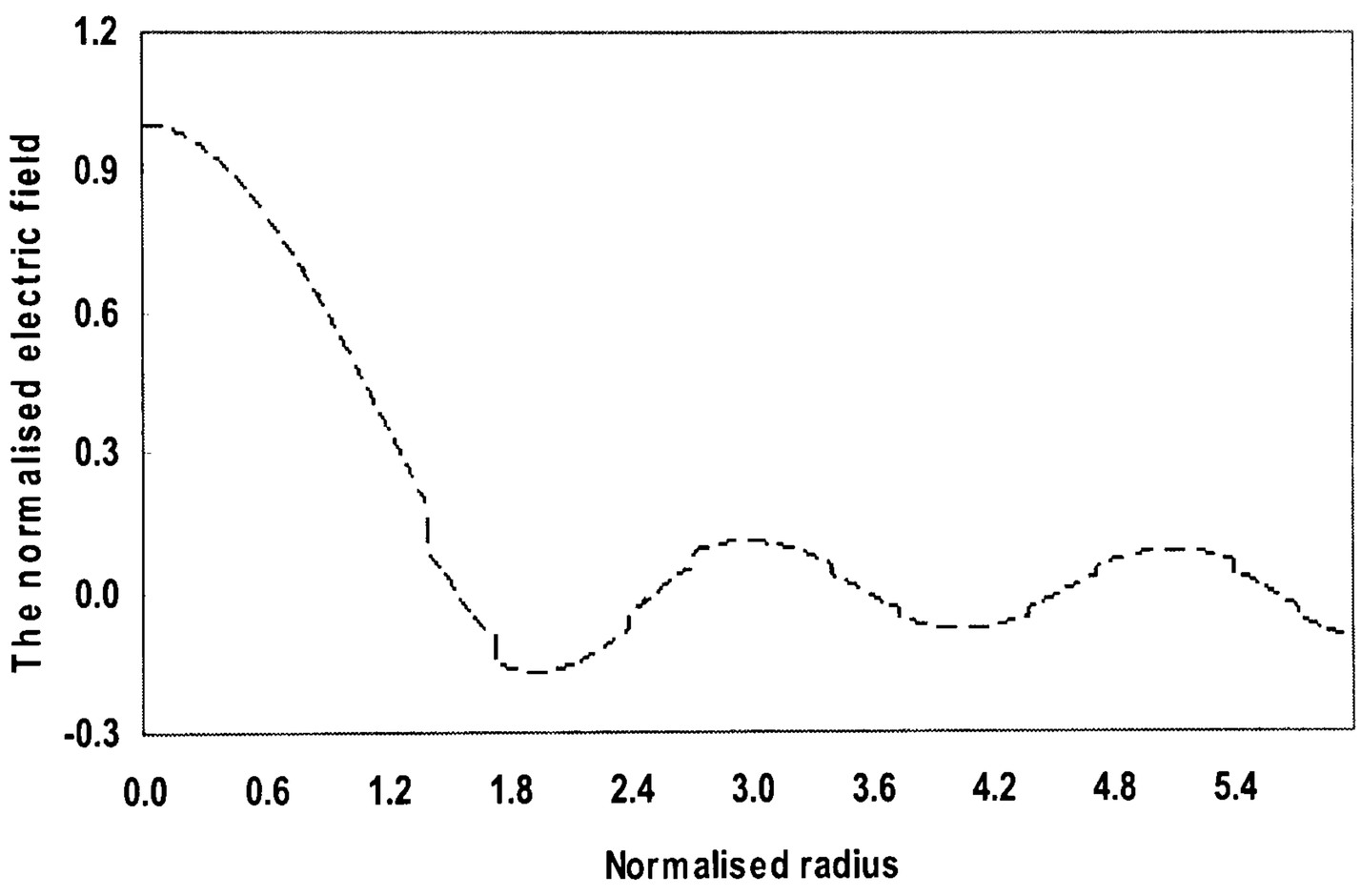

(b)

Figure 3.6 (a) The Bragg fibre structure: core index n_0=1, thickness r_0=1.4a, layer1 index n_1=4.6, thickness d_1=0.333d, layer2 index n_2=1.6, thickness d_2=0.667d. d=d_1+d_2 is the unit length of periodicity of the multilayered structure.

(b) E_r field distribution for the *TM* mode Bragg fibre with the Fig3.6a structure, the normalised propagation constant $\overline{\beta}$ =1.25, V-value V=8.

3.3 Complex Propagation Constant

With the advent of fibre lasers and doped fibre amplifiers, attention has been drawn to the analysis of optical fibres whose refractive index profile can be described in terms of complex numbers. Complex refractive index profiles result in complex mode propagation constants offering information on the loss or gain properties of optical fibres. Some approximate or numerically cumbersome methods have been reported in the literature (Reisinger 1973; Sader 1990; Sunanda and Sharma 1999; Singh and Sharma 2001) for evaluation of the propagation characteristics of such fibres.

In this section, a rapidly converging numerical technique is presented for the evaluation mode characteristics of circularly symmetric optical fibres with an arbitrary complex refractive index profile. The calculation process can be described as follows; since the normalized propagation constant is the function of the complex refractive index, the obtained normalized propagation constant is also complex. Using the *TL* technique and resonating the circuits to locate the real part of the complex refractive index at the root, the imaginary part gives the gain and loss. Therefore, the attenuation can be calculated using $8.686k_0\overline{\beta}_i(dB/m)$ (Desurvire 1994), where $\overline{\beta}_i$ is the imaginary part of the complex normalized propagation constant. To illustrate the capacity of the procedure, it has been applied to circularly symmetric fibres with complex step, parabolic and segmented refractive index profiles. This method has been used to evaluate and control the gain in a typical 980 *nm* pumped *EDF* as well as to calculate the attenuation of optical fibres when radial loss factors are presented.

3.3.1 Definition of Complex Refractive Index In Erbium-Doped Fibre

The signal gain in an *EDFA* is obtained by creating population inversion, using a pump at 980 *nm*. The assumption of a three-level laser system for the *EDFA* provides a means of defining a complex refractive index profile for the pumped *EDFA* at signal and pump wavelengths. The complex refractive index profile of the core-doped fibre can, in general, be written as (Sunanda and Sharma 1999):

$$n(r) = \begin{cases} n_1(r) + in_i(r) & r < a \\ n_2 & r > a \end{cases} \tag{3.17}$$

where a is the core radius.

The procedure is illustrated by analyzing a step index fibre with step index Erbium dopant concentration in the core, $\rho(r) = \rho_0$ for $r < a$ and $\rho(r) = 0$ for $r > a$, with $\rho_0 = 1.6 \times 10^{25}$ m^{-3}, and a pump wavelength of 980 *nm*. $\rho(r)$ is the Erbium-Dopant profile, $\psi_{p,s}^2(r)$ are the fibre mode profiles at the pump and signal wavelengths, and for step index refractive index profile are simply given by (Singh and Sharma 2001):

$$\psi_{p,s}^2(R < 1) = J_0^2(U_{p,s}R) \qquad \text{(in the core)} \tag{3.18}$$

$$\psi_{p,s}^2(R > 1) = \frac{J_0^2(U_{p,s})}{K_0^2(W_{p,s})} K_0^2(W_{p,s}R) \qquad \text{(in the cladding)} \tag{3.19}$$

where $R = r/a$, $U_{p,s}$, $V_{p,s}$, and $W_{p,s}$ are the conventional fibre parameters (Desurvire 1994) of the undoped fibre, and $J_0(Z)$ is the Bessel function of first kind of order zero. Equations (3.18) and (3.19) are valid only for step index profile waveguide, for other profile waveguides, (3.16) can be used to obtain the electric field, and the square of the field is $\psi_{p,s}^2(r)$.

$\sigma_a(\lambda_s)$ and $\sigma_e(\lambda_s)$ are the absorption and emission cross-sections respectively , at signal wavelength λ_s and $\eta(\lambda_s) = \sigma_e(\lambda_s)/\sigma_a(\lambda_s)$. Also, p and q indicate the signal and pump powers guided in the fundamental mode normalized to their respective saturation powers $p = P_s(z)/P_{sat}(\lambda_s)$, $q = P_p(z)/P_{sat}(\lambda_p)$, with $P_{sat}(\lambda_s)$ and $P_{sat}(\lambda_p)$ defined as:

$$P_{sat}(\lambda_s) = \frac{hc\pi\omega_s^2}{\lambda_s \sigma_a(\lambda_s)[1 + \eta(\lambda_s)]\tau} \tag{3.20}$$

$$P_{sat}(\lambda_p) = \frac{hc\pi\omega_p^2}{\lambda_p \sigma_a(\lambda_p)\tau} \tag{3.21}$$

where h is Planck's Constant 6.62×10^{-34} m$^2 kg/s$, c is the light speed in free space, τ is the life time of the upper laser level $1 \times 10^{-2} s$, $\omega_{p,s}$ is the mode power

radius given by (Sunanda and Sharma 1999):

$$\omega_{p,s}^{2} = 2\int_{0}^{\infty} \psi_{p,s}^{2}(r) r dr \tag{3.22}$$

The imaginary part of refractive index n_i in the pumped Erbium-Doped fibre can be written as in (Sunanda and Sharma 1999):

$$n_i(signal) = \frac{\rho(r)\sigma_{as}\lambda_s[\eta_s q|\psi_p(r)|^2 - 1]}{4\pi[1 + q|\psi_p(r)|^2 + p|\psi_s(r)|^2]} \tag{3.23}$$

$$n_i(pump) = \frac{-\rho(r)\sigma_{ap}\lambda_p[1 + (\eta_s)/(1+\eta_s)p|\psi_s(r)|^2]}{4\pi[1 + q|\psi_p(r)|^2 + p|\psi_s(r)|^2]} \tag{3.24}$$

The positive (negative) sign of the imaginary part indicates a gain (loss) medium. Once n_i is defined, the modal gain and loss can be obtained. The corresponding gain per unit length, defined as $g = (1/p)(dp/dZ)$, is given by $g = 2\beta_i$. The gain or loss of the propagation signal and pump power, in decibels per meter, is hence $8.686k_0\overline{\beta}_i(dB/m)$ (Desurvire 1994).

3.3.2 Numerical Results and Discussion

To compare the results presented here to those in (Sunanda and Sharma 1999), the same parameters are used in this work. The core radius of the analyzed optical fibre is $a = 1.5\mu m$, index in the core is $n_1 = 1.46$ and $NA = 0.24$. The absorption and emission cross-sections of the signal are $\sigma_{as} = 7\times10^{-25}m^2$ and $\sigma_{es} = 0.92\sigma_{as}$ respectively. The absorption cross section of the pump is $\sigma_{ap} = 2\times10^{-25}m^2$. Using the above (3.17), complex refractive index profile, and using the transmission line technique the complex index n_e and corresponding values of gain at different wavelengths can be obtained in the $1.53\mu m$ range. The typical radial index profiles of the imaginary part of the complex refractive index at pump and signal wavelengths respectively are shown in Figs. 3.7 and 3.8 (at $\lambda_s = 1.53\mu m$) for several pump power levels q under the small-signal approximation ($p = 2\times10^{-6}$). A

comparison is also shown with results in (Sunanda and Sharma 1999). As the pump power increases, the population density in the lower level decreases, and lower steady-state absorption of pump power is obtained. Positive and negative values of n_i represent gain and loss. Hence the curves imply that, in uniform dopant, at low pump levels the gain attained from a part of the fibre cross section is cancelled by loss from another part, a condition that can be corrected by the use of dopant only in the central region. The figures also show higher values of gain at higher pump levels but with a saturating behaviour. Associated with Figs.3.7 and 3.8 are in Tables 3.2 and 3.3 comparing the accuracy of the *TL* method with (Sunanda and Sharma 1999). From Tables 3.2 and 3.3, we can see that with the increase of the input pump power levels, the result differences between the *TL* method and Sunanda's are getting smaller.

Fig.3.9 and Fig.3.10 show examples for greater values for the imaginary part of the refractive index. The dopant concentration in the core is now increased to $2.68\times10^{27}\,m^{-3}$ (Yb^{3+}) (Limpert, Schreiber et al. 2002). For the ease of comparison with EDFA, the other parameters are same. This demonstrates that the *TL* technique is not only appropriate for profiles in which the imaginary part of the refractive index is very small, but can also be used for refractive index profiles with a much greater imaginary part.

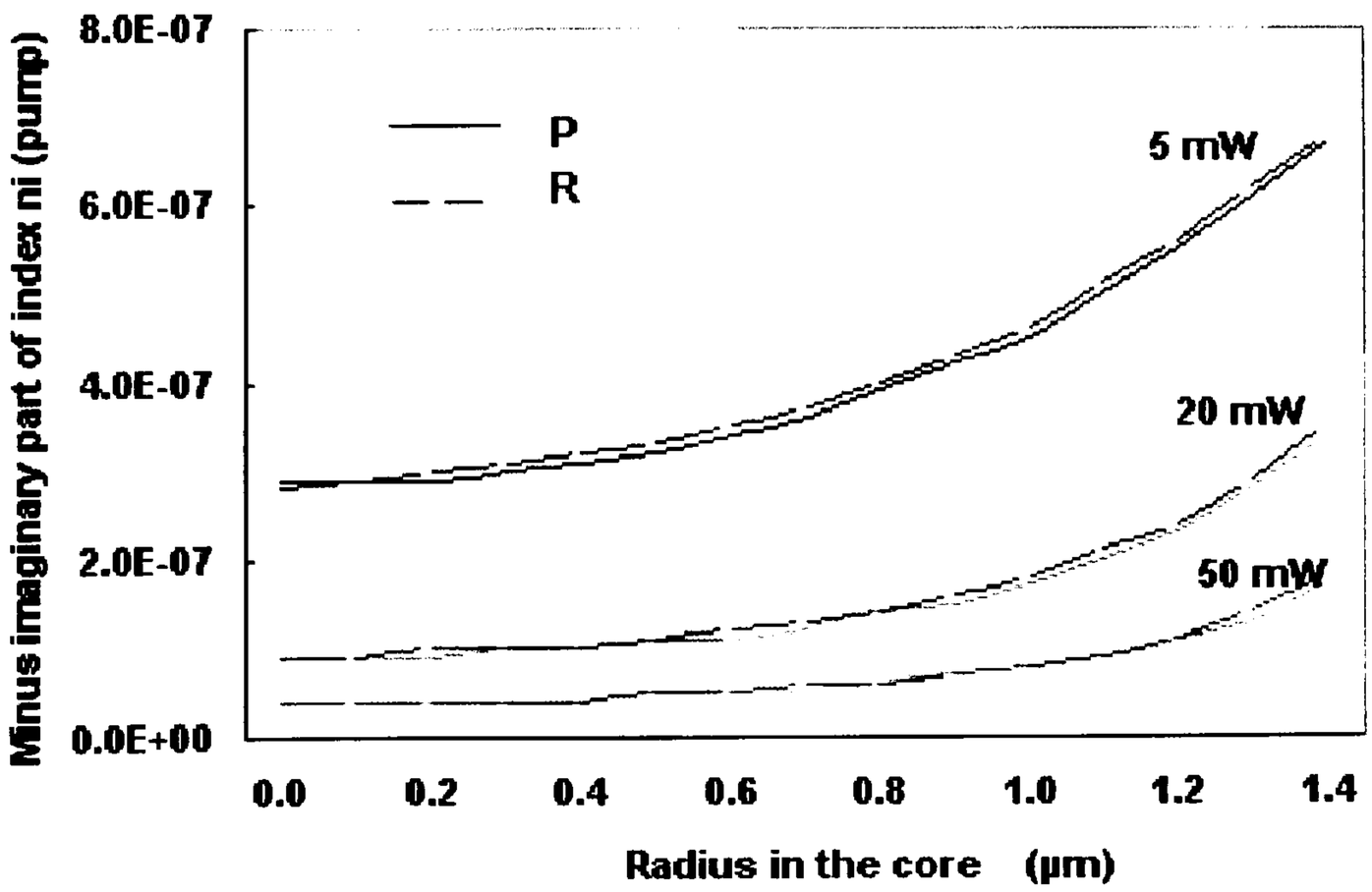

Figure 3.7 Radial profile of the minus imaginary part of the pump index against radius in the core at different input pump power levels q (marked in mW) by the present method (P) and Rayleigh-Ritz method (R) of (Sunanda and Sharma 1999).

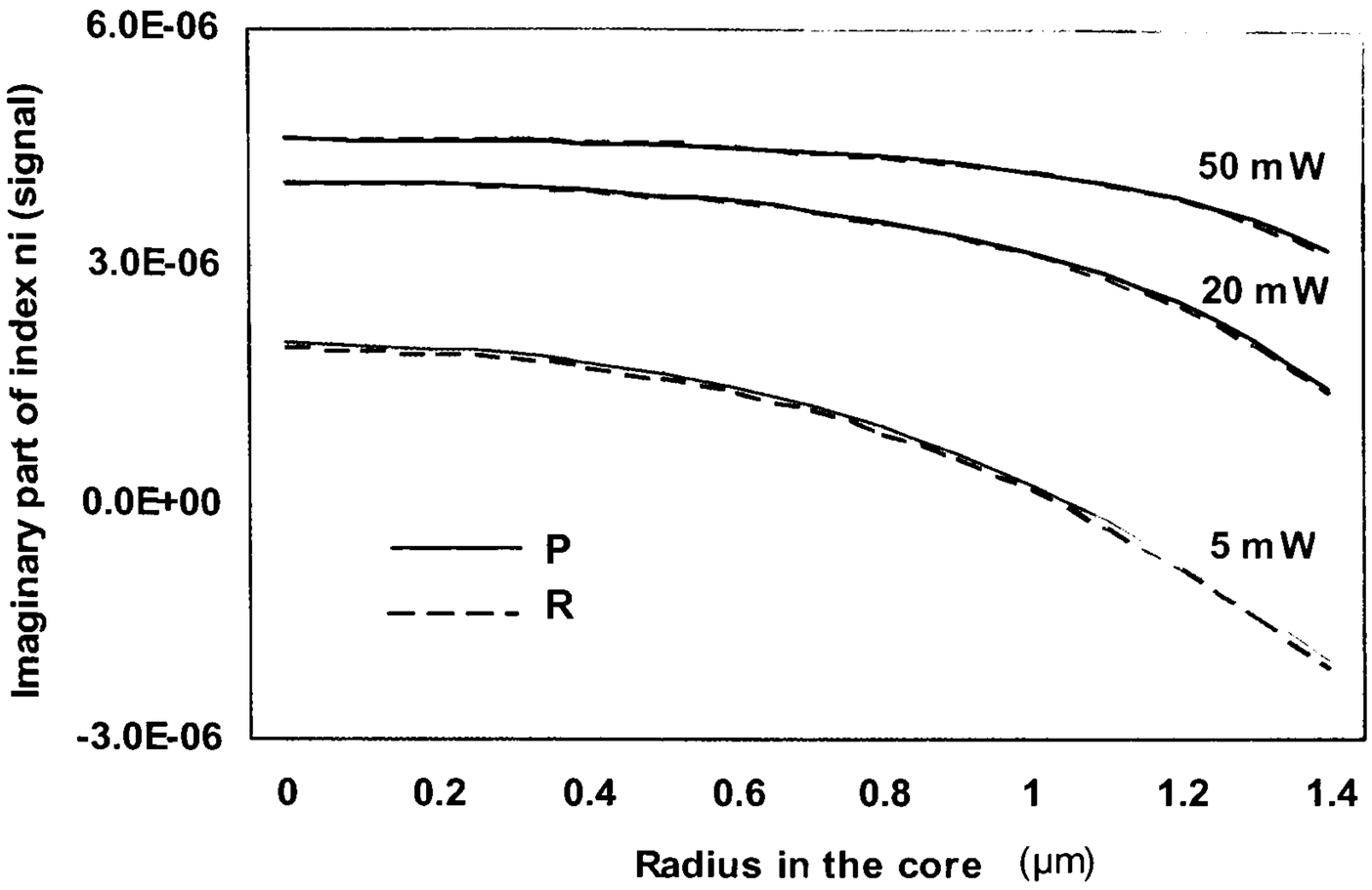

Figure 3.8 Radial profile of the imaginary part of the signal index against radius in the core at different input pump power levels q (marked in mW) by the present method (P) and Rayleigh-Ritz method (R) of (Sunanda and Sharma 1999).

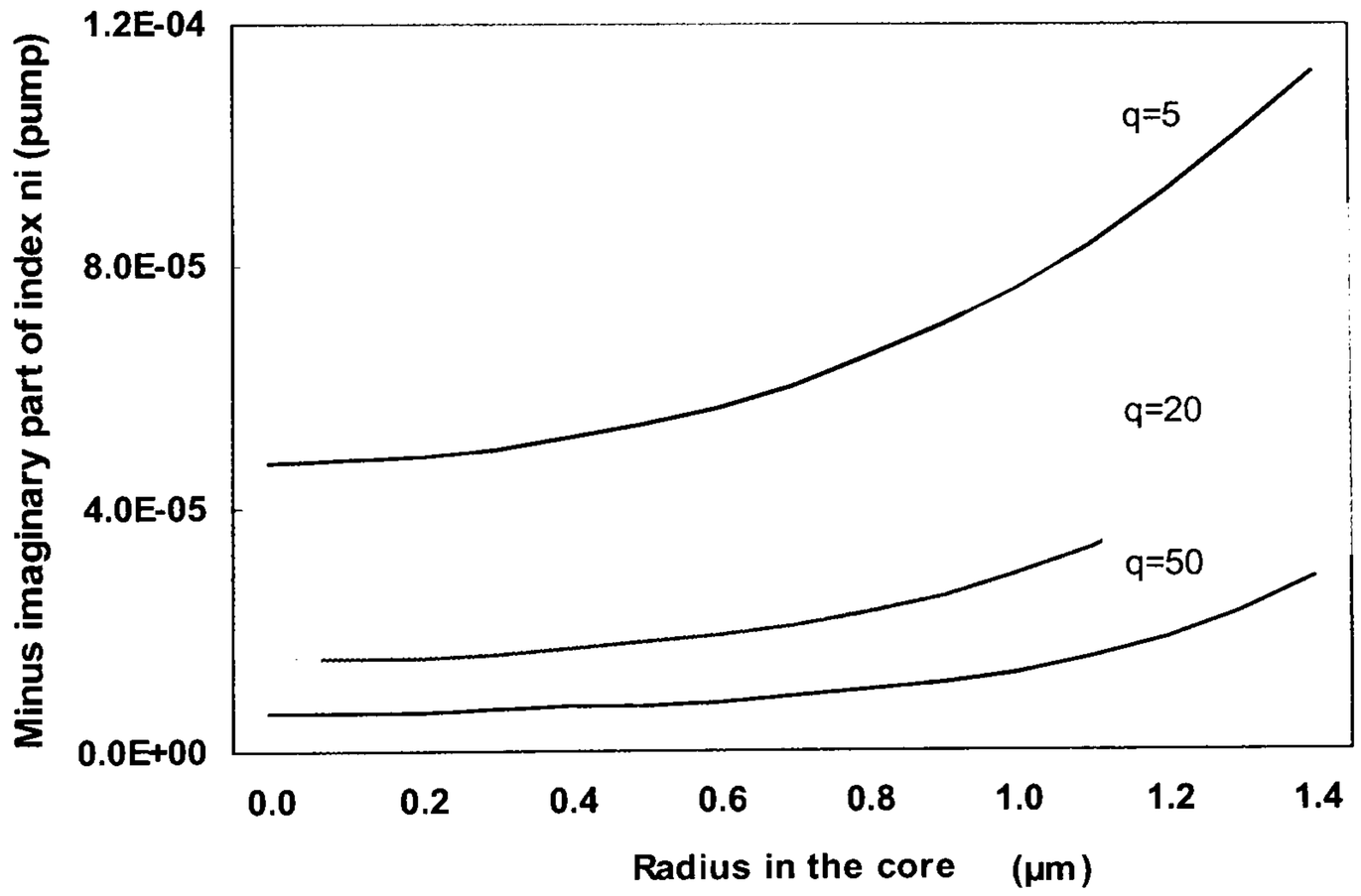

Figure 3.9 Radial profile of the minus imaginary part of the pump index against radius in the core at various input pump power levels q (marked in mW) by the present method (P).

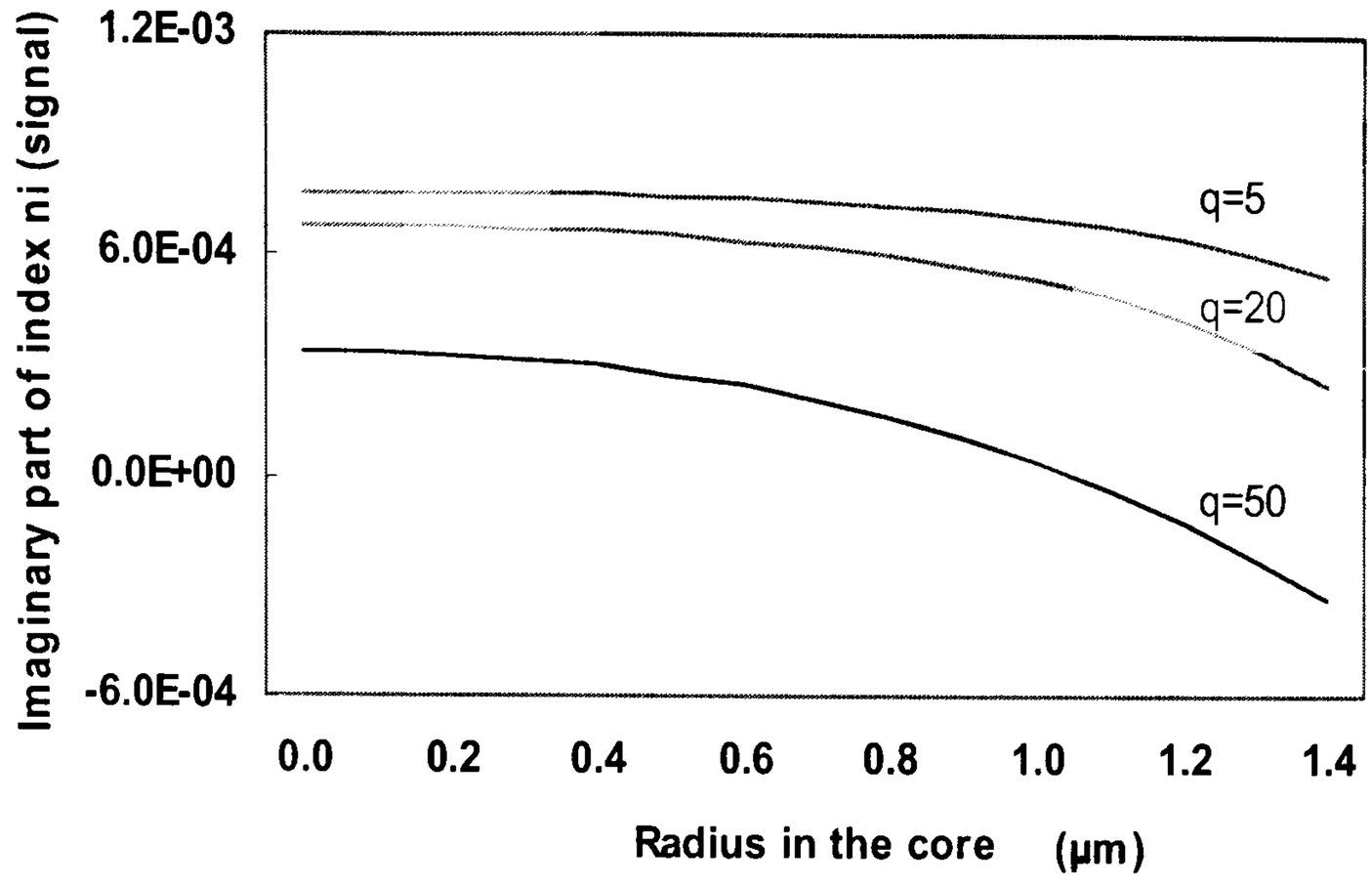

Figure 3.10 Radial profile of the imaginary part of the signal index against radius in the core at various input pump power levels q (marked in mW) by the present method (P).

TABLE 3.2
The difference of pump index imaginary part
$[\,100\% \times (R - P)/P\,]$

The difference (%) / Radius r (*nm*)	q=5mw	q=20mw	q=50mw
0	3.57	0	0
100	0	0	0
500	3.12	0	0
1000	2.22	5.88	0
1400	1.49	2.94	5.88

TABLE 3. 3
The difference of signal index imaginary part
$[\,100\% \times (R - P)/P\,]$

The difference (%) / Radius r (*nm*)	q=5mw	q=20mw	q=50mw
0	-4.41	-0.98	-0.43
100	-4.45	-0.739	-0.22
500	-6.02	-1.02	-0.44
1000	-1.69	-1.75	-0.69
1400	4.98	-6.76	-1.85

3.3.3 Gain in Optical Fibres

For different values of input pump power, a plot of signal gain for an input signal of $100nW$ versus wavelength is obtained by using the *TL* method. The results are compared with those in (Singh and Sharma 2001). The comparison is shown in Fig.3.11. As expected, the present results are practically coincident with the results of the more cumbersome Rayleigh-Ritz calculations. The uneven gain wavelength response of the Erbium-doped fibre is also readily recognizable. It is well known that the gain flatness of an optical amplifier is very important for *DWDM* optical systems, and that there have been many attempts to design gain flattened optical amplifiers for this reason. Next the *TL* method is demonstrated that it can be used in assisting with investigations into how to make the gain higher and flatter by modifying the optical fibre refractive index profile and the radial Erbium dopant concentration in the core.

a). Calculation of Gain By Varying Refractive Index Profile

Fig.3.12 shows the signal gain of a parabolic refractive index profile, but with uniform Erbium dopant concentration in the core. The parabolic refractive index profile step Erbium-doped fibre can not obtain the same gain as a step index profile fibre with the same Erbium dopant parameters, however, the gain is flatter compared to the step index case, Fig.3.11.

Fig.3.13 is another example of signal gain for a uniform doped core optical fibre with the segmented refractive index profile. We observe that the value of the derived achieved gain is similarly not as high as that obtained from a step index core (Fig.3.11), but the overall gain curve is flatter. Fig.3.14 shows the effect of gain flattening with varying the inner core index dip and for uniform core dopant. We see that the gain difference increases with increasing inner core index are not significant. Minimum gain ripple in this case occurs when the inner core index is less than 1.4420.

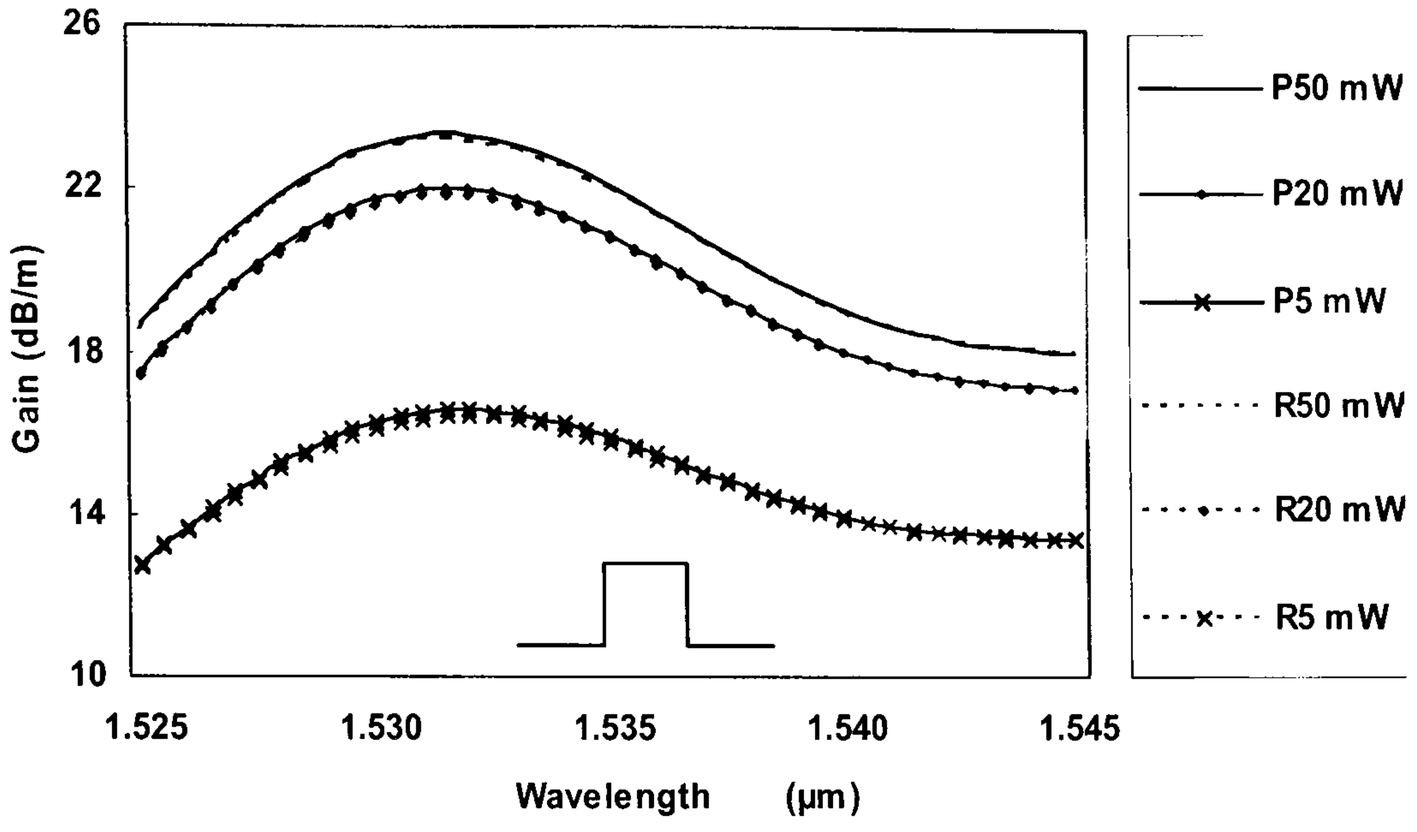

Figure 3.11 Signal gain against wavelength at different input pump power levels (marked in mW) by the present method (P) and Rayleigh-Ritz method (R) of (Singh and Sharma 2001) (core index=1.46, cladding index=1.4401).

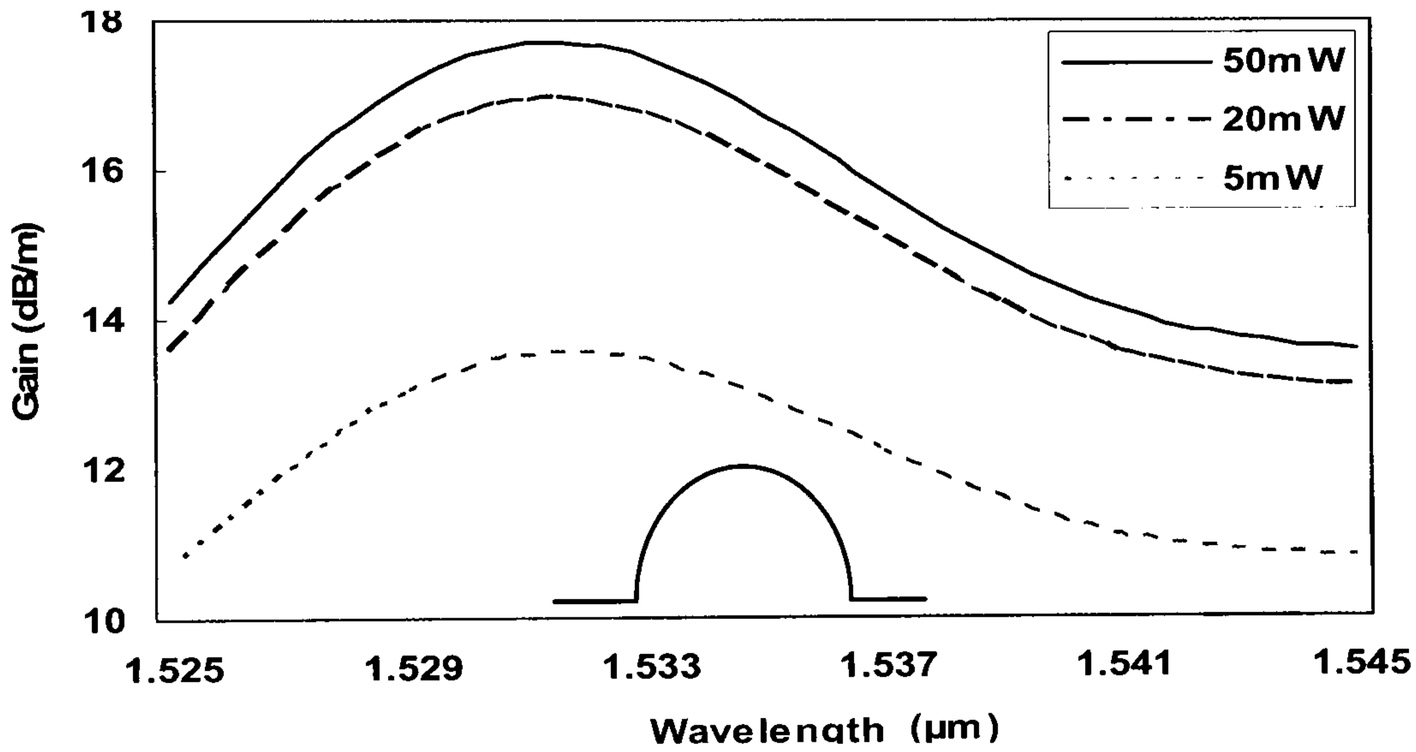

Figure 3.12 Signal gain of a parabolic refractive index against wavelength at different input pump power levels (marked in mW) for parabolic index waveguide (core index=1.46, cladding index=1.4401).

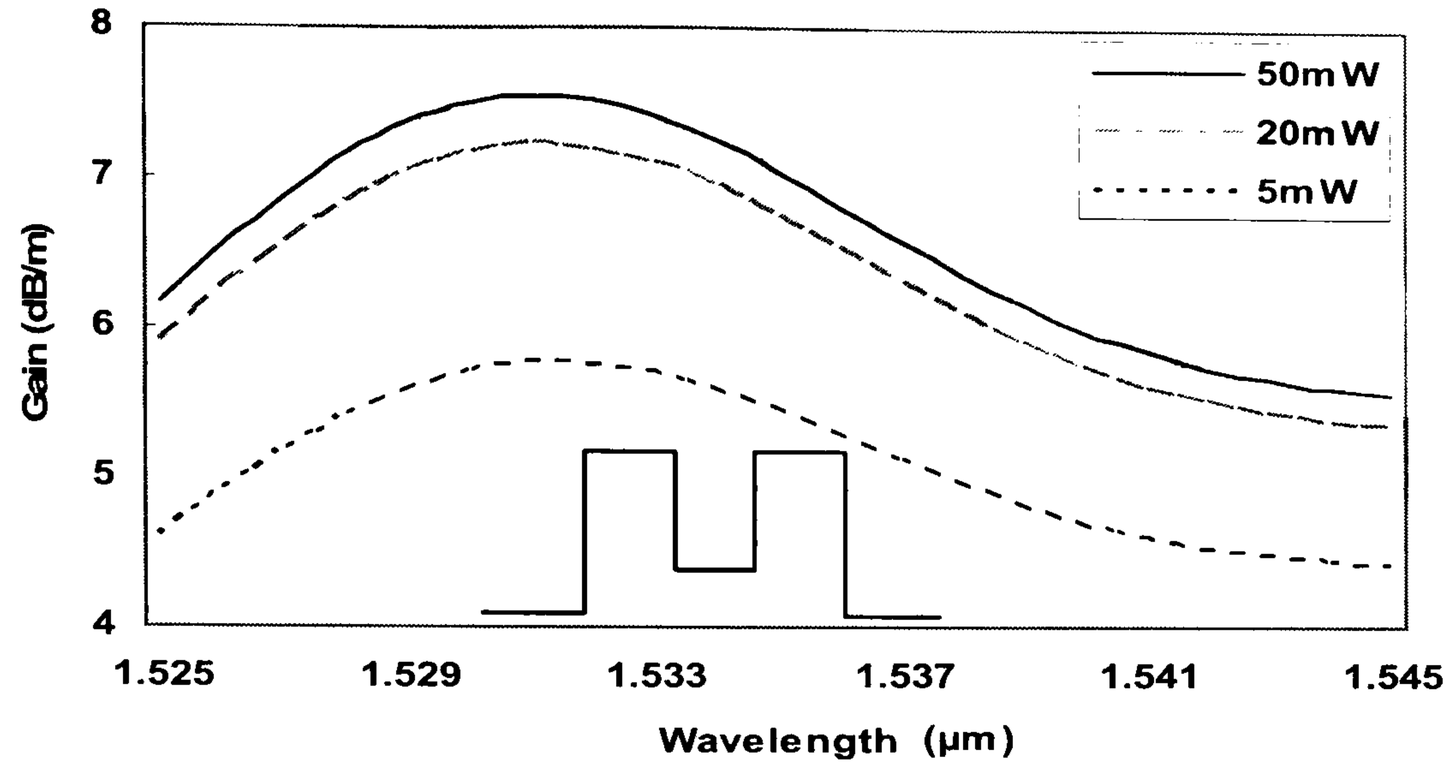

Figure 3.13 Signal gain of a segmented core refractive index against wavelength at different input pump power levels (marked in mW) for the segmented core refractive index waveguide (inner core index=1.4425, core index=1.46, cladding index=1.4401).

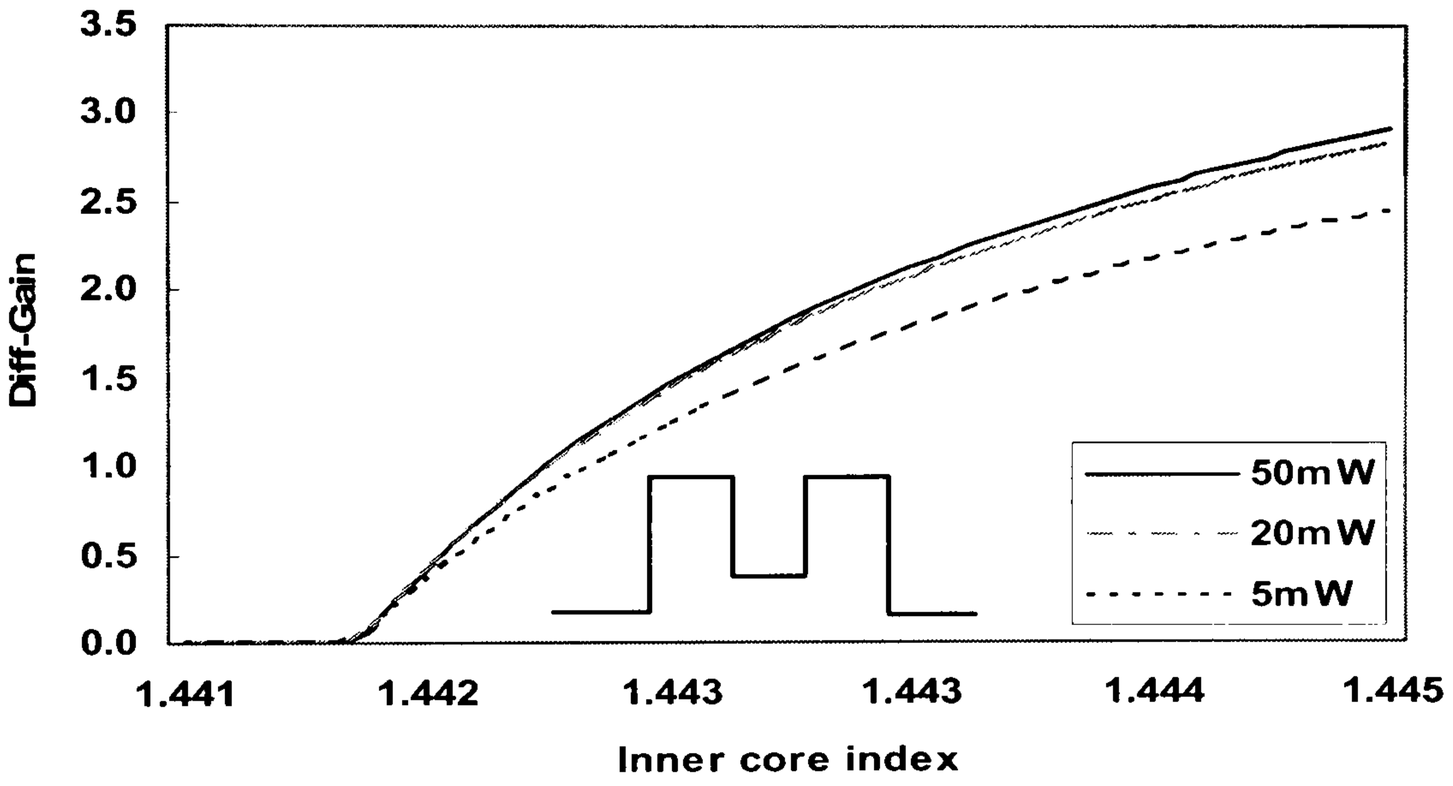

Figure 3.14 Gain difference (Diff gain=Maximum gain – $Gain_{\lambda=1.525\mu m}$) against inner core index, derived from Fig.3.13, at different input pump power levels (marked in mW) for the segmented core refractive index waveguide (core index=1.46, cladding index=1.4401).

b). Calculation of Gain By Varying Radial Dopant Concentration

The Erbium amplifier gain is a function of pump power, signal wavelength, fibre length and Erbium dopant concentration. Using the *TL* method, a test is attempted to ascertain if any improvements can be achieved by experimenting with radially varying the dopant concentration (normally constant) for different refractive index profiles. It is expected to result in an increase in the gain of the fibre amplifier. The dopant concentration is changed in inverse proportion to the radial field power, multiplied by the dopant constant at $r = 0$, of $1.6 \times 10^{25} m^{-3}$. The normalized powers

in the core for different refractive index profile optical fibers are shown in Fig.3.15(a). The corresponding radial dopant profiles for the three different refractive index profiles considered here are shown in Fig.3.15(b). All the dopant concentration values in the core are greater than the dopant constant $\rho_0 = 1.6 \times 10^{25} m^{-3}$, but vary radially and non-uniformly. Using the dopant profiles of Fig.3.15(b), the Erbium amplifier stored energy (related to gain) profiles are obtained, as shown in Figs.3.16-3.18. Fig.3.16 shows the increased gain profile resulting from step refractive index. The maximum gain is increased significantly while keeping the gain ripple nearly the same as in the case of in Fig. 3.11. Similar conclusions are drawn from Fig.3.17 and Fig.3.18 for parabolic and segmented core index profiles, with dopant distribution according to Fig.3.15(b).

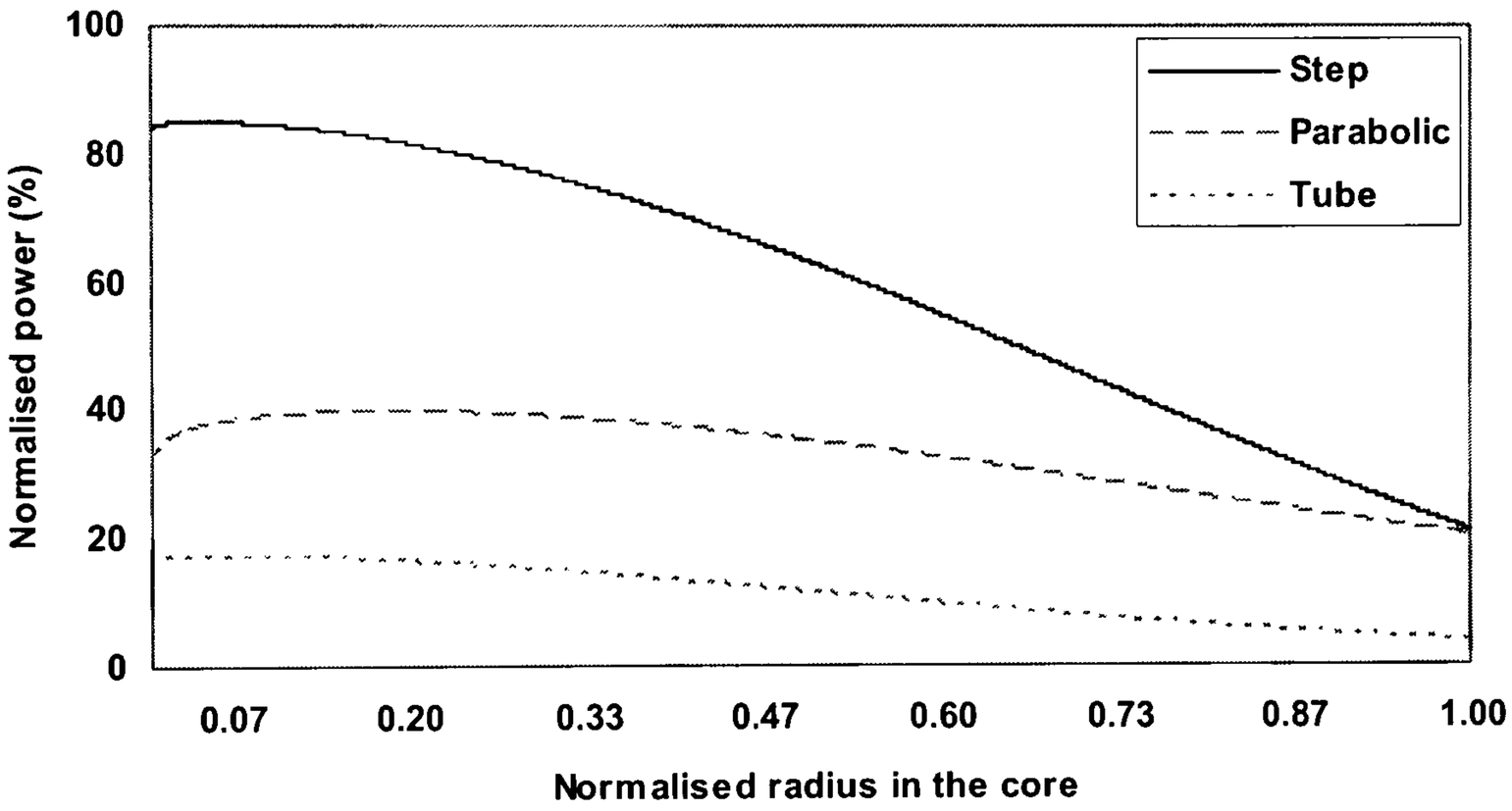

Figure 3.15 (a) Normalised power ((Power$_{core}$/ΣPower)100%) against core radius for different optical fiber refractive index profiles.

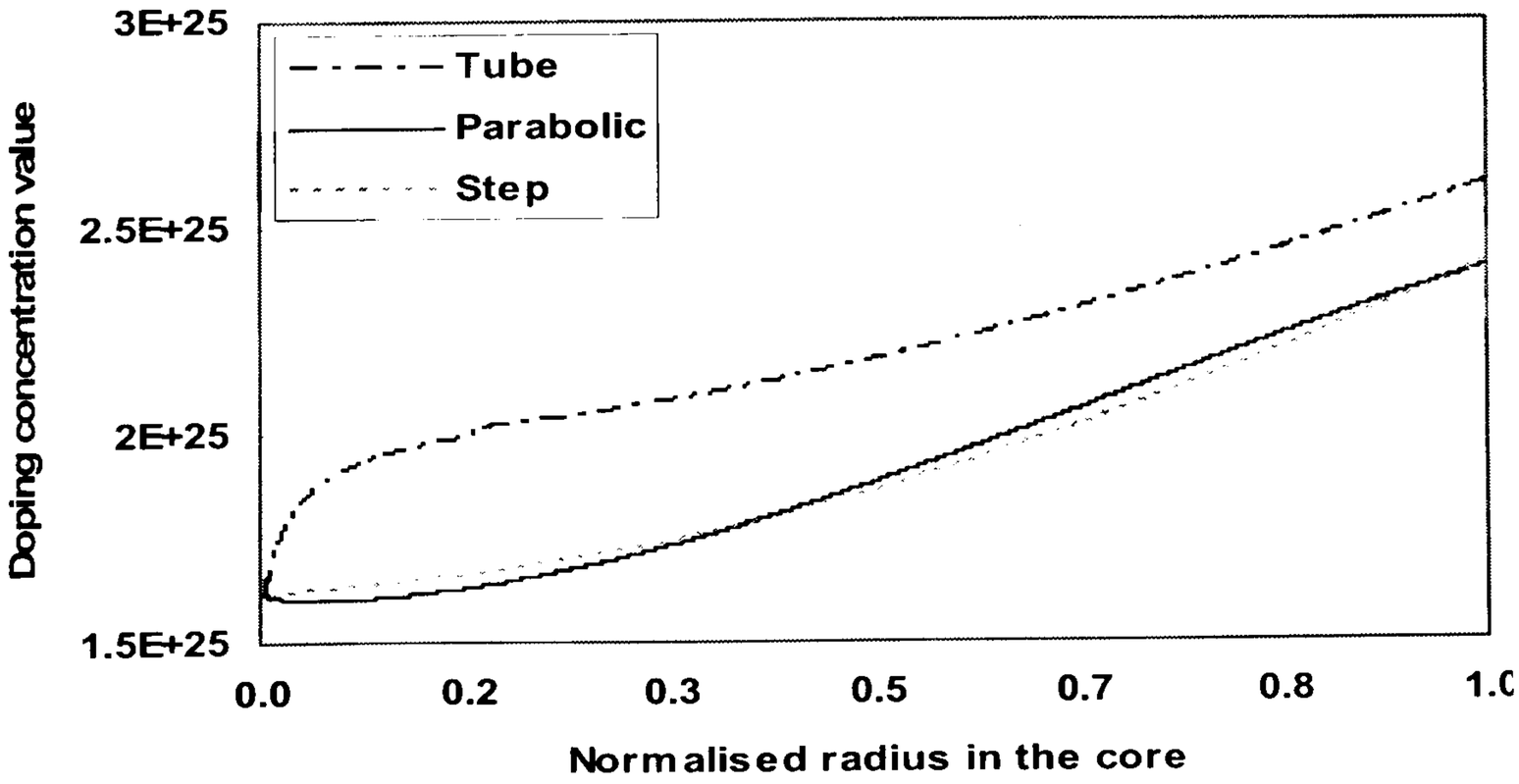

Figure 3.15 (b) Dopant concentration values changing with inverse field values of different optical fiber refractive index profiles, used for results of Figs. 3.16-3.18.

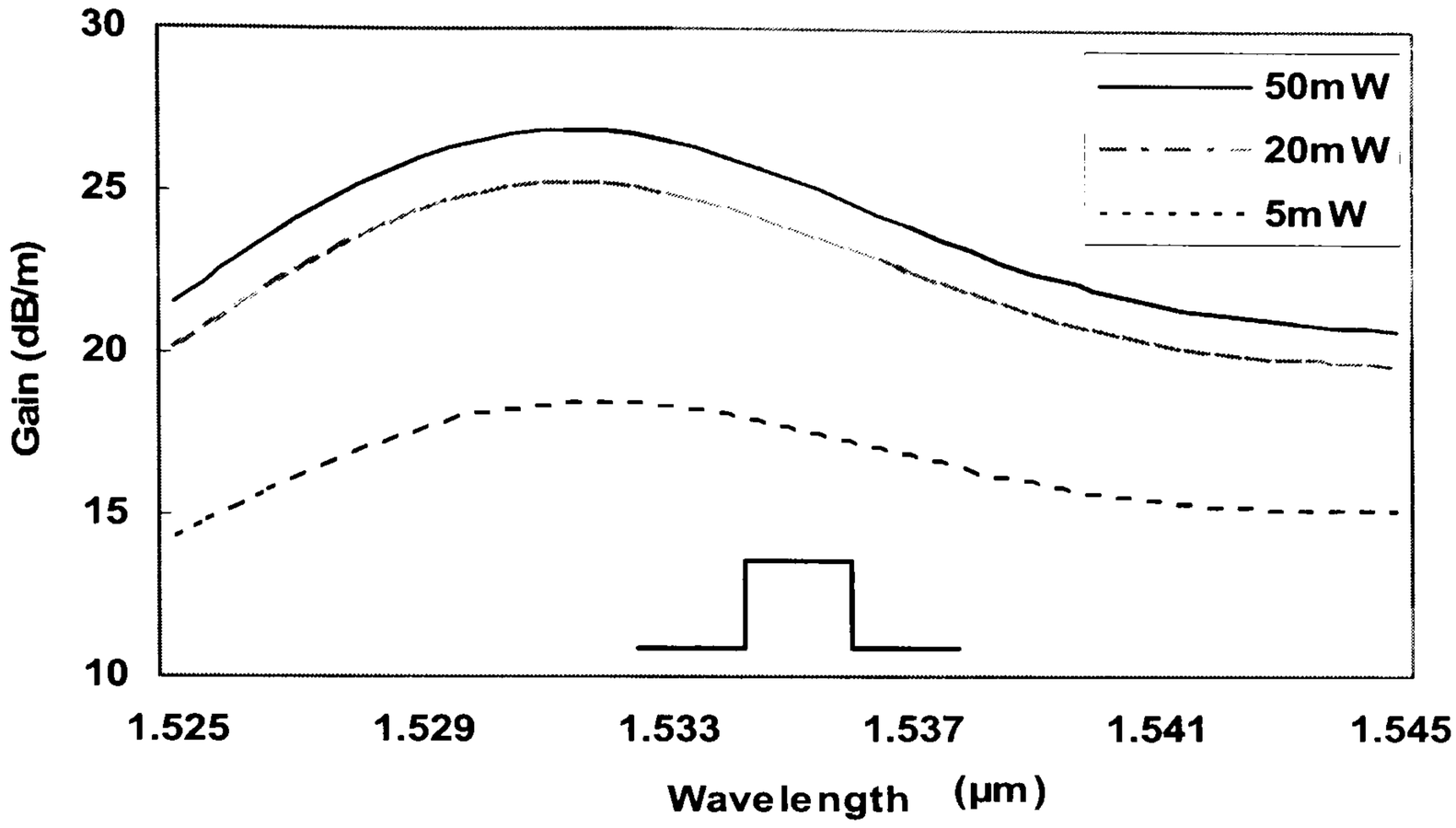

Figure 3.16 Signal gain in step index fibres against wavelength at different input pump power levels (marked in mW) using dopant profile of Fig. 3.15(b).

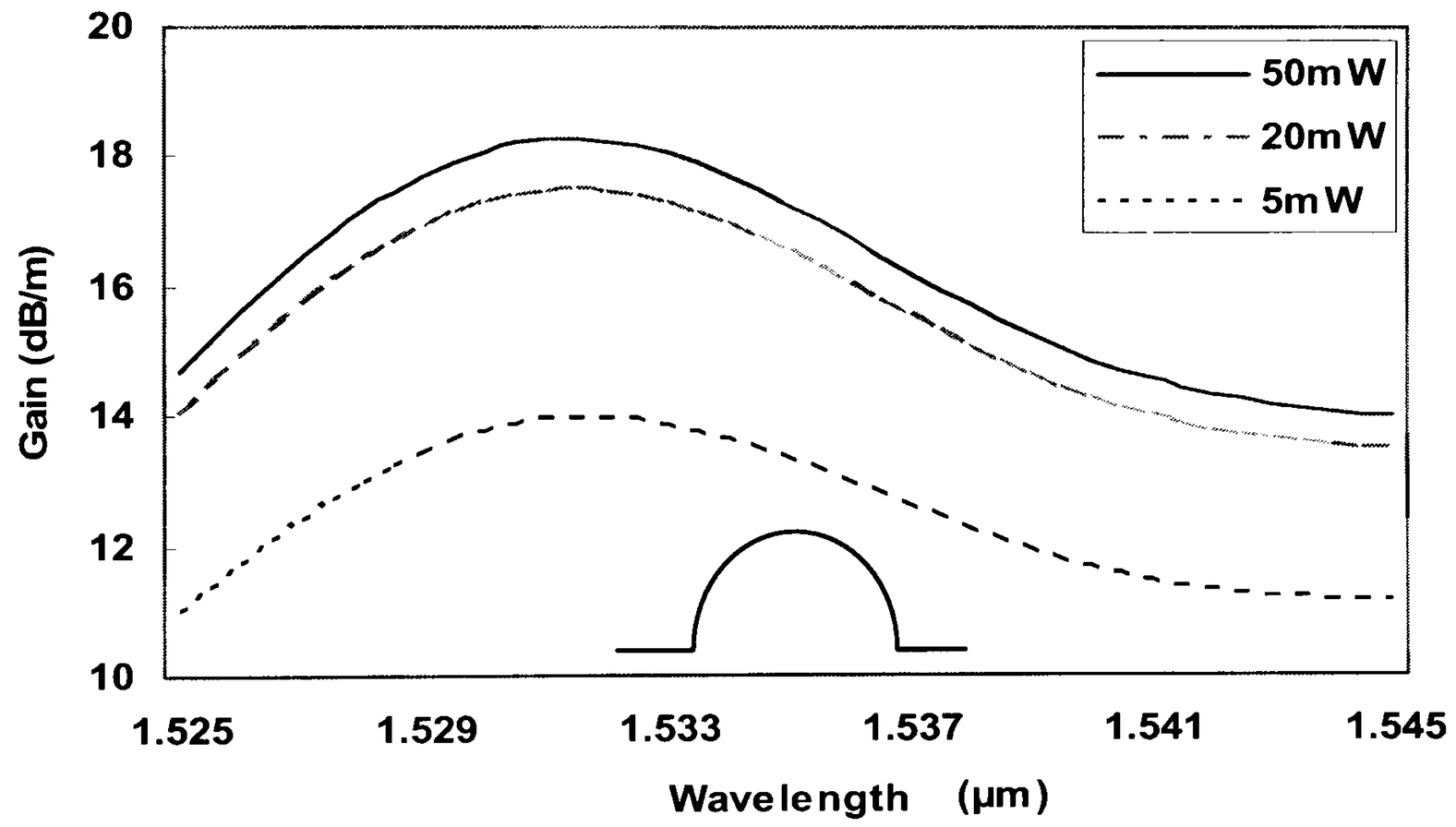

Figure 3.17 Signal gain in a parabolic refractive index fibres against wavelength at different input pump power levels (marked in mW) using dopant profile of Fig. 3.15(b).

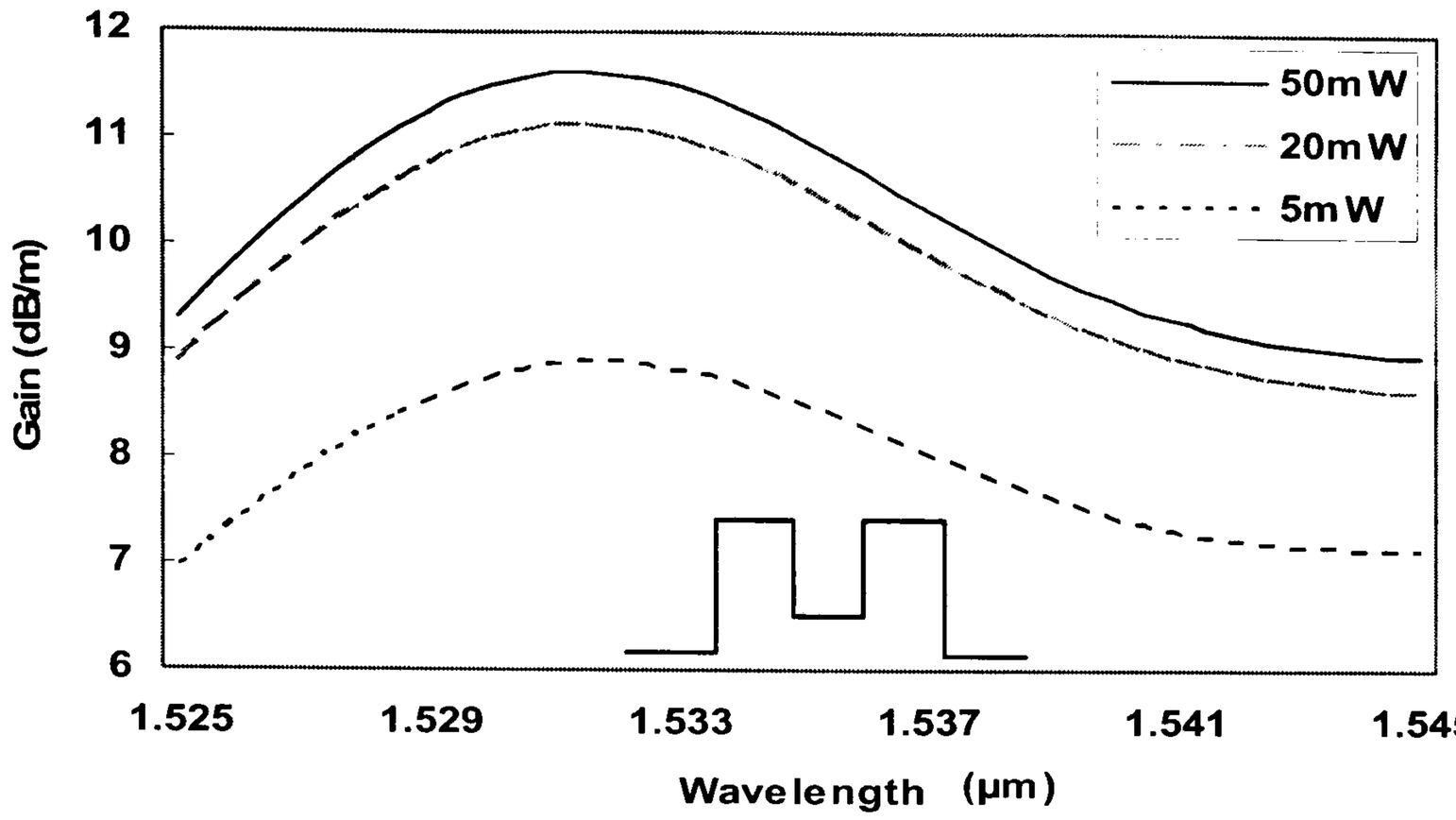

Figure 3.18 Signal gain in a segmented core refractive index fibres against wavelength at different input pump power levels (marked in mW) using dopant profile of Fig. 3.15(b).

3.3.4 Loss in Optical Fibres

In contrast and in order to illustrate further the capacity of the *TL* technique, let us now consider how to determine the optical fibre loss from varying radial attenuation. The spectrum of optical power loss in an optical fibre is a complicated function of absorption and scattering phenomena that are introduced during the drawing of the fibre, either because of impurities introduced during the drawing or because scattering centers increase or decrease according to the level of dopant used. In this work, for the purpose of comparison with results in (Gallawa, Goyal et al. 1993), the same parameters are used as only the following case is assumed:

a) The cladding is lossy.

b) The imaginary part of the refractive index is constant in the cladding, having the value 5×10^{-10}.

The fibre radial attenuation results of the electric circuit resonance technique are given in Table 3.4 for a step index single mode fibre having $V = 2.5$. The table includes the results in (Gallawa, Goyal et al. 1993) for comparison, and agreement with the *TL* technique is demonstrated.

To allow a comparison with the recently published perturbation method (Gallawa, Goyal et al. 1993), the following scenario is assumed although unlikely, which can facilitate the comparison as expected. The real part of the index is taken as a step

function. The electric field distribution is determined from a lossless step index fibre. However, the imaginary part of the index varies in the core according to different profiles as shown in Fig.3.19. Using the *TL* technique and the imaginary index profiles of Fig.3.19 for the distribution of absorption or scattering centers, the attenuation is subsequently calculated. The calculated attenuation results are given in Table 3.5. The step index fibre is used simply to allow comparison with published methods, but the *TL* method as demonstrated from the Tables 3.4 and 3.5 is accurate and applicable for determining arbitrary loss distributions and arbitrary fibre index profiles.

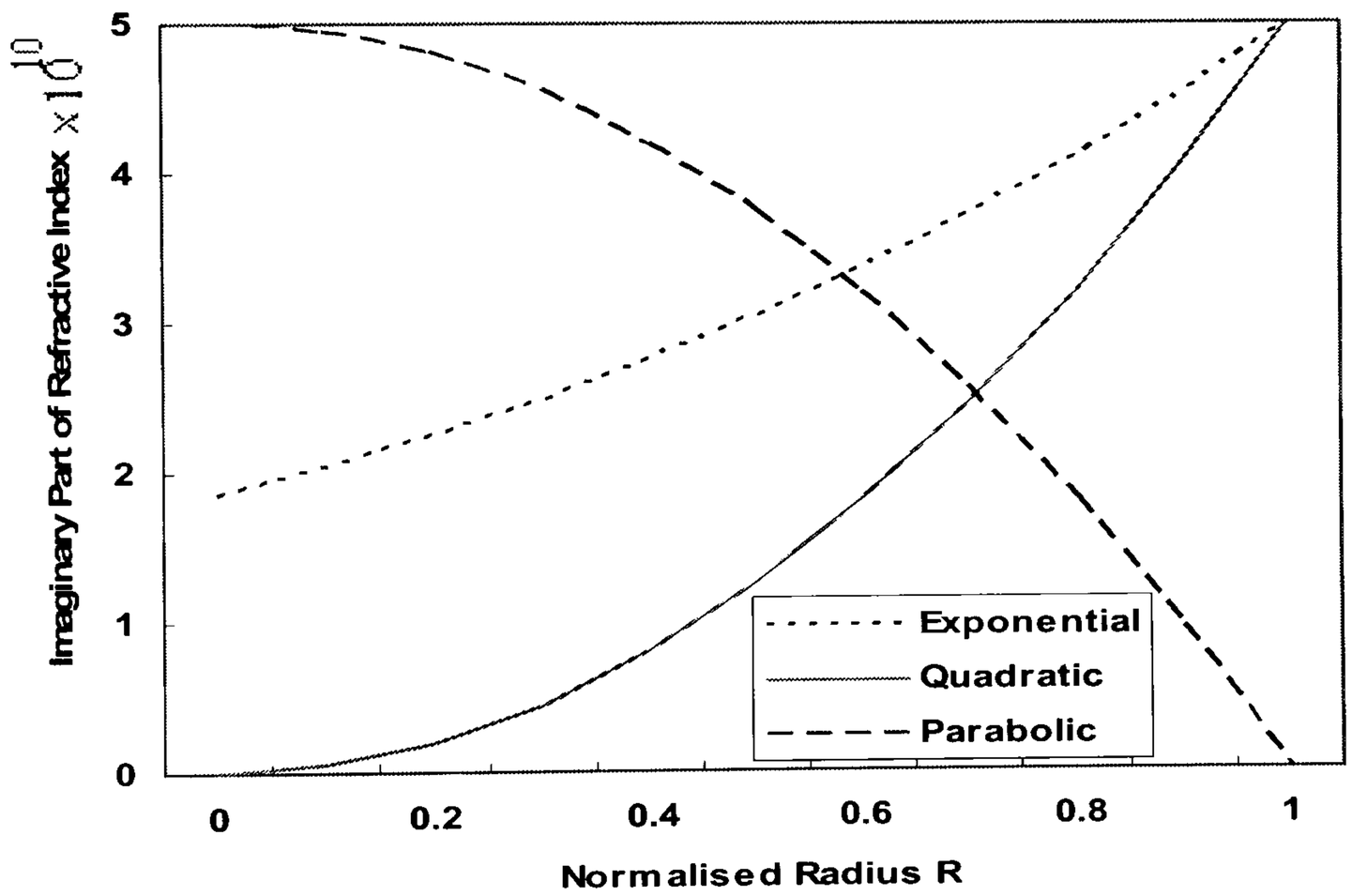

Figure 3.19 Loss profiles, Exponential, Quadratic, and Parabolic.

TABLE 3.4 ($\beta_i \times 10^{10}$) Loss only in the cladding, Step index fibre V=2.5			
Profiles	Exponential	Quadratic	Parabolic
Ref.	3.3228	3.3083	3.3059
Present Method	3.2459	3.2750	3.2662
Ratio (Ref./P)	1.0236	1.0101	1.0121

TABLE 3.5 ($\beta_i \times 10^{9}$) Loss only in the core, Step index fibre V=2.5			
Profiles	Exponential	Quadratic	Parabolic
Ref.	1.098	0.4121	1.353
Present Method	1.0938	0.41256	1.3325
Ratio (Ref./P)	1.0038	0.9988	1.0153

Note: Ref. in Tables 3.4 and 3.5 stands for the reference (Gallawa, Goyal et al. 1993).

3.4 Band-gap of Bragg Fibres

3.4.1 Characteristics of Bragg Fibres

In conventional optical fibres, the light is guided in the solid-core version by total internal reflection and photons propagate mainly in the high index centre core. A completely different confinement mechanism, air-core photonic crystal fibres or photonic band-gap fibres, such as a Bragg fibre, guides light by band-gap (so-called transmission window) effects in contrast to total internal reflection. Bragg reflection provides an alternative way of guiding light. Since Bragg fibres and conventional optical fibres utilize different guiding mechanisms, it is not surprising that Bragg fibres offer many possibilities that are difficult to achieve in conventional fibres. The biggest promise of air-core Bragg fibres has been the potential of guiding light in air, which allows low loss when material absorption is large for silica core fibres and low nonlinear (1000 times less than silica) transmission of light signals. This is a very attractive proposition for high-power applications (Cregan, Mangan et al. 1999). A

Bragg fibre within certain length can also be designed to support a single guided mode without azimuthal dependence (i.e. the *TE* or *TM* mode). In contrast with the fundamental mode in conventional fibres, which is always doubly degenerate, these Bragg fibre modes are truly single-moded. It is worth noting that there are no strictly guided modes in Bragg fibres, all the modes transmit on Bragg fibres are leaky modes. The structure around the Bragg fibre core that provides the guiding mechanism (pseudo-mirror) is finite in extent and therefore the Bragg fibre only support leaky modes. The single-modedness of a Bragg fibre means that the Bragg fibre only has one low-loss mode after a certain length.

In this work, the *TL* technique has been extended to calculate the effective index of leaky modes and it has been demonstrated by using the model of the Bragg fibre. In conventional step and graded index fibres there are strict definitions for guided and leaky modes: guided modes are radially evanescent in the depressed cladding layer whilst leaky modes have oscillatory fields in the cladding, allowing power to leak out of the fibre (Snyder and Love 1983). Equivalently, guided modes are described by real mode effective indices and leaky modes are described by complex mode effective indices, where the loss is proportional to the imaginary part of the effective index (Snyder and Love 1983).

Next, the *TL* technique has been extended and applied to leaky mode circular waveguides using the Bragg fibre with air core and periodic claddings as an example where the band-gap structures of *TM* modes can be obtained.

A Bragg fibre can be represented as a cascade of *T*-circuits connected in tandem. The series is terminated with the characteristic impedance of the medium at the axis (r=0) and the outer cladding (r=∞) of the fibre. Using *T*-circuit theory, starting from large r in the cladding, Z_{out} the total impedance up to the cladding-core boundary can be found and similarly, Z_{in} the total impedance from r=0 to that boundary. Z_{out} and Z_{in} can be easily determined by the following equation:

$$Z_{\substack{in \\ out}} = Z_B(a\pm1) + \cfrac{1}{\cfrac{1}{Z_P(a\pm1)} + \cfrac{1}{Z_B(a\pm1) + Z_B(a\pm2) + \cfrac{1}{\vdots\vdots\vdots\vdots \\ \cfrac{1}{Z_{Prev} + Z_B(n-1)}}}} \tag{3.25}$$

where the characteristic impedance Z_{prev}=0 at large r when the positive sign is used or it becomes Z_{prev}=∞ at r=0 when the negative sign is used, a is the core radius. The total circuit resonates when Z_{in} and Z_{out} are equal and opposite, hence Z_{total}=Z_{in}+Z_{out}=0, at the effective index value of any mode. Therefore, as before the unknown effective index $\overline{\beta}$ can be obtained by using a root searching method which locates the roots of the total impedance of the T-circuits, Z_{total}=0. In the case of air core Bragg fibres (n_0=1), the root searching for locating leaky mode effective index is carried out in the range of $0 < \overline{\beta} < n_0$.

In general, a Bragg fibre can be described by seven parameters: n_0, n_1, n_2, r_0, d_1, d_2, and N, Fig.3.20, where they represent the refractive indices of the core and the alternating high-low index layers, the core radius, layer thickness and the number of cladding pairs respectively. The effect of changing one or more of these parameters has been considered previously (Johnson, Ibanescu et al. 2001), but only over a limited range and not in the context of single-modedness.

Consider a Bragg fibre having the structure like the one shown in Fig.3.20. The core of the waveguide is an air hole, whose radius is denoted by r_0, at the center of the cross-section. The cladding consists of a coaxial periodic structure, where the radius of the ith boundary is defined by:

$$r_i = \begin{cases} n(d_1 + d_2) + r_0 & \mathrm{i} = 2\mathrm{n} \\ n(d_1 + d_2) + d_1 + r_0 & \mathrm{i} = 2\mathrm{n}+1 \end{cases} \quad (\mathrm{n} = 0,1,2,3\ldots) \qquad (3.26)$$

The refractive index for the ith layer is defined by:

$$n_i = \begin{cases} n_1 & \mathrm{i} = 2\mathrm{n}-1 \\ \mathrm{n}_2 & \mathrm{i} = 2\mathrm{n} \end{cases} \quad (\mathrm{n} = 1,2,3\ldots) \qquad (3.27)$$

To compare the present results with those of existing techniques, the same parameters for a Bragg fibre have been chosen from (Ouyang, Xu et al. 2001). The cladding structure of the Bragg fibre is: n_1=4.6 and thickness d_1=0.333d, n_2=1.6 and the thickness d_2=0.667d. Here, d=d_1+d_2 is the unit length of periodicity (cladding pair) of the multilayered structure. The Bragg fibre has a core with n_0=1 and the

radius r_0=1.4d. In practice, Bragg fibres have a finite number of layers and support only leaky modes (Johnson, Ibanescu et al. 2001).

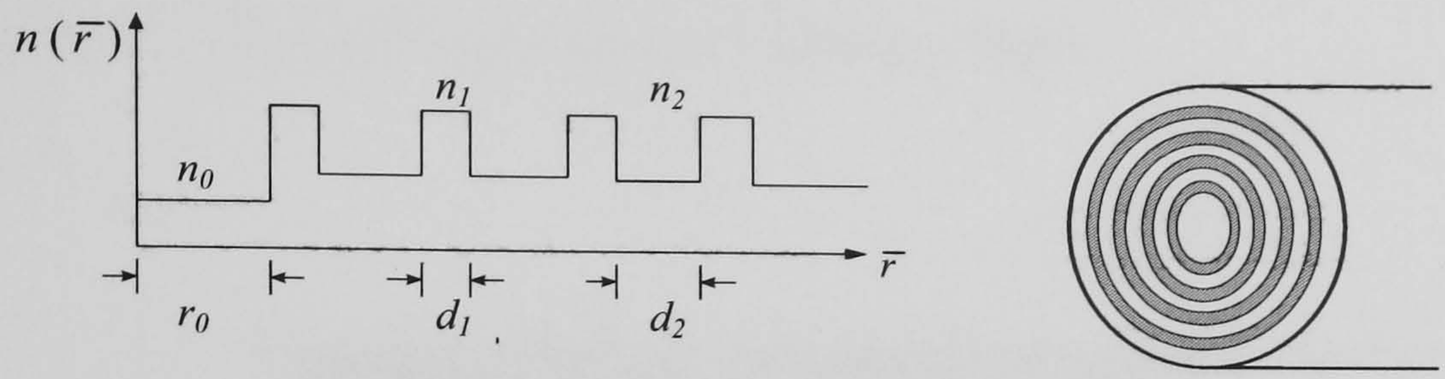

(a) (b)

Figure 3.20 (a) Refractive index profile of a Bragg fibre, the air-core n_0=1 and radius r_0, the alternating high-low indices and thickness $n_,$, d_1 and $n_,$, d_2 respectively. **(b)** Fibre side view. Shaded regions represent areas of higher refractive index and unshaded regions represent a uniform cladding region with lower refractive index.

3.4.2 Numerical Results and Discussion

The Bragg fibre leaky mode effective index can be achieved by using the root searching method locating the resonance of the electric *T*-circuit cascade. The solution to this problem allows working out the band-gap structures of *TM* modes for example and also the electric field distribution of the Bragg fibre. The effective index calculation is related to the number of concentric homogeneous cylindrical layers. In Fig.3.21(a)-(d), 200, 400, 600, 1000 layers (equivalent *T*-circuits) are used respectively. As we see, with the increase of the number of layers, a guided mode TM_{01} comes out in the band-gap. It is worth pointing out that there is no difference between Fig.3.21(c) and (d), the complete TM_{01} mode can be seen in the band-gap. To save computation time, 600 concentric homogeneous cylindrical layers will be used for the rest band-gap calculations of the Bragg fibre. A total of 5 cladding pairs are used for the Bragg fibre, which should provide good mode confinement based on the author's experience. Hence the thickness of the homogeneous cylindrical layers is $\delta\bar{r} = [5(d_1 + d_2) + r_0]/600$. This results in the band diagram of Fig.3.21(a)-(d). Only one guided mode (TM_{01}) exists in the band-gap. This implies that in this range only the TM_{01} mode can propagate in agreement with (Ouyang, Xu et al. 2001).

In this section, a novel and accurate *TL* technique has been extended to work out the propagation and band diagrams of leaky mode waveguides and specifically Bragg

fibre *TM* modes. The method uses transmission line principles and relies on the modeling of a cascade of thin uniform homogeneous cylindrical layers of a Bragg fibre to transmission line circuits. Simulation results demonstrate the potential of this new method for modeling properties of Bragg fibres.

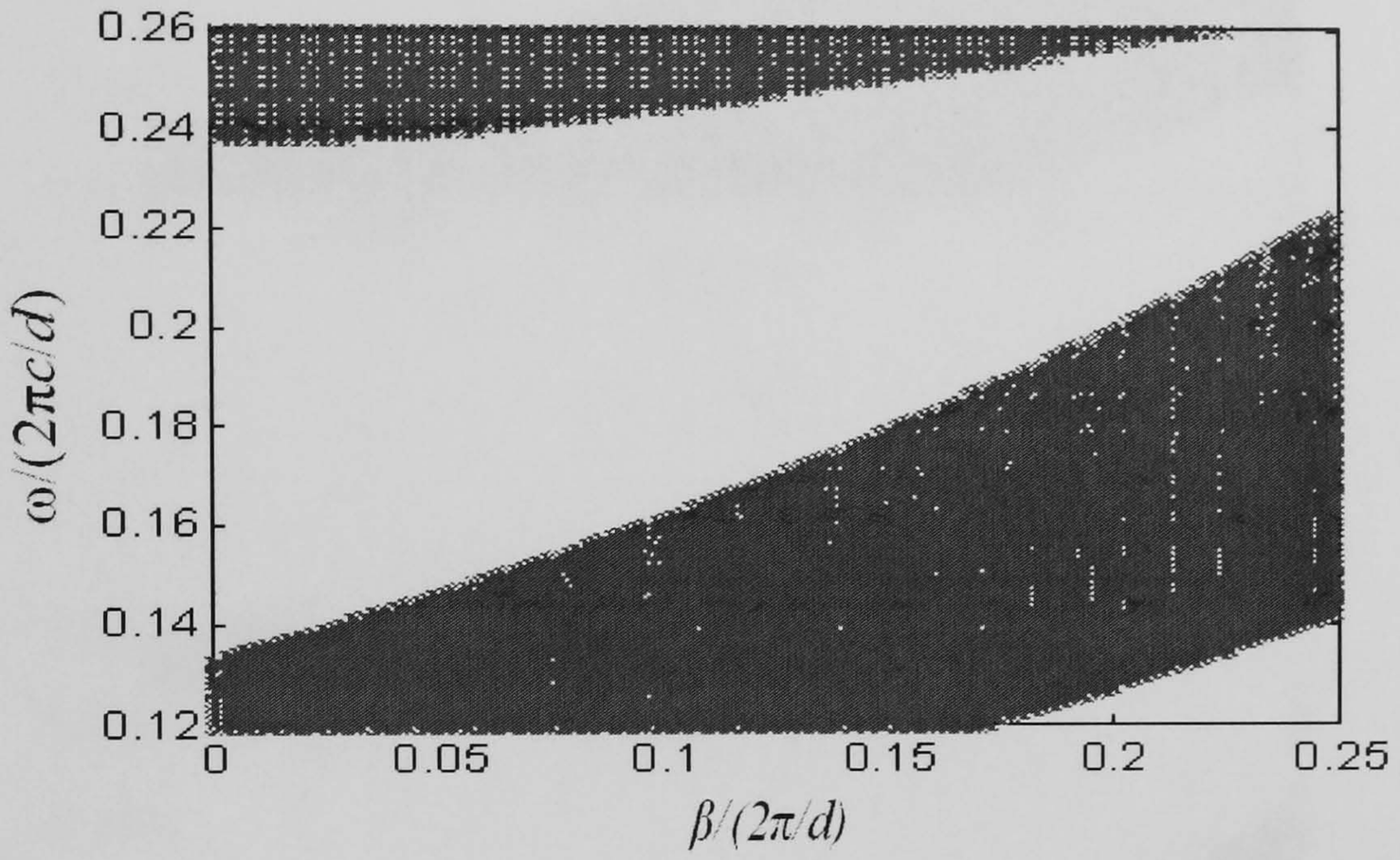

(a)

(b)

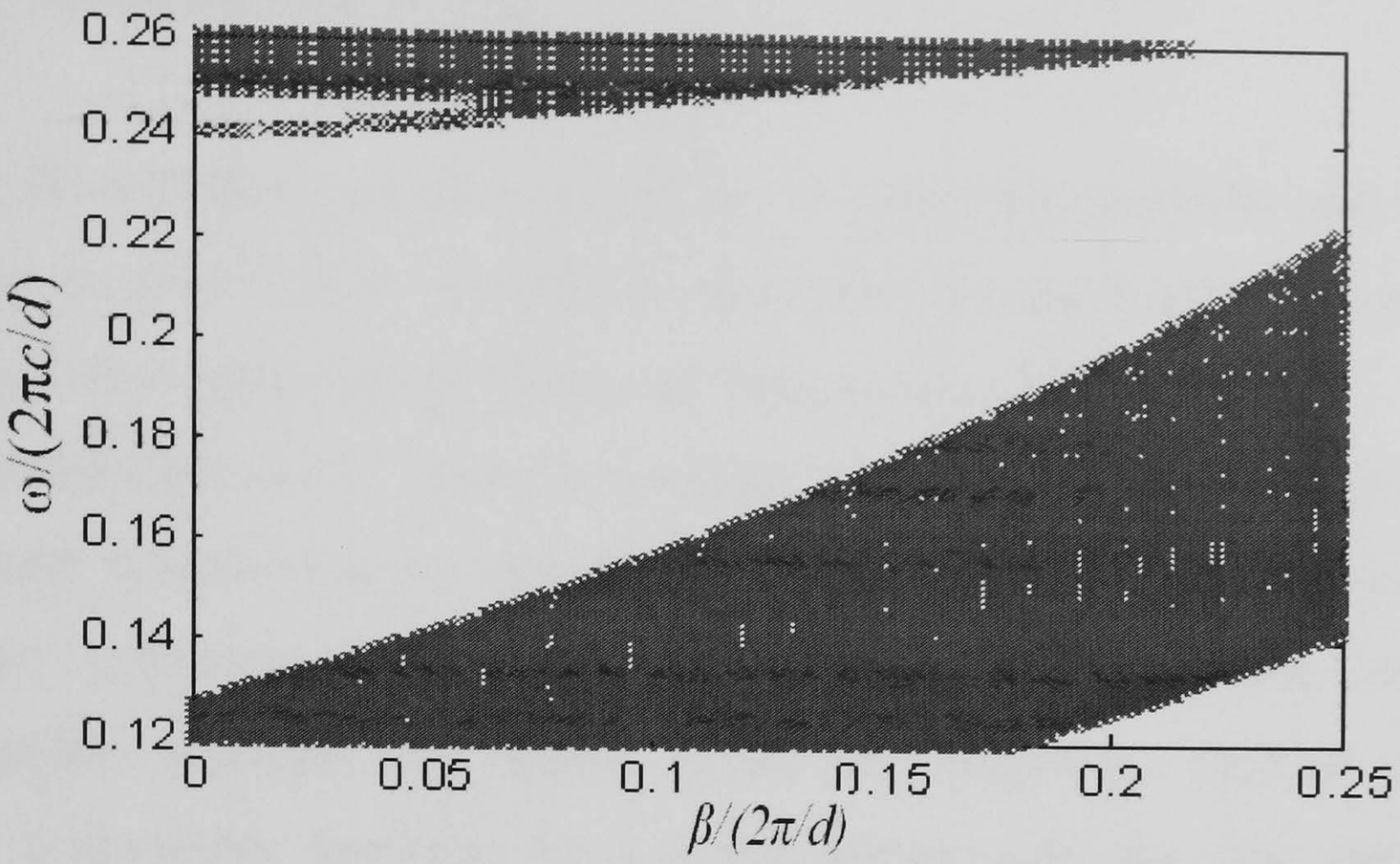

(c)

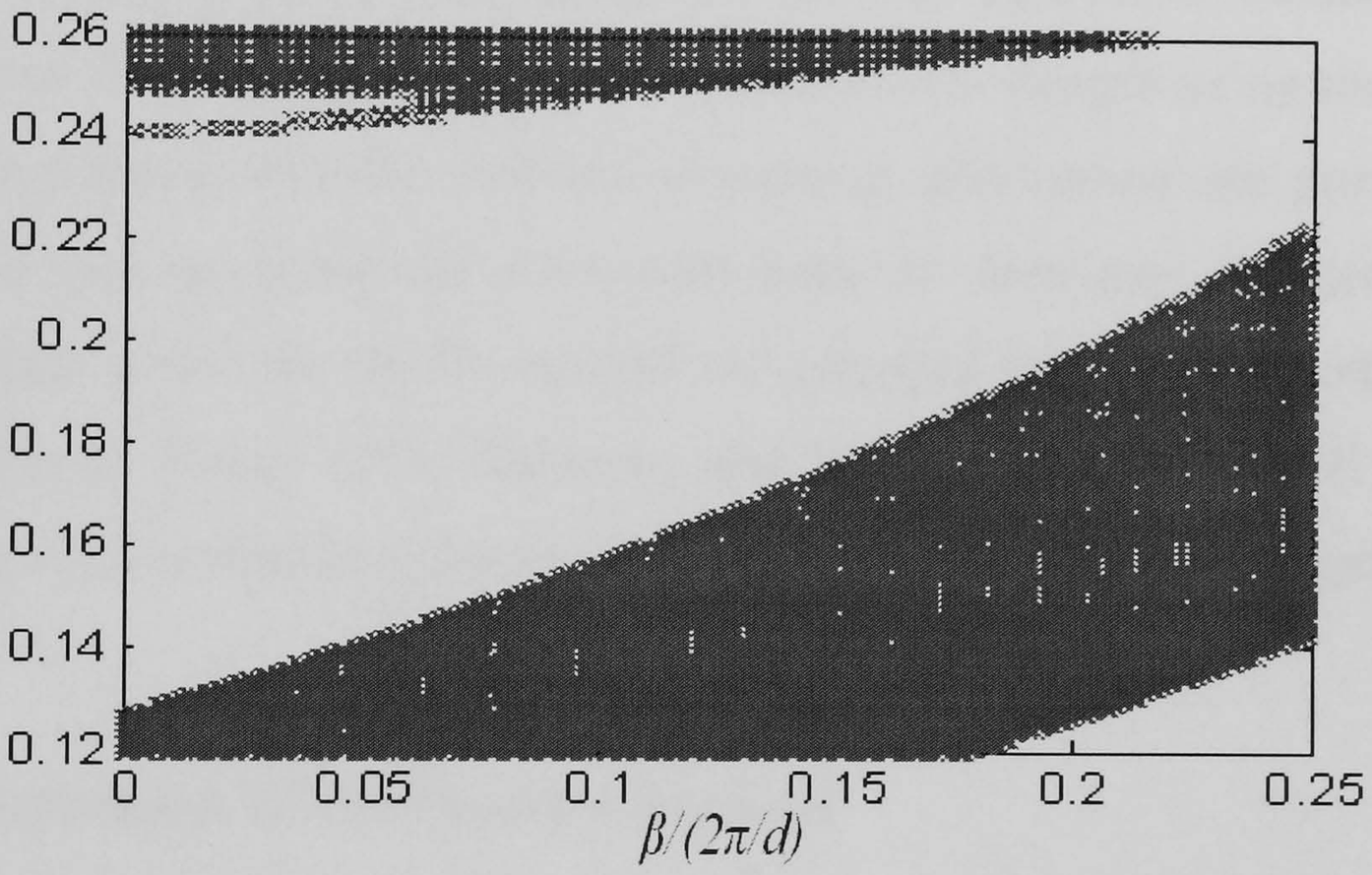

(d)

Figure 3.21 Band diagram of the Bragg fibre: core index n_0=1, thickness r_0=1.4d, layer1 index n_1=4.6, thickness d_1=0.333d, layer2 index n_2=1.6, thickness d_2=0.667d, d=d_1+d_2 is the unit length of periodicity of the multilayered structure. **(a)**200 layers, **(b)**400 layers, **(c)**600 layers, **(d)**1000 layers

3.5 Delay and Dispersion

The *TL* technique has been shown to be extremely powerful and it can be easily applied to optical fibres in order to determine the mode propagation constants and mode electric fields exactly (Qian and Boucouvalas 2004).

In this section, the *TL* theory is extended and a novel method based on the *T*-circuit technique is presented for calculating the dispersion of optical fibres of known but arbitrary refractive index profiles. Firstly, the equations for the derivatives of the propagation constant with respect to the wavelength are derived analytically. By using a recursive formula, for a given wavelength, the first derivative can be expressed in terms of equivalent circuit impedances at the wavelength of interest and the second derivative can be expressed in terms of circuit impedances and the first derivative. Secondly, by calculating the derived equivalent circuit formulas, the impedances can be worked out at the specified wavelength using the *TL* technique. Once these along with the material dispersion information are provided, the total dispersion can be accurately calculated from its definition. Numerical results on convergence speed for the *TL* method as compared with the methods (Ainslie and Day 1986; EL-Ibiary 1986; Survaiya and Shevgaonkar 1999) will be given. The following section describes the basic theory the technique is based upon.

3.5.1 Derivation of The Master Equations

From the *TL* forward solution, the following equations can be expressed for the parallel and vertical impedances of the *T*-circuit:

$$\left.\begin{aligned} Z_B &= \sinh(\gamma_{s_d}\delta r)\tanh(\gamma_{s_d}\frac{\delta r}{2})Z_P \\ Z_P &= \frac{\gamma_{s_d} Z_0}{jnrk_0(\beta^2+(\frac{l}{r})^2)\sinh(\gamma_{s_d}\delta r)} \end{aligned}\right\} \tag{3.28}$$

Since δr is infinitesimal, $\frac{\delta r}{r}$<<1, from (3.28) the following equations can be derived:

$$\left.\begin{aligned} Z_B &= \frac{1}{2}(\delta r)^2 \gamma_{s_d}^2 Z_P \\ Z_P &= \frac{Z_0}{jnr\delta r k_0 (\beta^2 + (\frac{l}{r})^2)} \end{aligned}\right\} \tag{3.29}$$

The equivalent *T*-circuit impedances (3.28) or (3.29) are functions of wavelength and the propagation constant, so the first and second derivatives of the propagation constant can be extended as follows:

$$\frac{\partial \beta}{\partial \lambda} = \frac{\frac{\partial Z_N}{\partial \lambda}\Big|_{\beta=\beta_0}}{\frac{\partial Z_N}{\partial \beta}\Big|_{\lambda=\lambda_0}} \tag{3.30}$$

$$\frac{\partial^2 \beta}{\partial \lambda^2} = \frac{\partial}{\partial \lambda}\left[\frac{\partial \beta}{\partial \lambda}\right] = \frac{\frac{\partial^2 Z_N}{\partial \lambda^2} - \frac{\partial \beta}{\partial \lambda}\frac{\partial^2 Z_N}{\partial \beta \partial \lambda}}{\frac{\partial Z_N}{\partial \beta}} \tag{3.31}$$

Where β_0 is the propagation constant at the wavelength of interest λ_0 (Boucouvalas and Papageorgiou 1982). Delay and dispersion can therefore be calculated if the derivatives in the equations (3.30) and (3.31) are known. Z_N can be calculated recurrently from $Z_n = Z_B + (\frac{1}{Z_B + Z_{n-1}} + \frac{1}{Z_P})^{-1}$, (n=1,2...N), which is the nth characteristic impedance of cylindrical layers. N is the total number of cylindrical layers, Z_N is the total impedance.

Equations (3.30) and (3.31) are equations related to derivatives of the impedances in each transmission line. The recursive equations can be used to determine delay and dispersion directly from equivalent *T*-circuit characteristic impedances.

3.5.2 Dispersion Solution Procedure

It is well known that the total dispersion in the single-mode regime includes material and waveguide dispersions. The concept of zero total dispersion by cancellation of the material and waveguide dispersions was proposed as long ago as 1970 in (Dyott and Stern 1970). The waveguide dispersion arises from the variation

in group velocity. It depends not only on the core radius and the refractive index difference between the core and the cladding of optical fibres, but also on the shape of the refractive index profile. The material contribution results from the wavelength dependence of the refractive index. The algorithm allows calculation of both material and waveguide dispersions. The material refractive index dependence on wavelength, (Survaiya and Shevgaonkar 1999), is included in the calculations and it is given by:

$$n_1(\lambda) = C_0 + C_1\lambda^2 + C_2\lambda^4 + \frac{C_3}{\lambda^2 - 0.035} + \frac{C_4}{(\lambda^2 - 0.035)^2} + \frac{C_5}{(\lambda^2 - 0.035)^3} \tag{3.32}$$

Where, C_0=1.4508554, C_1=-0.0031268, C_2=-0.0000381, C_3=0.0030270, C_4=-0.0000779, C_5=0.0000018.

The following steps detail the solution procedure for the mode delay and dispersion. From (3.30) and (3.31), delay and dispersion equations are given by (Safaai-Jazi and Lu 1990):

$$\tau = \frac{L\lambda^2}{2\pi c}\frac{\partial\beta}{\partial\lambda} \tag{3.33}$$

$$D = \frac{1}{L}\frac{\partial\tau}{\partial\lambda} = \frac{1}{2\pi c}(2\lambda\frac{\partial\beta}{\partial\lambda} + \lambda^2\frac{\partial^2\beta}{\partial\lambda^2}) \tag{3.34}$$

where τ is the delay, D is the dispersion, L is the optical fibre length, c is the velocity of light in free space.

The equations for $\frac{\partial Z_N}{\partial\lambda}$, $\frac{\partial Z_N}{\partial\beta}$, $\frac{\partial^2 Z_N}{\partial\lambda^2}$ and $\frac{\partial^2 Z_N}{\partial\beta\partial\lambda}$ are derived analytically which are to be used in the recursive algorithm:

$$\left.\begin{aligned}
\frac{\partial Z_N}{\partial\lambda} &= \frac{\partial Z_B}{\partial\lambda} + (\frac{1}{Z_B + Z_{n-1}} + \frac{1}{Z_P})^{-2}(\frac{\frac{\partial Z_B}{\partial\lambda} + \frac{\partial Z_{n-1}}{\partial\lambda}}{(Z_B + Z_{n-1})^2} + \frac{\frac{\partial Z_P}{\partial\lambda}}{Z_P^2}) \\
\frac{\partial Z_N}{\partial\beta} &= \frac{\partial Z_B}{\partial\beta} + (\frac{1}{Z_B + Z_{n-1}} + \frac{1}{Z_P})^{-2}(\frac{\frac{\partial Z_B}{\partial\beta} + \frac{\partial Z_{n-1}}{\partial\beta}}{(Z_B + Z_{n-1})^2} + \frac{\frac{\partial Z_P}{\partial\beta}}{Z_P^2})
\end{aligned}\right\} \tag{3.35}$$

$$\frac{\partial^2 Z_N}{\partial\lambda^2} = \frac{\partial^2 Z_B}{\partial\lambda^2} + 2\left(\frac{1}{Z_B + Z_{n-1}} + \frac{1}{Z_P}\right)^{-3}\left(\frac{\frac{\partial Z_B}{\partial\lambda} + \frac{\partial Z_{n-1}}{\partial\lambda}}{(Z_B + Z_{n-1})^2} + \frac{\frac{\partial Z_P}{\partial\lambda}}{Z_P^2}\right)^2 +$$

$$\left(\frac{1}{Z_B + Z_{n-1}} + \frac{1}{Z_P}\right)^{-2}\left(\frac{\frac{\partial^2 Z_B}{\partial\lambda^2} + \frac{\partial^2 Z_{n-1}}{\partial\lambda^2}}{(Z_B + Z_{n-1})^2} - \frac{2\left(\frac{\partial Z_B}{\partial\lambda} + \frac{\partial Z_{n-1}}{\partial\lambda}\right)^2}{(Z_B + Z_{n-1})^3} + \frac{\frac{\partial^2 Z_P}{\partial\lambda^2}}{Z_P^2} - \frac{2\left(\frac{\partial Z_P}{\partial\lambda}\right)^2}{Z_P^3}\right)$$

$$\left.\begin{aligned}\frac{\partial^2 Z_N}{\partial\beta\partial\lambda} = \frac{\partial^2 Z_B}{\partial\beta\partial\lambda} + 2\left(\frac{1}{Z_B + Z_{n-1}} + \frac{1}{Z_P}\right)^{-3}\left(\frac{\frac{\partial Z_B}{\partial\lambda} + \frac{\partial Z_{n-1}}{\partial\lambda}}{(Z_B + Z_{n-1})^2} + \frac{\frac{\partial Z_P}{\partial\lambda}}{Z_P^2}\right)\left(\frac{\frac{\partial Z_B}{\partial\beta} + \frac{\partial Z_{n-1}}{\partial\beta}}{(Z_B + Z_{n-1})^2} + \frac{\frac{\partial Z_P}{\partial\beta}}{Z_P^2}\right) +\\ \left(\frac{1}{Z_B + Z_{n-1}} + \frac{1}{Z_P}\right)^{-2}\left(\frac{\frac{\partial^2 Z_B}{\partial\beta\partial\lambda} + \frac{\partial^2 Z_{n-1}}{\partial\beta\partial\lambda}}{(Z_B + Z_{n-1})^2} - \frac{2\left(\frac{\partial Z_B}{\partial\lambda} + \frac{\partial Z_{n-1}}{\partial\lambda}\right)\left(\frac{\partial Z_B}{\partial\beta} + \frac{\partial Z_{n-1}}{\partial\beta}\right)}{(Z_B + Z_{n-1})^3} + \frac{\frac{\partial^2 Z_P}{\partial\beta\partial\lambda}}{Z_P^2} - \frac{2\frac{\partial Z_P}{\partial\lambda}\frac{\partial Z_P}{\partial\beta}}{Z_P^3}\right)\end{aligned}\right\} \quad (3.36)$$

The first derivatives of the impedance equations (3.29) as a function of the fibre layer physical and optical parameters are given by:

$$\left.\begin{aligned}\frac{\partial Z_P}{\partial\beta} &= \frac{-2Z_0\beta}{nr\,\delta rk_0\left(\beta^2 + \left(\frac{l}{r}\right)^2\right)^2}\\ \frac{\partial Z_P}{\partial\lambda} &= \frac{-Z_0}{r\,\delta rk_0\left(\beta^2 + \left(\frac{l}{r}\right)^2\right)^2}\frac{\frac{\partial n}{\partial\lambda}}{n^2}\end{aligned}\right\} \quad (3.37)$$

$$\left.\begin{aligned}\frac{\partial Z_B}{\partial\beta} &= \frac{\delta r^2}{2}\left(\frac{\partial\gamma^2}{\partial\beta}Z_P + \gamma^2\frac{\partial Z_P}{\partial\beta}\right)\\ \frac{\partial Z_B}{\partial\lambda} &= \frac{\delta r^2}{2}\left(\frac{\partial\gamma^2}{\partial\lambda}Z_P + \gamma^2\frac{\partial Z_P}{\partial\lambda}\right)\end{aligned}\right\} \quad (3.38)$$

Where

$$\gamma^2 = \beta^2 + \left(\frac{l}{r}\right)^2 - n^2k_0^2 - \frac{2n\beta lk_0}{(\beta r)^2 + l^2}),$$

$$\frac{\partial\gamma^2}{\partial\beta} = 2\beta - \frac{2nlk_0(l^2 - (\beta r)^2)}{((\beta r)^2 + l^2)^2},$$

$$\frac{\partial\gamma^2}{\partial\lambda} = -2n\frac{\partial n}{\partial\lambda}k_0{}^2 - \frac{2k_0\beta l}{(\beta r)^2 + l^2}\frac{\partial n}{\partial\lambda},$$

$$\frac{\partial n}{\partial \lambda} = 2C_1\lambda + 4C_2\lambda^3 - \frac{2C_3\lambda}{(\lambda^2 - 0.035)^2} - \frac{4C_4\lambda}{(\lambda^2 - 0.035)^3} - \frac{6C_5\lambda}{(\lambda^2 - 0.035)^4}$$

For the second derivatives of the impedance equations (3.29):

$$\left.\begin{aligned} \frac{\partial^2 Z_P}{\partial\beta\partial\lambda} &= \frac{2Z_0\beta}{r\delta rk_0(\beta^2 + (\frac{l}{r})^2)^2}\frac{\frac{\partial n}{\partial\lambda}}{n^2} \\ \frac{\partial^2 Z_P}{\partial\lambda^2} &= \frac{-Z_0}{r\delta rk_0(\beta^2 + (\frac{l}{r})^2)}(\frac{\frac{\partial^2 n}{\partial\lambda^2}}{n^2} - \frac{2(\frac{\partial n}{\partial\lambda})^2}{n^3}) \end{aligned}\right\} \quad (3.39)$$

$$\left.\begin{aligned} \frac{\partial^2 Z_B}{\partial\beta\partial\lambda} &= \frac{\delta r^2}{2}(\frac{\partial^2\gamma^2}{\partial\beta\partial\lambda}Z_P + \frac{\partial\gamma^2}{\partial\beta}\frac{\partial Z_P}{\partial\lambda} + \frac{\partial\gamma^2}{\partial\lambda}\frac{\partial Z_P}{\partial\beta} + \gamma^2\frac{\partial^2 Z_P}{\partial\beta\partial\lambda}) \\ \frac{\partial^2 Z_B}{\partial\lambda^2} &= \frac{\delta r^2}{2}(\frac{\partial^2\gamma^2}{\partial\lambda^2}Z_P + 2\frac{\partial\gamma^2}{\partial\lambda}\frac{\partial Z_P}{\partial\lambda} + \gamma^2\frac{\partial^2 Z_P}{\partial\lambda^2}) \end{aligned}\right\} \quad (3.40)$$

Where

$$\frac{\partial^2\gamma^2}{\partial\beta\partial\lambda} = \frac{-2lk_0(l^2 - (\beta r)^2)}{((\beta r)^2 + l^2)^2}\frac{\partial n}{\partial\lambda}$$

$$\frac{\partial^2\gamma^2}{\partial\lambda^2} = -2k_0{}^2((\frac{\partial n}{\partial\lambda})^2 + n\frac{\partial^2 n}{\partial\lambda^2}) - \frac{2\beta k_0 l}{(\beta r)^2 + l^2}\frac{\partial^2 n}{\partial\lambda^2}$$

$$\frac{\partial^2 n}{\partial\lambda^2} = 2C_1 + 12C_2\lambda^2 + \frac{6C_3\lambda^2 + 0.07C_3}{(\lambda^2 - 0.035)^3} + \frac{20C_4\lambda^2 + 0.14C_4}{(\lambda^2 - 0.035)^4} - \frac{42C_5\lambda^2 + 0.21C_5}{(\lambda^2 - 0.035)^5}$$

To test the accuracy of (3.37)-(3.40) derived from the approximate impedance equations (3.29), the exact first and second derivatives from the exact impedance equations (3.28) have also been worked out, in Appendix C. The equations (3.37)-(3.40) have been found to be accurate for the purpose. Approximations are not however essential in this analysis and if the exact equivalent equations are preferred they can be used. In this solution procedure, almost all the computation time is spent in calculating (3.35) and (3.36). The derivatives $\frac{\partial Z_N}{\partial\lambda}$, $\frac{\partial Z_N}{\partial\beta}$ and $\frac{\partial^2 Z_N}{\partial\lambda^2}$, $\frac{\partial^2 Z_N}{\partial\beta\partial\lambda}$ can now

be obtained very efficiently. Therefore, delay and dispersion can be calculated accurately and recursively.

3.5.3 Numerical Results and Discussion

For the comparative numerical results, an optical fibre with a well known refractive index profile radial dependence is considered as follows (Adams 1981):

$$n(\bar{r}) = \begin{cases} n_1(1 - \Delta(\dfrac{\bar{r}}{\bar{a}})^{\alpha}) & \dfrac{\bar{r}}{\bar{a}} < 1 \\ n_2 & \dfrac{\bar{r}}{\bar{a}} > 1 \end{cases} \tag{3.41}$$

where $\Delta \equiv (n_1 - n_2)/n_1$, n_1 is the maximal refractive index, n_2 is the refractive index of the outer and uniform cladding, α controls the decay or growth of the profile envelope, $\bar{a}$ is the normalized core radius, and $\bar{r}$ is the normalized cylindrical layer radius. A variety of refractive index profiles can be generated by varying α (α = 1 triangular profile, α = 2 parabolic profile, $\alpha = \infty$ step profile).

Furthermore, in order to introduce refractive index wavelength dependence, since (3.41) is proportional to n, it scales as a function of wavelength according to (3.32).

Convergence and accuracy are important factors for any numerical techniques. The typical standard step, triangular, and linear chirp index fibre profiles have been chosen as the results are well known. For all the computations, the thickness of the cylindrical layers, inside and outside the core, is taken to be $\delta\bar{r}/\bar{r}$ =0.02. 600 to 1000 homogeneous cylindrical layers are, in general, sufficient for this $\delta\bar{r}/\bar{r}$ ratio.

The dispersion characteristics for step index optical fibres are calculated by applying the novel technique and using delay and dispersion equations, (3.33) and (3.34), within the wavelength range used in optical communications. The step index profile optical fibre used has typical values of core radius a_1=2.2 μm and index difference Δ =0.012 (Ainslie and Day 1986). In Fig.3.22, the exact normalised propagation constants (effective indices) for the step index fibre calculated using Bessel functions are compared with the results obtained with the *TL* technique. The *TL* results are presented in two curves, one using the exact impedance equations

(3.28) and the other plot using the approximate impedance equations (3.29). The curves are also presented by varying as a parameter the number of layers set to 600 and 1000 for this algorithm. The numerical results show $\delta\bar{r}/\bar{r}$ =0.02 offers good homogeneity to the cylindrical layers and the accurate results can be obtained. With 1000 layers, the algorithm using either (3.28) or (3.29) gives accurate results in agreement with the Bessel functions while maintaining efficient computation speed. Therefore, the number of 1000 layers is chosen for the dispersion calculation. Table3.6 shows the accuracy of the *TL* method in calculating the effective mode indices at the wavelength 1.30103 μm using (3.28) and (3.29). Both compare very well to the exact Bessel functions solution. Results based on (3.28) are slightly closer to the result from Bessel functions. Both (3.28) and (3.29) however offer excellent accuracy. Fig.3.23 compares dispersion results using this algorithm for the range 1.2 μm and 1.6 μm. It includes a dispersion curve generated using Bessel functions for the effective index and dispersion plots using an effective index obtained by the *TL* method, (3.28) and (3.29). As expected, for the step index optical fibre the zero dispersion point is at 1.30103 μm. Table3.7 shows a comparison of some numerical results of calculated zero dispersion wavelengths. The results of the *TL* method agree very well with the result from Bessel Functions. As expected, using (3.28) gives slightly more accurate results than (3.29), however, for 1000 layers this difference is not significant. The two dispersion curves in Fig.3.24 are derived using Bessel functions for the exact effective mode index. One dispersion plot uses numerical differentiation and the other uses the dispersion algorithm. The zero dispersion wavelength obtained using this algorithm is λ_0=1.30133 μm and λ_0=1.30835 μm is based on numerical differentiation respectively. The result demonstrates the accuracy of this algorithm (exact λ_0=1.30103 μm).

To allow further comparison with the existing publication on the dispersion calculation (EL-Ibiary 1986), the triangular refractive index profile fibres are also considered. Fig.3.25 shows dispersion curves plotted against wavelength for the two values of core radius a_1, namely, 1.92 μm and 3.29 μm, and index difference Δ =0.01, with zero dispersion wavelength at 1.55 μm. Fig.3.25 shows the excellent agreement in the calculated dispersion for triangular optical fibres using the different methods with different core radii. In this case there is negligible difference between

the results using (3.28) and (3.29). The results match perfectly with those given in (EL-Ibiary 1986).

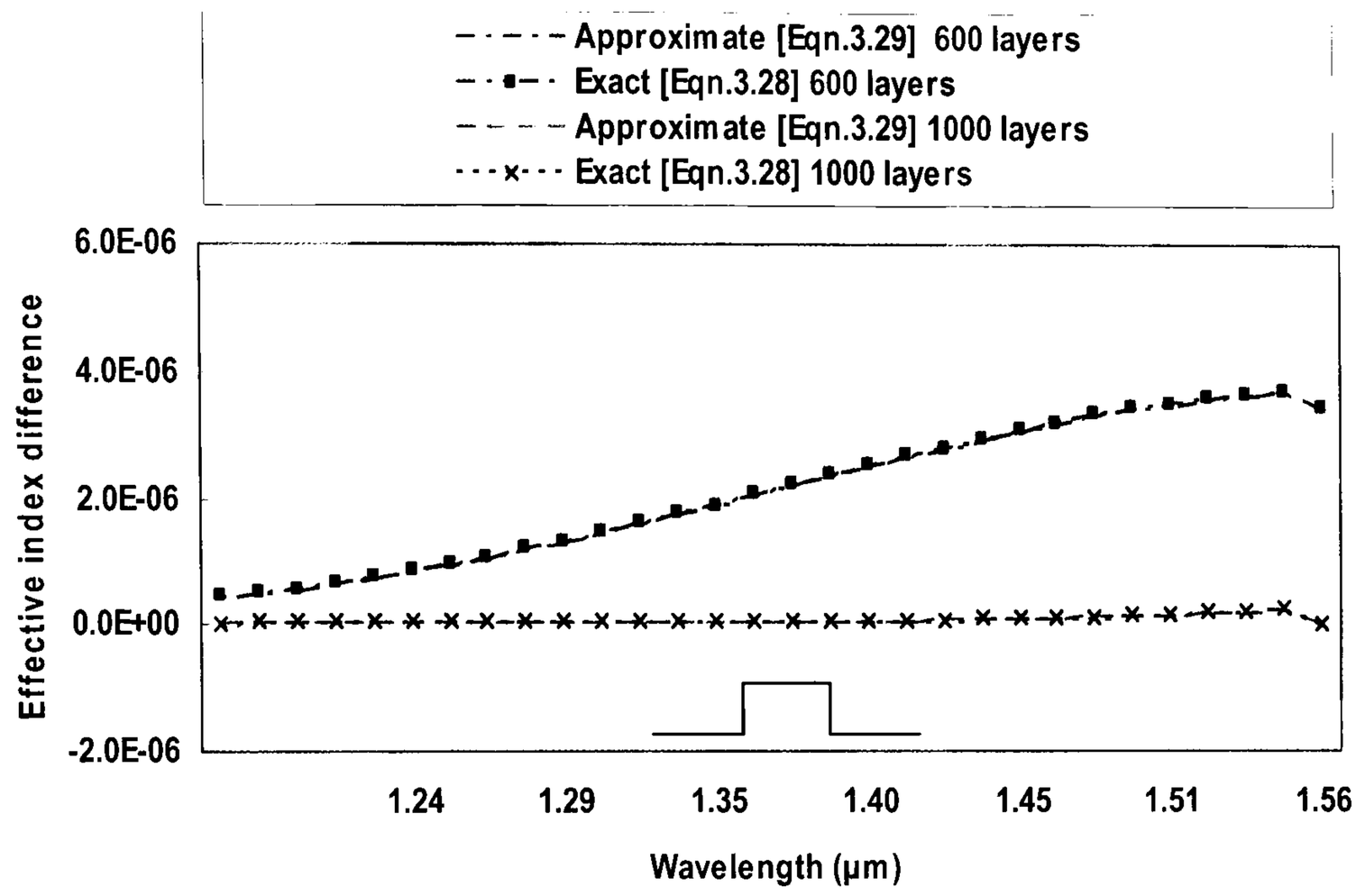

Figure 3.22 Effective mode index difference versus wavelength curves for the step index single-mode optical fibre with core radius a_1=2.2μm and Δ =0.012. ($\Delta\overline{\beta} = \dfrac{(\overline{\beta} - \overline{\beta}_{bessel})}{\overline{\beta}_{bessel}}$)

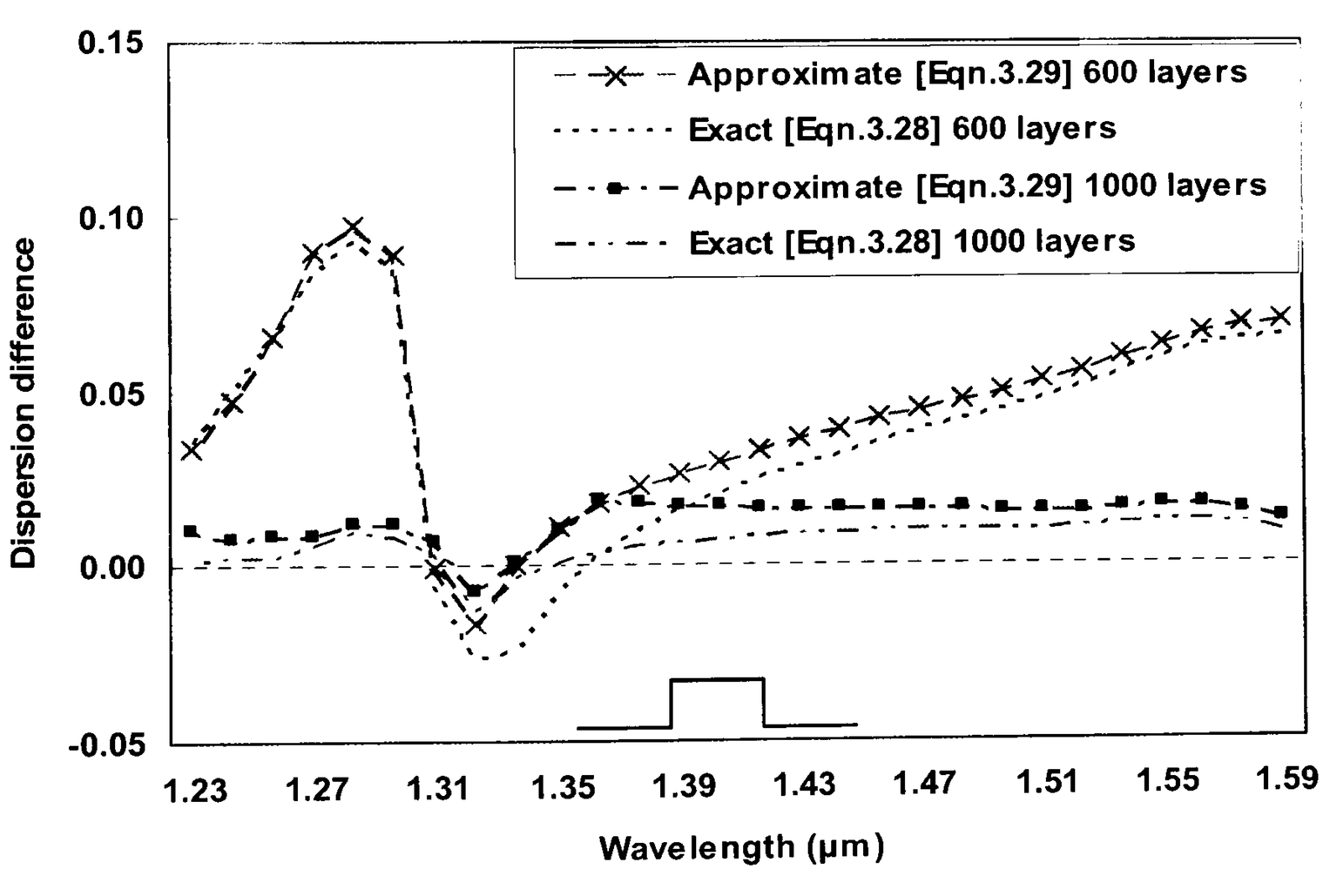

Figure 3.23 The dispersion difference versus wavelength curves for the step index optical fibre with core radius a_1=2.2μm and Δ =0.012. ($\Delta D = \dfrac{(D - D_{bessel})}{D_{bessel}}$, D stands for dispersion)

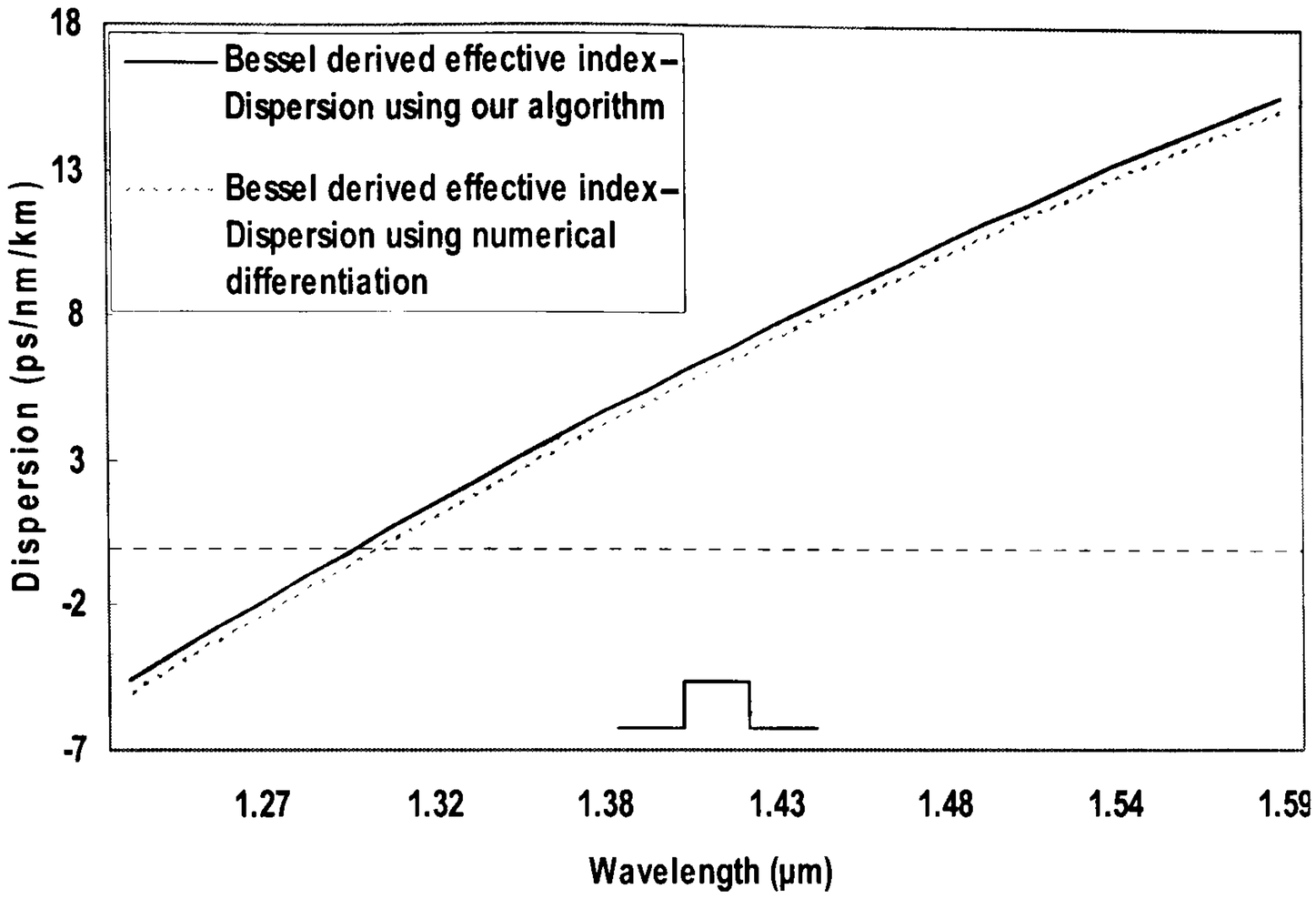

Figure 3.24 The dispersion of fundamental mode of a step index optical fibre using the algorithm compared to the result using numerical differentiation for a core radius a_1=2.2μm and Δ =0.012.

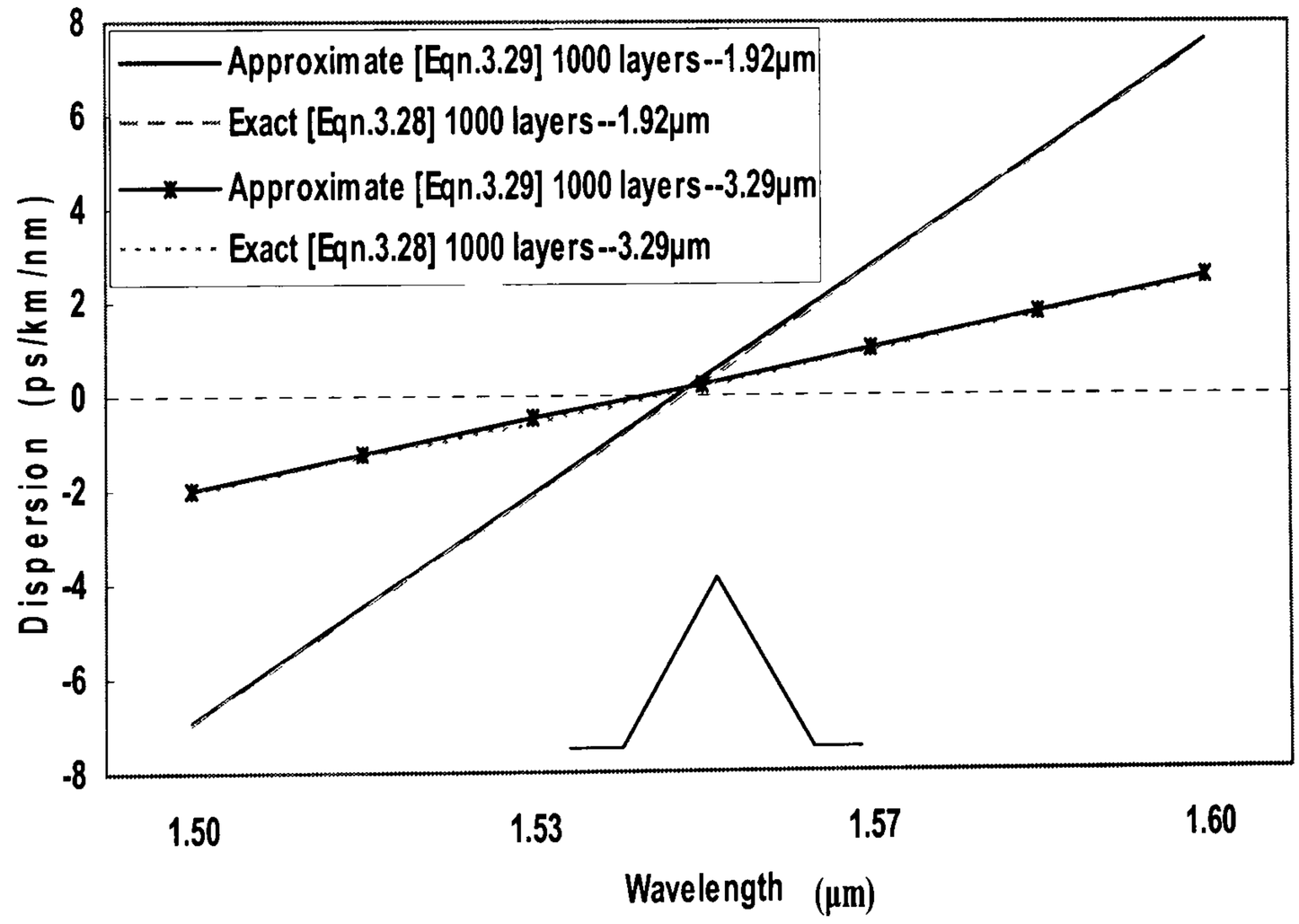

Figure 3.25 The variation of dispersion versus wavelength curves for the triangular refractive index profile optical fibre with Δ =0.01at the two values of core radius which attain the zero dispersion point at 1.55μm.

TABLE 3.6

The accuracy of the *TL* method for calculating $\overline{\beta}$ for a step index optical fibre at $\lambda_{1.3}$ =1.30103 μm

		$\overline{\beta}$ at $\lambda_{1.3}$	$\Delta\overline{\beta} = \frac{(\overline{\beta} - \overline{\beta}_{bessel})}{\overline{\beta}_{bessel}}(\%)$
Bessel Function ($\overline{\beta}_{bessel}$)		1.48020635	0.0
TL Method	Exact [Eqn.3.28] 600 layers	1.48020794	1.0742×10^{-4}
	Approximate [Eqn.3.29] 600 layers	1.48020795	1.0809×10^{-4}
	Exact [Eqn.3.28] 1000 layers	1.48020644	6.0802×10^{-6}
	Approximate [Eqn.3.29] 1000 layers	1.48020645	6.7558×10^{-6}

TABLE 3.7

The accuracy of the *TL* method for calculating the zero dispersion wavelength λ_0 for a step index optical fibre.

		$\lambda_0(10^{-6})$	$\Delta\lambda = \frac{(\lambda_0 - \lambda_{1.3})}{\lambda_{1.3}}(\%)$
Bessel Function ($\lambda_{1.3}$)		1.30103	0.0
TL Method	Exact [Eqn.3.28] 600 layers	1.30183	0.06149
	Approximate [Eqn.3.29] 600 layers	1.30218	0.08839
	Exact [Eqn.3.28] 1000 layers	1.30133	0.02306
	Approximate [Eqn.3.29] 1000 layers	1.30168	0.04996

It is well known that the dispersion flattened characteristics of an optical fibre are very important for *WDM* optical systems. There have been many attempts to design dispersion flattened optical fibres (Francois 1983; Davies and Sahm 1986; Safaai-Jazi and Lu 1990). The *TL* method can be used in the design of dispersion flattened optical fibres quite efficiently. The optical fibre considered here is with linear chirp refractive index profile, of core radius a_1=7.2 μm and index difference Δ=0.0102, as shown in Fig.3.26, and it has been studied in (Safaai-Jazi and Lu 1990). Fig.3.27 shows the calculated dispersion as a function of wavelength using the *TL* method. It can be seen that the dispersion magnitude is less than 2 *ps/nm/km* over the entire range of 1.35-1.6 μm wavelength. There is no significant difference using the *TL* method with (3.28) or (3.29). The results in Fig.3.27 also agree very well with the results in (Safaai-Jazi and Lu 1990).

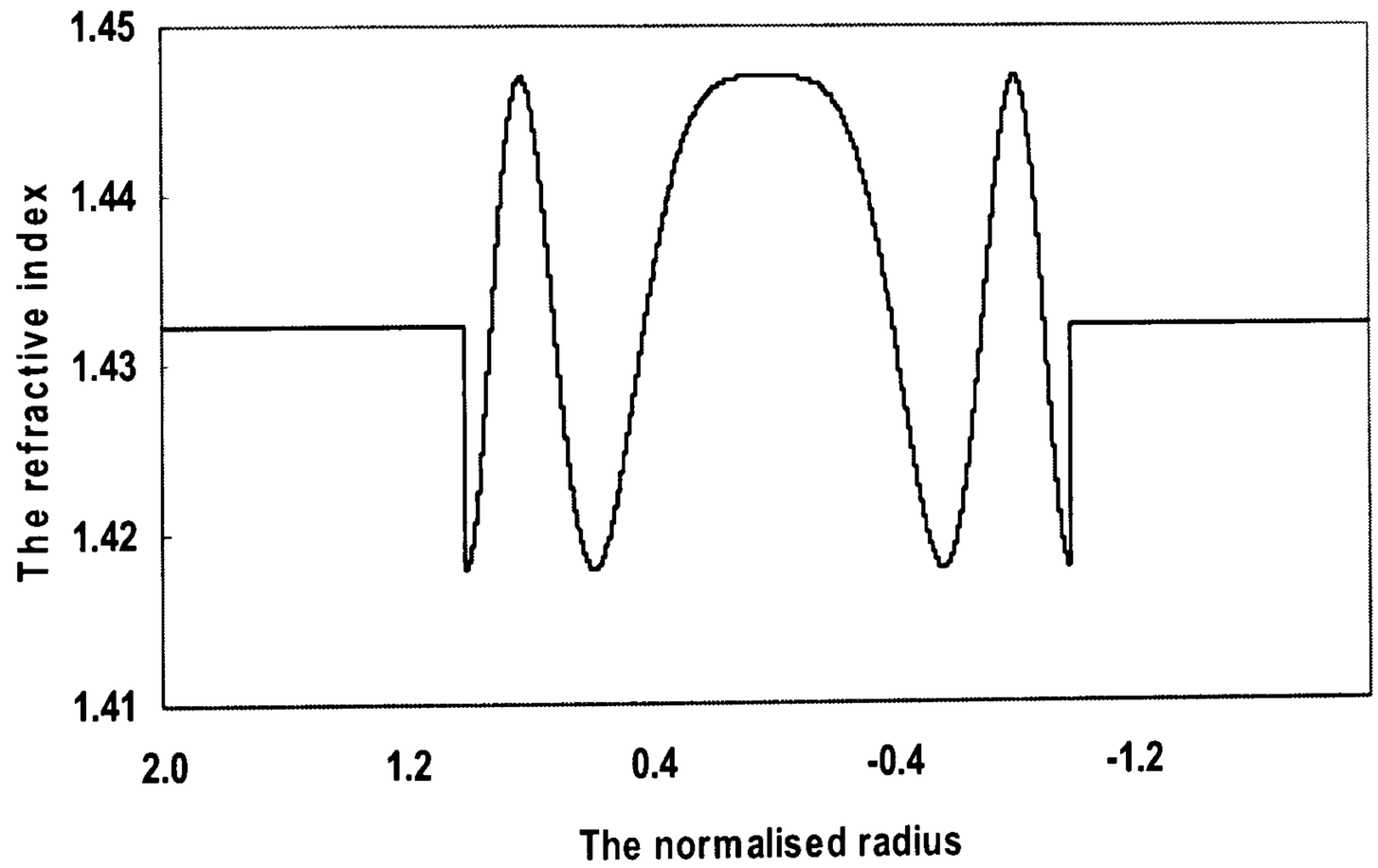

Figure 3.26 The linear chirp refractive index profile of core radius a_1=7.2μm and Δ=0.0102.

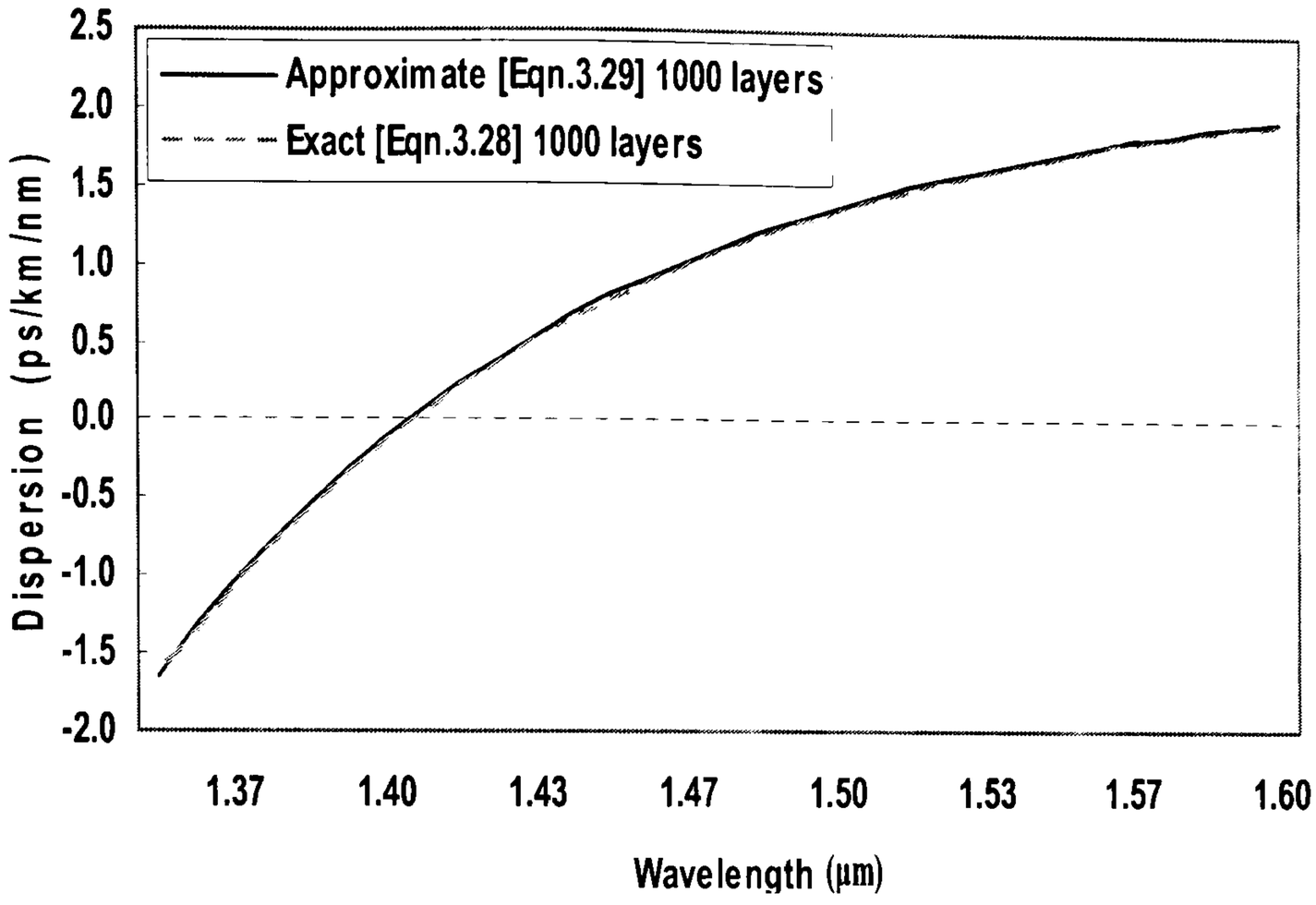

Figure 3.27 The dispersion versus wavelength curves for the linear chirp refractive index profile of Fig. 3.26 over a wavelength range from 1.35 to 1.6μm.

In this section, a novel, efficient and accurate algorithm for calculating the mode dispersion of cylindrical dielectric waveguides has been developed from *TL* principles. This method uses Transmission-Line representation of cylindrical dielectric waveguides and relies on the modeling of a thin uniform concentric cylindrical layer of an optical fibre to a *T*-circuit. The method requires knowledge of only the mode propagation constant and the refractive index profile. It is direct and exact, and avoids the use of numerical differentiation twice. From the mathematical point of view, it may be especially useful for designing and predicting complicated refractive index profile optical fibres where the earlier reported approximate methods are slow. The performance of this technique has been demonstrated by evaluating dispersion versus wavelength for step, triangular and linear chirp index profile optical fibres. The results support the claim that this algorithm provides direct calculation of dispersion with high degree of accuracy.

In the following chapter, the inverse solution of *TL* technique will be presented. The problem addressed can be stated as follows: the guided mode electric field is known, can the inverse transmission line principles be used for determining the refractive index profile? It is well known that inverse problems are much more difficult to solve, they often are non-linear, and suffer from stability problems. A new simple inverse *TL* technique is offered which does not require direct inversion of

the scalar wave equation, but uses a recursive algorithm which reconstructs the refractive index directly with the appropriate radius.

CHAPTER 4

Inverse Solution of Maxwell's Equations for Cylindrical Waveguides From Mode Electric Field

4.1 Inverse *TL* Theory

The refractive index profile of the optical fibre plays an important role in characterizing the properties of the optical fibre. It allows the determination of the fibre's numerical aperture and of the number of modes propagating within the optical fibre, while defining intermodal and material dispersion caused by the optical fibre itself. Furthermore, since the impulse response and, consequently, the information-carrying capacity of the optical fibre is refractive index profile-dependent, it is essential for optical fibre manufacturers to produce controlled optical fibre index profiles with great accuracy. It is important to establish an efficient and accurate method for measuring the refractive index profile. Accurate knowledge of the refractive index profile allows designers to reduce optical fibre device manufacturing costs through tight control of the optical fibre fabrication processes. As a result, there is a need for accurate methods of optical fibre refractive index profiling.

In this chapter, the inverse solution of the *TL* method will be applied to the optical fibre refractive index reconstruction from the mode electric field. The equivalent T-circuit for a cylindrical thin dielectric layer, Fig.3.1, of constant refractive index n and thickness $\delta\bar{r}$ at distance $\bar{r}$ from the core is represented as an electric circuit in Fig. 4.1. At $r = \infty$, $Z_{prev} = 0$ and $n(\infty) = n_2$ are assumed. From circuit theory, the following recursive relation has been derived to determine the values of $Z_{p,n}$, $Z_{B,n}$ and $Z_{prev} = Z_n$ for the nth layer.

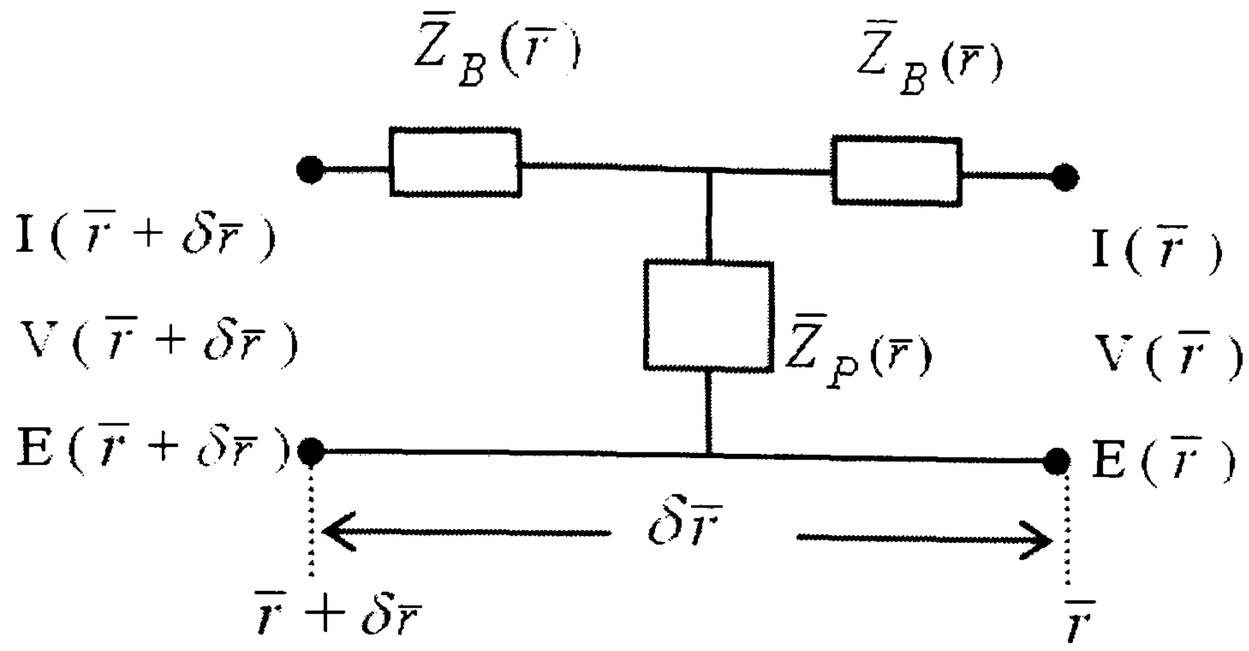

Figure 4.1 Equivalent circuit for a cylindrical thin layer at constant refractive index n and thickness $\delta\bar{r}$ at distance $\bar{r}$ from the core

$$\left.\begin{aligned}
\bar{Z}_n &= \frac{(\bar{Z}_{n-1}+\bar{Z}_{B,n})\bar{Z}_{P,n}}{\bar{Z}_{n-1}+\bar{Z}_{B,n}+\bar{Z}_{P,n}}+\bar{Z}_{B,n} \\
\bar{Z}_{B,n} &= \frac{1}{2}\bar{\gamma}^2\delta\bar{r}^2\bar{Z}_{P,n} \\
\bar{Z}_{P,n} &= \frac{Z_0}{n(\bar{r})\bar{r}\delta\bar{r}(\bar{\beta}^2+\frac{l^2}{\bar{r}^2})}
\end{aligned}\right\} \qquad (4.1)$$

where $\bar{\gamma}^2 = \bar{\beta}^2 + \frac{l^2}{\bar{r}^2} - n^2(\bar{r}) - \frac{2\bar{\beta}n(\bar{r})l}{\bar{\beta}^2\bar{r}^2+l^2}$.

$\bar{\beta}$ is the effective refractive index and for typical waveguides lies between n_1 and n_2. For the time being, the knowledge of $\bar{\beta}$, λ_0, $\bar{r}$, $\delta\bar{r}$ and $n(\infty)=n_2$ is assumed to be known. Hence $I(\bar{r}+\delta\bar{r})$, $V(\bar{r}+\delta\bar{r})$ can be calculated for any radius.

Hence the refractive index $n(\bar{r})$ can be worked out as follows:

$$\left.\begin{aligned}
I_s(\bar{r}) &= \frac{2I_E(\bar{r})}{\sqrt{n(\bar{r})}} \\
E_{\bar{r}}(\bar{r}) &= \frac{I_E(\bar{r})Z_0}{n^2(\bar{r})\bar{r}}
\end{aligned}\right\} \qquad (4.2)$$

and finally

$$E_{\bar{r}}(\bar{r}) = \frac{I_s(\bar{r})Z_0}{2n^{3/2}(\bar{r})\bar{r}} \qquad (4.3)$$

$$n(\bar{r}) = \left(\frac{I_s(\bar{r})Z_0}{2E_{\bar{r}}(\bar{r})\bar{r}}\right)^{2/3} \tag{4.4}$$

Since mode electric field $E_{\bar{r}}(\bar{r})$ and current $I_s(\bar{r})$ are known, hence the refractive index $n(\bar{r})$ can be reconstructed. This formula can be applied to single-mode and multimode optical fibres and Bragg fibres.

The inverse solution of the *TL* method can be stated as follows: the guided mode electric field $E_{\bar{r}}(\bar{r})$ is known. At $r = \infty$, $Z_{prev} = 0$, $I_{prev} = 10^{-3}$, and $n(\infty) = n_2$. Z_n is computed starting with Z_{prev} as Z_{n-1} and using $Z_n = \frac{(Z_{n-1} + Z_{B,n})Z_{p,n}}{Z_{n-1} + Z_{B,n} + Z_{p,n}} + Z_{B,n}$ for n=1,2,3…,N. Similarly, $I_n = I_{n-1}(1 + \frac{Z_{B,n} + Z_{n-1}}{Z_{p,n}})$. From (4.4), the refractive index profile of the optical fibre can be reconstructed directly with radius. It can be applied to any kind of cylindrical and angularly uniform optical fibres. The advantages of this method are that no prior information is needed on the functional form of the unknown quantities, no iterations in the calculating process are necessary. Some essential examples are shown in the following sections.

4.2 Refractive Index Synthesis from the Fundamental Mode Electric Field

In this section, the *TL* method is used to determine the refractive index profile of an single-mode optical fibre from the electric field of the HE_{11} mode. Fig.4.2(a) shows the electric field distribution of the HE_{11} mode of the optical fibre used. Fig.4.2(b) shows the reconstructed refractive index profile of a single-mode step index optical fibre. It has a refractive index n_1=1.4811 and n_2=1.4801, core radius a =4.583 μm, and V=2.5. In order to compare its accuracy with the original refractive index which has been used to derive the electric field of Fig.4.2(a), Fig.4.2(c) shows the % error versus the normalised radius.

The error in the refractive index oscillates about the exact value in the core. The error in the cladding is zero. The error oscillations in the core are centred about the exact value of n_1 and the ripple depends on the number of homogeneous cylindrical

layers used for the reconstruction of the index as shown in Fig.4.3. We see in Fig.4.3 that less than 1% error due to the ripple in Δn can be achieved with up to 30,000 homogeneous layers. There are two factors that are responsible for the obtained error; one factor is due to the use of the approximate impedance equations (3.29) instead of the exact impedance equations (3.28), the other factor is that the homogeneous cylindrical layers must be very thin in order to apply the inverse solution of the *TL* method accurately.

Fig.4.4(a) shows the effect of inaccuracies in $\overline{\beta}$ on the ripple in the reconstructed Δn. The ripple increases with the use of the incorrect $\overline{\beta}$. The minimum error occurs at the exact $\overline{\beta}$. However, this is not a problem if it is unknown, since the reconstruction can be simply started with $\overline{\beta} = n_2$ and the process is repeated with a $\overline{\beta}$ change within $n_2 \leq \overline{\beta} \leq n_1$ until the ripple is at a minimum. At this minimum ripple point the exact $\overline{\beta}$ is achieved, and the reconstructed refractive index is also exact. The same conclusion can also be obtained from (4.4), as with the exact $\overline{\beta}$ the mode electric field is also exact, hence the reconstructed refractive index is the most accurate. To further illustrate the accuracy of the inverse *TL* technique, β =1.4805 is chosen from Fig.4.4(a) to reconstruct the refractive index, as shown in Fig.4.4(b). For this kind of refractive index profile, $\overline{\beta}$ =1.4805 is the exact $\overline{\beta}$, shown in Fig.4.4(c).

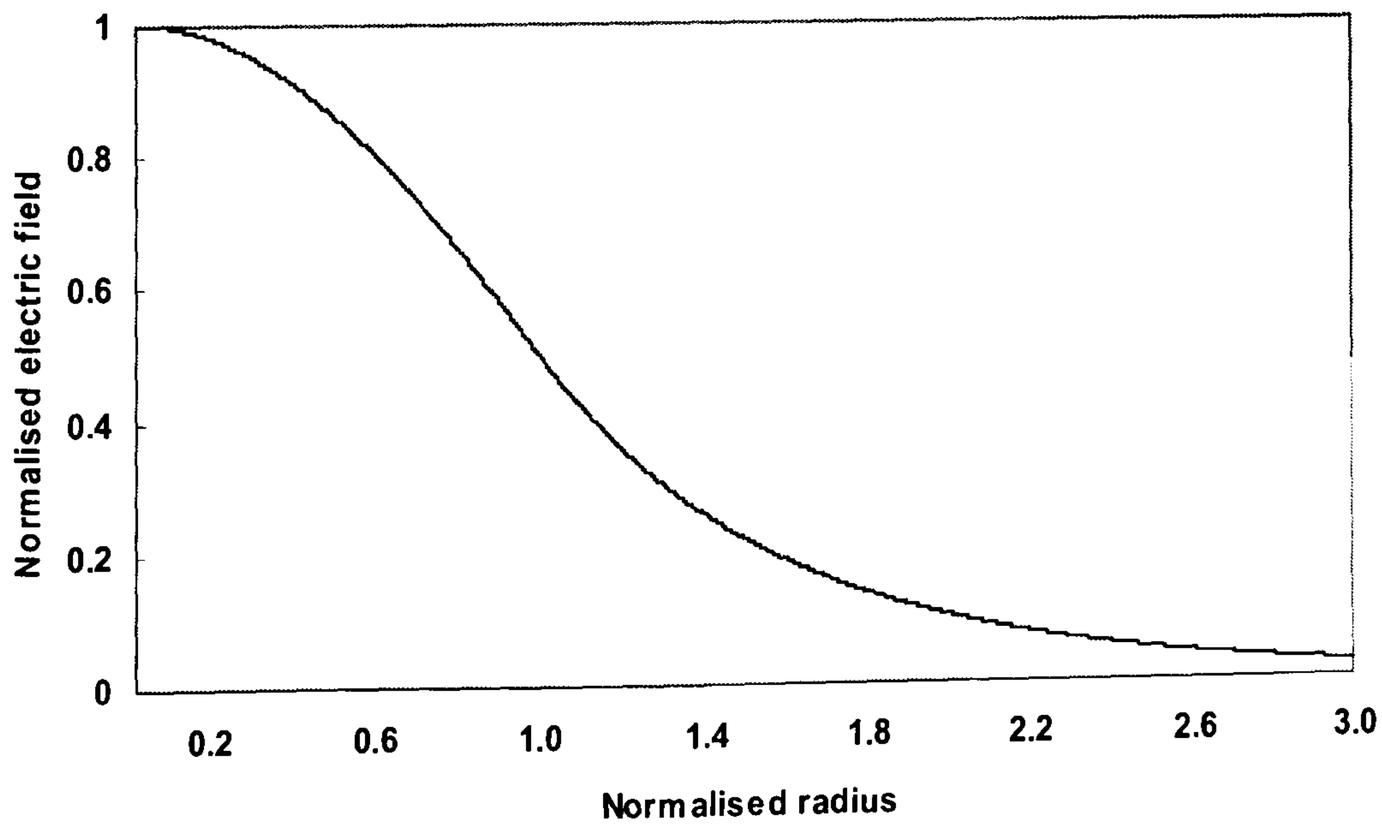

(a)

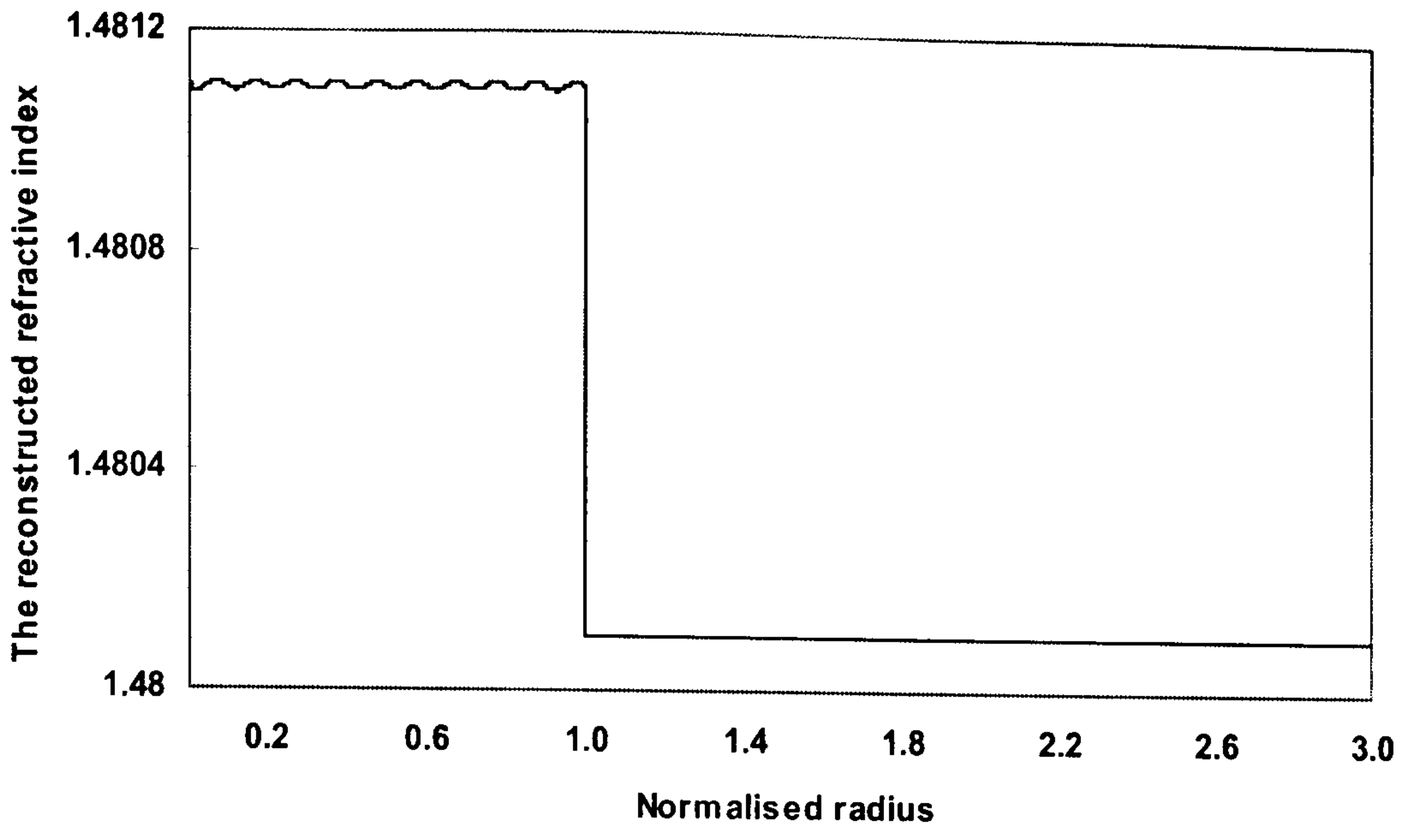

(b)

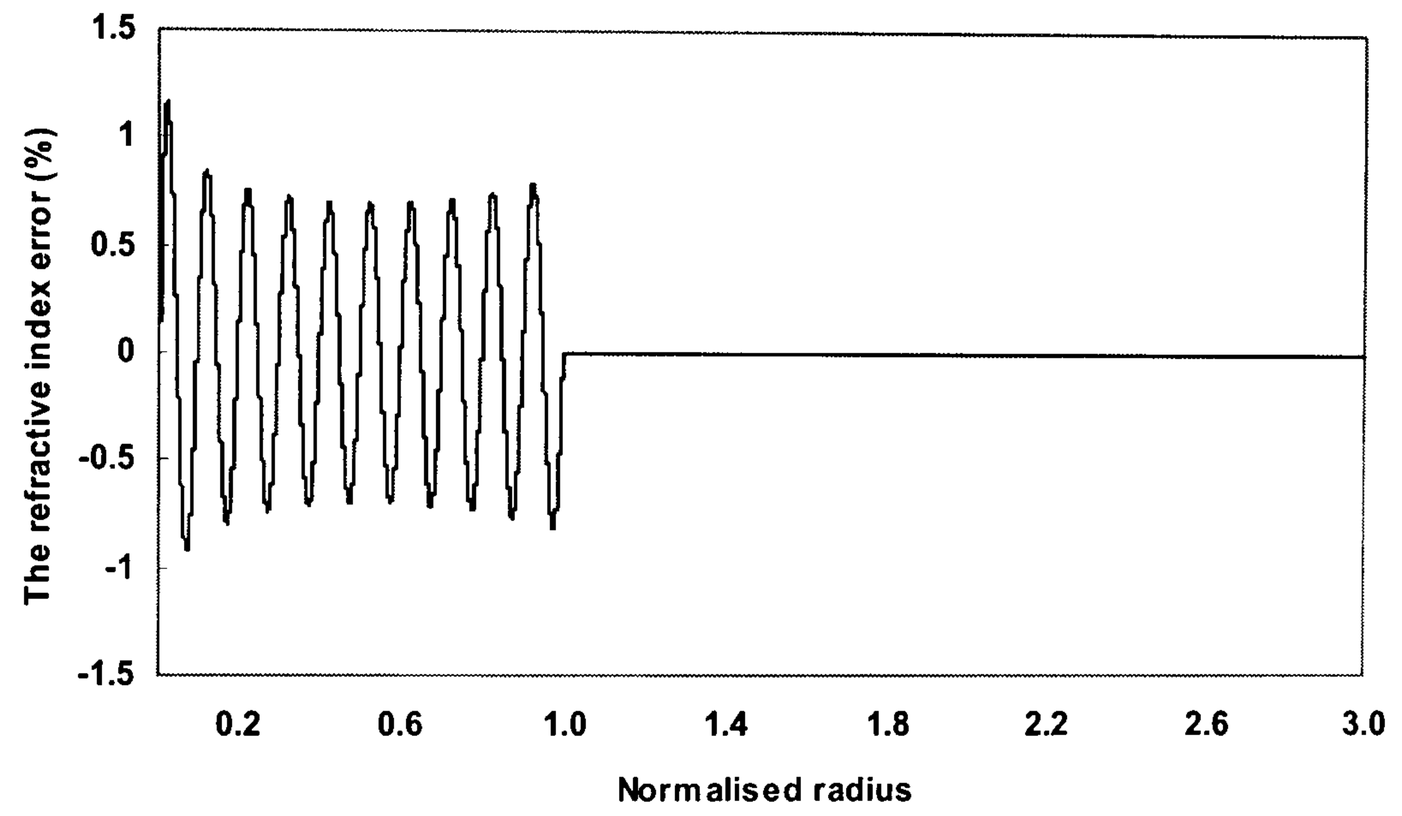

(c)

Figure 4.2 (a) Electric field plot for single-mode step index profile optical fibre with core index n_1=1.4811 and cladding index n_2=1.4801, core radius a=4.583 μm, V=2.5.
(b) The reconstructed refractive index using (4.4).
(c) The error (%) in refractive index difference due to ripple
$(100(n_{exact} - n_{reconstructed})/n_{exact})\%$

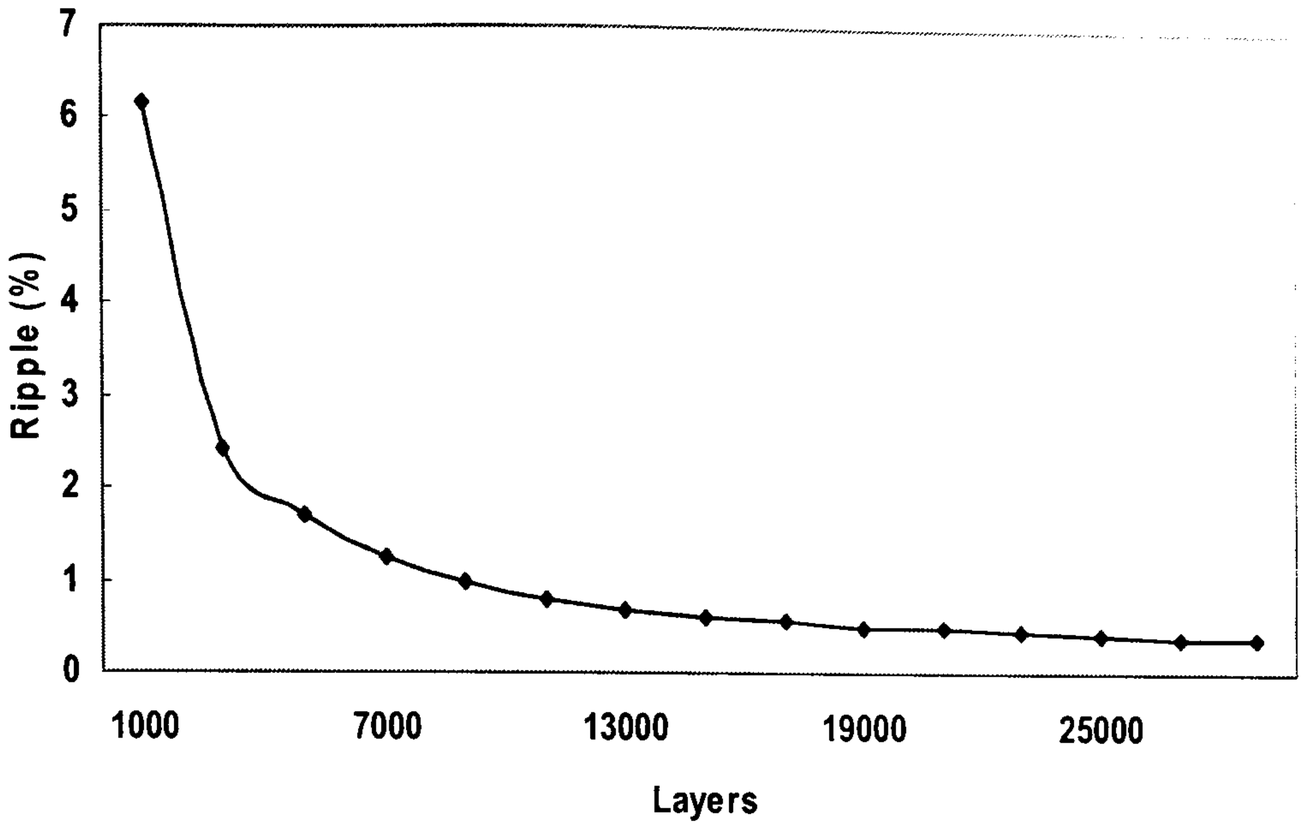

Figure 4.3 The refractive index difference, error (%) of the synthesized refractive index versus the number of homogeneous layers.

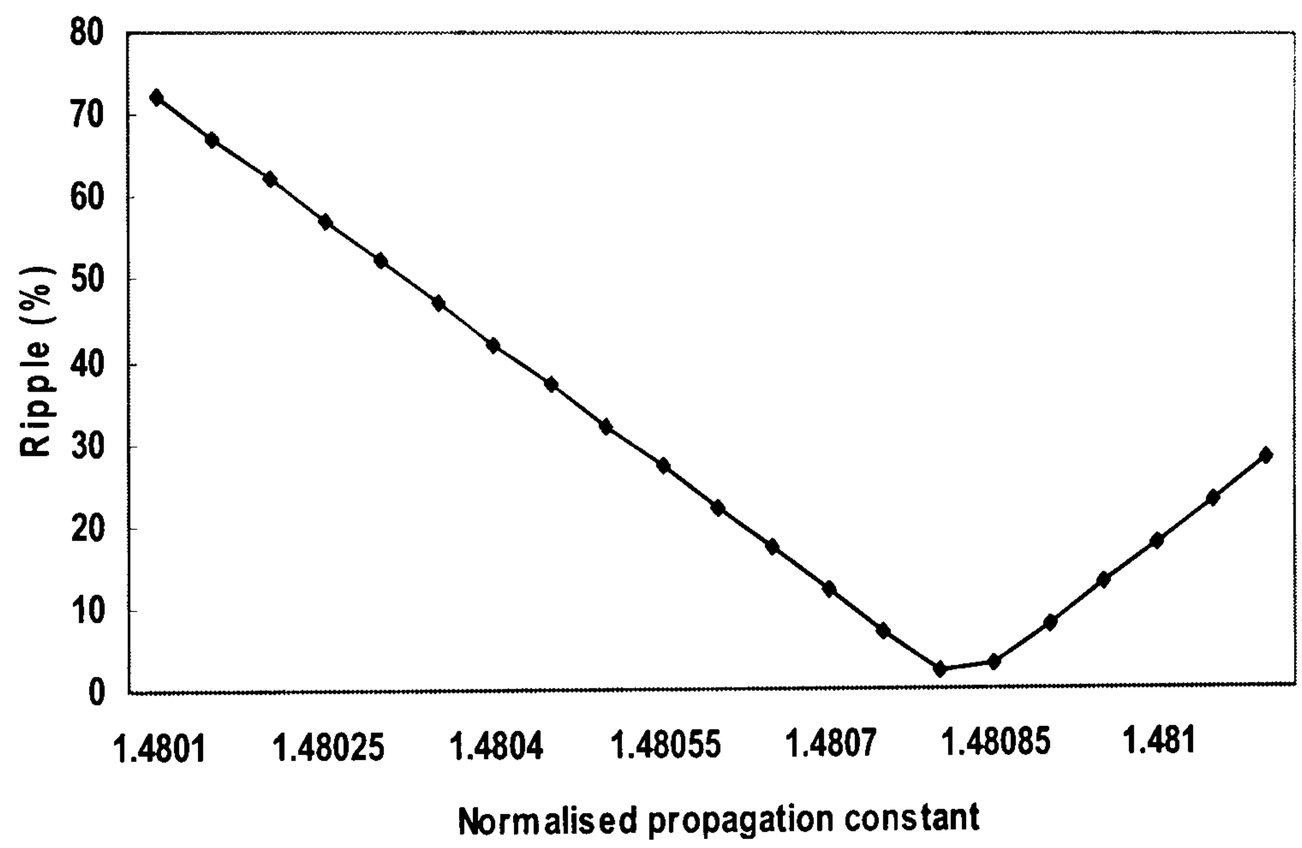

Figure 4.4 (a) The refractive index difference, error (%) of the synthesized refractive index versus values for $\bar{\beta}$ offset from the exact.

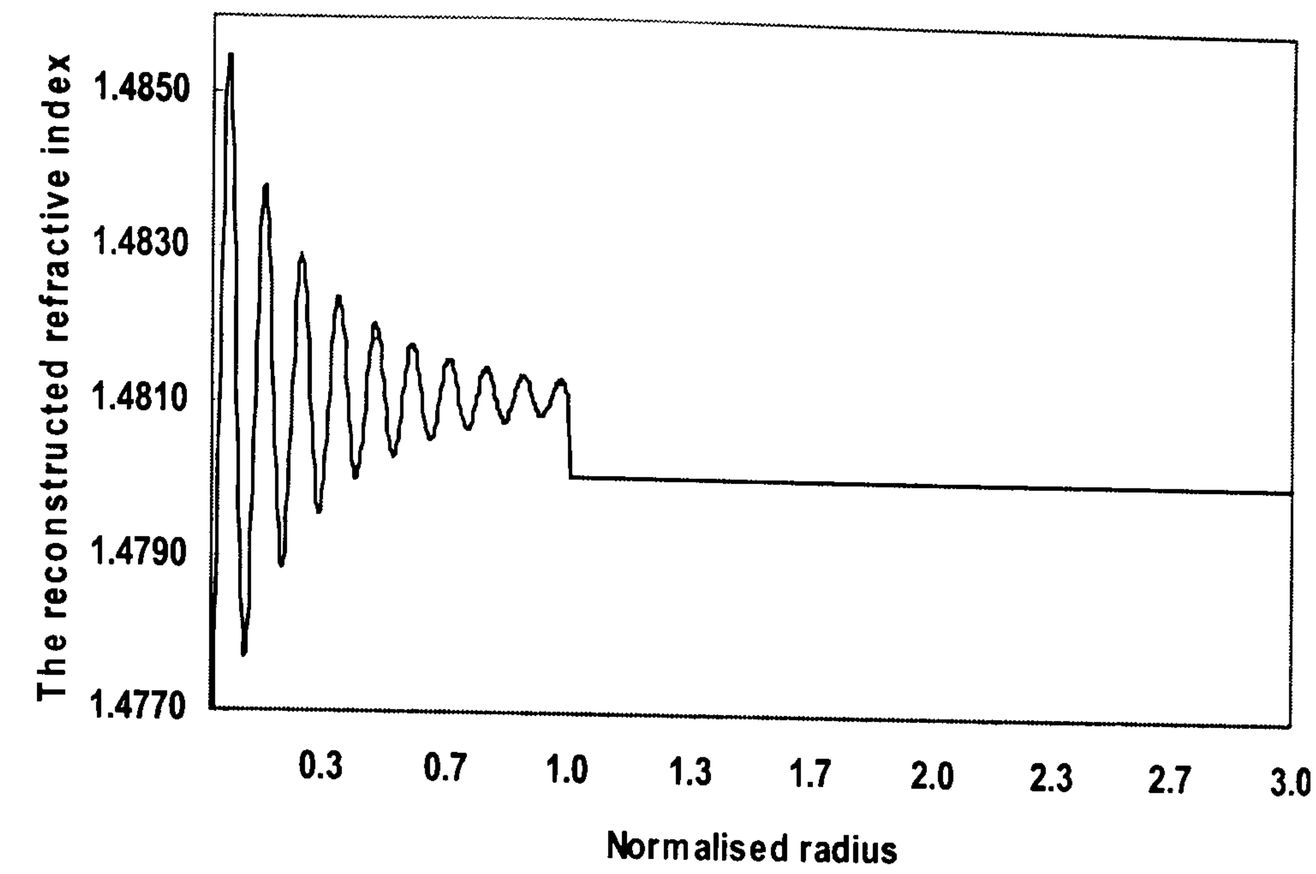

(b)

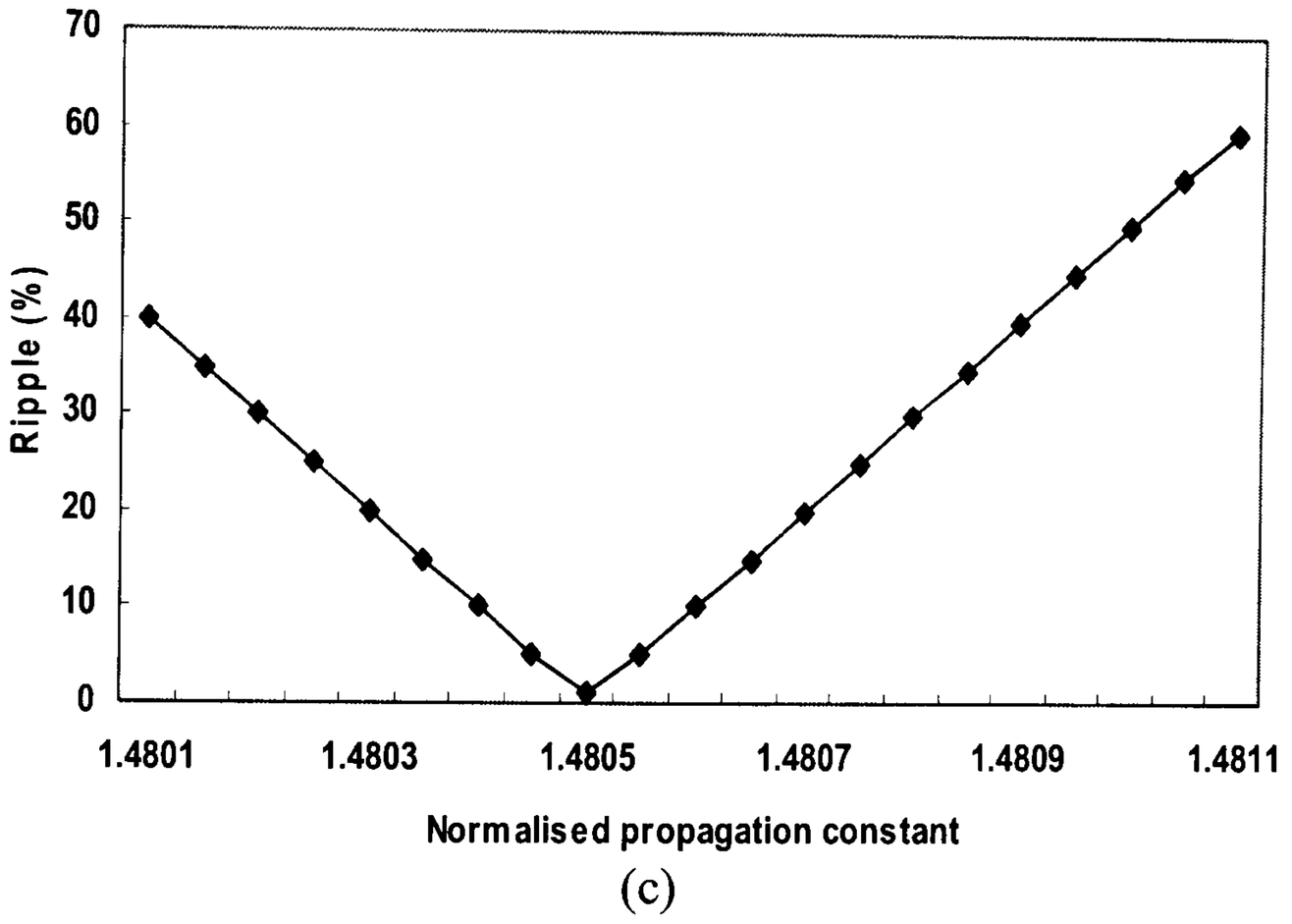

(c)

Figure 4.4 (b) The reconstructed refractive index
(c) The refractive index difference, error (%) of the synthesized refractive index versus values for $\bar{\beta}$ offset from the exact.

In another example, Fig.4.5(b) shows the reconstructed segmented refractive index profile obtained from the electric field of HE_{11} mode as shown in Fig.4.5(a). The high degree of accuracy of the reconstruction is demonstrated in Fig.4.5(c), where the % error in Δn is shown. The % error is less than 1.6%.

Finally, Fig.4.6(b) shows the example reconstruction of a parabolic refractive index profile from the HE_{11} mode electric field of Fig.4.6(a). Fig.4.6(c) shows the % error in Δn which is less than 0.06%. Clearly the parabolic index profile optical fibre is less demanding in reconstruction than the step and segmented index profile optical fibres.

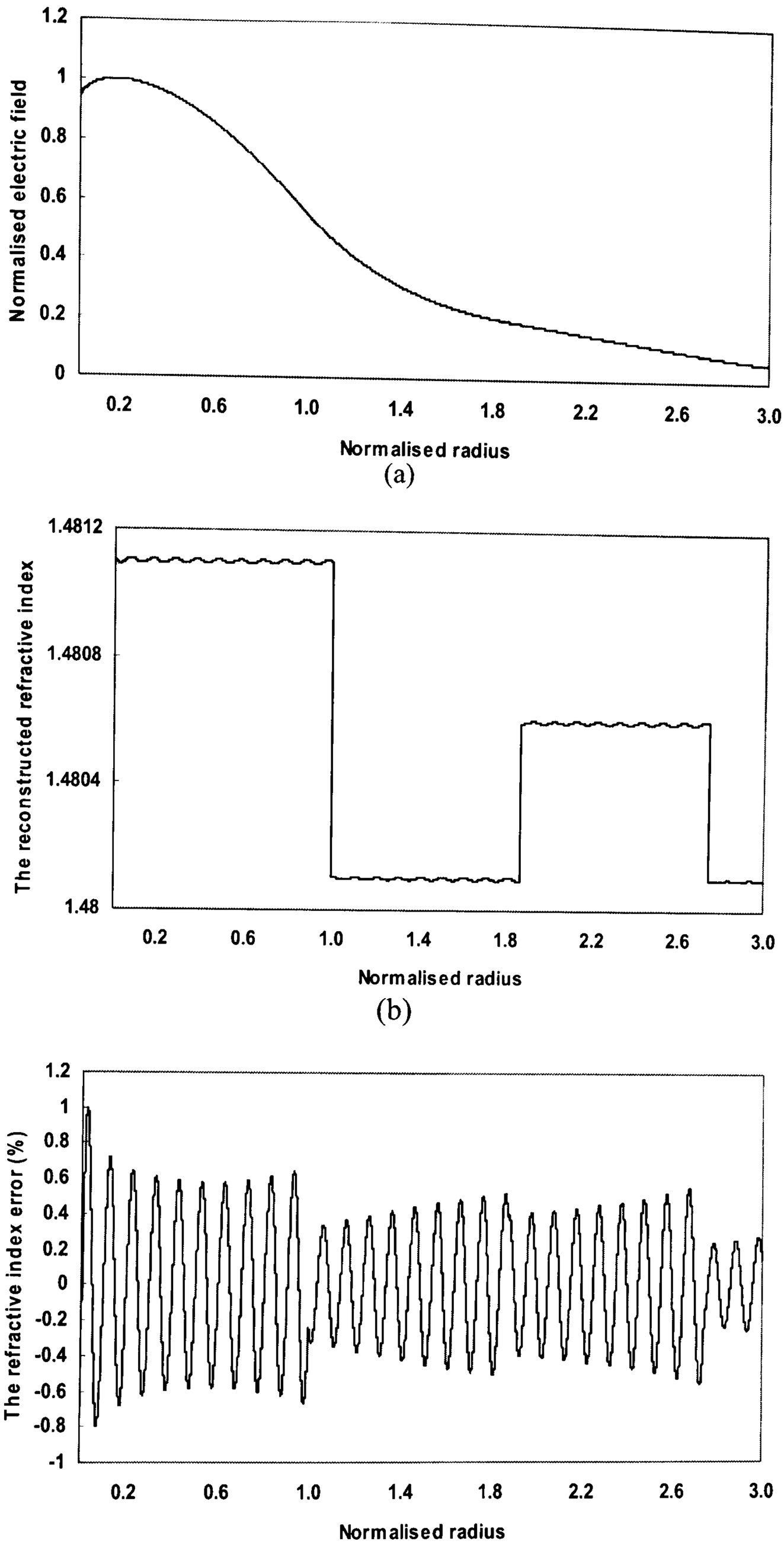

Figure 4.5 (a) Electric field plot of HE_{11} mode from a segmented index profile optical fibre with core radius a_1 =4.583 μm, inner cladding radius a_2 =8.685 μm, outer cladding radius a_3 =1.315 μm, core index n_1=1.4811, cladding index n_2 =1.4801, n_3=1.4806, and V=2.5 **(b)** Example of a reconstructed segmented refractive index profile from the electric field **(c)** The refractive index difference, error (%) of the synthesized segmented refractive index of Fig. 4.5(b).

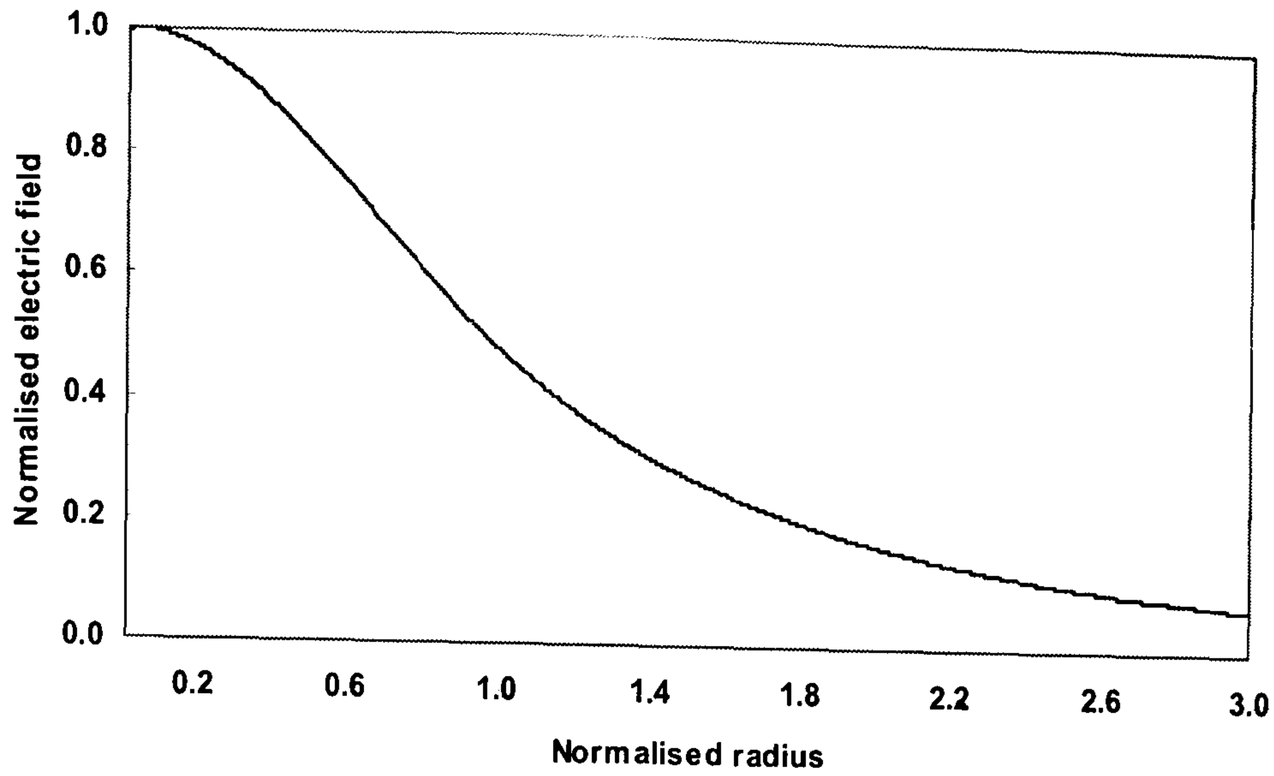

(a)

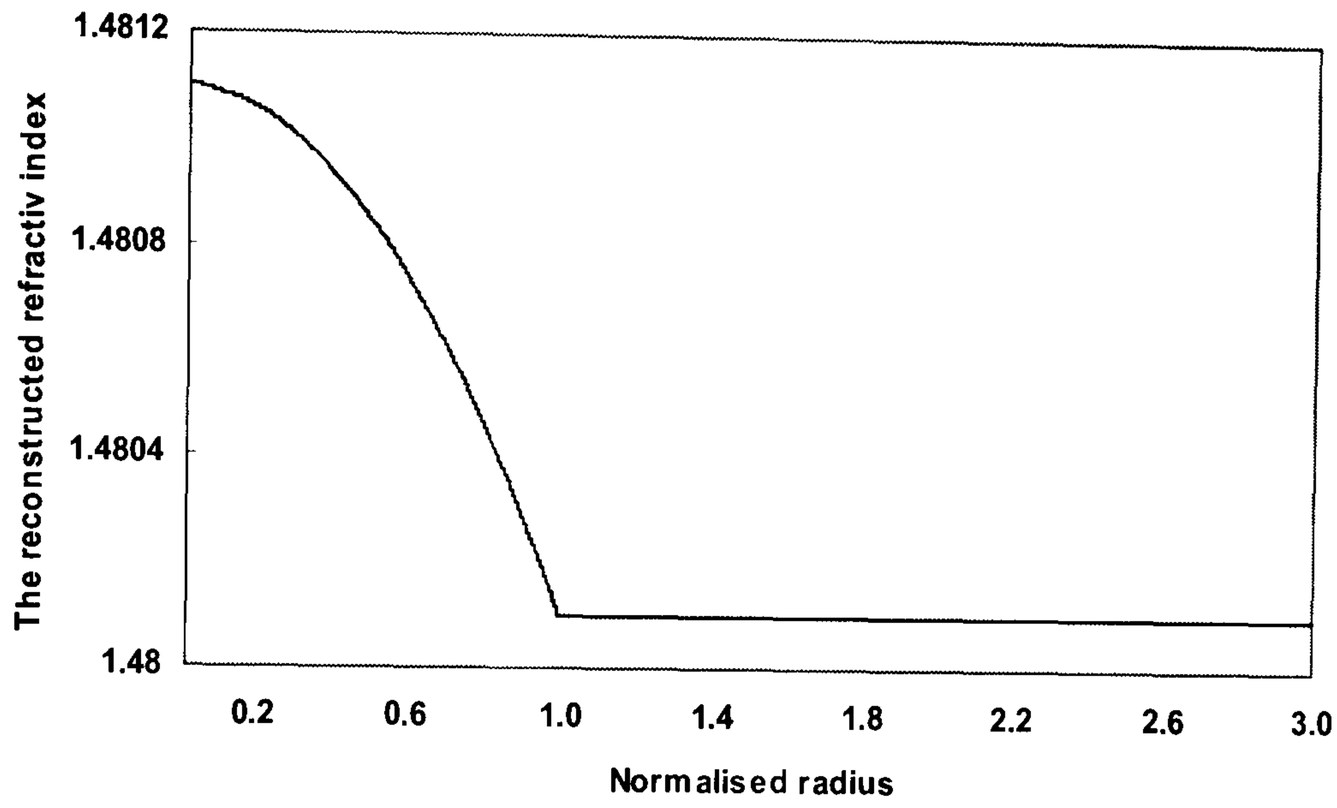

(b)

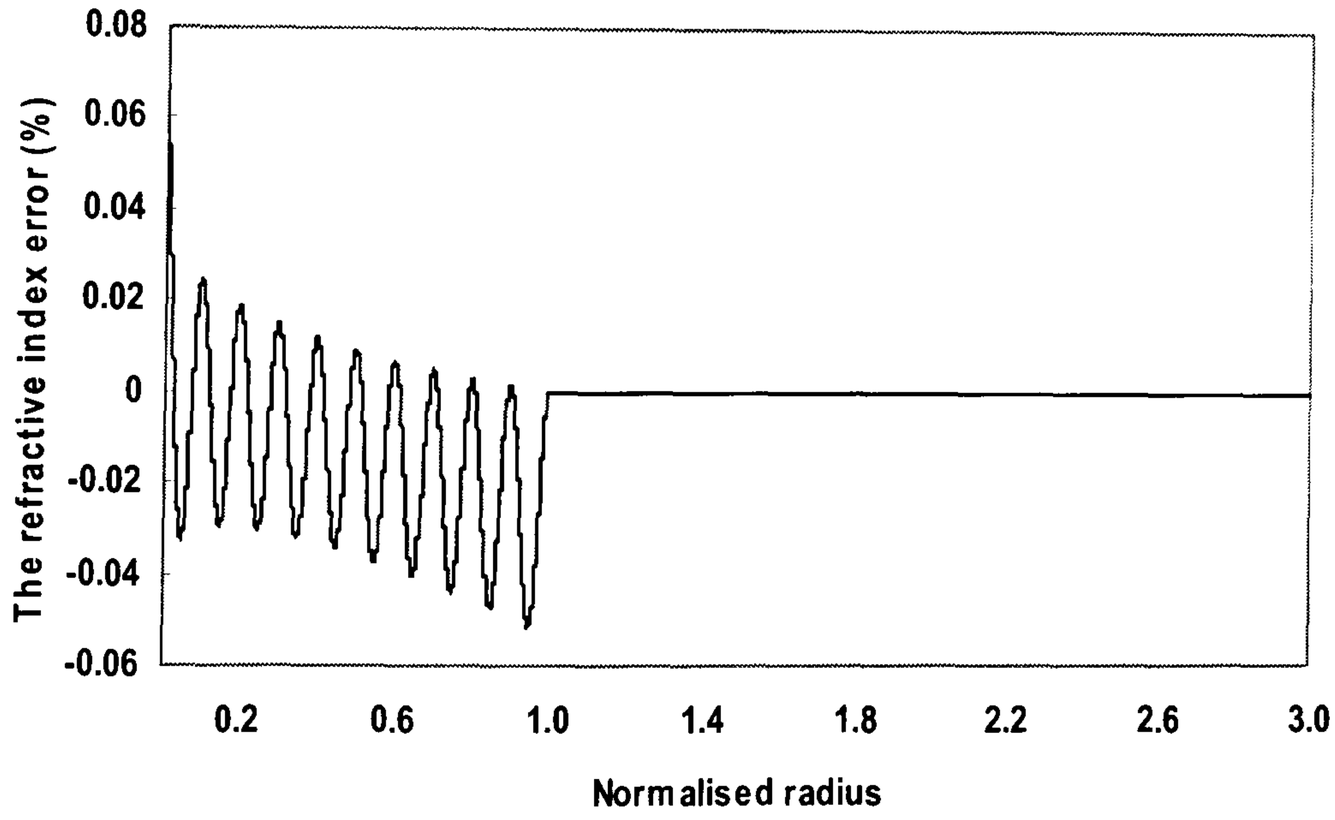

(c)

Figure 4.6 (a) Electric field plot of single-mode parabolic index profile optical fibre with core radius a_1 =4.583 μm, core index n_1=1.4811, cladding index n_2 =1.4801, and V=2.5

(b) A parabolic refractive index reconstruction from the electric field.

(c) The refractive index difference, error (%) of the synthesized parabolic refractive index of Fig.4.6(b).

In order to illustrate further the power of the inverse *TL* technique, optical fibres with arbitrary specific electric field distributions are considered. Fig.4.7(a) shows two examples of desired triangular HE_{11} mode electric fields with different slopes. In Fig.4.7(b), we can see the refractive index reconstructions supporting the fields. It is demonstrated that the inverse *TL* method can reconstruct the refractive index profiles successfully for these special electric fields. In Fig.4.7(c), the cladding index has been forced to be constant n_2. This is allowed with the inverse *TL* technique and results in deeper grating in the core since the technique is compensating for this enforcement in a shorter radius range (core only). Fig.4.8(a) is another example of sigmoid electric field profiles. Sigmoid fields are very interesting because they offer mode field distributions in the core which are very flat, unlike ordinary step index fibres which support Bessel functions mode field distributions. Sigmoids show constant core field intensities. The fibre refractive index reconstructions using sigmoid electric fields are demonstrated in Fig.4.8(b). Also, the cladding index has been forced to be constant n_2. By comparing Fig.4.7(c) and Fig.4.8(b), we can see that the larger the contrast of the electric field distribution in the core and cladding, the deeper the grating in the core is.

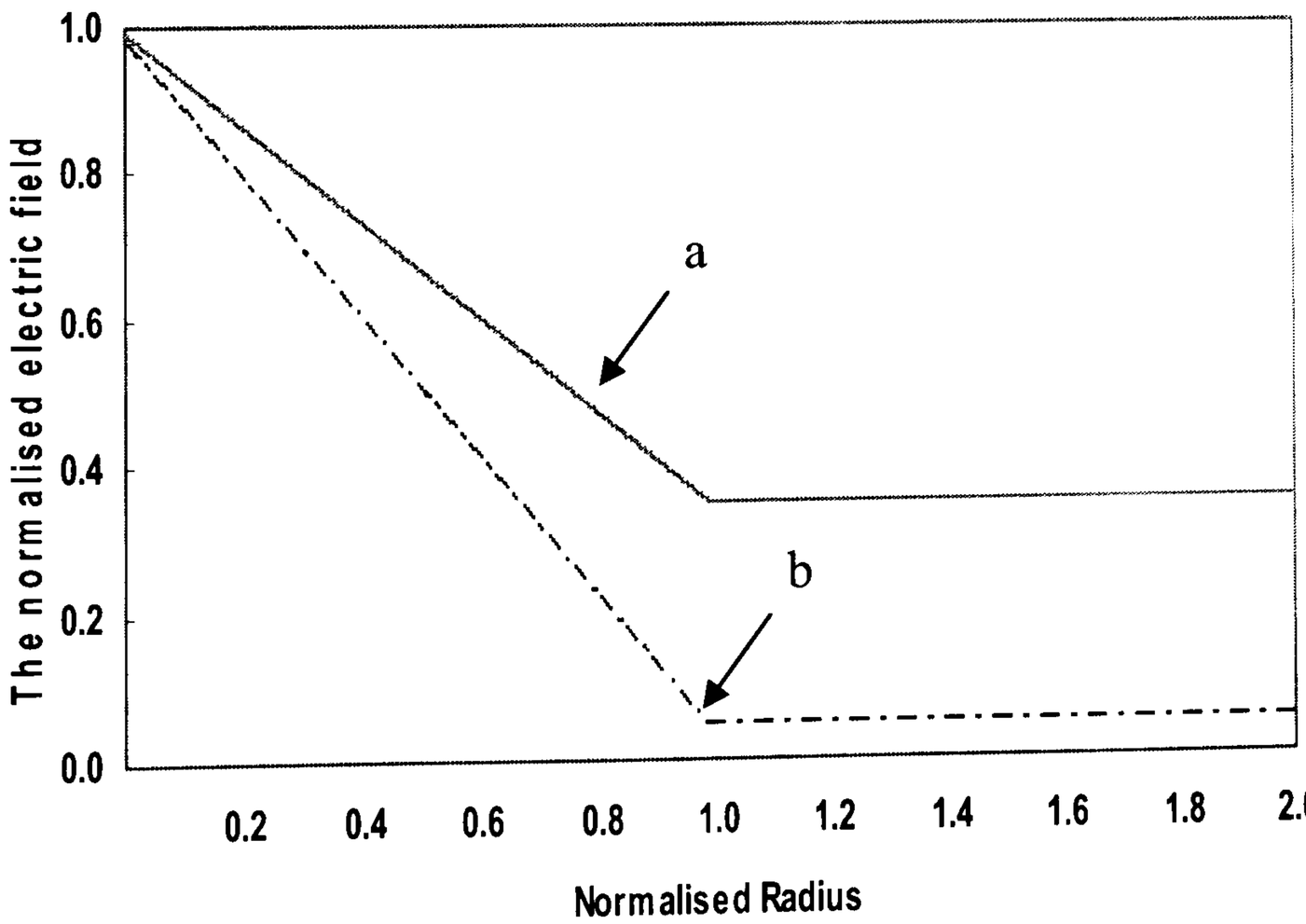

(a)

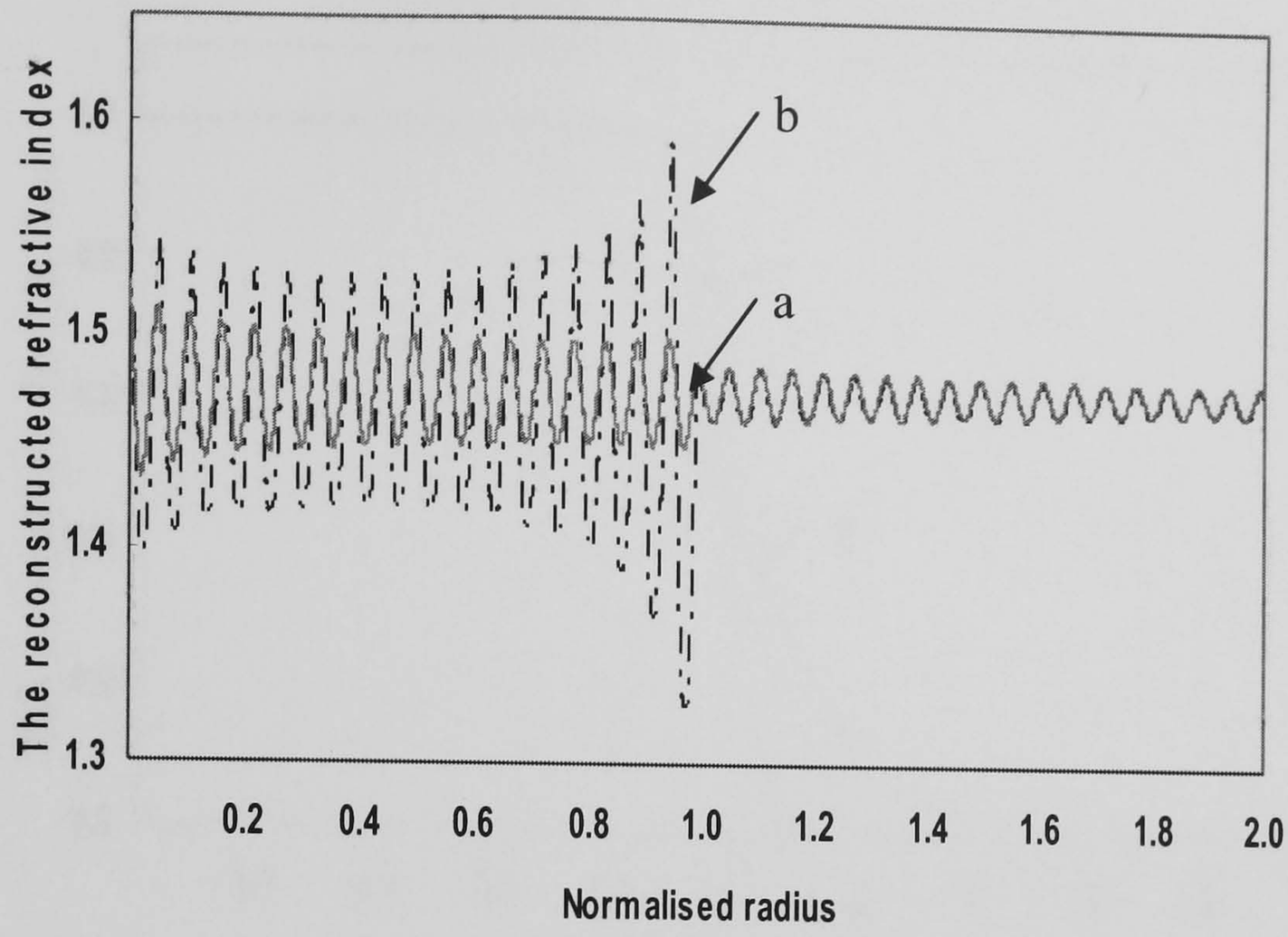

(b)

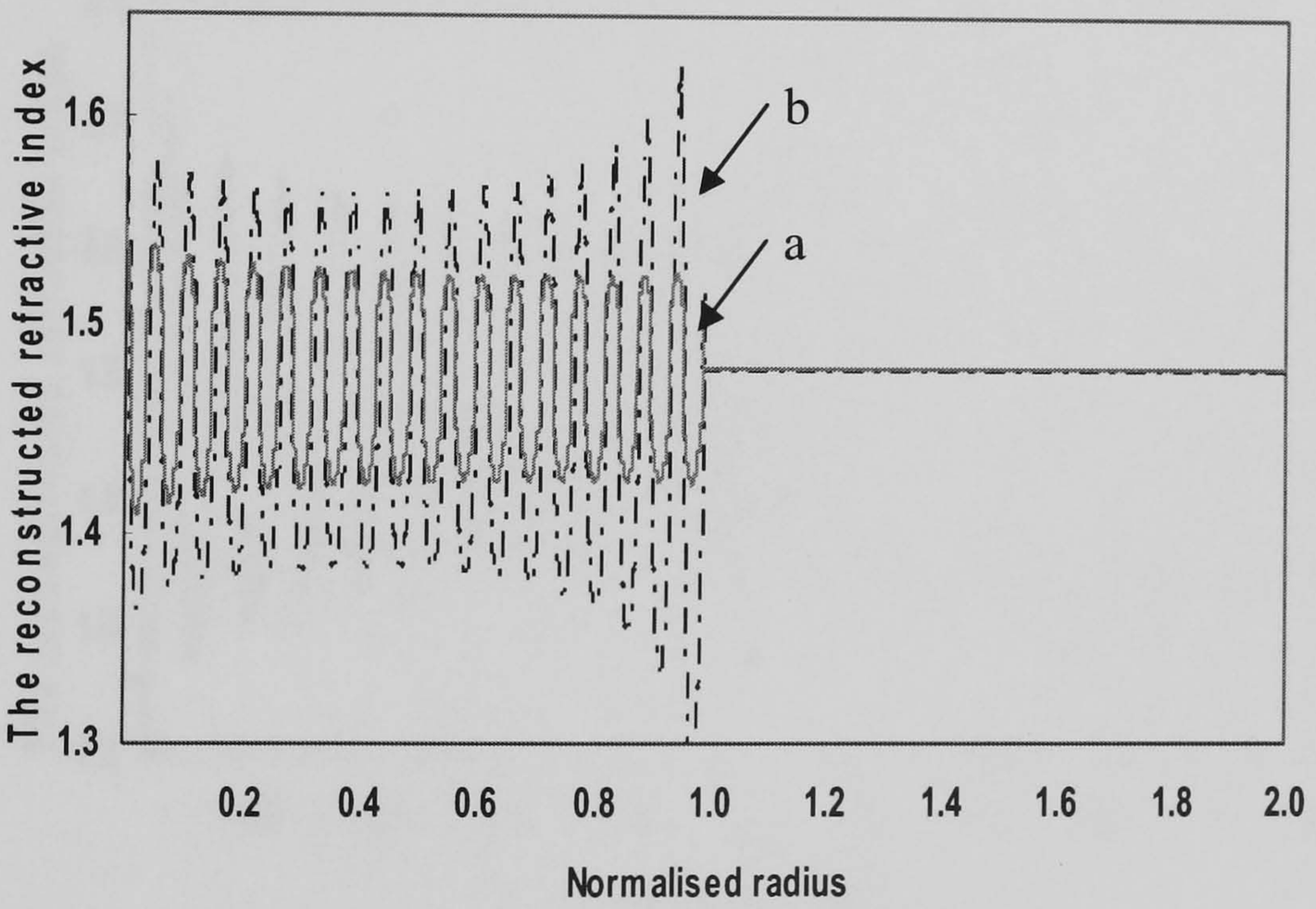

(c)

Figure 4.7 (a). Examples of HE_{11} mode electric field (triangular profile) with different slopes. **(b).**The reconstructed refractive index profiles from the triangular profile electric fields. **(c).**The reconstructed refractive index profiles with constant cladding index from the triangular profile electric fields.

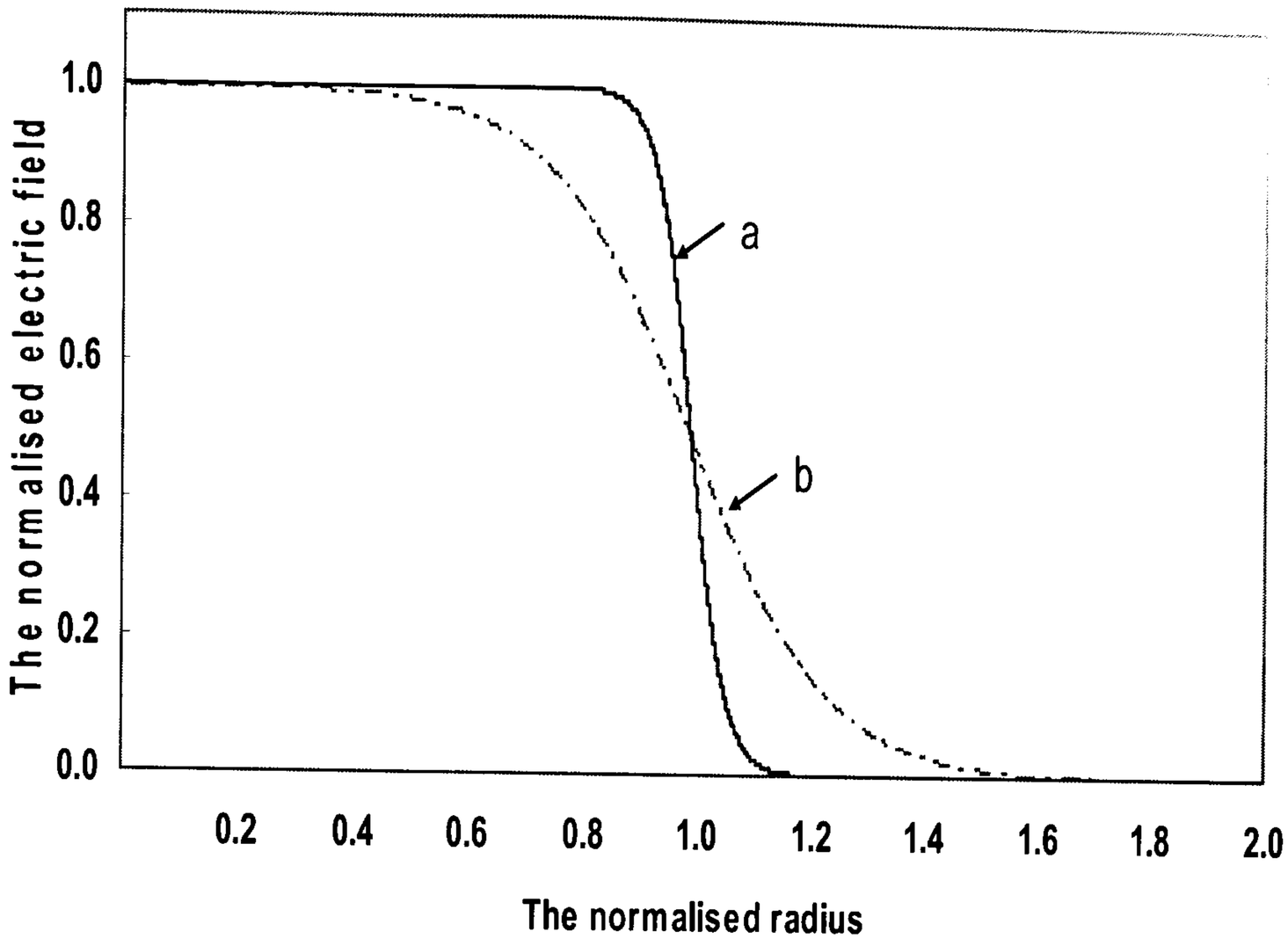

(a)

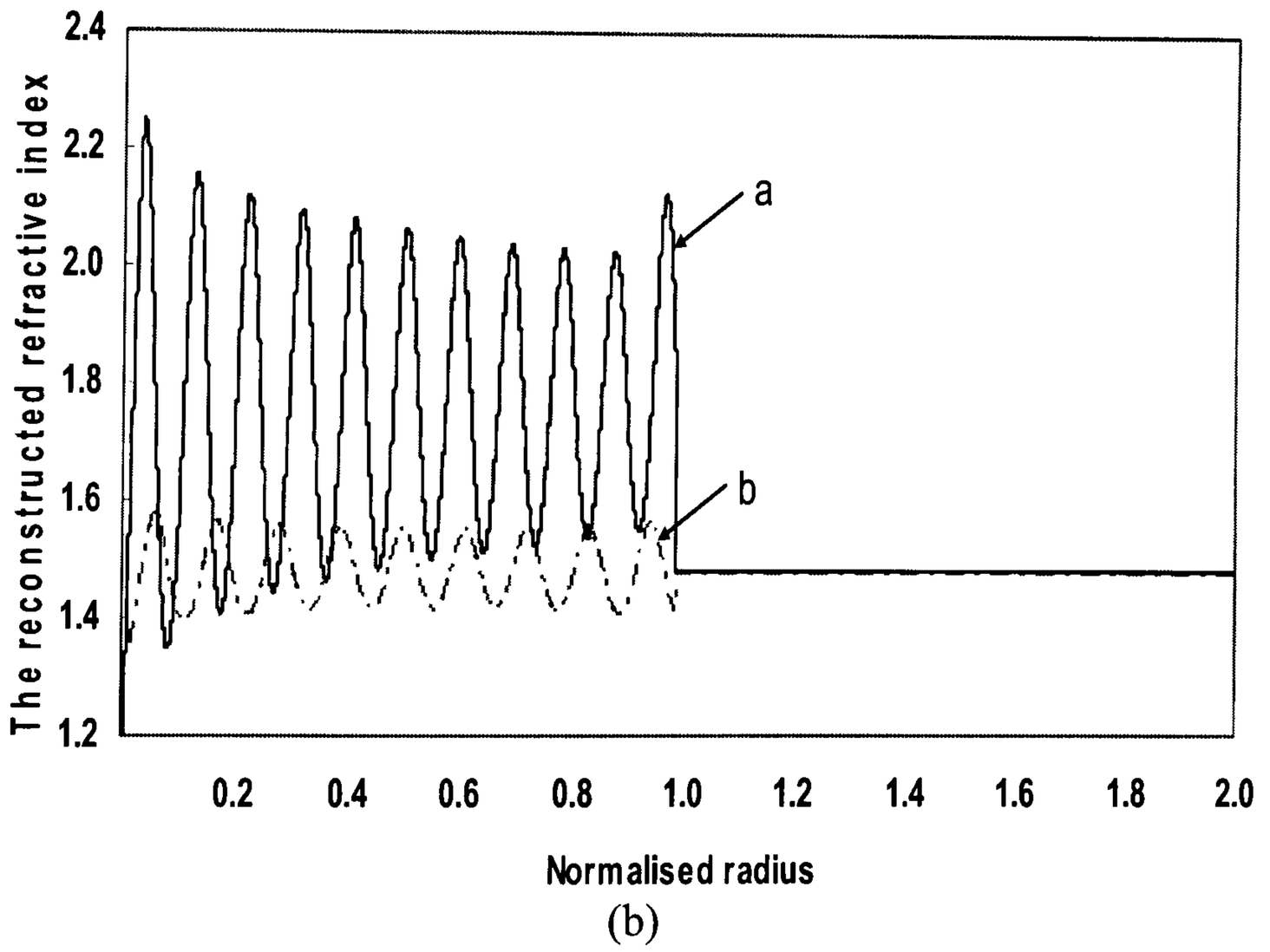

(b)

Figure 4.8 (a).Examples of HE_{11} mode electric field (sigmoid profile) with different slopes. **(b)**.The reconstructed refractive index profiles with constant cladding index from the sigmoid profile electric fields.

4.3 Refractive Index Synthesis from Higher Order Mode Electric Fields

In this section, the same refractive index profile can be reconstructed by not only using the fundamental mode electric field, but also the HE_{12} and HE_{21} higher order mode electric fields, demonstrating that the *TL* technique can be generally applied to any guided mode electric fields.

Fig.4.9 shows the exact electric field amplitude of HE_{11}, HE_{12} and HE_{21} modes of a segmented optical fibre. By using (4.4) with wave number $l = 1$ for HE_{11} and HE_{12}, and $l = 2$ for HE_{21}, the inverse *TL* method can be used to reconstruct the refractive index profile of the segmented optical fibre.

Fig.4.10(a) shows the reconstructed refractive index profile of a segmented optical fibre of refractive index n_1=1.51508, n_2=1.508, and n_3=1.512 using the HE_{11} field data of Fig.4.9. In order to compare its accuracy with the original refractive index, Fig.4.10(b) shows the % error versus the normalised radius. The error in refractive index shows small oscillations about the exact value in the core. The error in the cladding is smaller.

Fig.4.10(c) shows the effect of inaccuracies in β on the ripple in the reconstructed Δn. The ripple increases by using the incorrect $\overline{\beta}$, and the minimum error can be obtained at the exact $\overline{\beta}$. At the observed minimum error ripple corresponding to the exact $\overline{\beta}$, the reconstructed refracted index is also exact.

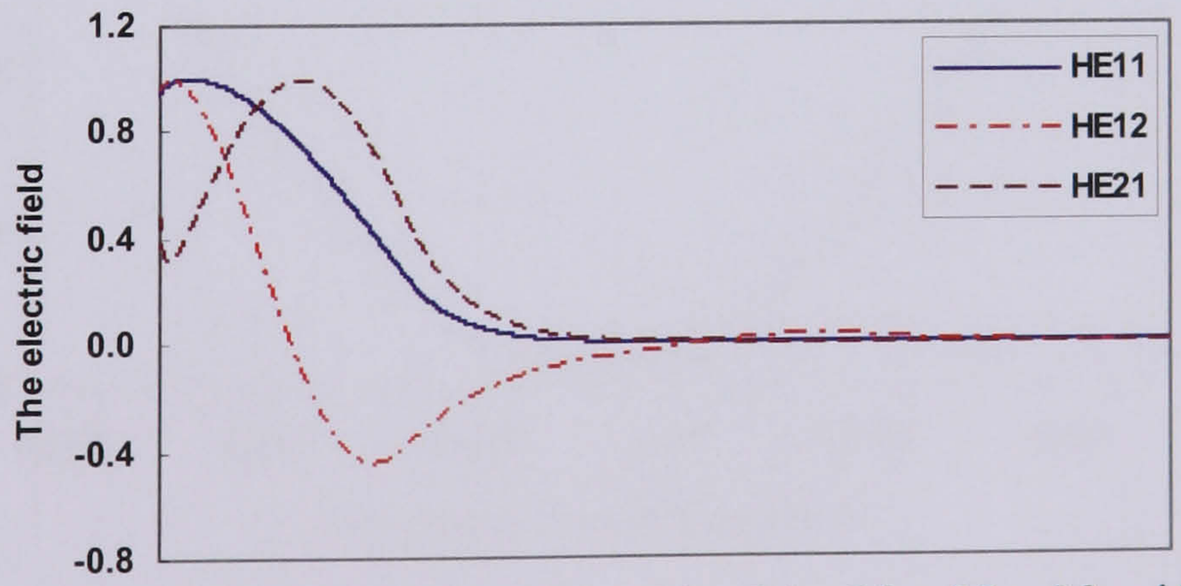

Figure 4.9 Electric field plots for HE_{11}, HE_{12}, and HE_{21} modes on the segmented index profile optical fibre with core radius a_1=4.583 μm, inner cladding radius a_2=8.685 μm, outer cladding radius a_3=1.315 μm, core index n_1=1.51508, cladding index n_2=1.508, n_3=1.512, and V=5

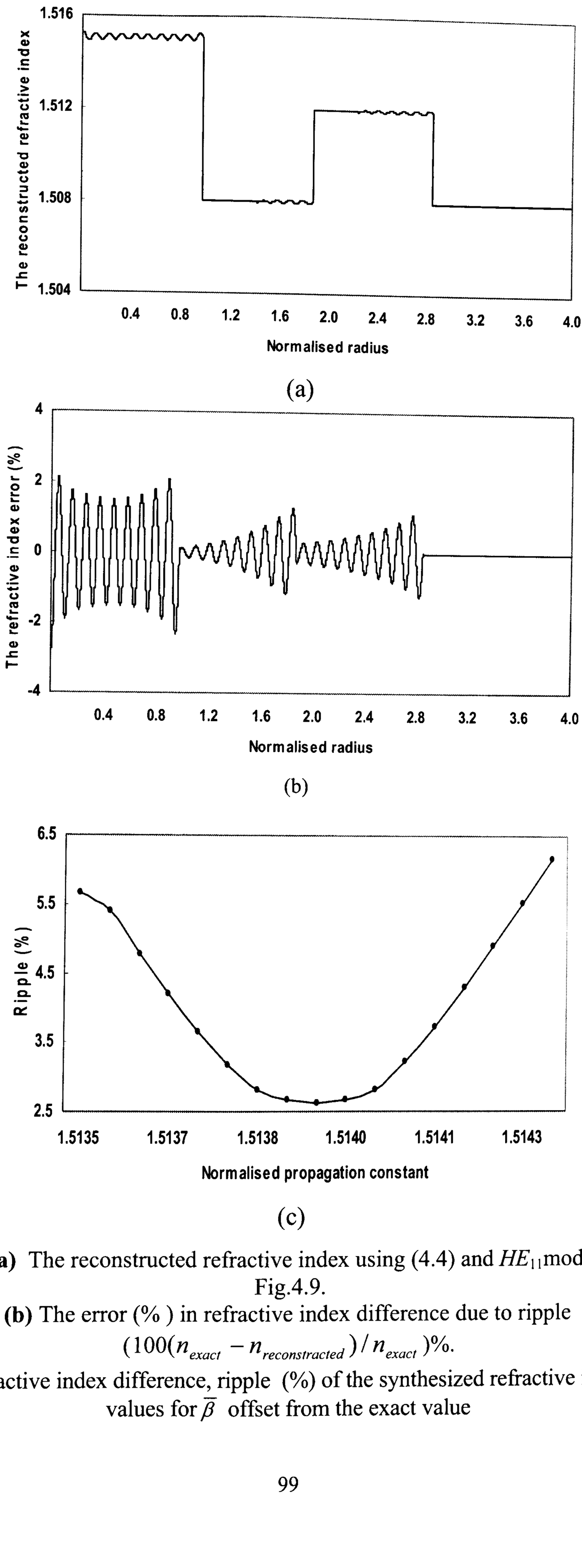

Figure 4.10 **(a)** The reconstructed refractive index using (4.4) and HE_{11}mode field data in Fig.4.9.

(b) The error (%) in refractive index difference due to ripple $(100(n_{exact} - n_{reconstracted})/n_{exact})\%$.

(c) The refractive index difference, ripple (%) of the synthesized refractive index versus values for $\overline{\beta}$ offset from the exact value

Fig.4.11(a) shows an example refractive index reconstruction for multimode segmented fibre using the HE_{12} mode electric field of Fig.4.9. The inverse *TL* method can reconstruct the refractive index profile successfully for this and other higher order mode electric fields using 30,000 homogeneous cylindrical layers. In Fig.4.11(a), we can notice that there are two spikes in the reconstructed refractive index profile. The reason is because the HE_{12} mode field goes to zero at these radii (divided by zero). We can also reach the same conclusion from the equation (4.4). The good accuracy of the index reconstruction using the HE_{12} mode is demonstrated in Fig.4.11(b), where the % error in Δn is shown. The % error is less than 5%. Clearly the HE_{11} mode is less demanding in reconstructing the refractive index profile than the HE_{12} mode. Fig.4.11(c) shows the effect of inaccuracies in $\overline{\beta}$ on the ripple in the reconstructed Δn.

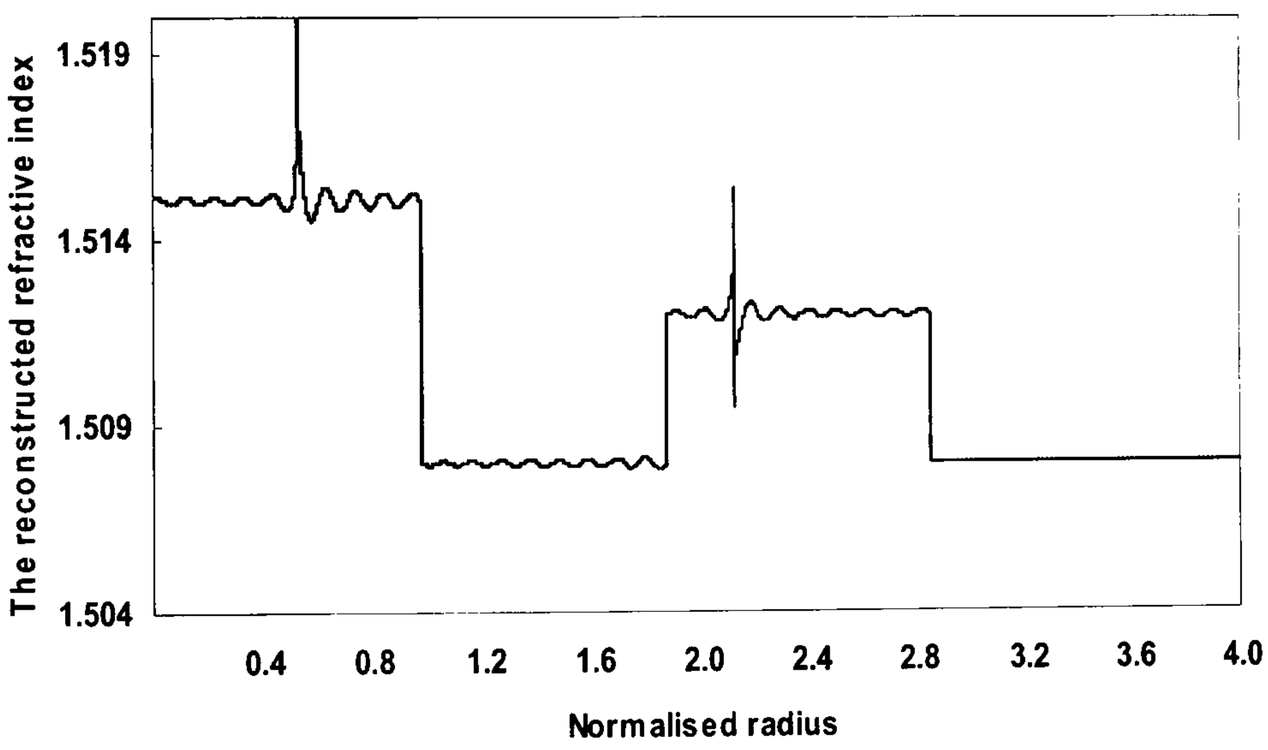

(a)

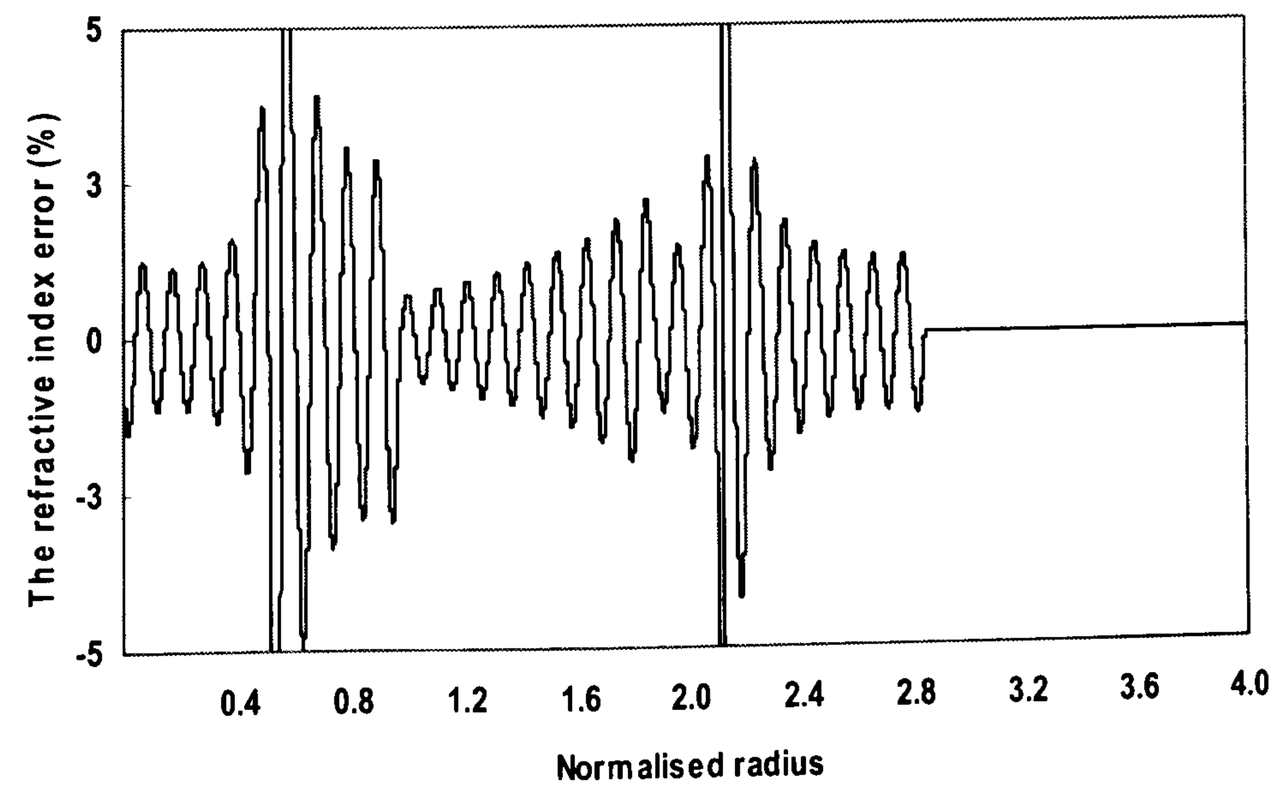

(b)

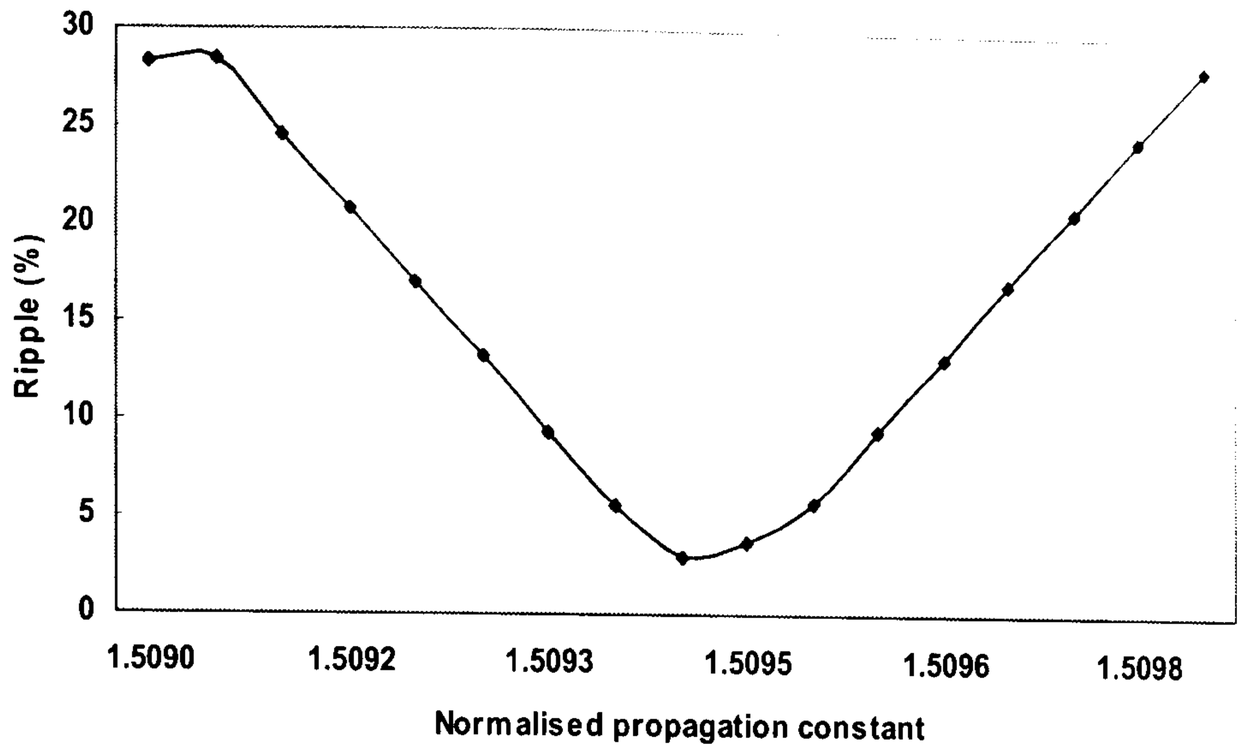

(c)

Figure 4.11 **(a)** Example of a reconstructed segmented core refractive index profile from the electric field of the HE_{12} mode Fig.4.9.
(b) The % error in the reconstructed refractive index profile, (the difference between the exact and reconstructed refractive index profile).
(c) The refractive index difference, ripple (%) of the synthesized refractive index versus values for $\overline{\beta}$ offset from the exact value

Fig.4.12(a) shows another example refractive index reconstruction for multimode segmented fibre using the HE_{21} mode electric field of Fig.4.9. The notable accuracy of the index reconstruction using the HE_{21} mode electric field is shown in Fig.4.12(b), where the % error in Δn is less than 8%. The HE_{12} mode seems to be less demanding in reconstructing the refractive index profile than the HE_{21} mode. Fig.4.12(c) also shows the effect of inaccuracies in $\overline{\beta}$ on the ripple in the reconstructed Δn.

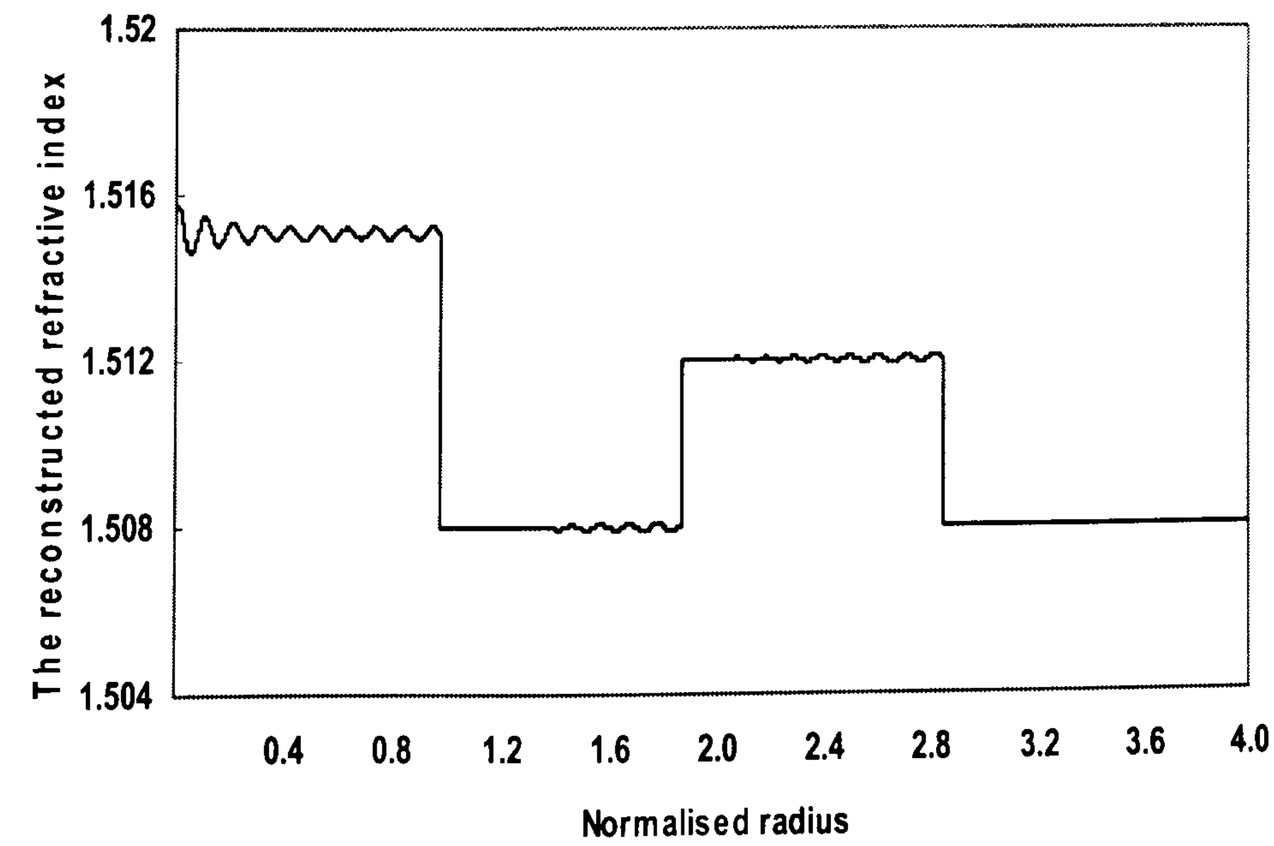

(a)

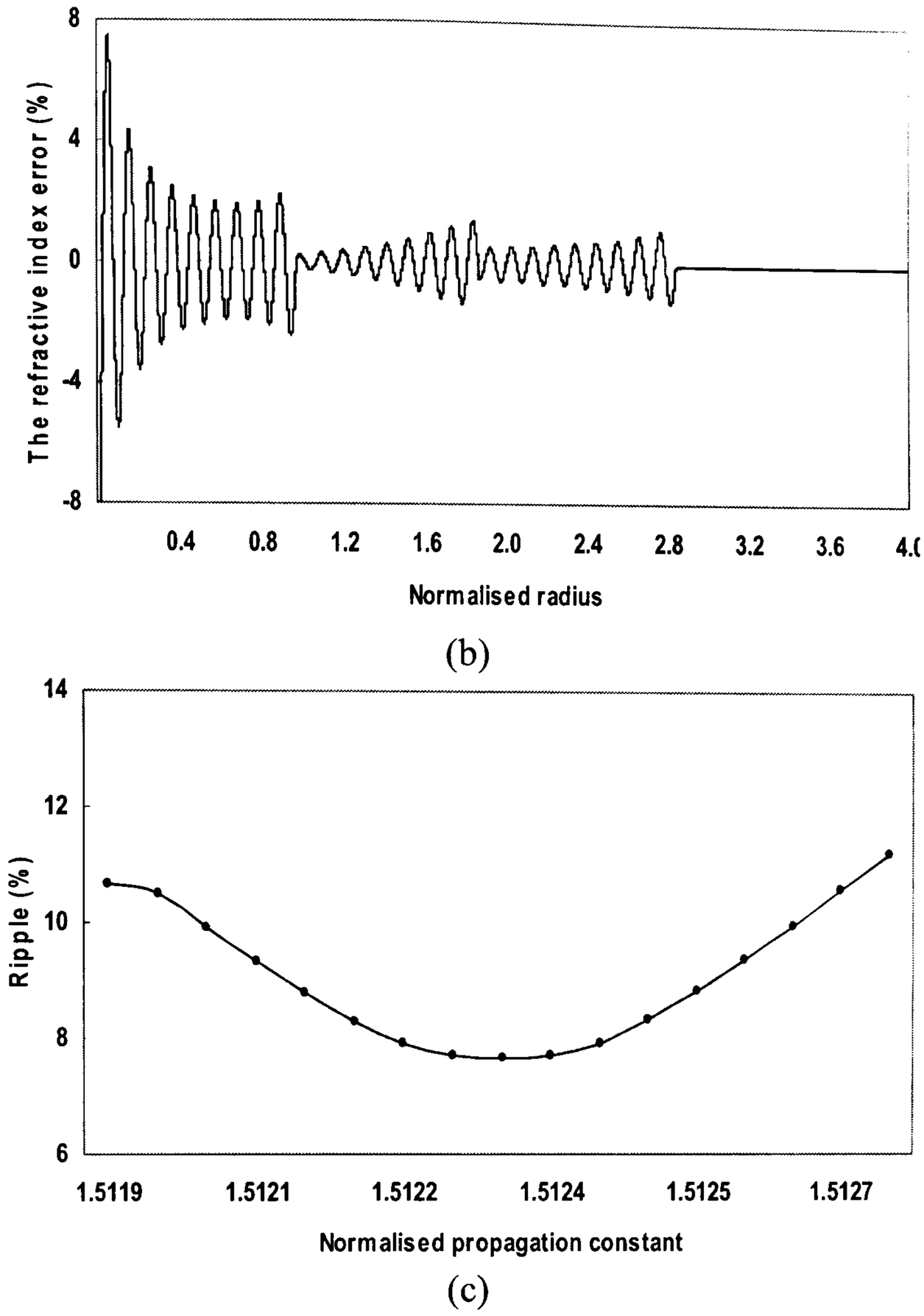

Figure 4.12 **(a)** Example of a reconstructed segmented core refractive index profile from the electric field of the HE_{21} mode Fig.4.9.
(b) The % error in the reconstructed refractive index profile, (the difference between the exact and reconstructed refractive index profile).
(c) The refractive index difference, ripple (%) of the synthesized refractive index versus values for $\overline{\beta}$ offset from the exact value

4.4 Refractive Index Synthesis from the Noisy Electric Field

In this section, to examine the possibility and accuracy of the inverse *TL* method for refractive index profiling from the noisy electric field of an optical fibre, the white Gaussian noise (*S/N*=20) is added to the original single-mode step index optical fibre electric field data. *S/N* is the signal to noise ratio. The noisy HE_{11} mode electric field is shown in Fig.4.13(a). The next step is to compare the refractive index reconstruction results both from the noisy field and the smoothed field, as well as the effect of the smoothing filter can affect the inverse *TL* technique results. Here, the least squares smoothing filter (also called digital smoothing polynomial filter) is applied. It is typically used to "smooth out" a noisy signal. Fig.4.13(b) shows the smoothed field obtained by using a polynomial filter.

Since the noisy mode electric field in the cladding is asymptotic to zero, the refractive index reconstruction result is very sensitive to the noisy electric field distribution in the cladding of the optical fibre. To examine how the noisy electric field distribution in the core and cladding affect the refractive index reconstruction results, the refractive index is to be reconstructed from two directions; one direction is from the cladding to the core of the optical fibre, and the other direction is from the core to the cladding. Fig.4.14(a) shows the reconstructed refractive index error of single-mode step index optical fibre against the *S/N* for the direction from the cladding to the core, while Fig.4.14(b) shows the reconstructed refractive index error against the *S/N* for the direction from the core to the cladding. In fact, the reconstructed refractive index error of step index single-mode fibre in Fig.4.14(a) and Fig.4.14(b) decreases with the increase of *S/N* value. In this work, to demonstrate the accuracy of the inverse *TL* technique, the worst noise condition *S/N*=20 is used for the rest calculation. It can also be seen that the reconstructed refractive index error in Fig.4.14(a) is much smaller than that in Fig.4.14(b). There are two reasons that are responsible for this fact; one reason is because when the refractive index reconstruction is started from the cladding to the core, it matches the *TL* forward solution direction. In the *TL* forward solution, the electric field is plotted from the cladding to the core. The other reason is because the electric field value in the cladding is much closer to zero than the field value in the core. When the refractive index is reconstructed from the cladding to the core, the reconstructed index error is

mainly from the cladding, on the contrary when the refractive index is reconstructed from the core to the cladding, the reconstructed index error from the core is accumulated in the cladding.

For the reasons mentioned above, the direction from the cladding to the core is used to reconstruct the refractive index profile from both the noisy electric field and the smoothed electric field of the single-mode step index optical fibre. Fig.4.15(a) shows the reconstructed refractive index profile of a step index optical fibre with refractive index n_1 =1.4811, n_2 =1.4801 by using the noisy HE_{11} field data of Fig.4.13(a). In order to compare its accuracy with the original refractive index, Fig.4.15(b) shows the reconstructed refractive index % error versus the normalised radius. The error in refractive index shows small oscillations about the exact value in the core. The error in the cladding is larger. Fig.4.16(a) and (b) show that by using the least squares smoothing filter, the accurate refractive index profile can also be reconstructed from the smoothed HE_{11} mode electric field of Fig.4.13(b).

In the case of a set of examples, we can see that the % error in the computed profiles is not very sensitive to the accuracy of the measured electric field intensity distribution and smoothing using filtering. By using the efficient inverse *TL* technique presented above, even the noise in the measurements is considered, the refractive index profiles can still be successfully reconstructed without complexity or loss of accuracy.

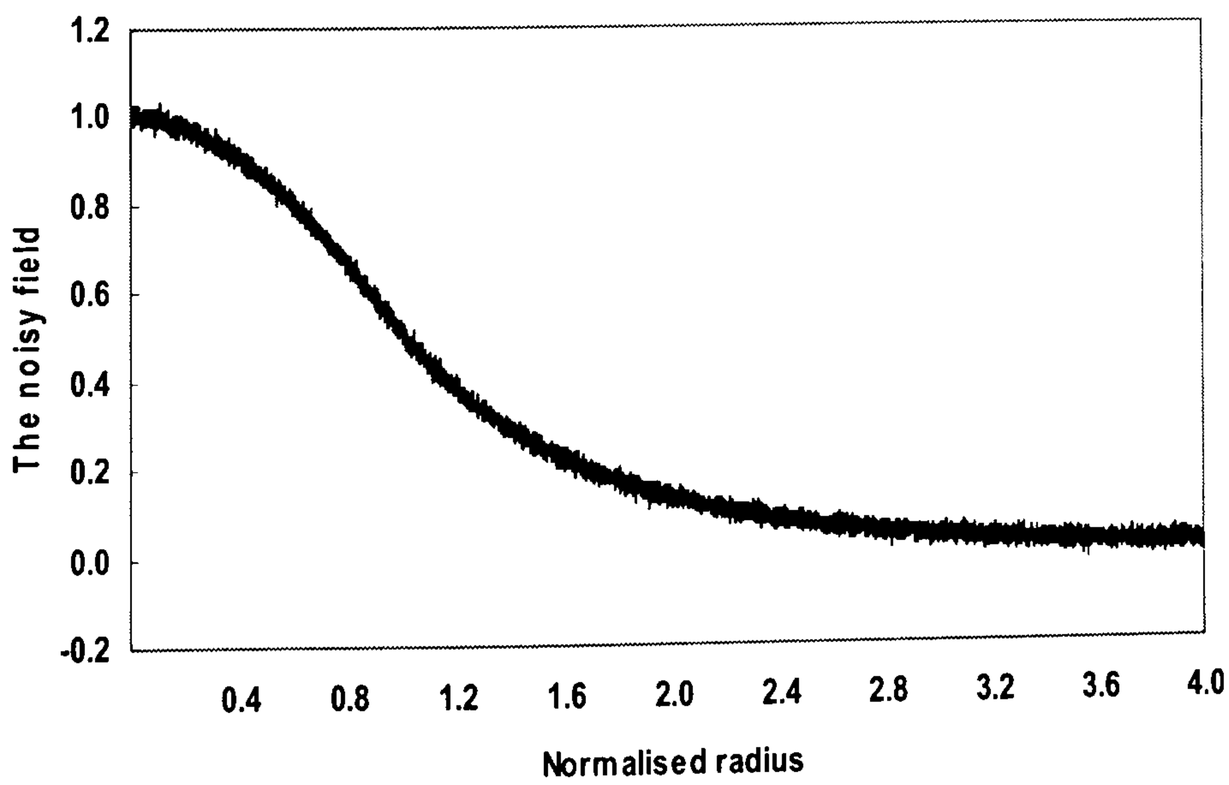

(a)

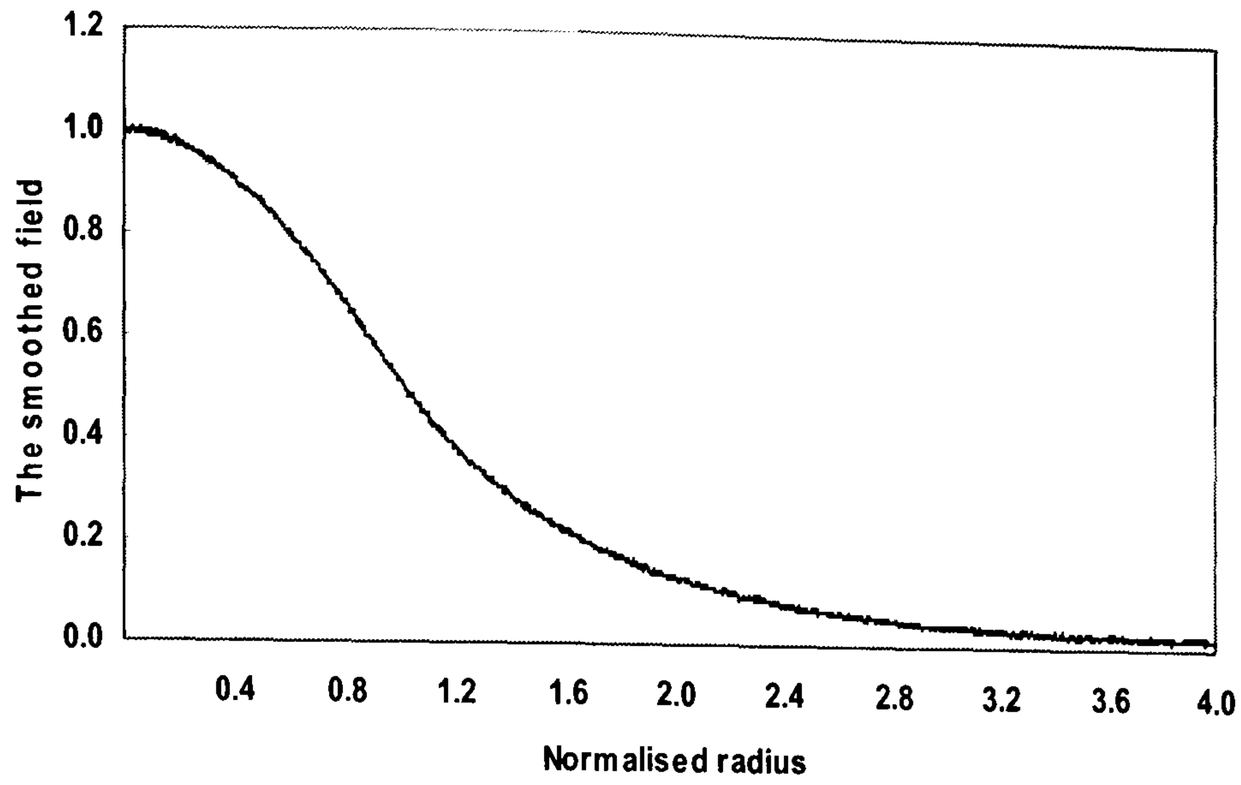

(b)

Figure 4.13 **(a)** Noisy electric field plot for single-mode step index optical fibre with core radius a=4.583 μm, core index n_1=1.4811, cladding index n_2=1.4801, and V=2.5
(b) Smoothed electric field from Fig.4.13(a) by least squares smoothing filter

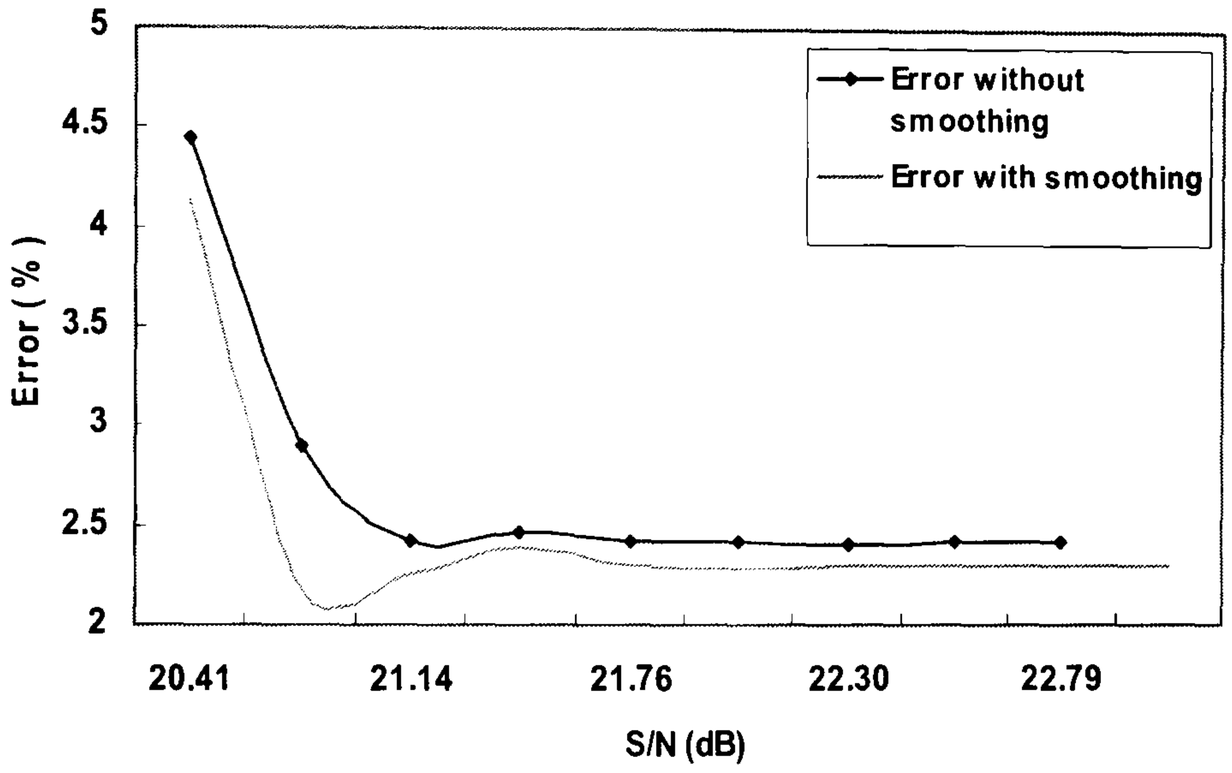

(a)

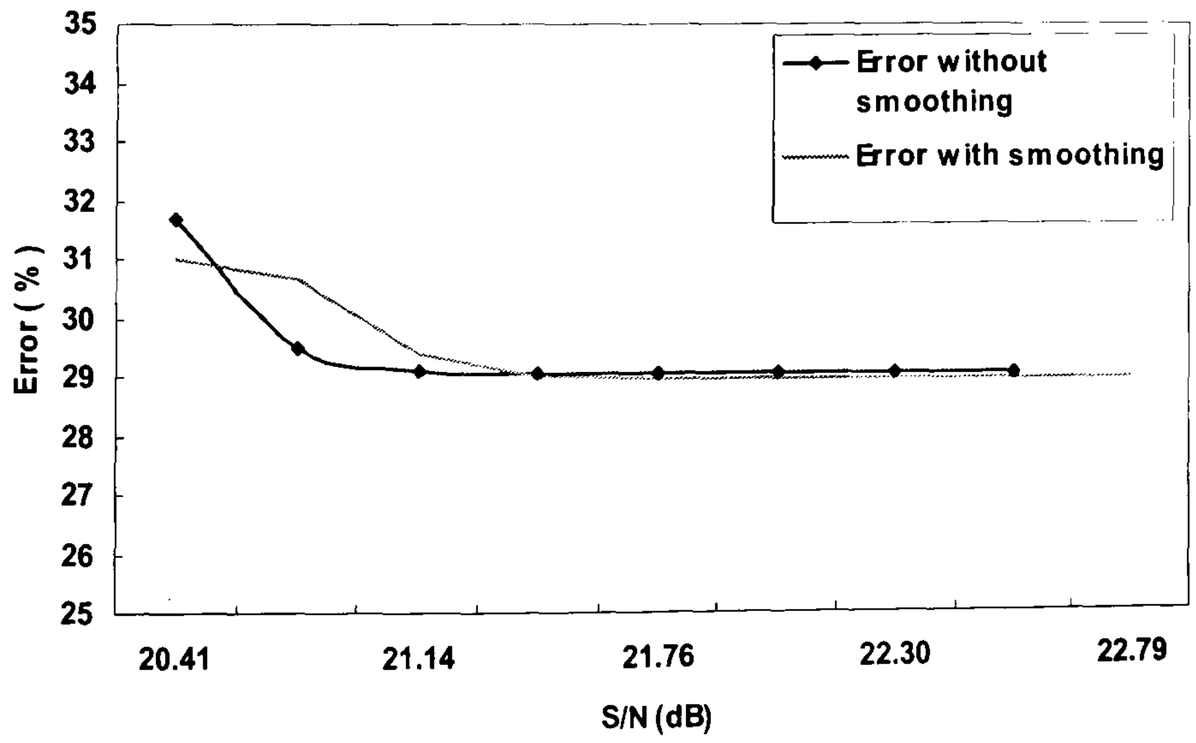

(b)

Figure 4.14 The refractive index error of single-mode step index profile optical fibre against *S/N* value, error = $[100\% \times (n_{old} - n_{new}) / (n_{core} - n_{cladding})]$, **(a)** the reconstruction direction is from the cladding to the core, **(b)** the reconstruction direction is from the core to the cladding

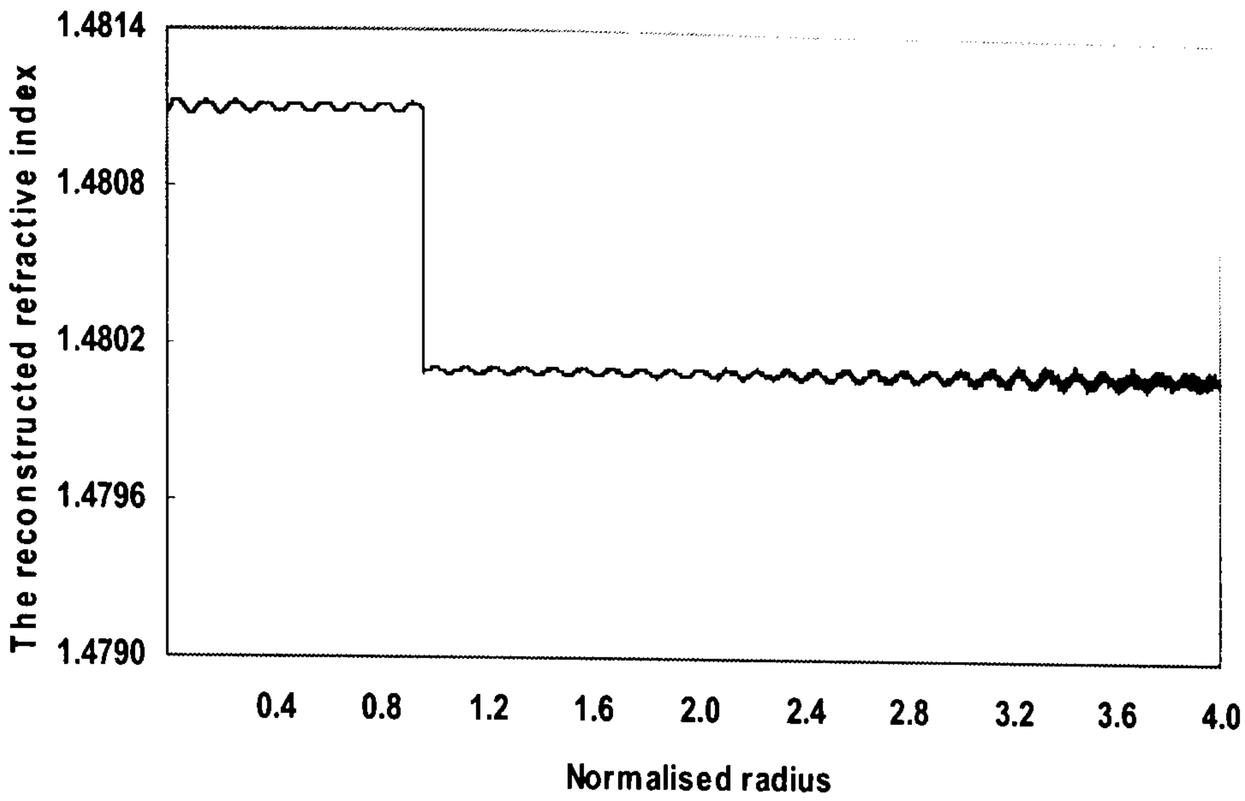

(a)

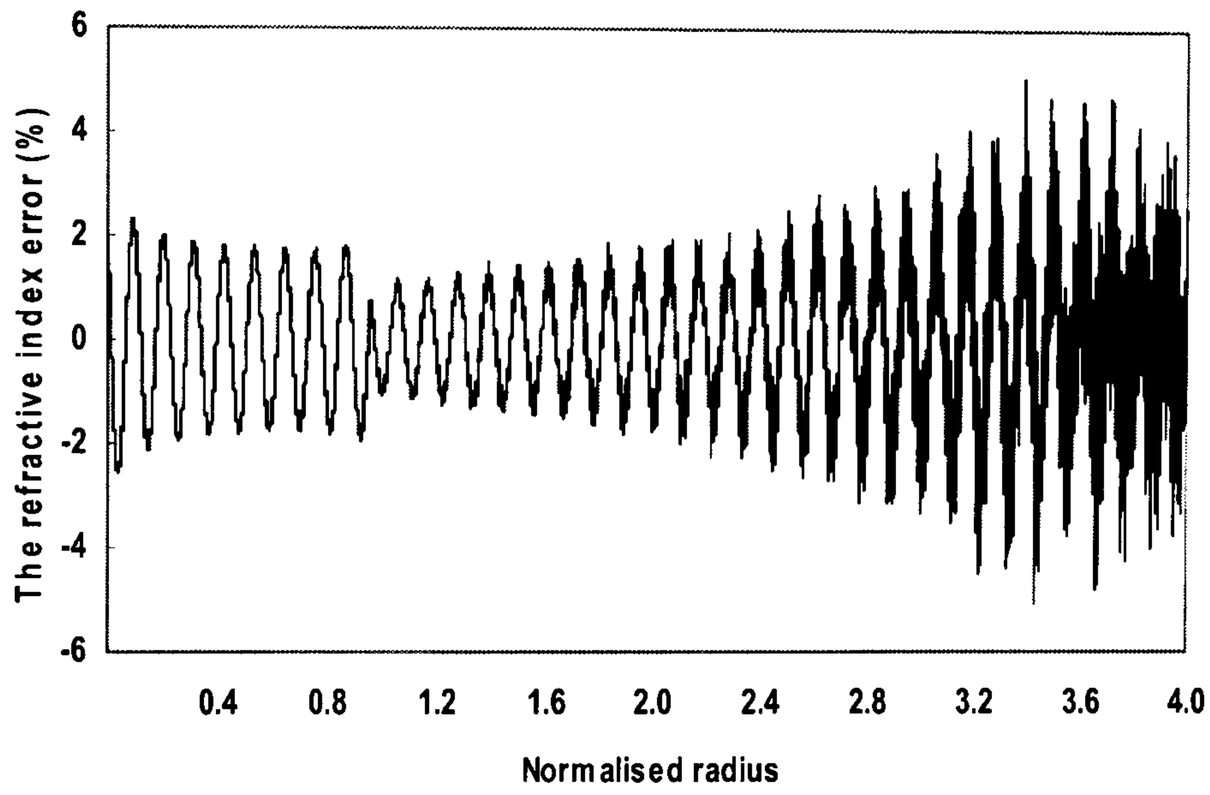

(b)

Figure 4.15 (a) Example of a reconstructed step refractive index profile from the noisy electric field of the single-mode Fig.4.13(a), at *S/N*=20
(b) The % error in the reconstructed refractive index profile, (the difference between the exact and reconstructed refractive index profile).

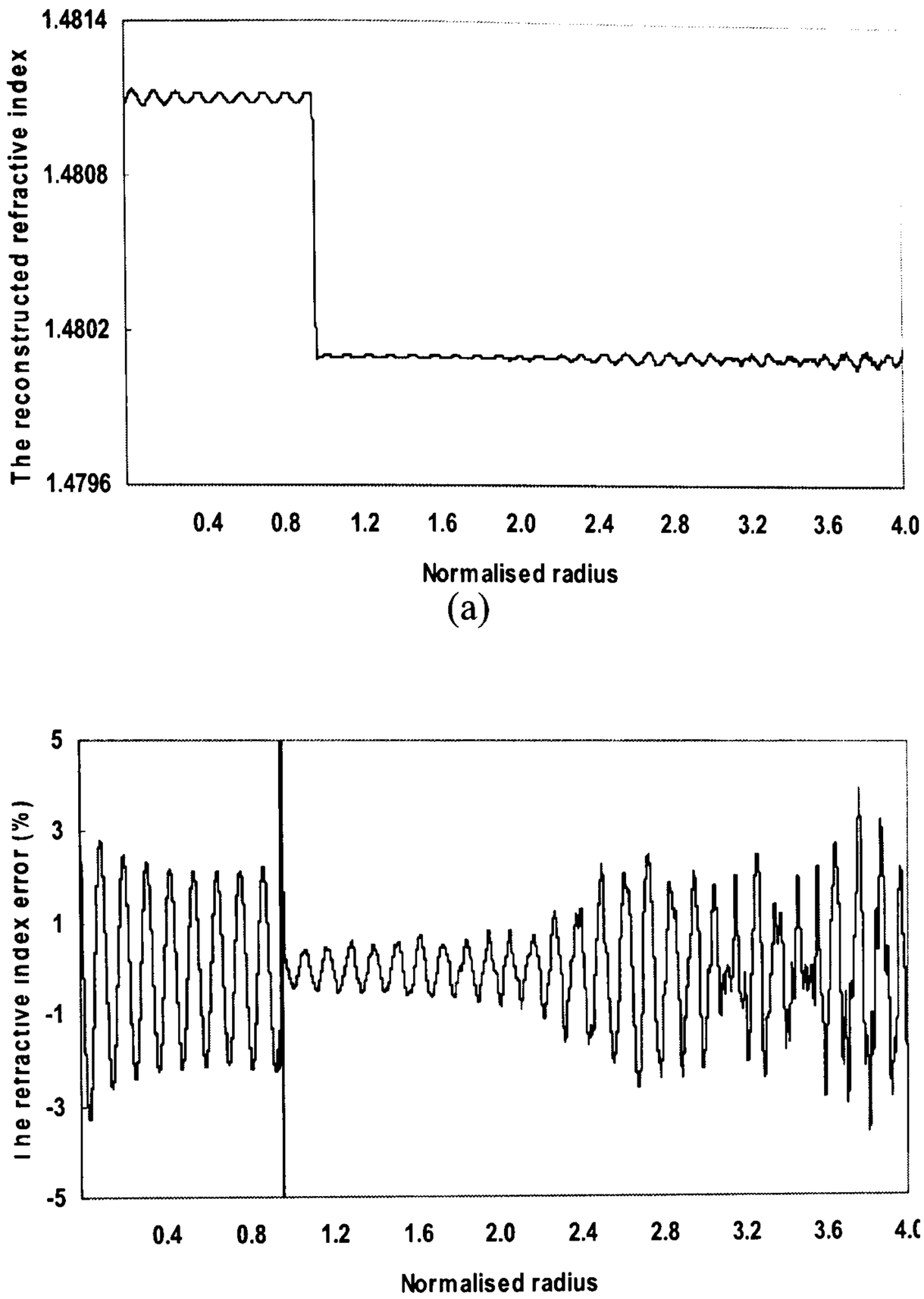

Figure 4.16 (a) Example of a reconstructed step refractive index profile from the smoothed electric field of the single-mode Fig.4.13(b), at *S/N*=20
(b) The % error in the reconstructed refractive index profile, (the difference between the exact and reconstructed refractive index profile).

4.5 Refractive Index Synthesis from the Bragg Fibre Electric Field

The calculation of Bragg fibre electric fields in the band-gap is very sensitive to the propagation constants. In order to get a decaying mode field, the propagation constant should have a high degree of accuracy, which can be obtained by finding the root to satisfy the resonance condition. It is necessary to know the Bragg fibre effective index $\overline{\beta}$ for the inverse problem. The structure of the Bragg fibre considered here is as follows: layer1 has an index of refraction n_1 =4.6 and a thickness d_1 =0.333d, whereas layer2 has an index of refraction n_2 =1.6 and the thickness d_2 =0.667d. Here, d= d_1 + d_2 is the unit length of periodicity of the multilayered structure. The Bragg fibre has a uniform core with an index of refraction n_0 =1 (air-core Bragg fibre) and a radius r_0 =1.4d.

Using (4.3), the TM_{01} electric field $E_{\bar{r}}(\bar{r})$ is plotted in Fig. 4.17(a) with parameters, effective index $\overline{\beta}$ =1.25 and V-value V=8. For high index difference, boundary matching imposes jump discontinuities at the periodic layer interfaces for $E_{\bar{r}}(\bar{r})$. For the inverse problem, applying the refractive index profile synthesis method developed in (Boucouvalas and Qian 2003), and using (4.4), together with the electric field $E_{\bar{r}}(\bar{r})$ of the TM_{01}, the Bragg refractive index profile can be synthesized directly. The result is shown in Fig.4.17(b). In order to compare its accuracy with the original refractive index, Fig.4.17(c) shows the % error versus the normalized radius. The error in refractive index shows small oscillations about the exact value in the cladding, and the values in the air core are very accurate. The oscillations in the cladding depend on the number of homogeneous cylindrical layers used for the reconstruction of the index as shown in Fig.4.18, where less than 8% error due to the ripple in Δn can be achieved with 6000 up to 10000 homogeneous layers. This could be due to the use of the approximations (3.29) instead of the exact ones (3.28), as well as the fact that the layer must be very thin in order to apply this theory accurately. To save computation time, 6000 homogeneous cylindrical layers are used in the inverse calculations.

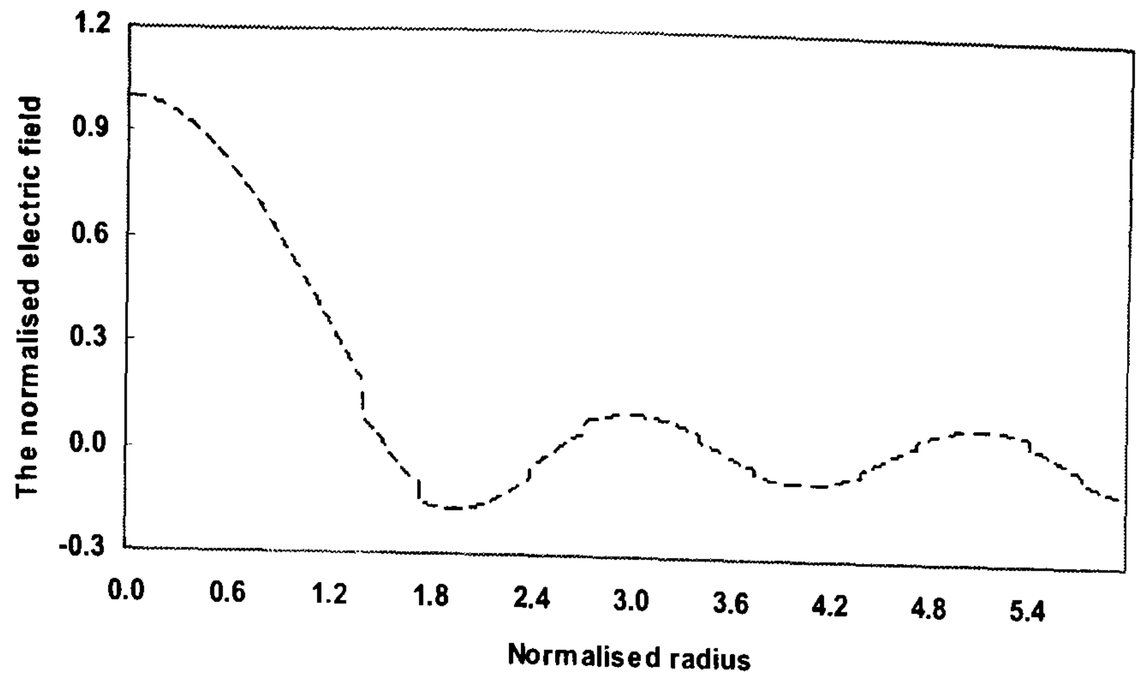

(a)

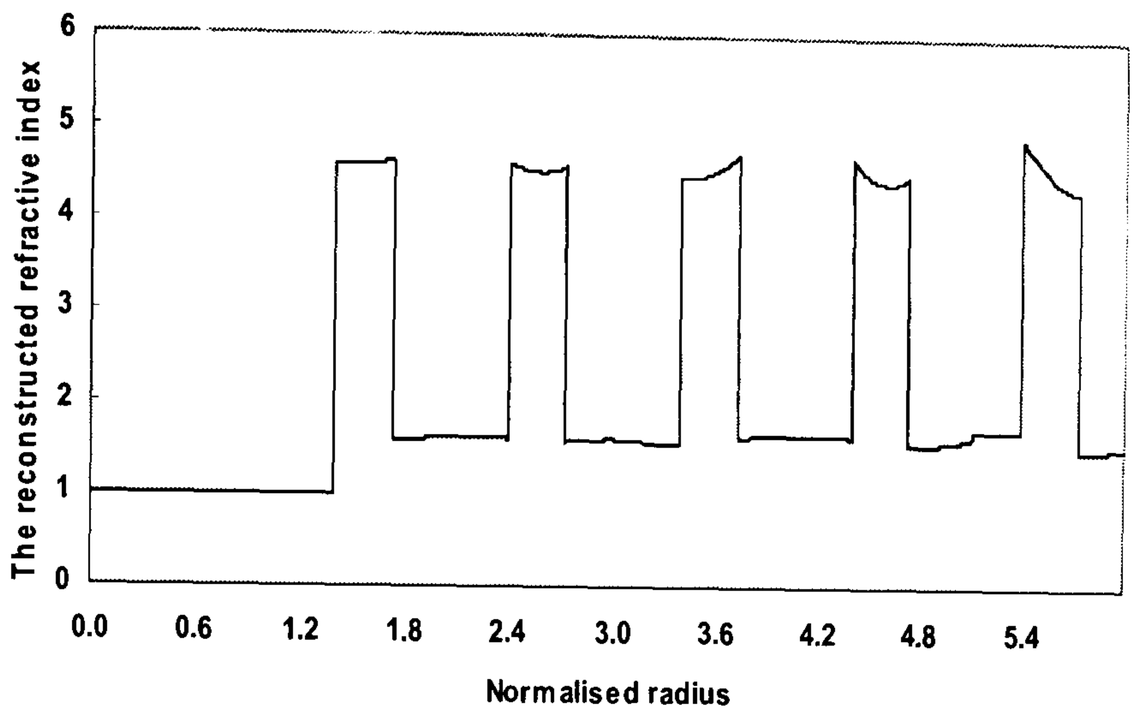

(b)

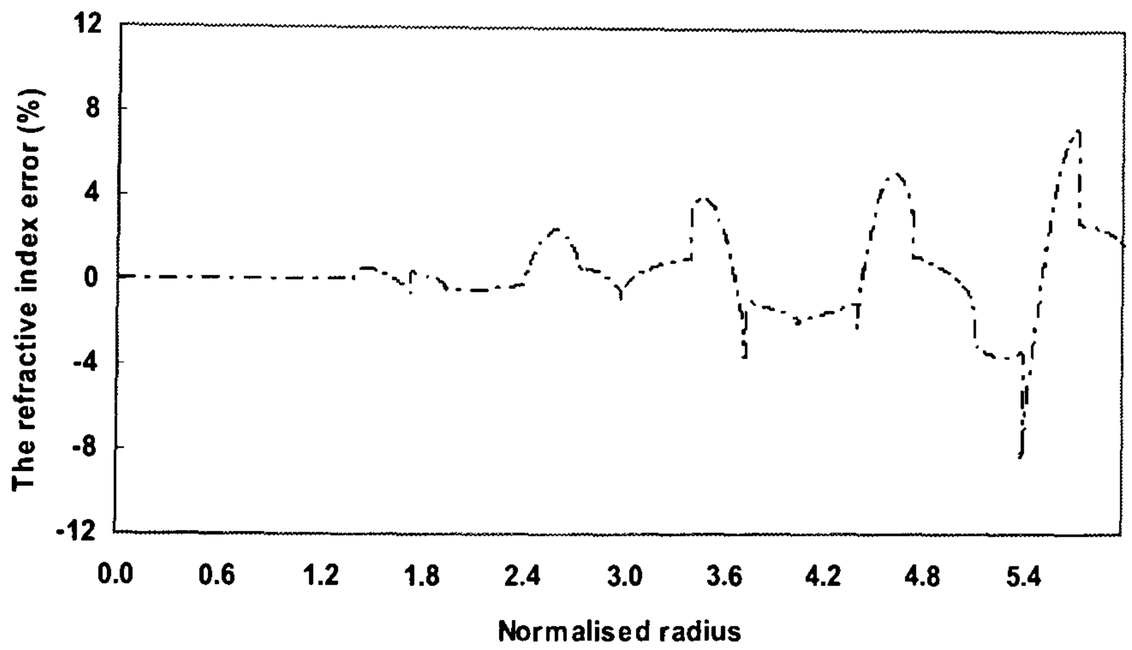

(c)

Figure 4.17 (a) Electric field profile for the *TM* mode Bragg fibre with the core index n_0 =1, thickness r_0 =1.4d, layer1 index n_1 =4.6, thickness d_1 =0.333d, layer2 index n_2 =1.6, thickness d_2 =0.667d.

$d = d_1 + d_2$ is the unit length of periodicity of the multilayered structure, the normalised propagation constant $\bar{\beta}$ =1.25, V=8.

(b) Example of a reconstructed Bragg structure refractive index profile from the electric field of the *TM* mode Fig.4.17(a)

(c) The % error in the reconstructed refractive index profile, (the difference between the exact and reconstructed refractive index profile).

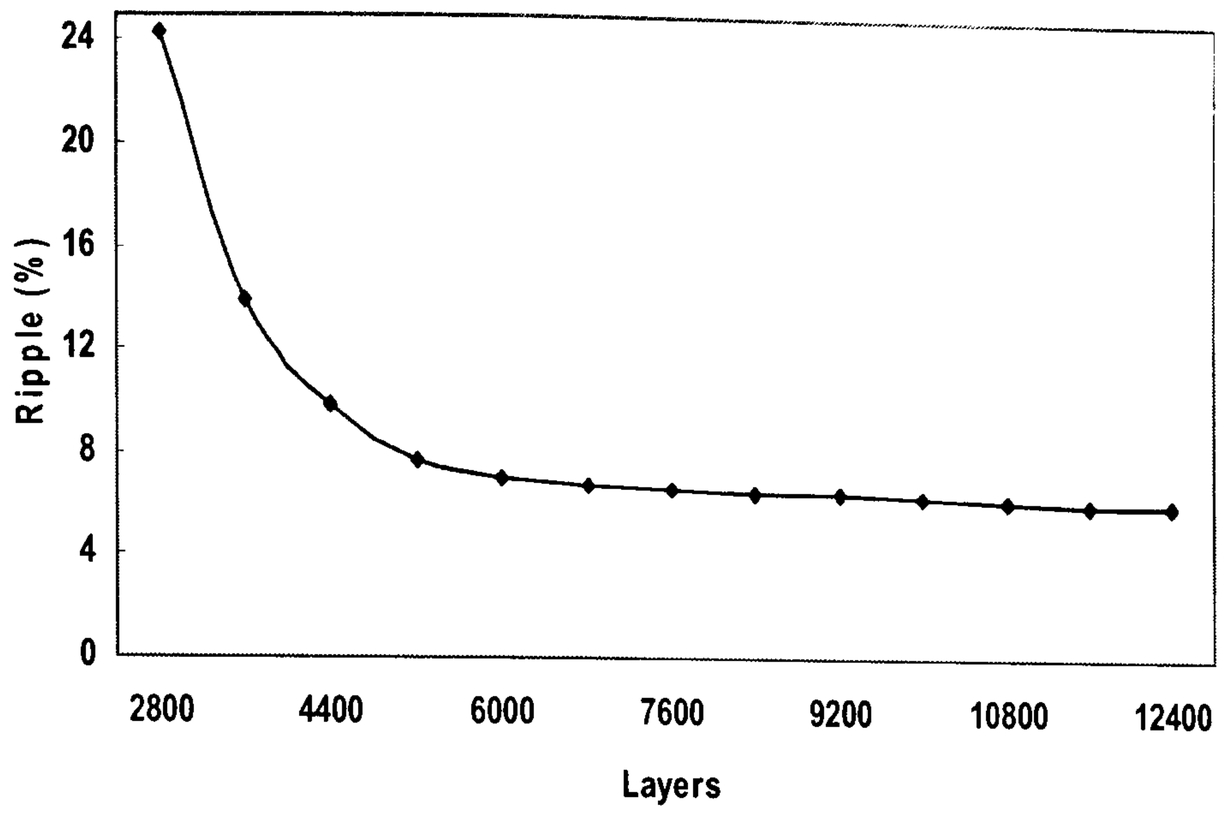

Figure 4.18 The refractive index difference, maximum % ripple (error) of the synthesized refractive index versus the number of cylindrical layers.

From the results obtained in chapter 4, it appears that sufficient accuracy and robustness of the solutions can be achieved by using the inverse *TL* technique, which is based on the propagation mode electric field scanning technique. The inverse *TL* technique is examined by reconstructing the refractive index profile of single-mode, multimode optical fibres and Bragg fibres. The inverse *TL* technique is also able to reconstruct optical fibre refractive index profile supporting modes of nearly arbitrary field distributions, which can be very useful in many applications in fibre optic sensing and other applications such as refractive index profiling instrumentation. It can be concluded that the inverse *TL* technique is useful for refractive index profiling from the practical point of view. In the next chapter, the capability of the inverse *TL* technique will be examined by reconstructing planar optical waveguide refractive index profiles form mode electric fields.

CHAPTER 5

Forward and Inverse Electric Field Solutions of Maxwell's Equations for Planar Optical Waveguides

In this chapter, the *TL* method will be developed for the forward and inverse electric field solutions of Maxwell's equations for planar optical waveguides. The case of both symmetric and asymmetric arbitrary refractive index profile planar optical waveguides will be discussed. Maxwell's equations for source-free, time-dependent fields are:

$$\left.\begin{aligned} \nabla \times \vec{E} &= -\frac{\partial \vec{B}}{\partial t} \\ \nabla \times \vec{H} &= \frac{\partial \vec{D}}{\partial t} \end{aligned}\right\} \tag{5.1}$$

where $\vec{E}(t)$, $\vec{H}(t)$, $\vec{B}(t)$ and $\vec{D}(t)$ are time-dependent vectors of the electric and magnetic fields, and magnetic and electric flux densities, respectively.

5.1 Physical Model of The Planar Optical Waveguide

An inhomogeneous planar optical waveguide is shown in Fig.5.1. The top and bottom cladding indices are n_3 and n_2 and the core index profile is $n(z)$. The thickness of the thin planar layer in the core is *d*, *a* is the radius of the core. It is assumed that the transverse electric and transverse magnetic fields have periodic time dependence of the form $\exp(j\omega t)$ and a direction of propagation along the y axis of an anisotropic medium with dielectric constants ε_y along the *x* and *y* directions and ε_z along the *z* direction, where ω presents the frequency of laser radiation.

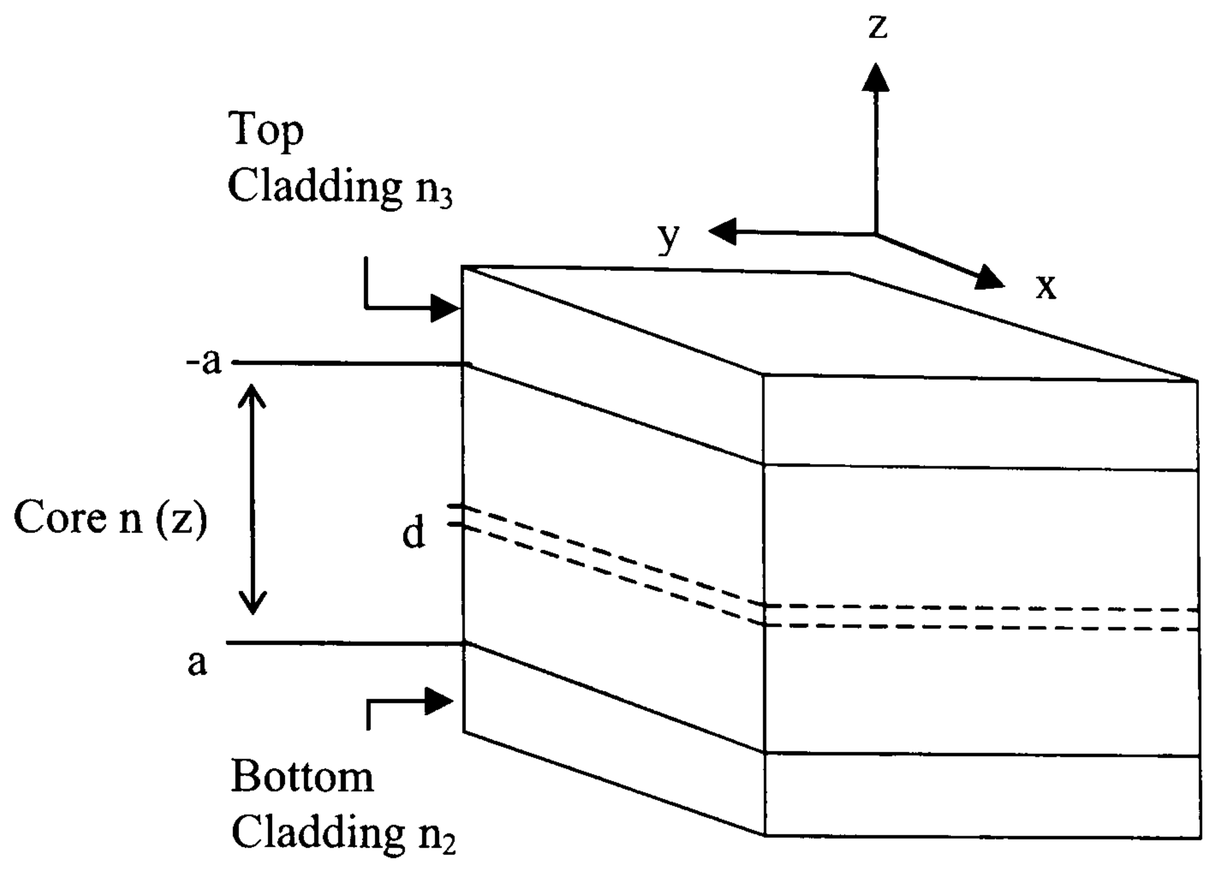

Figure 5.1 Physical structure of the inhomogeneous planar optical waveguide.

It is now necessary to transfer the field components equations (5.1) into the following reduced equations by applying the space Fourier transforms along the x and y axes with respective wave numbers l and β :

$$\left.\begin{aligned}
&\frac{j\beta B_z}{\mu_0} - \frac{\partial H_y}{\partial z} = j\omega\varepsilon_0\varepsilon_y E_x \\
&\frac{\partial H_x}{\partial z} - \frac{jlB_z}{\mu_0} = j\omega\varepsilon_0\varepsilon_y E_y \\
&lH_y - \beta H_x = \omega D_z \\
&\frac{j\beta D_z}{\varepsilon_0\varepsilon_z} - \frac{\partial E_y}{\partial z} = -j\omega\mu_0 H_x \\
&\frac{\partial E_x}{\partial z} - \frac{jlD_z}{\varepsilon_0\varepsilon_z} = -j\omega\mu_0 H_y \\
&lE_y - \beta E_x = -\omega B_z
\end{aligned}\right\} \qquad (5.2)$$

By defining the variables

$V_M = lH_x + \beta H_y$ (Magnetic Voltage)

$V_E = lE_x + \beta E_y$ (Electric Voltage)

$\mathrm{I_M} = \omega B_z = \omega\mu_0 H_z = \beta E_x - lE_y$ (Magnetic Current)

$\mathrm{I_E} = \omega D_z = \omega\varepsilon_z E_z = lH_y - \beta H_x$ (Electric Current)

The relationships deduced from (5.2):

$$\left.\begin{aligned}\frac{\partial V_M}{\partial z} &= -\frac{\gamma_y^2}{j\omega\mu_0} I_M \\ \frac{\partial I_M}{\partial z} &= -j\omega\mu_0 V_M\end{aligned}\right\} \tag{5.3}$$

$$\left.\begin{aligned}\frac{\partial V_E}{\partial z} &= -\frac{\gamma_z^2}{j\omega\varepsilon_0 n_z^2} I_E \\ \frac{\partial I_E}{\partial z} &= -j\omega\varepsilon_0 n_y^2 V_E\end{aligned}\right\} \tag{5.4}$$

where $\gamma_y^2 = l^2 + \beta^2 - n_y^2 k_0^2$ and $\gamma_z^2 = l^2 + \beta^2 - n_z^2 k_0^2$, $k_0 = 2\pi/\lambda_0$ (λ_0 is the free-space wavelength), $\varepsilon_y = n_y^2$ and $\varepsilon_z = n_z^2$ (n_y, n_z are the corresponding refractive indices). Equations (5.3) and (5.4) are the well-known transmission line equations. Equations (5.3) are defined to represent a magnetic line, and equations (5.4) to represent an electric line. They have different propagation factors, γ_y and γ_z, and different characteristic impedances, Z_M and Z_E:

$$\left.\begin{aligned}Z_M &= \frac{\gamma_y}{j\omega\mu_0} \\ Z_E &= \frac{\gamma_z}{j\omega\varepsilon_0 n_y n_z}\end{aligned}\right\} \tag{5.5}$$

Let us now consider a dielectric planar layer of thickness *d* and refractive indices n_y and n_z along the *y* and *z* directions, as shown in Fig.5.1. With the *z* axis chosen to be normal to the layer boundary planes, a wave is to be propagating along the *y* axis. For the planar layer $\partial/\partial x = 0$ and equations (5.3), (5.4) and (5.5) are independent of *l*, hence:

$$\left.\begin{aligned}\gamma_y^2 &= \beta^2 - n_y^2 k_0^2 \\ \gamma_z^2 &= \beta^2 - n_z^2 k_0^2\end{aligned}\right\} \tag{5.6}$$

The thin planar layer in the core (thickness d) can be represented by two transmission lines, and therefore by two equivalent T-circuits, Fig.5.2, with elements given by:

$$\left.\begin{aligned} Z_{S,M} &= Z_M \tanh(\gamma_y d/2) \\ Z_{P,M} &= Z_M / \sinh(\gamma_y d) \end{aligned}\right\} \tag{5.7}$$

$$\left.\begin{aligned} Z_{S,E} &= Z_E \tanh(\gamma_z d/2) \\ Z_{P,E} &= Z_E / \sinh(\gamma_z d) \end{aligned}\right\} \tag{5.8}$$

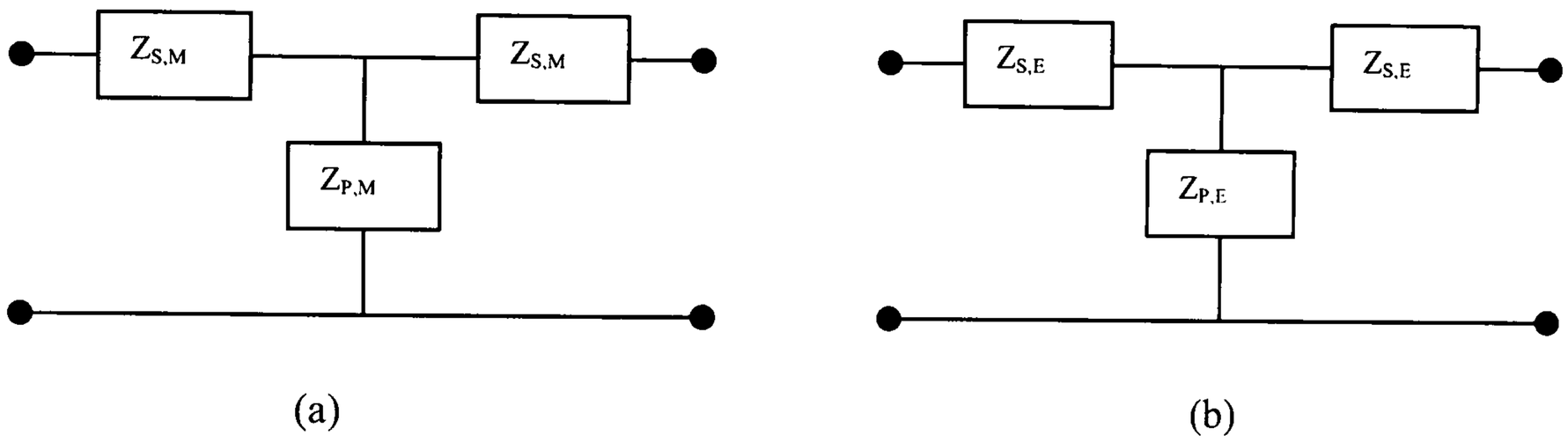

(a) (b)

Figure 5.2 Equivalent T-circuits of the transmission lines representing the thin planar layer in the core shown in Fig.5.1, **(a)** Magnetic equivalent circuit, **(b)** Electric equivalent circuit

Therefore, a set of successive thin planar layers can now be represented by a set of equivalent T-circuits connected in tandem with their elements given by equations (5.7) and (5.8).

The resonance condition gives the propagation constants of the *TE* modes by using the magnetic equivalent circuit Fig.5.2(a), and of the *TM* modes by using the electric equivalent circuit Fig.5.2(b). In such circumstances, equations (5.3) and (5.4) can be solved by using the resonance technique, which has the advantages of providing an easily understood physical representation of the problem and keeping the numerical computations involved fairly simple. An inhomogeneous anisotropic core between two uniform, anisotropic cladding is considered, shown in Fig.5.3(a). The top cladding (left hand side) has refractive indices $n_{y,T}$ and $n_{z,T}$, the bottom cladding (right hand side) has indices $n_{y,B}$ and $n_{z,B}$, along the y and z directions respectively.

Propagation is in the y direction. For TM modes, the characteristic impedances of the top cladding Z_T and the bottom cladding Z_B are given by (5.9), similarly for TE modes (5.10):

$$\left.\begin{aligned} Z_T &= -\frac{j(\beta^2 - n_{z,T}^2 k_0^2)^{1/2}}{\omega\varepsilon_0 n_{y,T} n_{z,T}} \\ Z_B &= -\frac{j(\beta^2 - n_{z,B}^2 k_0^2)^{1/2}}{\omega\varepsilon_0 n_{y,B} n_{z,B}} \end{aligned}\right\} \tag{5.9}$$

$$\left.\begin{aligned} Z_T &= -\frac{j(\beta^2 - n_{y,T}^2 k_0^2)^{1/2}}{\omega\mu_0} \\ Z_B &= -\frac{j(\beta^2 - n_{y,B}^2 k_0^2)^{1/2}}{\omega\mu_0} \end{aligned}\right\} \tag{5.10}$$

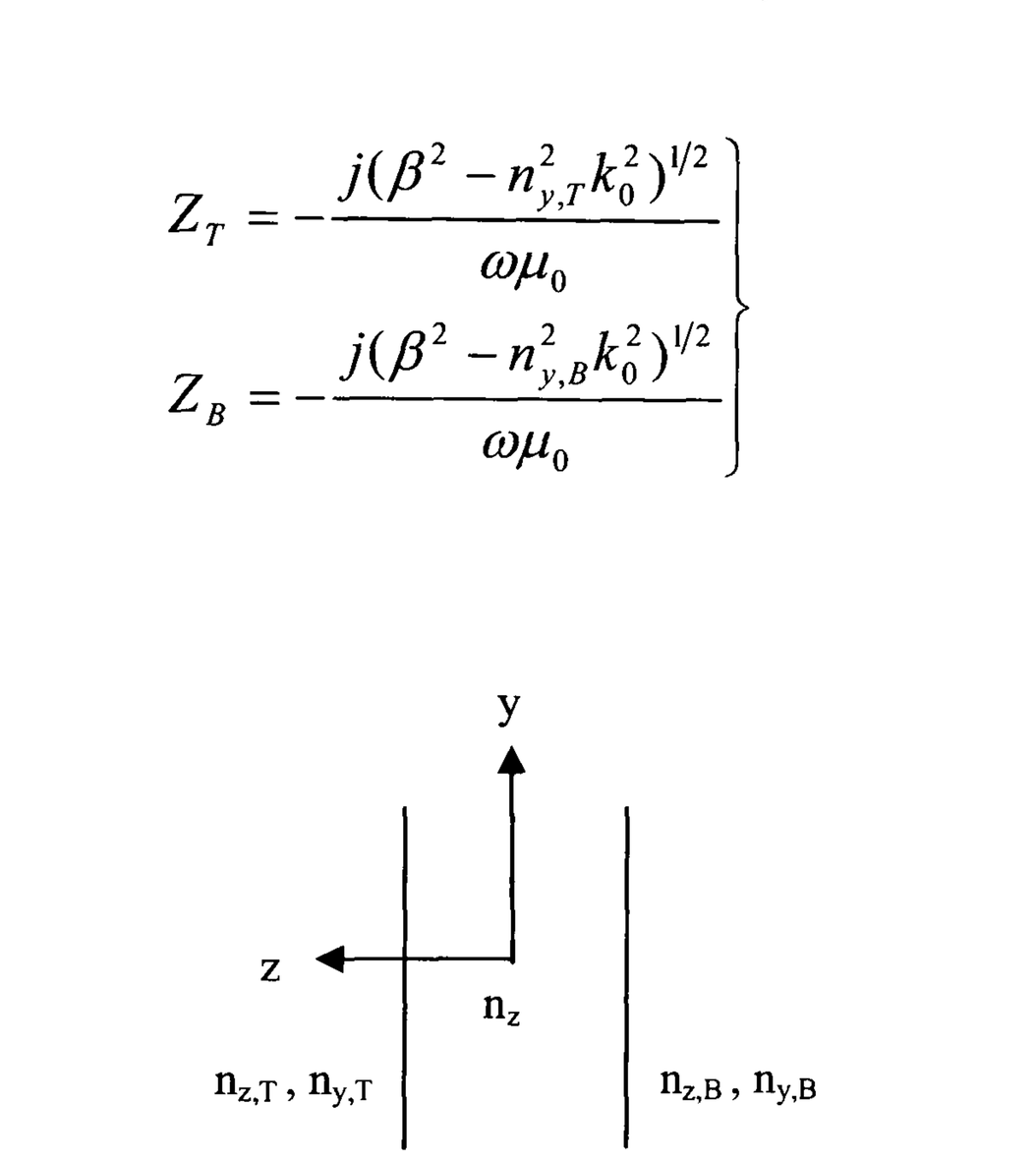

Figure 5.3 **(a)** An inhomogeneous anisotropic planar waveguide,
(b) The equivalent transmission line consisting of a large number of equivalent T-circuits of thin layers in tandem.

The arbitrary index profile core is represented by a large number, N, of adjacent uniform thin layers (thickness d) in a stair-like configuration. The equivalent T-circuits of the successive layers are connected in tandem, as shown in Fig.5.3(b), and are terminated by Z_T and Z_B. Using elementary circuit theory, the impedance of the nth layer can be expressed in terms of the impedance of the $(n\text{-}1)$th layer by the recurrence relation:

$$Z_n = \frac{(Z_{n-1} + Z_{S,n})Z_{P,n}}{Z_{n-1} + Z_{S,n} + Z_{P,n}} + Z_{S,n} \quad (n=1, 2, 3 \ldots, N) \tag{5.11}$$

where $Z_{S,n}$, $Z_{P,n}$ are the series and parallel elements of the T-circuit representation of the nth layer.

For there to be resonance, the total impedance of the circuits is determined as the sum of Z_N and Z_T. Z_N is computed by starting with the bottom cladding impedance Z_B as Z_{n-1} and using (5.11). Z_T is the characteristic impedance of the top cladding. Resonance occurs when the condition (5.12) is satisfied:

$$Z_N + Z_T = 0 \tag{5.12}$$

As we noted previously, the analysis for *TE* and *TM* modes are similar, so that for the rest of this work only the *TM* case is examined. By using the propagation constant β obtained from the resonance technique, the electric field E_z can be worked out, which is derived from the variables of (5.2):

$$E_z = \frac{I_E}{\omega\varepsilon_0 n^2(z)} = \frac{Z_0 I_E}{k_0 n^2(z)} \tag{5.13}$$

Therefore if the refractive index $n(z)$ as the function of radius is known, the electric field E_z can be plotted out precisely by using (5.13).

For determining the refractive index profile from knowledge of E_z, the following boundary condition is assumed: At $r = \infty$, $Z_{prev} = Z_B$ and $n(\infty) = n_2$. From circuit theory, using Fig.5.3(b), the values of $Z_{S,z}$ and $Z_{P,z}$ are determined. $\overline{\beta} = \beta / k_0$ is the effective refractive index and for typical waveguides lies between the indices of the core and the cladding. Both the free space wavelength λ_0 and the thin uniform layer thickness d are known. Since electric field E_z and current I_E are known, the planar optical waveguide refractive index $n(z)$ can be calculated as follows:

$$n(z) = \left(\frac{Z_0 I_E}{k_0 E_z}\right)^{1/2} \tag{5.14}$$

5.2 Design Examples and Discussion

5.2.1 The Isotropic Symmetric Planar Waveguide

In the case of *TM* modes, for the isotropic symmetric planar optical waveguides, dielectric constant ε_y equals to ε_z (refractive indices $n_y = n_z$) and the bottom cladding impedance Z_B equals to the top cladding impedance Z_T. By using a root searching technique, propagation constant β can be located. Results of sample computations for the well-known step index profile for *TM* modes in the isotropic case are given in Fig.5.4. In this work, the same parameters are used as Figure 2.26 in (Adams 1981) for the ease of comparison, core radius $a = 1\mu m$, wavelength $\lambda = 0.633\mu m$, core index $n_1 = 1.517$, the bottom and top cladding indices $n_2 = n_3 = 1.5$.

Fig.5.5 shows the TM_{01} mode field distribution and the reconstructed refractive index profile of the step index planar optical waveguide. In order to show the accuracy of the inverse *TL* technique, Fig.5.6 shows the % error versus the normalized radius by comparing the reconstructed index with the original refractive index. The error in refractive index oscillates about the exact value in the core and the top cladding, while the error in the bottom cladding is zero. The reconstruction

calculation is started from the bottom cladding to the top cladding, so the error in the bottom cladding is at a minimum and it is accumulated in the core and the top cladding. The oscillations in the core and the top cladding depend on the number of uniform thin layers used for the reconstruction of the index as shown in Fig.5.7. This figure shows that less than 5% error due to the ripple in Δn can be achieved with up to 30,000 layers. As expected, the larger the number of uniform thin layers, the better the accuracy and convergence can be achieved. However, the error ripple obtained by using 10,000 layers is almost the same as the error ripple obtained by using 30,000 layers. To save computation time, 10,000 layers are used for the remaining calculations. The application of this method to arbitrary refractive index profile planar waveguides is favoured by the simplicity of the computing program and its accuracy and efficiency.

For the reconstructed Δn, Fig.5.8 shows the effect of inaccuracies in $\overline{\beta}$ on the error ripple. We can see that the error ripple increases with the use of the incorrect $\overline{\beta}$. The minimum error can be achieved at the exact $\overline{\beta}$. The reconstructed refractive index is also exact at this minimum ripple point.

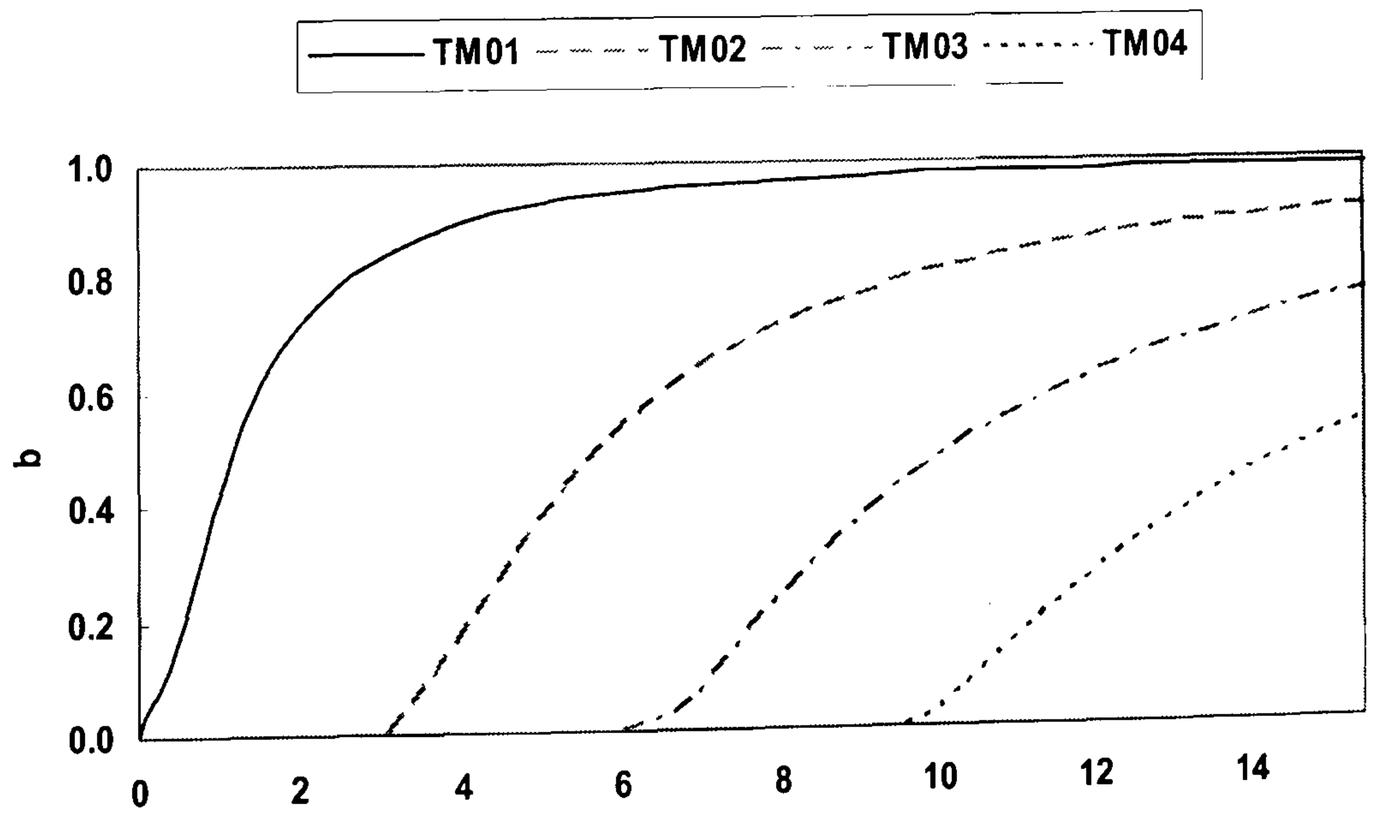

Figure 5.4 b-V for step index planar waveguide $V = k_0 a (n_1^2 - n_2^2)^{1/2}$ and $b = [(\beta / k_0)^2 - n_2^2] / (n_1^2 - n_2^2)$.

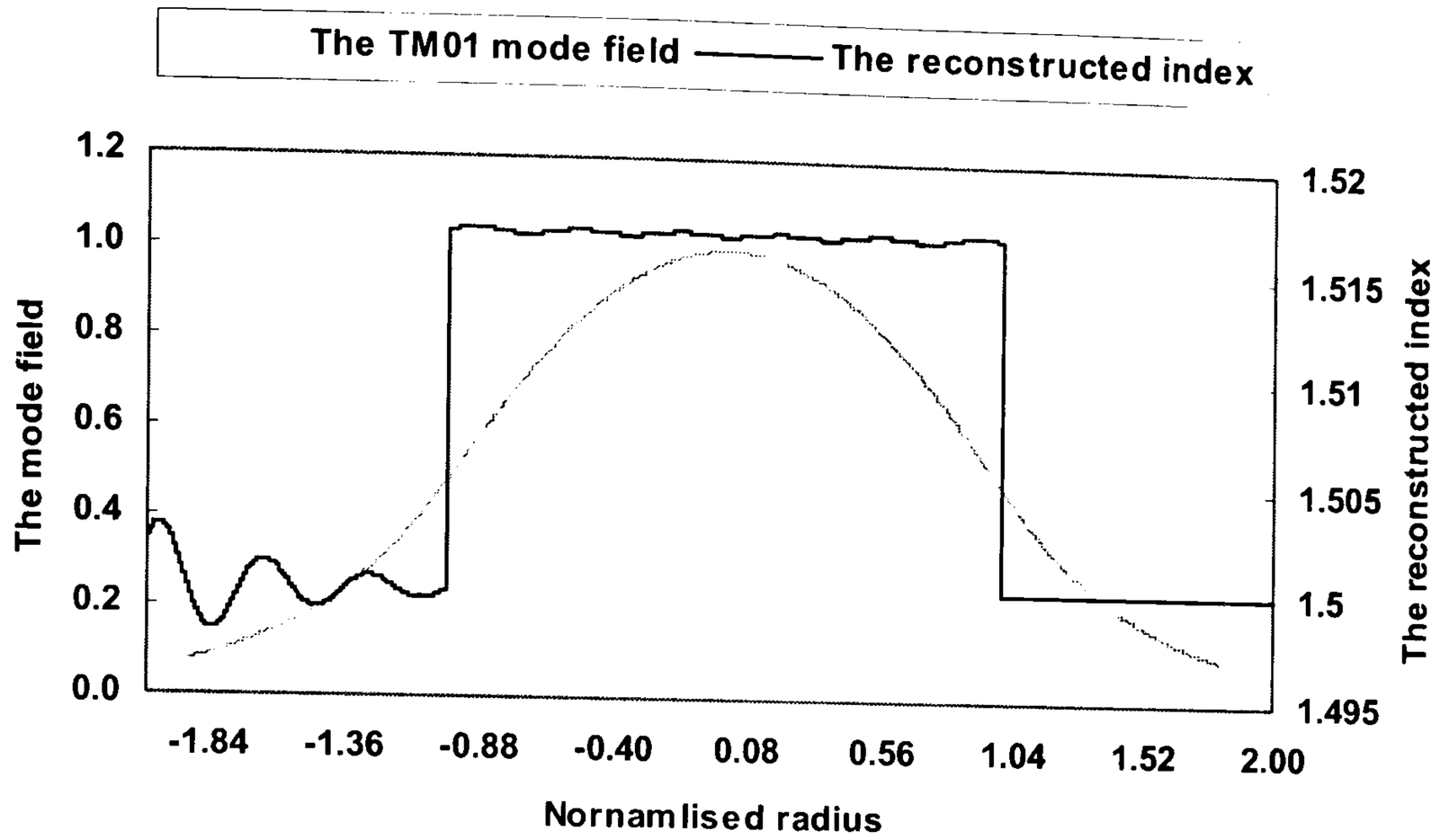

Figure 5.5 The reconstructed step index profile from the step index planar waveguide TM_{01} mode electric field.

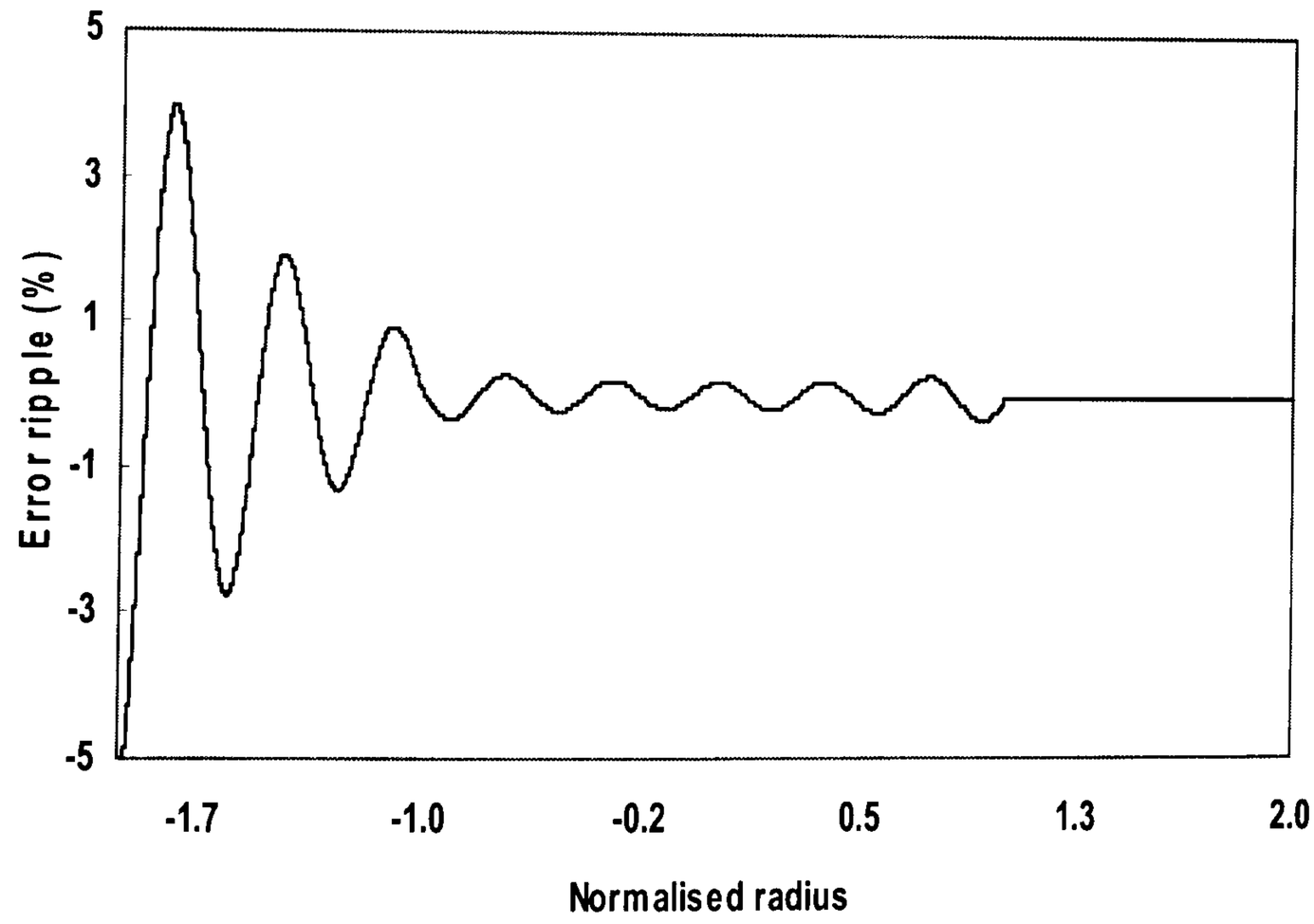

Figure 5.6 The % error in the reconstructed refractive index profile, (the difference between the exact and reconstructed refractive index profile) $(100 \times (n_{exact} - n_{reconstructed}) / n_{exact})\%$.

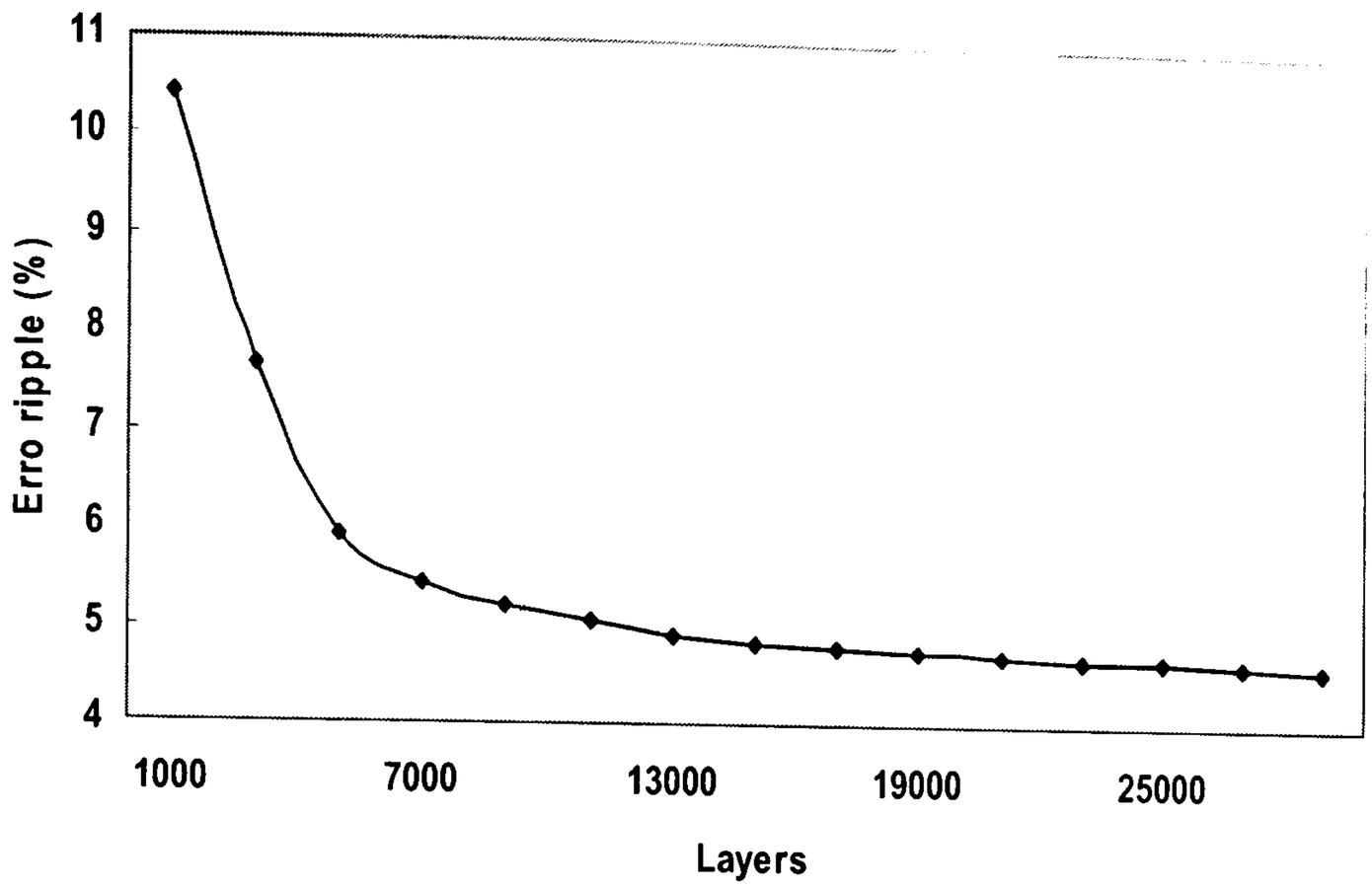

Figure 5.7 The refractive index difference, maximum % ripple (error) of the synthesized refractive index versus the number of T-circuit equivalent planar layers.

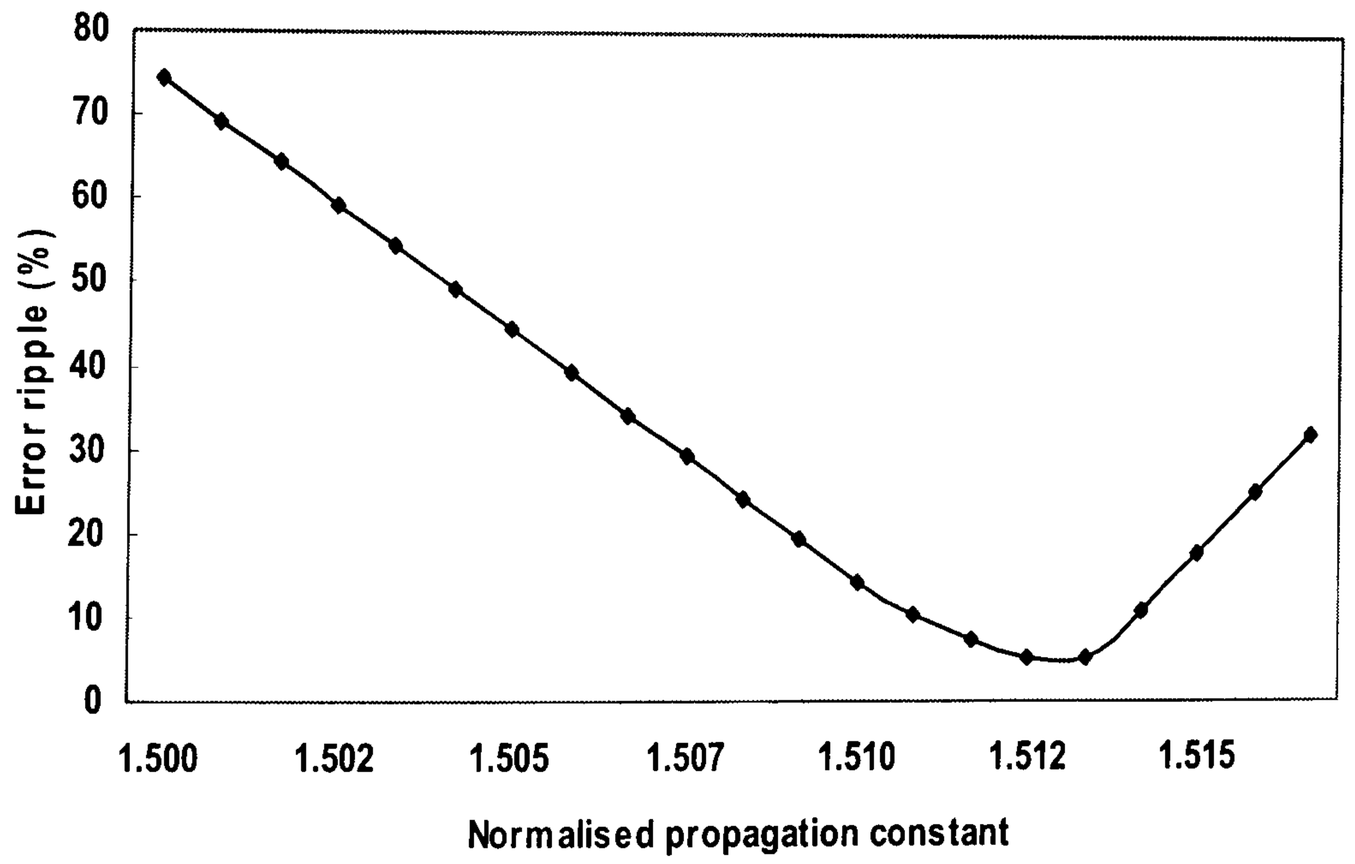

Figure 5.8 The refractive index difference, maximum % ripple (error) of the synthesized refractive index versus values for $\overline{\beta}$ offset from exact.

Fig.5.9 shows the refractive index reconstruction for a parabolic core planar waveguide. The remarkable accuracy of the reconstruction is demonstrated in Fig.5.10, where the % error in Δn is shown. The % error is less than 0.5%. Clearly the parabolic profile is less demanding in reconstruction than a step index profile planar optical waveguide.

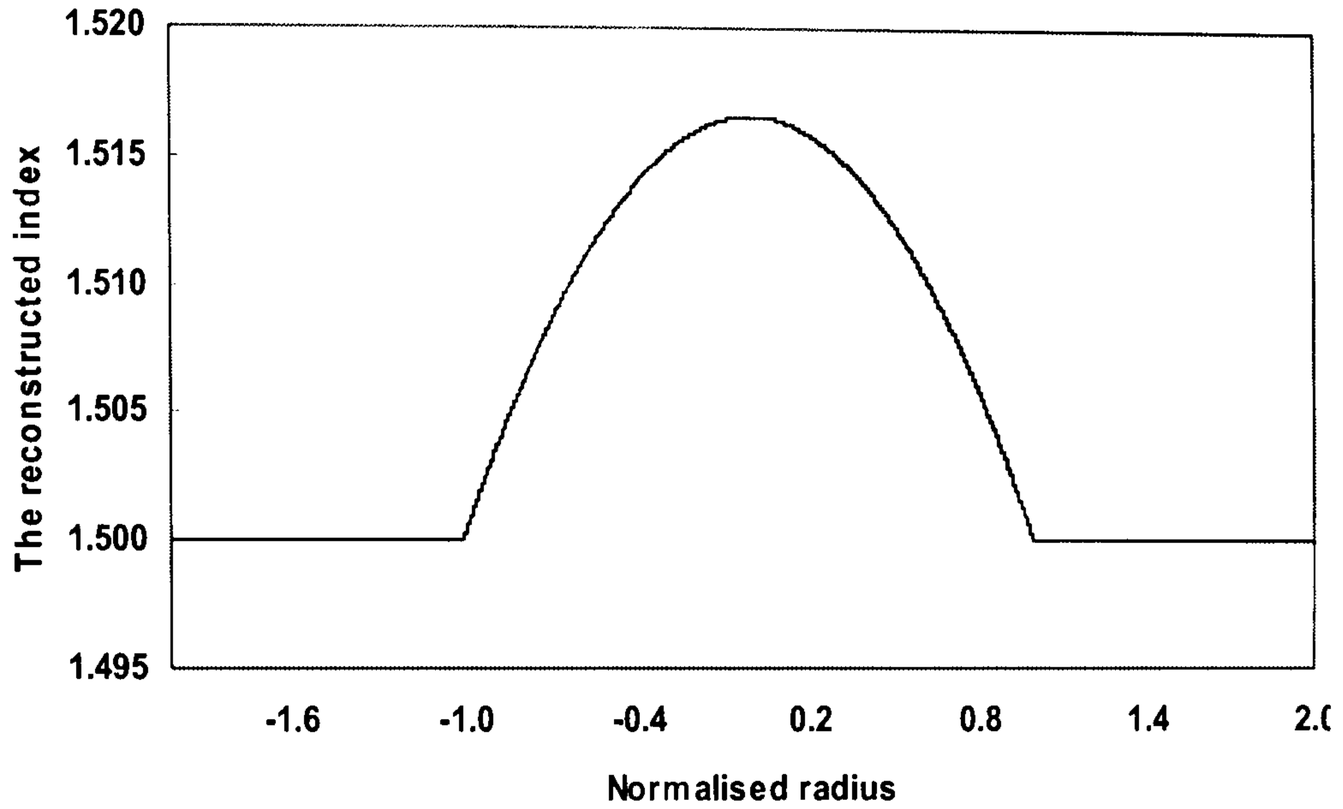

Figure 5.9 The reconstructed parabolic index profile from the parabolic index planar waveguide electric field.

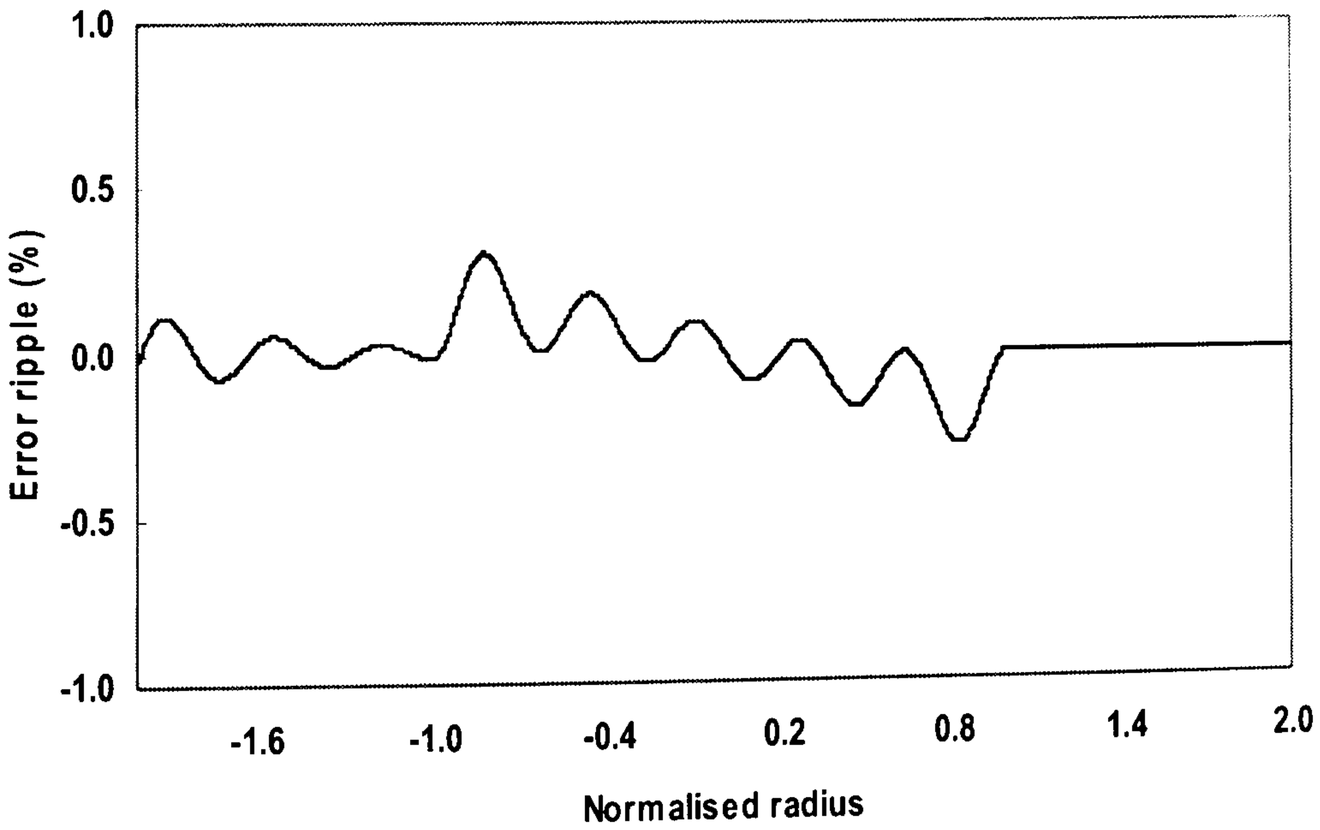

Figure 5.10 The % error in the reconstructed refractive index profile, (the difference between the exact and reconstructed refractive index profile)

$$(100 \times (n_{exact} - n_{reconstructed}) / n_{exact})\% .$$

Inverse *TL* technique can be applied to synthesize the refractive index profile of a planar optical waveguide from a desired fundamental mode electric field, as well as from higher order mode electric fields. Fig.5.11(a) and (b) show the reconstructed refractive index profiles of isotropic symmetric planar optical waveguides from given higher order mode electric fields.

Fig.5.11(a) shows a given higher order *TM* mode (TM_{02}) electric field distribution and the reconstructed refractive index profile from it the corresponding step index planar optical waveguide. In Fig.5.11(a), we notice that there are two spikes in the reconstructed refractive index profile. The reason is because the TM_{02} mode electric field goes to zero at these radii. The same conclusion can also be obtained from (5.13). The extraordinary accuracy of the index reconstruction using the TM_{02} mode electric field is demonstrated in Fig.5.11(b), where the % error in Δn is shown. The error in refractive index shows small oscillations about the exact value in the core and the top cladding. The error in the bottom cladding is zero, this is because the inverse calculation is started from the bottom cladding to the top cladding and the error can be accumulated.

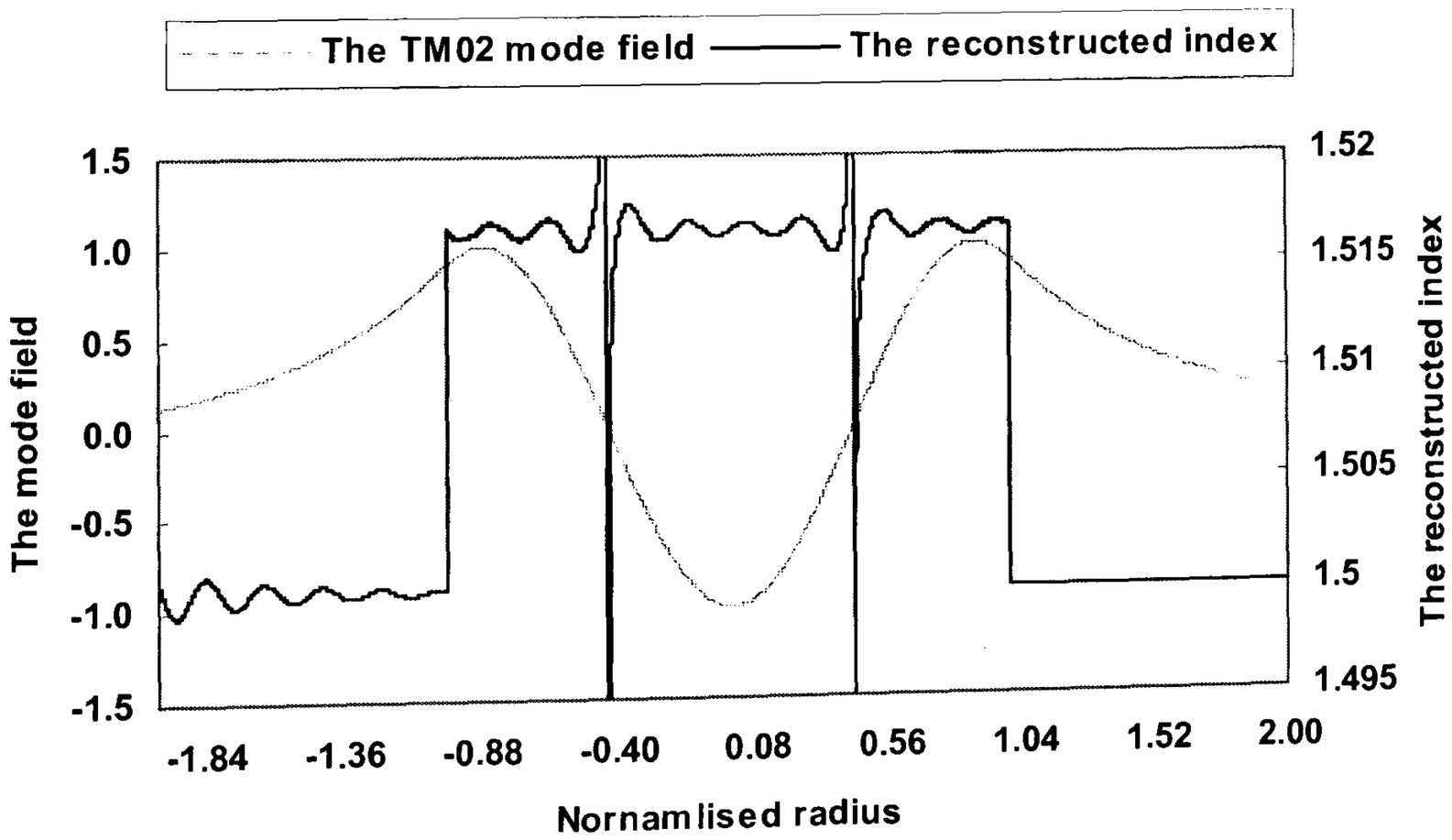

(a)

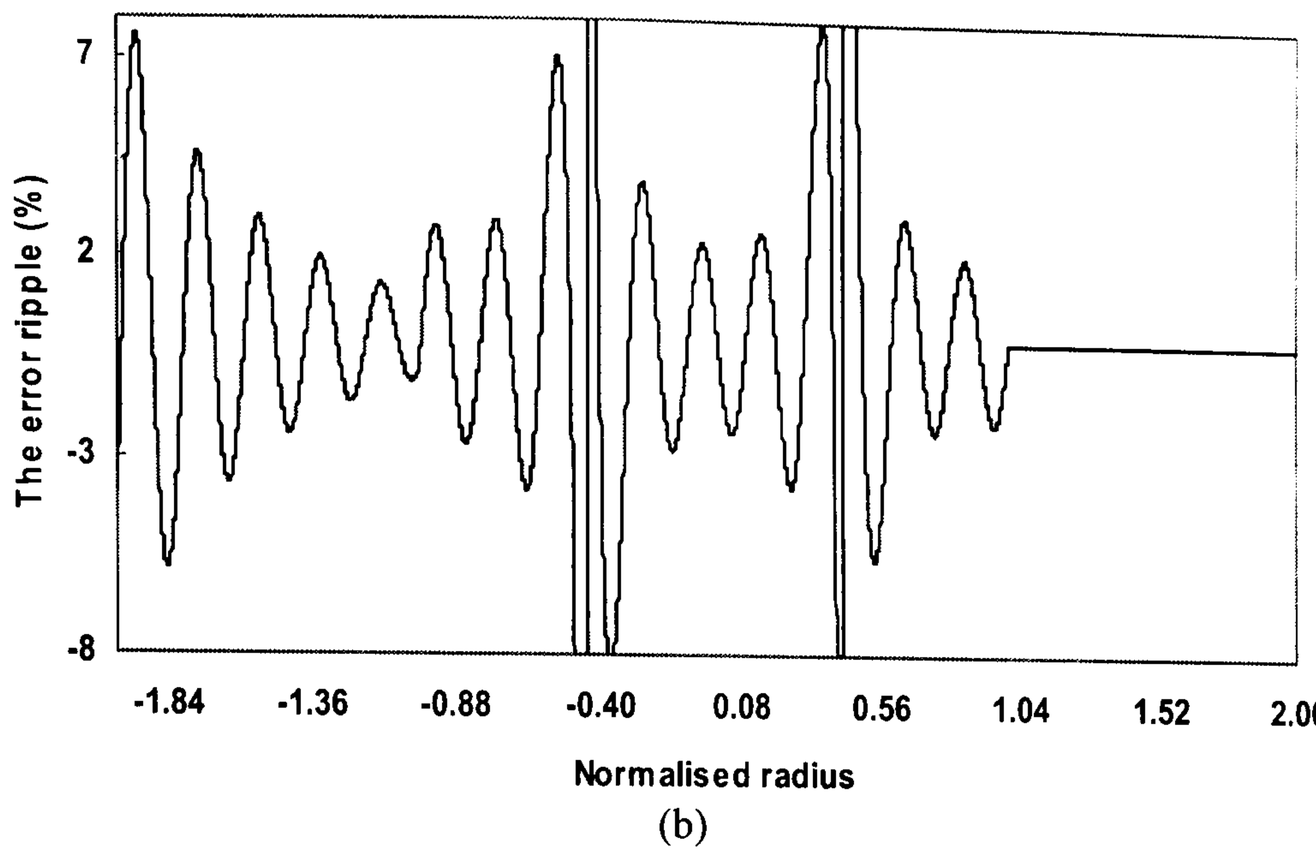

(b)

Figure 5.11 **(a)** Example of a reconstructed step core refractive index profile from the electric field of TM_{02} mode. **(b)** The % error in the reconstructed refractive index profile, (the difference between the exact and reconstructed refractive index profile)

$(100 \times (n_{exact} - n_{reconstructed}) / n_{exact})\%$.

The error oscillations in the core and the top cladding depend on the number of thin planar layers used for the numerical reconstruction of the index as shown in Fig.5.12. As expected, the larger the number of layers is, the better the accuracy and convergence can be obtained. Again, 10,000 layers are used for the rest calculations.

Fig.5.13 shows the effect of inaccuracies in the given $\overline{\beta}$ on the ripple in the reconstructed Δn. We can see that the ripple increases by using the incorrect $\overline{\beta}$. The minimum error occurs at the exact $\overline{\beta}$. Hence the prior knowledge of $\overline{\beta}$ can be avoided.

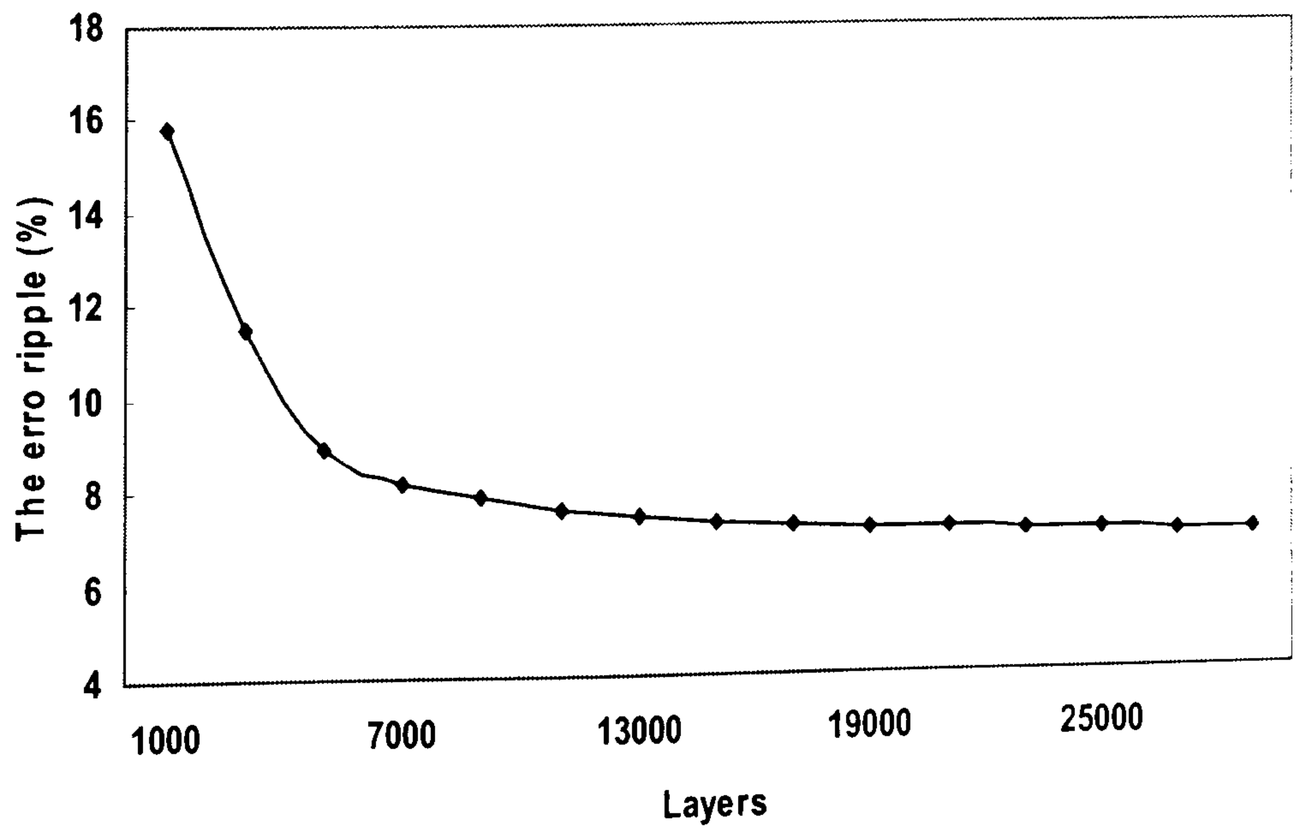

Figure 5.12 The refractive index difference, maximum % ripple (error) of the synthesized refractive index versus the number of planar layers.

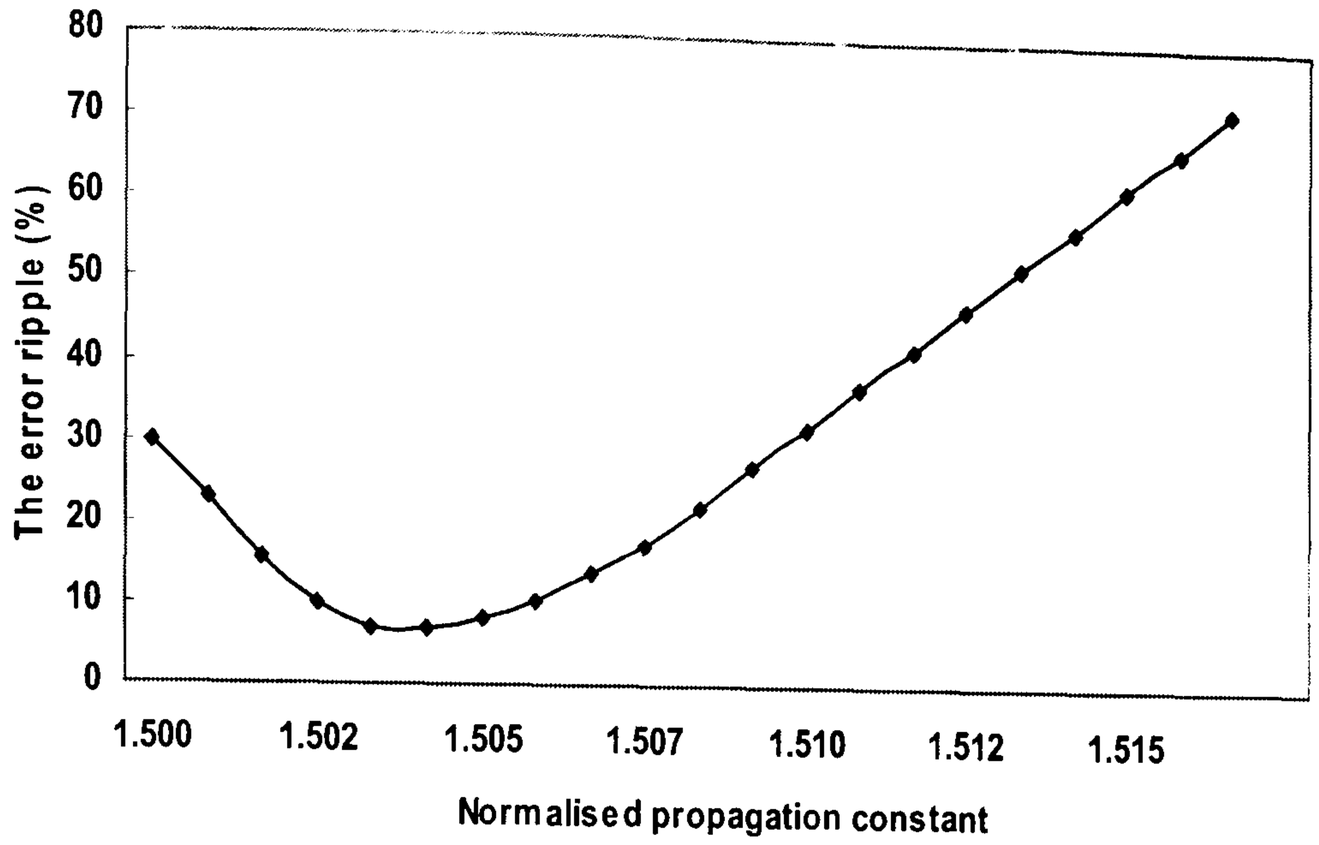

Figure 5.13 The refractive index difference, ripple (%) of the synthesized refractive index versus values for $\bar{\beta}$ offset from the exact.

In order to illustrate further the power of the inverse *TL* technique, the arbitrary refractive index profile reconstruction for the asymmetric planar waveguides is considered in the next section.

5.2.2 The Isotropic Asymmetric Planar Waveguide

For the isotropic asymmetric planar optical waveguide, dielectric constant ε_y equals to ε_z (refractive indices $n_y = n_z$), while $Z_T > Z_B$, $n_3 > n_2$ and the effective index $n_3 < \bar{\beta} < n_1$.

The reconstructed refractive index profile of an asymmetric step index planar waveguide with top cladding index $n_3 = 1.504$ is shown in Fig.5.14. The accuracy compared with the original refractive index shows the % error against the normalized radius, Fig.5.15. The error in the bottom cladding is the smallest compared to those in the core and the top cladding. Also, we can see that the % error difference between Fig5.6 and Fig.5.15. For the asymmetric step index planar waveguide, the % error in refractive index difference is larger than for the symmetric step index planar waveguides. By varying the top cladding index n_3 between the bottom cladding index n_2 and the core index n_1, ($n_2 < n_3 < n_1$), it is possible to obtain the exact

normalised propagation constants and the related reconstructed index errors against the increasing top cladding indices, Fig.5.16. From which we see that the % error becomes larger as the top cladding index n_3 increases.

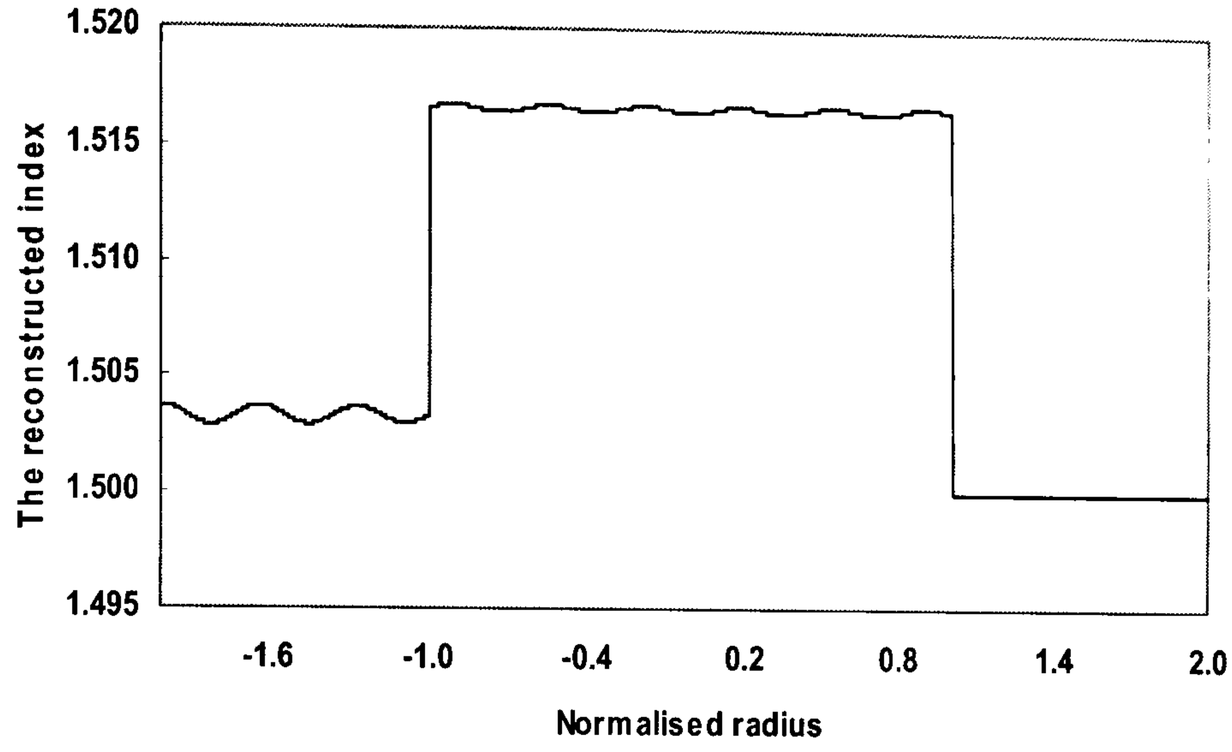

Figure 5.14 The reconstructed asymmetric step index profile from the step index planar waveguide electric field.

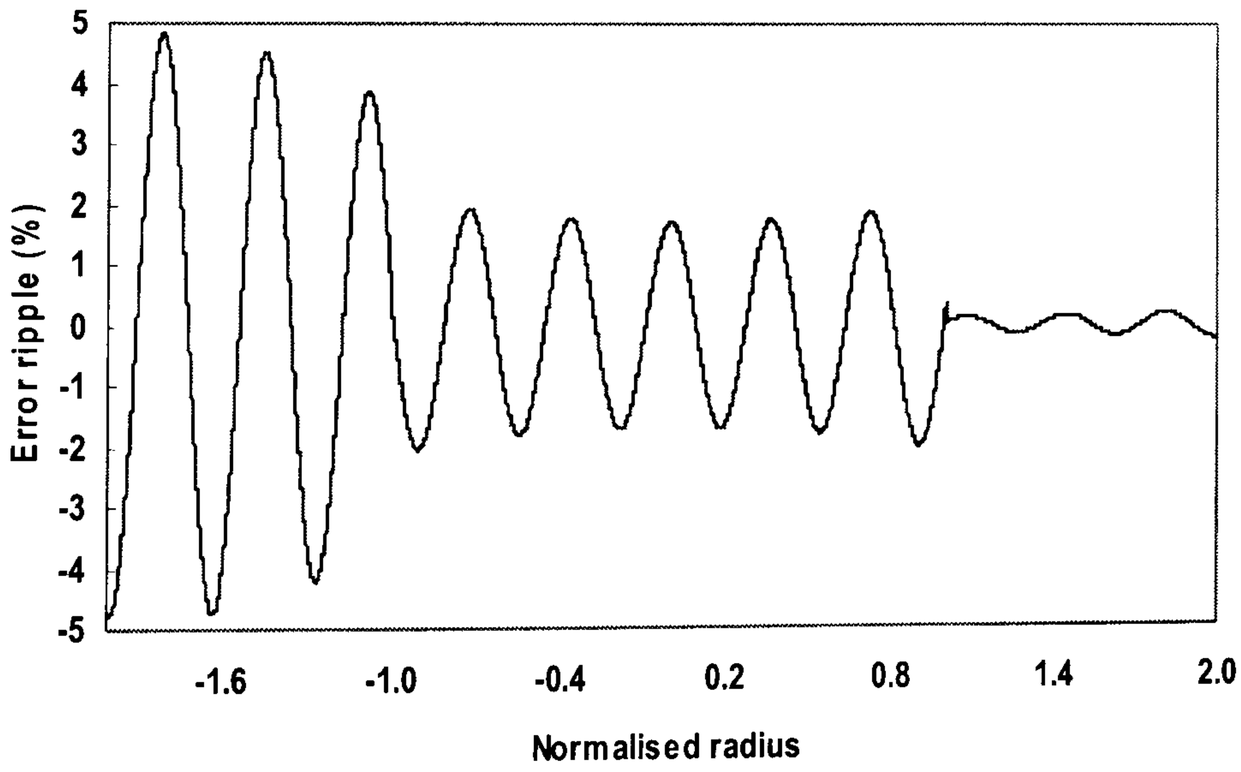

Figure 5.15 The % error in the reconstructed refractive index profile, (the difference between the exact and reconstructed refractive index profile)

$$(100 \times (n_{exact} - n_{reconstructed}) / n_{exact})\% .$$

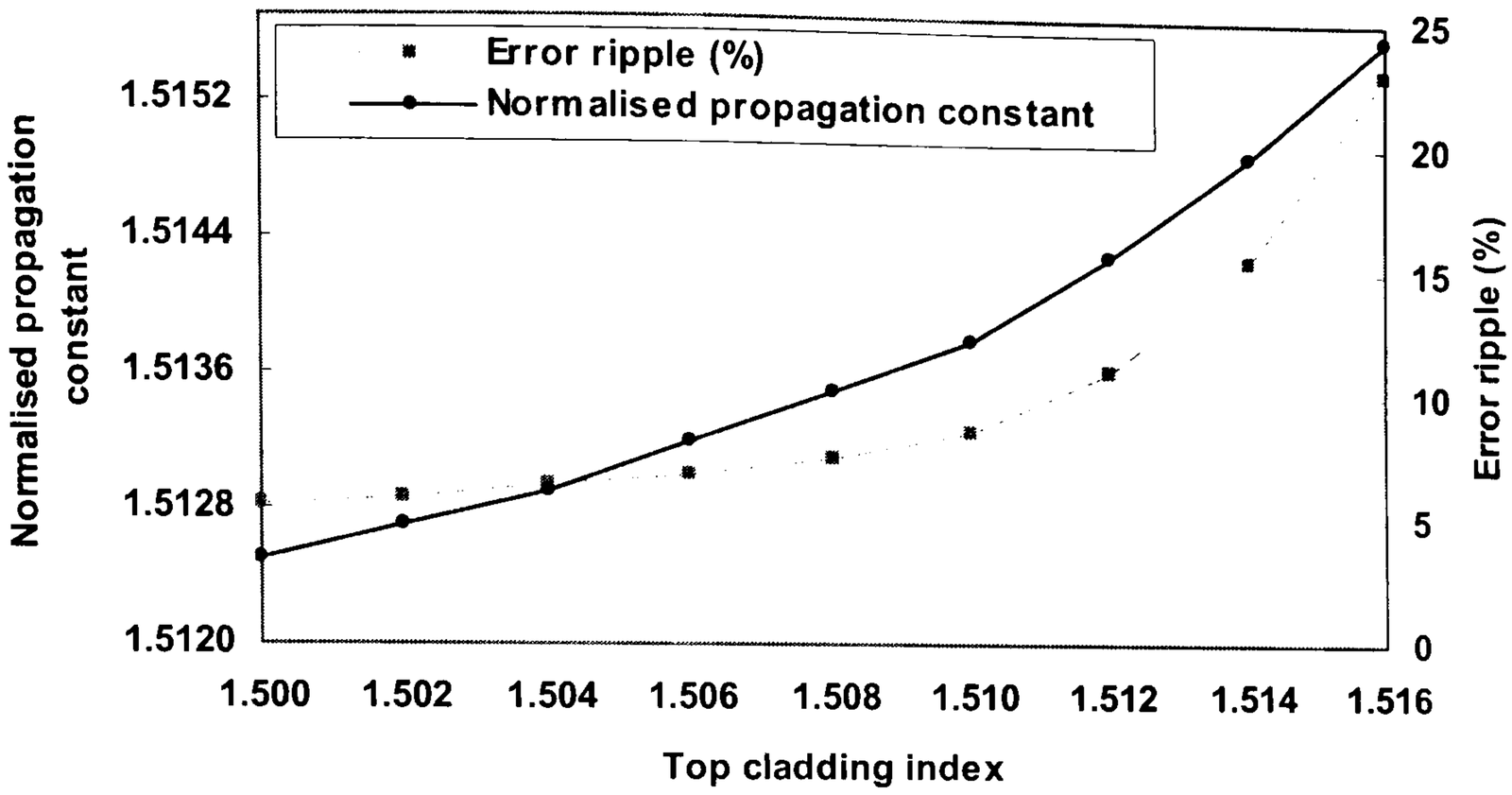

Figure 5.16 The % maximum error in refractive index difference due to ripple versus the top cladding index.

Fig.5.17 shows another example of the asymmetric parabolic planar waveguide refractive index reconstruction. The top cladding index is n_3 =1.504. Fig.5.18 demonstrates the accuracy of the asymmetric parabolic refractive index reconstruction, in which the % error in Δn is less accurate compared to the % error in Fig.5.10. The maximum % error is about 0.7%. Obviously the asymmetric parabolic planar waveguide is less demanding in reconstruction than the asymmetric step index planar waveguide described above. The obtained exact normalised propagation constants and the related reconstructed index errors against the increasing top cladding indices n_3 have also been plotted for the asymmetric parabolic planar waveguide, as shown in Fig.5.19.

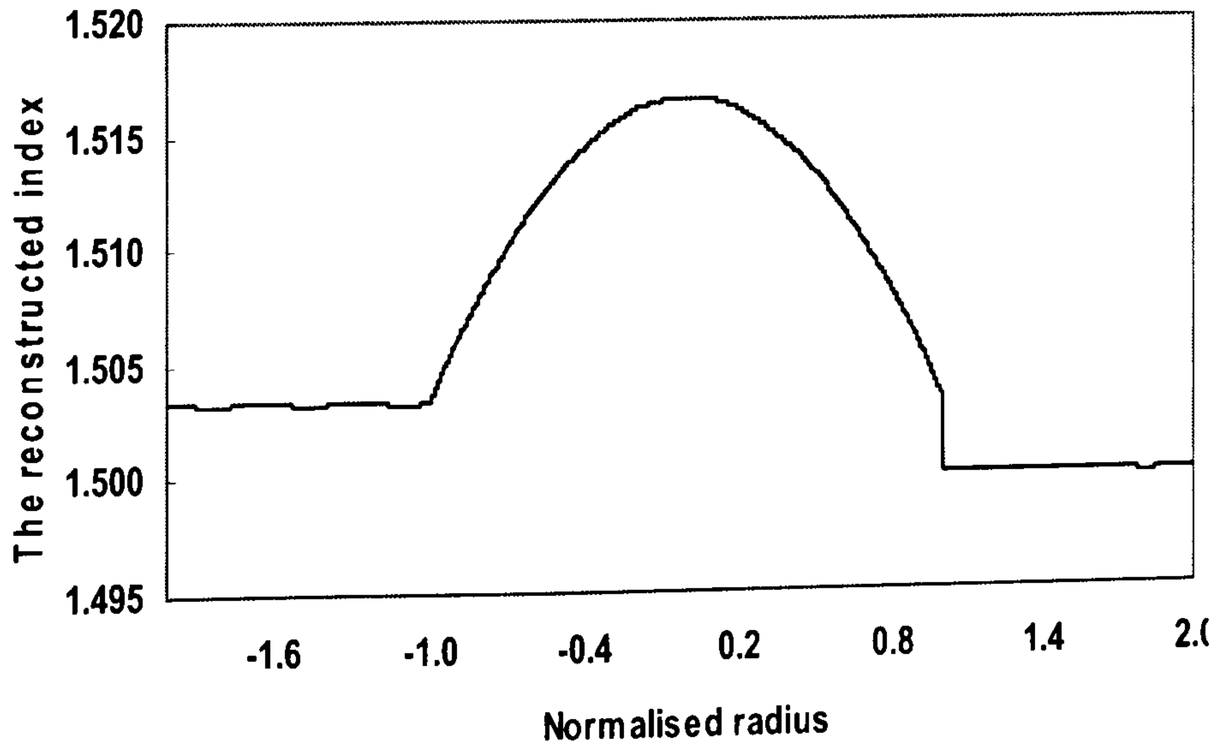

Figure 5.17 The reconstructed asymmetric parabolic index profile from the parabolic index planar waveguide electric field.

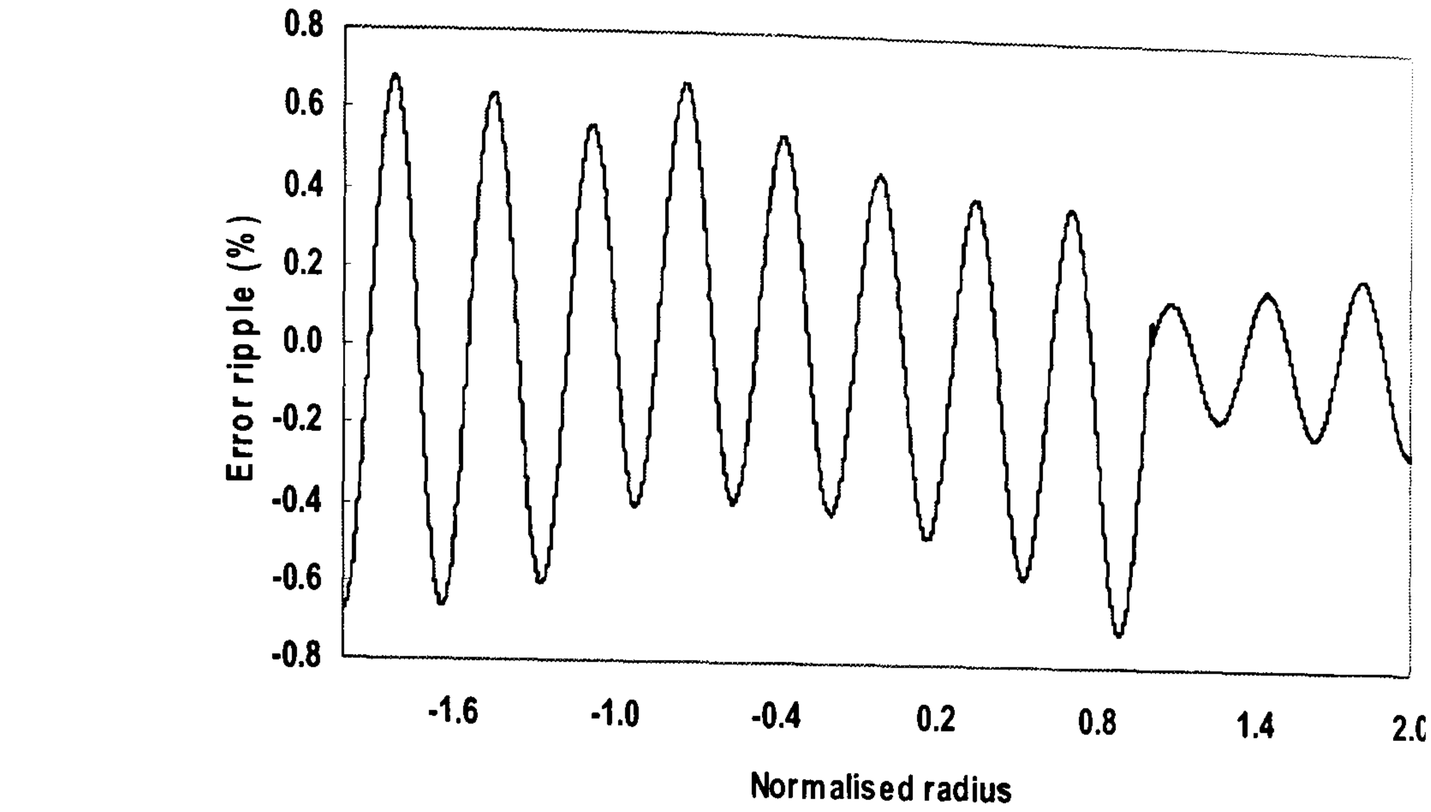

Figure 5.18 The % error in the reconstructed refractive index profile, (the difference between the exact and reconstructed refractive index profile)

$(100 \times (n_{exact} - n_{reconstructed}) / n_{exact})\%$.

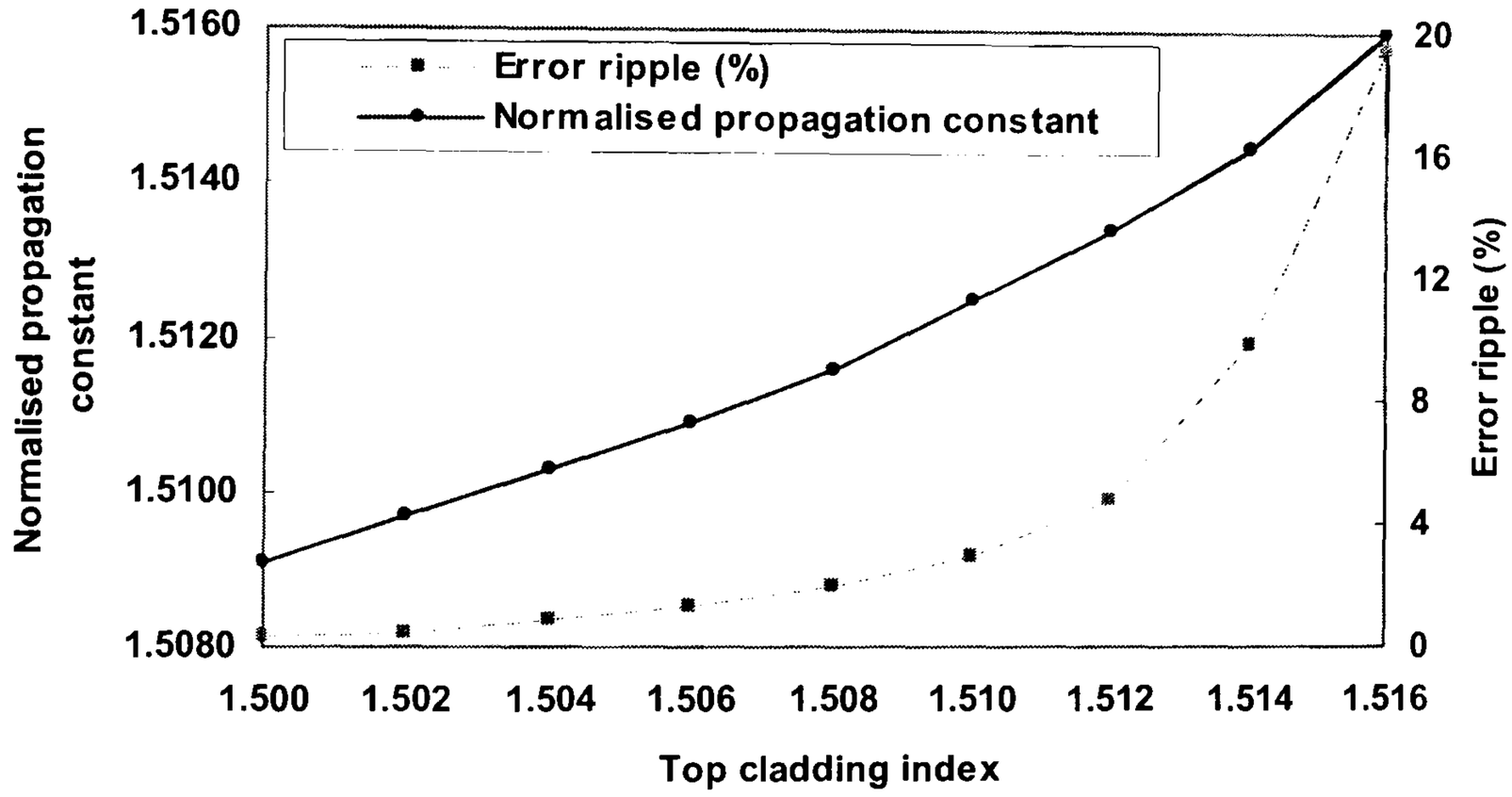

Figure 5.19 The % maximum error in refractive index difference due to ripple versus the top cladding index.

In chapter 5, the inverse *TL* technique has been discussed for the planar optical waveguide refractive index profile reconstruction. The concept of this work is based on modelling a planar optical waveguide as simple equivalent electric circuits, such that the waveguide modal properties translate and can be derived from the resonant frequencies of the equivalent circuits. This is common sense in electrical

engineering, and standard circuit theory can subsequently be applied to the circuits. From Maxwell's equations, the *T*-circuits are derived for the arbitrary refractive index profile isotropic symmetric planar waveguide. This model is used to carry out the inverse problem and synthesize the exact refractive index profiles of isotropic symmetric planar waveguides numerically from the electric fields. The numerical simulations performed show the effectiveness of this method. Reconstructions with arbitrary isotropic asymmetric refractive index profile planar optical waveguides have also been carried out in order to test the robustness of this algorithm.

CHAPTER 6

Conclusions and Suggestions for Further Research Work

6.1 Conclusions

The aim of this thesis, the analysis of optical waveguides using the *TL* forward and inverse solutions has been achieved. Both optical fibres and planar optical waveguides have been studied. The main contributions of this thesis are:

- In the forward solution, the *TL* technique has been applied to circularly symmetric optical fibres with complex step and graded index profiles. This method has been used to evaluate and manipulate the gain in a typical 980 *nm* pumped *EDF* as well as to calculate the attenuation of optical fibres when radial loss factors are presented.
- The *TL* technique has been applied to calculate the effective index of leaky modes and demonstrated by using the model of the Bragg fibre with air core and periodic coaxial claddings as an example of where the band-gap structures of *TM* modes can be obtained.
- A new analysis leading to a novel algorithm has been presented for calculating directly and without numerical differentiation the dispersion characteristics. This method only requires knowledge of the mode propagation constant and the refractive index profile. It is straightforward and avoids the use of numerical differentiation twice. It is useful for designing complicated refractive index profile optical fibres.
- In the inverse solution of the *TL* technique, the refractive indices have been accurately reconstructed from the electric fields for both optical fibres and planar optical waveguides.

6.1.1 Conclusions for The Forward Solution of The *TL* Technique

a) In the forward solution of Maxwell's equations for optical waveguides, the resonance technique, which uses transmission line principles to locate the propagation constants of optical waveguides has been presented. Because different modes transmitted on the optical waveguides have their own propagation constant, when the propagation constant is obtained by using the root searching method on the basis of the resonance technique, it can be used to plot the electric field for different modes and different refractive index profile optical waveguides.

b) To illustrate the capacity of the *TL* procedure, it has been applied to calculate the complex propagation constant of optical fibres with complex refractive index profile. The potential of this technique has been examined by describing two methods to flatten the gain spectrum: one is by varying refractive index profile, and the other one is by varying the core dopant concentration. In contrast and in order to illustrate further the power of this technique, it has been applied to determine the optical fibre radial attenuation.

c) The Bragg fibre leaky mode effective index can be obtained by using the root searching method locating the resonances of the electric *T*-circuit cascade. The solution of this problem allows the band-gap structures of *TM* modes to be worked out and the electric field distribution of the Bragg fibre to be plotted.

d) The forward *TL* theory has been extended and a novel method based on it has been presented for calculating the dispersion of optical fibres of known but arbitrary refractive index profiles. Two master equations have been analytically derived for the derivatives of the propagation constant with respect to the wavelength. The first derivative can be expressed in terms of equivalent circuit impedances at the wavelength of interest and the second derivative can be expressed in terms of circuit impedances and the first derivative. Once the information along with the material dispersion is given, the dispersion can be accurately calculated from its definition.

6.1.2 Conclusions for The Inverse Solution of The *TL* Technique

a) In the inverse solution, equivalent *T*-circuits for the optical fibre have been derived from Maxwell's equations. Based on knowledge of the electric field, the numerical reconstruction results of single-mode and multimode step, graded index optical fibre and Bragg fibre refractive index profiles have been successfully demonstrated. The accuracy of the reconstructed waveguides has been examined numerically. In contrast to the traditional approach, this proposed inverse method requires no prior information on the functional form of the unknown quantity, no iterations in the calculating process and no intensity smoothing in advance. Furthermore, the advantage of this method is that the unknown quantity of the refractive index can be reconstructed directly. This implies that the present model offers a great deal of flexibility. Consequently, the results show that the proposed inverse method is an accurate, robust and efficient inverse technique for reconstructing the refractive index of any kind of single-mode and multimode optical fibres.

b) A method based on the inverse *TL* technique has also been developed. This method can be used to design planar optical waveguides. The method uses inverse *TL* principles and relies on the modelling of a thin uniform layer of a planar waveguide to a *T*-circuit. The method requires knowledge of the electric field of the planar waveguide and the reconstruction is theoretically exact. Simulation results demonstrate the potential of this novel method for reconstructing arbitrary refractive index profiles of isotropic symmetric and asymmetric planar optical waveguides.

In this thesis, the research results and directions will be timely and applicable in practical implementation. This type of conclusion can indicate the direction to be taken by further research work.

6.2 Suggestions for Further Research Work

a) The problem of designing an optical fibre from the mode electric field has previously been resolved within this thesis. Knowledge of the electric field will allow the design of suitable fibre refractive index profiles. The *TL* technique can be extended even further into the more difficult problem of designing a fibre profile starting from knowledge of fibre dispersion. There are no easy methods for dealing with this problem, and all available techniques are difficult to work with. The exact design of the optical fibre refractive index profile from dispersion is very important. It allows the zero dispersion point to be shifted to any desired wavelength, thereby increasing the bandwidth of the optical fibre. Dispersion of an optical fibre is one of the main limitations on the bit rate and length of the fibre within optical communication systems. By using the extension of the inverse *TL* technique developed in this thesis, the suitable refractive index profiles can be designed from the desired dispersion characteristics. This would be a great demonstration of the capability of *TL* technique. From the mathematical point of view, it is much harder than the forward solution of dispersion.

b) The *TL* technique, which is an efficient tool in analyzing linear optical waveguides, can be modified to analyze nonlinear waveguides, both in planar and cylindrical geometry. The similar deduction developed for linear optical waveguides can be applied directly in a fibre with a nonlinear index behavior in the core and/or in the cladding. However, the complication of mode analysis in nonlinear fibres requires an in-depth study, giving attention to combined nonlinearity and geometry. The use of nonlinear materials for the core and/or the cladding of the optical waveguide either for Kerr or Saturable type lead to more complicated power depending phenomena for the propagation constant and field profiles (Stathopoulos 2004). A strong motivation exists in order to extend the *TL* technique to calculate the nonlinear refractive index profile from knowledge of the mode electric field radial distribution. This is an inverse problem corresponding to the linear inverse problem already tackled in this thesis. If this is possible it would be

interesting to be able to examine the influence of the finite thickness and number of the cladding layers in the calculation of the nonlinear refractive index. The problem could be examined in both planar and cylindrical coordinates. Both Kerr and Saturable nonlinearities are considered and different strengths of nonlinearities in the core and cladding can be examined.

c) Bragg fibres are optical fibres that consist of a core surrounded by layers of alternating high and low refractive index. The light is confined to the core by Bragg reflection off the alternating layers, which approximately form a Bragg grating and have a one dimensional band-gap. In practice, Bragg fibres have a finite number of layers and support only leaky modes. The band-gap of TM_{01} mode has been evaluated by using the *TL* technique within this thesis. If the Bragg fibre supports a leaky mode with a sufficiently lower loss than all other leaky modes, it can be considered effectively single-moded. The same method developed for calculating the loss in conventional optical fibres can be applied to obtain the loss in Bragg fibres. The response of the modes of a Bragg fibre to changes in the core radius and the number of layers can be examined and explained in terms of simple models for the cavity condition and the guiding mechanism. The results allow for the role of the core radius and number of layers to be better incorporated into the design and optimization process, when designing such Bragg fibres for particular applications. Further optimization of these single polarization non-degenerate mode fibre designs, especially relating to minimizing confinement loss, will be investigated in the future.

REFERENCES

Adams, M. J. (1981). An Introduction to Optical Waveguides. Binghamton, John Wiley & Sons.

Agraweal, G. P. (1995). Nonlinear Fiber Optics, New York: Academic.

Ainslie, B. J. and C. R. Day (1986). "A Review of Single Mode Fiber with Modified Dispersion Characteristics." IEEE Journal of Lightwave Technology **LT-4**(8): 967-979.

Argyros, A. (2002). "Guided Modes and Loss in Bragg Fibres." Optics Letters **10**(24): 1411-1417.

Argyros, A. and I. M. Bassett (2002). Counting Modes in Optical Fibres with Leaky Modes. Symposium on Optical Fiber Measurements SOFM 2002, National Institute of Standards and Technology, Colorado.

Badolo, M. and P. Emplit (1997). "Prediction of Close to Zero Modal Dispersion Over a Wide Range of Wavelengths in Singly Clad Multimode Fibers." IEEE Journal of Lightwave Technology **15**(1): 121-124.

Barnes, W. L., R. I. Laming, et al. (1991). "Absorption and Emission Cross Section of Er Doped Silica Fibers." IEEE Journal of Quantum Electronics **27**(4): 1004-1010.

Boucouvalas, A. C. (1983). "Use of Far-Field Radiation Pattern to Characterise Single-Mode Symmetric Slab Waveguides." Electronics Letters **19**(3): 120-121.

Boucouvalas, A. C. and C. D. Papageorgiou (1982). "Cutoff Frequencies in Optical Fibres of Arbitrary Refractive Index Profile using the 'Resonance' Technique." IEEE Journal of Quantum Electronics **18**(12): 2027-2031.

Boucouvalas, A. C. and X. Qian (2003). Optical Fiber Refractive Index Profile Synthesis from Near Field. IEEE Globecom 2003, San Francisco, CA, IEEE GLOBECOM.

Boucouvalas, A. C. and X. Qian (2005). "Mode Dispersion and Delay Characteristics of Optical Waveguides Using Equivalent TL Circuits." IEEE Journal of Quantum Electronics **41**(7): 951-957.

Boucouvalas, A. C. and S. C. Robertson (1985). "Optical Waveguide Transverse Transmission Line Equations and Their use in Determining Mode Properties." Joers Advanced Fiber Measurement Symposium.

Bourillot, E., S. I. Hosain, et al. (1995). "Determination of Mode-Cutoff Wavelengths and Refractive-Index Profile of Planar Optical Waveguides with a Photon Scanning Tunnelling Microscope." Physical Review B **51**(16): 11225-11228.

Brooks, D. and S. Ruschin (1996). "Improved Near-Field Method for Refractive Index Measurement of Optical Waveguides." IEEE Photonics Technology Letters **8**(2): 254-256.

Caccavale, F., P. Chakraborty, et al. (1995). "Secondary Ion Mass Spectrometry and Near Field Studies of Ti : LiNbO Optical Waveguides." Journal of Applied Physics **78**: 5345-5350.

Caccavale, F., F. Gonella, et al. (1996). "Iterative Simplex-Finite Difference Method for the Characterization of Optical Waveguides." IEEE Journal of Lightwave Technology **14**(8): 1825-1830.

Caccavale, F., F. Segato, et al. (1998). "A Finite Differences Method for the Reconstruction of Refractive Index Profiles from Near-Field Measurements." IEEE Journal of Lightwave Technology **16**(7): 1348-1353.

CCITT, Ed. (1985). Cut-off Wavelength of Cabled Single-Mode Fibers. USA, COM.

Chew, W. C. (1999). Waves and Fields in Inhomogeneous Media. New York, Wiley-IEEE Press.

Chiang, K. S., C. L. Wong, et al. (1996). "Refractive Index Profiling of Graded Index Planar Waveguides From Effective Indexes Measured for Both Mode Types and at Different Wavelengths." IEEE Journal of Lightwave Technology **14**(5): 827-832.

Cregan, R. F., B. J. Mangan, et al. (1999). Single-Mode Photonic Band Gap Guidance of Light in Air. Science. **285:** 1537-1539.

Davies, R. W. and D. Sahm (1986). "Correlation of Zero-Dispersion Wavelength with Mode Confinement Parameters in Single-Mode Fibers--Analysis for Simple Step, Triangular Core, and Dispersion-Shifted Models." IEEE Journal of Lightwave Technology **LT-4**(9): 1393-1401.

Desurvire, E. (1994). Erbium-Doped Fiber Amplifiers. New York, A Wiley-Interscience Publication, John Wiley&Sons, INC.

Desurvire, E., J. L. Zyskind, et al. (1990). "Design Optimization for Efficient Erbium-Doped Fiber Amplifiers." IEEE Journal of Lightwave Technology **8**(11): 1730-1741.

Dhar, L., H. J. Lee, et al. (1996). Refractive Index Profiling of Optical Waveguides Using Near-Field Scanning Optical Microscopy. OFC'96 Technical Digest: 303-304.

Doran, N. J. and K. J. Blow (1983). "Cylindrical Bragg Fibers: A Design and Feasibility Study For Optical Communications." IEEE Journal of Lightwave Technology **LT-1**(4): 588-590.

Dyott, R. B. and J. R. Stern (1970). Group Delay in Glass Fibre Waveguide. Trunk Telecommun. Guided Waves, London, UK, IEE Conference Publication.

EL-Ibiary, M. Y. (1986). "Parameter Optimization in Graded-Index Dispersion-Shifted Single-Mode Fibers." IEEE Journal of Lightwave Technology **LT-4**(3): 364-367.

Ennser, K., M. Ibsen, et al. (1998). "Influence of Nonideal Chirped Fiber Grating Characteristics on Dispersion Cancellation." IEEE Photonics Technology Letters **10**(10): 1476-1478.

Fink, Y., D. J. Ripin, et al. (1999). "Guiding Optical Light in Air Using an All-Dielectric Structure." IEEE Journal of Lightwave Technology **17**(11): 2039-2041.

Fleming, J. G., S. Y. Lin, et al. (2002). Proceeding of The Solid-State Sensor Actuator and Microsystems Workshop. Hilton Head, S.C.

Fleming, S. C. and T. J. Whitley (1996). "Measurement and Analysis of Pump-Dependent Refractive Index and Dispersion Effects in Erbium-Doped Fiber Amplifiers." IEEE Journal of Quantum Electronics **32**(7): 1113-1121.

Francois, P. (1983). "Zero Dispersion in Attenuation Optimized Doubly Clad Fibers." IEEE Journal of Lightwave Technology **LT-1**(1): 26-37.

Frenkel, A., J. P. Heritage, et al. (1989). "Compensation of Dispersion in Optical Fibers for the 1300-1600 nm Region with a Grating and Telescope." IEEE Journal of Quantum Electronics **25**(9): 1981-1984.

Gallawa, R. L., I. C. Goyal, et al. (1993). "Calculated Fiber Attenuation: A General Method Yielding Stationary Values." IEEE Journal of Lightwave Technology **11**(12): 1900-1904.

Gambling, W. A., D. N. Payne, et al. (1976). "Determination of Core Diameter and Refractive Index Difference of Single-Mode Fibres by Observation of the Far-Field Radiation Pattern." IEE Journal of Microwaves, Optics & Acoustics **1**: 13-17.

Garrett, I. (1983). "Towars the Fundamental Limits of Optical-Fiber Communications." IEEE Journal of Lightwave Technology **LT-1**(1): 131-138.

Gauthier, F., J. Auge, et al. (1981). "Consistent Refractive Index Profile Measurements of a Step-Index Monomode Optical Fiber Attained by Several Techniques." IEEE Journal of Quantum Electronics **17**(6): 885-889.

Giles, C. R. and E. Desurvire (1991). "Propagation of Signal and Noise in Concatenated Erbium Doped Fiber Optical Amplifiers." IEEE Journal of Lightwave Technology **9**(2): 147-154.

Hadjiloucas, S., R. K. H. Galvao, et al. (2003). "Measurement of Propagation Constant in Waveguides With Wideband Coherent Terahertz Spectroscopy." Journal of the Optical Society America B **20**(2): 391-401.

Hakki, B. W. (1996). "Polarization Mode Dispersion in a Single Mode Fiber." IEEE Journal of Lightwave Technology **14**(9): 2202-2208.

Hartog, A. H. and M. J. Adams (1977). "On the Accuracy of the WKB Approximation in Optical Dielectric Waveguides." IBID **9**: 223-232.

Hartog, A. H. and M. P. Gold (1984). "On the Theory of Backscattering in Single-Mode Optical Fibers." IEEE Journal of Lightwave Technology **LT-2**: 76-83.

Hattori, H. T. and A. Safaai-Jazi (1998). "Fiber Designs With Significantly Reduced Nonlinearity for Very Long Distance Transmission." Applied Optics **37**: 3190-3197.

Heitmann, W. and K. F. Klein (2004). "Infrared Absorption of Silica Fibers." Optical Communications **25**(3): 106-109.

Helms, J., J. Schmidtchen, et al. (1990). "Error Analysis for Refractive-Index Profile from Near-Field Measurements." IEEE Journal of Lightwave Technology **8**(5): 625-633.

Hinata, T., S. Furukawa, et al. (1994). "A Single-Polarization Optical Fiber of Hollow Pit Type with Zero Total Dispersion at Wavelength of 1550 nm." IEEE Journal of Lightwave Technology **12**(11): 1921-1925.

Hotate, K. and K. Okoshi (1979). "Measurement of Refractive Index Profile and Transmission Characteristics of A Single-Mode Optical Fiber From Its Exit-Radiation Pattern." Applied Optics **18**: 3265-3271.

Hou, C. H., B. G. Grossman, et al. (2003). "Experimental Determination of Propagation Constant Using End-Etched Fiber." Optics and Laser Technology **35**(5): 355-360.

Ibanescu, M., Y. Fink, et al. (2000). An All-Dielectric Coaxial Waveguide. Science. **289:** 415-418.

Inoue, K., T. Kominato, et al. (1991). "Tunable Gain Equalization Using a Mach-Zehnder Optical Filter in Multistage Fiber Amplifiers." IEEE Photonics Technology Letters **3**(8): 718-720.

Issa, N. A., A. Argyros, et al. (2003). "Identifying Hollow Waveguide Guidance in Air-Cored Microstructured Optical Fibres." Optics Express **11**(9): 996-1001.

Issa, N. A. and L. Poladian (2003). "Vector Wave Expansion Method for Leaky Modes of Microstructured Optical Fibers." IEEE Journal of Lightwave Technology **21**(4): 1005-1012.

Jeunhomme, L. B. (1983). Single Mode Fiber Optics, Marcel Dekker Inc.

Joannopoulos, J. D., R. D. Meade, et al. (1995). Photonic Crystals: Molding the Flow of Light. Princeton, Princeton University Press.

Johnson, S. G., M. Ibanescu, et al. (2001). "Low-Loss Asymptotically Single-Mode Propagation in Large-Core OmniGuide Fibers." Optics Express **9**(13): 748-779.

Kaman, V., X. Z. Zheng, et al. (2005). "A 32 10 Gb/s DWDM Metropolitan Network Demonstration Using Wavelength-Selective Photonic Cross-Connects and Narrow-Band EDFAs." IEEE Photonics Technol Letters **17**(9): 1977-1979.

Kaminow, I. P. and J. R. Carruthers (1973). "Optical waveguiding layers in LiNbO and LiTaO." Applied Physics Letter **22**: 326.

Krijnen, G. J. M., H. J. W. M. Hoekstra, et al. (1994). "A New Method for the Calculation of Propagation Constants and Field Profiles of Guided Modes of Nonlinear Channel Waveguides Based on The Effective Index Method." IEEE Journal of Quantum Electronics **12**(9): 1550-1559.

Lahart, M. J. (1998). "Analysis of a Cylindrical Dielectric Waveguide With Three Regions By Use of An Inverted Mode-Definition Parameter." Journal of the Optical Society America A **15**: 727-735.

Laming, R. I., J. D. Minelly, et al. (1993). "Twin Core Erbium Doped Fiber Equalization with Passive Spectral Gain Equalization." Electronics Letters **29**: 509-510.

Lassen, E. A., S. T. Huntington, et al. (2005). "Refractive Index Profiling of Axially Symmetric Optical Fibers: A New Technique." Optics Express **13**(9): 3277-3282.

Lidgard, A., D. J. Digiovanni, et al. (1992). "A Comparative Study of an Erbium Doped Fiber Amplifier Pumped at 811 and 980 nm." IEEE Journal of Quantum Electronics **28**(1): 43-47.

Limpert, J., T. Schreiber, et al. (2002). "High-Power Femtosecond Yb-Doped Fiber Amplifier." Optics Express **10**(14): 628-638.

Lin, H. Y., R. B. Wu, et al. (1992). "An Efficient Algorithm for Determining the Dispersion Characteristics of Single-Mode Optical Fibers." IEEE Journal of Lightwave Technology **10**(6): 705-711.

Lin, J. H. and C. K. Chen (2002). "An Inverse Algorithm to Calculate the Refractive Index Profiles of Periodically Segmented Waveguides from the Measured

Near-Field Intensities." IEEE Journal of Lightwave Technology **20**(1): 58-64.

Liu, P. L. and S. De (2003). "Fiber Design—From Optical Mode to Index Profile." Optical Engineering **42**(4): 981-984.

Lu, P., L. Chen, et al. (2001). "Polarization Mode Dispersion and Polarization Dependent Loss for a Pulse in Single-Mode Fibers." IEEE Journal of Lightwave Technology **19**(6): 856-860.

Lundin, R. (1993). "Minimization of the Chromatic Dispersion Over a Broad Wavelength Range In A Single Mode Optical Fiber." Applied Optics **32**: 3241-3245.

Lundin, R. (1994). "Dispersion Flattening in A W-Fiber." Applied Optics **33**: 1011-1014.

Mammel, W. L. and L. G. Cohen (1982). "Numerical Prediction of Fiber Transmission as Characteristics from Arbitrary Refractive-Index Profiles." APPLIED OPTICS **21**: 699-703.

Marcuse, D. (1993). "Bend Loss of Slab and Fiber Modes Computed with Diffraction Theory." IEEE Journal of Quantum Electronics **29**(12): 2957-2961.

Martynkien, T., S. Harris, et al. (2000). "Determination of The Core Dimensions in Elliptical Core Fibers Using Cut-Off Wavelengths for Higher Order Modes." Optik **111**(10): 454-458.

Mathey, P., P. Jullien, et al. (1995). "Refractive-Index Profile Reconstructions in Planar Waveguides by the WKB Inverse Method and Reflectivity Calculations." Journal of Optical Society America B **12**: 1663-1670.

Matsuda, T., A. Naka, et al. (1996). "10gbit/s, 6000km NRZ and 4400km RZ signal transmission experiments at zero dispersion wavelength." Electronics Letters **32**(3): 229-231.

Mazzali, C., D. F. Grosz, et al. (1999). "Simple Method for Measuring Dispersion and Nonlinear Coefficient Near the Zero-Dispersion Wavelength of Optical Fibers." IEEE Photonics Technology Letters **11**(2): 251-253.

Miya, T., M. Nakahara, et al. (1983). "Fabrication of Dispersion-Free VAD Single-Mode Fibers in the 1500 nm Wavelength Region." IEEE Journal of Lightwave Technology **LT-1**(1): 14-19.

Miyagi, M. and S. Kawakami (1984). "Design Theory of Dielectric-Coated Circular Metallic Waveguides for Infrared Transmission." IEEE Journal of Lightwave Technology **LT-2**(2): 116-126.

Mizrahi, A. and L. Schachter (2004). "Bragg Reflection Waveguides with a Matching Layer." Optics Express **12**(14): 3156-3170.

Morishita, K. (1983). "Refractive-Index-Profile Determination of Single Mode Optical Fibres by a Propagation-Mode Near Field Scanning Technique." IEEE Journal of Lightwave Technology **1**(3): 445-449.

Murakami, Y. and H.Tsuchiya (1978). "Bending Losses of Coated Single-Mode Optical Fibers." IEEE Journal of Quantum Electronics **QE-14**(7): 495-501.

Oksanen, M. and I. V. Lindell (1990). "Nonstandard Variational Method for Calculating Attenuation in Optical Fibers." Microwave and Optical Technology Letters **3**: 160-164.

Ouyang, G., Y. Xu, et al. (2001). "Comparative Study of Air-Core and Coaxial Bragg Fibers: Single-Mode Transmission and Dispersion Characteristics." Optics Letters **9**(13): 733-747.

Ouyang, G., Y. Xu, et al. (2002). "Theoretical Study on Dispersion Compensation In Air-Core Bragg Fibers." Optics Express **10**(17): 899-908.

Papageorgiou, C. D. and A. C. Boucouvalas (1982). "Propagation Constants of Cylindrical Dielectric Waveguides with Arbitrary Refractive Index Profile, using the 'Resonance' Technique." Electronics Letters **18**(18): 786-788.

Payne, D. N. and W. A. Gambling (1975). "Zero Material Dispersion in Optical Fibers." Electronics Letters **11**: 176-178.

Qian, X. and A. C. Boucouvalas (2003). Optical Fiber Refractive Index Profile Synthesis from Near Field. IEEE Globecom 2003, San Francisco, CA, IEEE.

Qian, X. and A. C. Boucouvalas (2004). Optical Fibre Refractive Index Reconstruction from Mode Near Field. CSNDSP 2004, The University of Newcastle, UK, IEEE.

Qian, X. and A. C. Boucouvalas (2004). "Propagation Characteristics of Single-Mode Optical Fibers with Arbitrary Complex Index Profiles." IEEE Journal of Quantum Electronics **40**(6): 771-777.

Qian, X. and A. C. Boucouvalas (2005). "Analysis of Leaky Modes and Bragg Fibers Using Transmission Line Equivalent T-Circuits." IEEE Photonics Technol Letters **17**(5): 1031-1033.

Ramadan, W. A., E. Fazio, et al. (1996). "Measurements of The Refractive-Index Profile of Planar Waveguides by the Use of A Double Lloyd's Interferometer." Applied Optics **35**: 6173–6178.

Rego, G., O. Frazao, et al. (2001). Long-Period Fiber Gratings Produced Using the Electric Arc Technique for DWDM Communication Systems. 5th World Multi-Conference on Systemics, Cybernetics and Informatics, Orlando, USA.

Reisinger, A. (1973). "Characteristics of Optical Guided Modes in Lossy Waveguides." Applied Optics **12**: 1015 -1025.

Rochette, M., S. Larochelle, et al. (1999). Experimental Investigation of Erbium-Doped Fiber Amplifier Gain Equalization Schemes Using Short-Period Bragg Gratings. CLEO'99 Tech. Dig.

Sabadash, V. V. and G. E. Chaika (1991). Attenuation of Electromagnetic Waves in Lightguide Cladding When Exact Solutions of Maxwell's Equations are Allowed. Optic Spectrosc, USSR.

Sader, J. E. (1990). "Method for Analysis of Complex Refractive-Index-Profile Fibers." Optics Letters **15**(2): 105-107.

Safaai-Jazi, A. and L. J. Lu (1990). "Accuracy of Approximate Methods for the Evaluation of Chromatic Dispersion in Dispersion-Flattened Fibers." IEEE Journal of Lightwave Technology **8**(8): 1145-1150.

Saleh, B. E. A. and M. C. Teich (1991). Fundamentals of Photonics. New York, Wiley.

Sammut, R. A. (1979). "Analysis of Approximations for the Mode Dispersion in Monomode Fiber." Electron Letters **15**: 590-591.

Schar, M. (1999). "What is "Technical"? A Contribution to the Concept of "Technicality" in the Light of the European Patent Convention." Journal of World Intellectual Property **2**(1): 93-130.

Sharma, A. and S. Banerjee (1989). "Chromatic Dispersion in Single Mode Fiber with Arbitrary Index Profile: A Simple Method for Exact Numerical Evaluation." IEEE Journal of Lightwave Technology **7**(12): 1919-1923.

Sharma, E. K., A. Sharma, et al. (1982). "Propagation Characteristics of Single Mode Optical Fibers with Arbitrary Index Profiles: A Simple Numerical Approach." IEEE Journal of Quantum Electronics **QE-18**(10): 1484-1489.

Shimizu, M., M. Yamada, et al. (1990). "Erbium Doped Fibre Amplifiers with an Extremely High Gain Coefficient of 11.0 dB/mW." Electron Letters **26**(20): 1641-1643.

Singh, R. and E. K. Sharma (2001). "Propagation Characteristics of Single-Mode Optical Fibres with Arbitrary Complex Index Profiles: A Direct Numerical Approach." IEEE Journal of Quantum Electronics **37**(5): 635-640.

Snyder, A. W. and J. D. Love (1983). Optical Waveguide Theory, Chapman & Hall, London.

Stathopoulos, N. A. (2004). "Calculation of Nonlinear Modes Guided by Step-Index Fibers with Finite Cladding Thickness." Optical and Quantum Electronics **36**(4): 367-381.

Strohhofer, C. and A. Polman (2001). "Relationship Between Gain and Yb3+ concentration in Er3+ - Yb3+ doped waveguide amplifiers." Applied Physics **90**(9): 4314-4320.

Sunanda and E. K. Sharma (1999). "Field Variational Analysis for Modal Gain in Erbium-Doped Fiber Amplifiers." Journal of the Optical Society America **16**(9): 1344-1347.

Survaiya, S. P. and R. K. Shevgaonkar (1996). "Design of Subpicosecond Dispersion-Flattened Fibers." IEEE Photonics Technology Letters **8**(6): 803-805.

Survaiya, S. P. and R. K. Shevgaonkar (1999). "Dispersion Characteristics of an Optical Fiber Having Linear Chirp Refractive Index profile." IEEE Journal of Lightwave Technology **17**(10): 1797-1805.

Takagi, A., K. Jinguji, et al. (1992). "Design and Fabrication of Broad-Band Silica-Based Optical Waveguide Couplers with Asymmetric Structure." IEEE Journal of Quantum Electronics **28**(4): 848-855.

Themistos, C., B. M. A. Rahman, et al. (1995). "Loss/Gain Characterization of Optical Waveguides." IEEE Journal of Lightwave Technology **13**(8): 1760-1765.

Tonova, D., A. Paneva, et al. (1998). "Determination of Refractive Index Profiles of Gradient Optical Waveguides by Ellipsometry." Optics Communications **150**: 121-125.

Ulrich, R. and R. Torge (1973). "Measurement of Thin Film Parameters with a Prism Coupler." Applied Optics **12**: 2901-2908.

Urquhart, P. (2003). "Component Technologies for Future Optical Networks." IEE Proc-Optoelectron **150**(1): 3-9.

Von-der-Weid, J. P., R. Passy, et al. (1998). "High-Resolution Distributed-Gain Measurements in Erbium-doped Fibers." IEEE Photonics Technology Letters **10**(7).

Waldron, R. A. (1969). Theory of Guide Electromagnetic Waves. London, Van Nostrand Reinhold.

Wang, L. and C.S.Hsiao (2001). "A Matrix Method for Studying TM Modes of Optical Planar Waveguides With Arbitrary Index Profiles." IEEE Journal of Quantum Electronics **37**(12): 1654-1660.

Wang, L. and N. Huang (1999). "A New Numerical Method for Solving Planar Waveguide Problems with Arbitrary Index Profiles: TE Mode Solutions." IEEE Journal of Quantum Electronics **35**(9): 1351-1353.

White, J. M. and P. F. Heidrich (1976). "Optical Waveguide Refractive Index Profiles Determined from Measurement of Mode Indices: A Simple Analysis." Applied Optics **15**: 151-155.

White, T. P., B. T. Kuhlmey, et al. (2002). "Multipole Method For Microstructured Optical Fibers. I. Formulation." Journal of the Optical Society America B **19**(10): 2322-2330.

Wu, B. and P. L. Chu (1994). "A Twin-Core Erbium-Doped Fiber Amplifier." Optical Communications **110**: 545-548.

Xu, Y., G. X. Ouyang, et al. (2002). "Asymptotic Matrix Theory of Bragg Fibers." IEEE Journal of Lightwave Technology **20**(3): 428-440.

Xu, Y., A. Yariv, et al. (2003). "Asymptotic Analysis of Silicon Based Bragg Fibers." Optics Letters **11**(9): 1039-1049.

Yabre, G. (2000). "Comprehensive Theory of Dispersion in Graded-Index Optical Fibers." IEEE Journal of Lightwave Technology **18**(2): 166-177.

Yamada, M., M. Shimizu, et al. (1990). "Noise Characteristics of Erbium-Doped Fiber Amplifiers Pumped by 980 and 1480 nm Laser Diodes." IEEE Photonics Technology Letters **2**(3): 205-207.

Yeh, P., A. Yariv, et al. (1978). "Theory of Bragg Fiber." Journal of the Optical Society America **68**: 1196-1201.

Yun, S. H., B. W. Lee, et al. (1999). "Dynamic Erbium-Doped Fiber Amplifier Based On Active Gain Flattening with Fiber Acoustooptic Tunable Filters." IEEE Photonics Technology Letters **11**: 1229-1231.

Zervas, M. N. and R. I. Laming (1995). "Rayleigh Scattering Effect on the Gain Efficiency and Noise of Erbium Doped Fiber Amplifiers." IEEE Journal of Quantum Electronics **31**(3): 468-471.

Zhao, Y., J. Bryce, et al. (1997). "Gain Clamped Erbium-Doped Fiber Amplifiers-Modeling and Experiment." IEEE Journal of Selected Topics Quantum Electron **3**: 1008-1012.

APPENDICES

Appendix A. Physical Properties of Optical Fibres

V- value

This optical fibre parameter is defined so as to include most of the physical fibre parameters. It is given by $v = \frac{2\pi a}{\lambda}\sqrt{n_1^2 - n_2^2}$, where a is the fibre core radius, and λ is the operating optical wavelength.

Multimode

For step index fibres, (i.e. fibres with core and cladding refractive indices uniform, of values n_1 and n_2 respectively), when the V-value of the fibre is greater than 2.405, then the optical fibre can support more than one mode, hence it is called multimode . Multimode in ray theory terms means that there are many angles of preferential propagation of the light inside the fibre.

Single-mode

If a waveguide can support only one mode, (a single ray parallel to the fibre axis, of nearly zero incidence angle) then it is called single-mode. This mode is the lowest order bound mode, which can propagate at the wavelength of interest. It is notable that the lowest order bound mode is ascertained for the wavelength of interest by solving Maxwell's equations for the boundary conditions imposed by the fibre, *e.g.* , core (spot) size and the refractive indices of the core and cladding. The solution of Maxwell's equations for the lowest order bound mode will permit a pair of orthogonally polarized fields in the fibre, and this is the usual case in a communication fibre. In step index guides, single-mode operation occurs when the normalized frequency V is less than 2.405.

Classification of Optical Fibres

Optical fibres are manufactured as single-mode, or multimode as mentioned above. Optical fibres have also a refractive index profile such as step index, and graded index. Step index single-mode and multimode waveguides have constant refractive index in the core and cladding. The basic structure of a step index optical fibre is

shown in Fig.A1. It consists of a cylindrical dielectric rod, surrounded by a tubular cladding. For a wavelength of operation λ, the core and cladding are transparent to the light. The core is of higher refractive index n_1, than the cladding, of refractive index n_2.

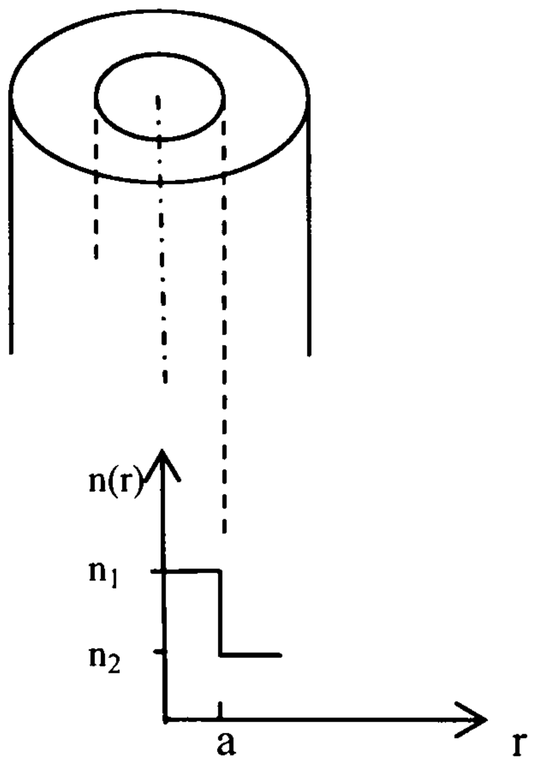

Figure A1 The cross section of a step index optical fibre, the core n_1, surrounded by the cladding of slightly lower refractive index n_2, a the radius of the core.

Graded index fibres do not have a constant refractive index in the core, but a decreasing core index $n(r)$, with radial distance from a maximum value of n_1 at the axis, to a constant value n_2 beyond the core radius 'a' in the cladding. This refractive index variation may be represented as:

$$n(\bar{r}) = \begin{cases} n_1 \times \left[1 - \Delta \times (\frac{\bar{r}}{\bar{a}})^{\alpha}\right] & \bar{r} < \bar{a} \\ n_2 & \bar{r} > \bar{a} \end{cases} \qquad \text{(A.1)}$$

where $\Delta \equiv (n_1 - n_2)/n_1$, n_1 is the refractive index at the axis of the optical fibre, α controls the decay or growth of the profile envelope, $\bar{a}$ is normalised core radius.

A variety of profiles can be generated by varying α, as shown in Fig.A2 below

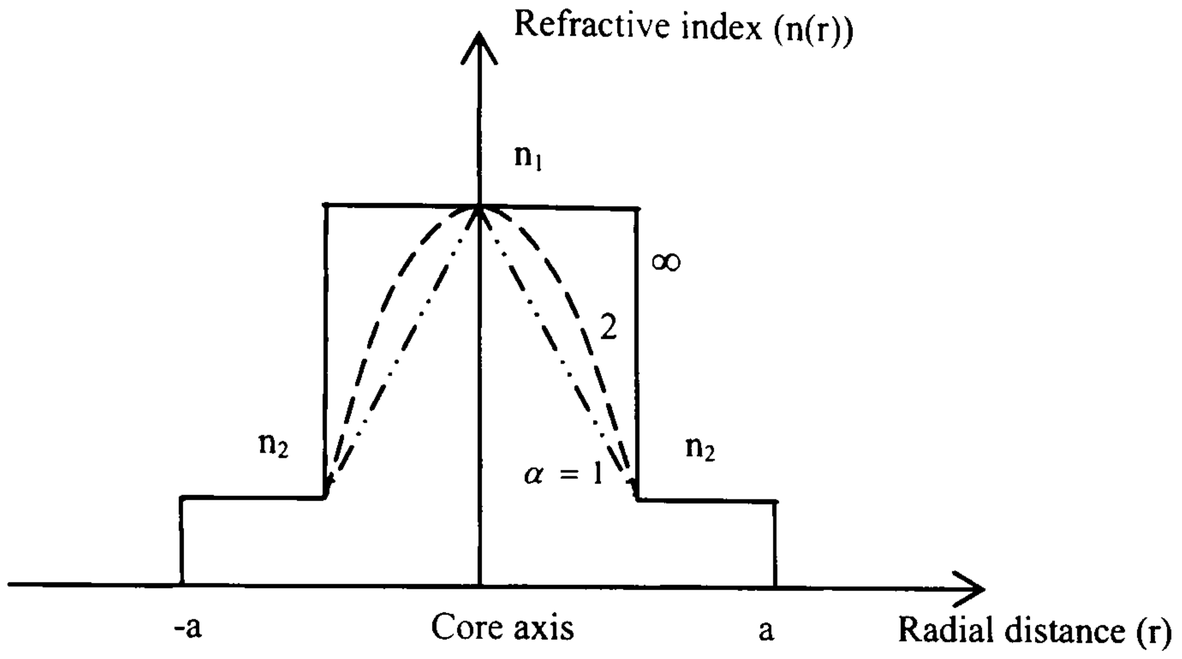

$\alpha = 1$	Triangular index profile
$\alpha = 2$	Parabolic index profile
$\alpha = \infty$	Step index profile

Figure A2 Possible fibre refractive index profiles for different values of α

Appendix B. Impedance Z for Different Modes

Mode	γ^2	Z_P	$Z(r=0)$	$Z(r=\infty)$	$I(r=0)$	$I(r=\infty)$	l
TE	$\beta^2 - n^2 K_0^2$	$\frac{-jZ_0\gamma}{K_0 r\beta^2}$	∞	0	$\frac{1}{Z(r=0)}$	1	0
TM	$\beta^2 - n^2 K_0^2$	$\frac{-jZ_0\gamma}{K_0 r\beta^2 n^2}$	∞	0	$\frac{1}{Z(r=0)}$	1	0
HE/EH	$\beta^2 + (\frac{l}{r})^2 - nK_0{}^2 \mp \frac{2nK_0\beta l}{(\beta r)^2 + l^2}$	$\frac{-j\gamma Z_0}{nrk_0(\beta^2 + (\frac{l}{r})^2)}$	$\frac{Z_0}{jn_1 l}$	0	$\frac{1}{Z(r=0)}$	1	1

After normalization

Mode	$\bar{\gamma}^2$	$\bar{Z}_P$	$Z(r=0)$	$Z(r=\infty)$	$I(r=0)$	$I(r=\infty)$	l
TE	$\bar{\beta}^2 - n^2$	$\frac{Z_0\bar{\gamma}}{j\bar{r}\bar{\beta}^2}$	∞	0	$\frac{1}{Z(r=0)}$	1	0
TM	$\bar{\beta}^2 - n^2$	$\frac{Z_0\bar{\gamma}}{j\bar{r}\bar{\beta}^2 n^2}$	∞	0	$\frac{1}{Z(r=0)}$	1	0
HE/EH	$\bar{\beta}^2 + (\frac{l}{\bar{r}})^2 - n^2 \mp \frac{2n\bar{\beta}l}{(\bar{\beta}\bar{r})^2 + l^2}$	$\frac{\bar{\gamma}Z_0}{jn\bar{r}(\bar{\beta}^2 + (\frac{l}{\bar{r}})^2)}$	$\frac{Z_0}{jn_1 l}$	0	$\frac{1}{Z(r=0)}$	1	1

Where $Z_0 = 120\pi$, l is the wave number.

Appendix C. Derivation of The Exact Impedance Equations

To shorten the equations, the following definitions are made:

$$A = \beta^2 + (\frac{l}{r})^2, \quad B = \sinh(\gamma\delta r), \quad C = \cosh(\gamma\delta r), \quad D = \cosh(\gamma\frac{\delta r}{2}), \quad E = \tanh(\gamma\frac{\delta r}{2})$$

The first derivatives of the exact impedance equations (3.28):

$$\left.\begin{aligned}\frac{\partial Z_P}{\partial \beta} &= \frac{Z_0}{nrk_0}\left(\frac{\frac{\partial \gamma}{\partial \beta}}{AB} - \gamma\left(\frac{2\beta}{A^2B} + \frac{C\,\delta r\,\frac{\partial \gamma}{\partial \beta}}{AB^2}\right)\right)\\ \frac{\partial Z_P}{\partial \lambda} &= \frac{Z_0}{rk_0 A}\frac{\frac{\partial \gamma}{\partial \lambda}(nB) - \gamma\left(\frac{\partial n}{\partial \lambda}B + nC\,\delta r\,\frac{\partial \gamma}{\partial \lambda}\right)}{n^2B^2}\end{aligned}\right\} \tag{C.1}$$

$$\left.\begin{aligned}\frac{\partial Z_B}{\partial \beta} &= \left(C\,\delta r\,\frac{\partial \gamma}{\partial \beta}E + \frac{B}{D^2}\frac{\delta r}{2}\frac{\partial \gamma}{\partial \beta}\right)Z_P + BE\,\frac{\partial Z_P}{\partial \beta}\\ \frac{\partial Z_B}{\partial \lambda} &= \left(C\,\delta r\,\frac{\partial \gamma}{\partial \lambda}E + \frac{B}{D^2}\frac{\delta r}{2}\frac{\partial \gamma}{\partial \lambda}\right)Z_P + BE\,\frac{\partial Z_P}{\partial \lambda}\end{aligned}\right\} \tag{C.2}$$

Where

$$\frac{\partial \gamma}{\partial \beta} = \frac{\partial}{\partial \beta}(\sqrt{\gamma^2}) = \frac{1}{2}\frac{2\beta - \frac{2nlk_0(l^2 - \beta^2 r^2)}{A^2 r^4}}{\sqrt{A - n^2k_0^2 - \frac{2n\beta lk_0}{Ar^2}}}, \qquad \frac{\partial \gamma}{\partial \lambda} = \frac{1}{2}\frac{-\frac{\partial n}{\partial \lambda}k_0\left(2nk_0 + \frac{2\beta l}{Ar^2}\right)}{\sqrt{A - n^2k_0^2 - \frac{2n\beta lk_0}{Ar^2}}}$$

The second derivatives of the exact impedance equations (3.28):

$$\begin{aligned}\frac{\partial^2 Z_P}{\partial\beta\partial\lambda} = &-\frac{\frac{\partial n}{\partial \lambda}}{n^2}\frac{Z_0}{rk_0}\left(\frac{\frac{\partial \gamma}{\partial \beta}}{AB} - \gamma\left(\frac{2\beta}{A^2B} + \frac{C\delta r\,\frac{\partial \gamma}{\partial \beta}}{AB^2}\right)\right) + \frac{Z_0}{nrk_0}\left(\frac{1}{A}\frac{\frac{\partial^2 \gamma}{\partial\beta\partial\lambda}B - \frac{\partial \gamma}{\partial \beta}C\delta r\frac{\partial \gamma}{\partial \lambda}}{\sinh^2(\gamma\frac{\delta r}{k_0})} - \frac{\partial \gamma}{\partial \lambda}\left(\frac{2\beta}{A^2B} + \frac{C\delta r\,\frac{\partial \gamma}{\partial \beta}}{AB^2}\right) - \right.\\ &\left.\gamma\left(\frac{2\beta}{A^2}\frac{-C\delta r\,\frac{\partial \gamma}{\partial \lambda}}{B^2} + \frac{\delta r}{A}\frac{\left(B\delta r\,\frac{\partial \gamma}{\partial \lambda}\frac{\partial \gamma}{\partial \beta} + C\,\frac{\partial^2 \gamma}{\partial\beta\partial\lambda}\right)B^2 - 2C^2\,\frac{\partial \gamma}{\partial \lambda}\frac{\partial \gamma}{\partial \beta}B\delta r}{B^4}\right)\right)\end{aligned} \tag{C.3}$$

$$\frac{\partial^2 Z_P}{\partial \lambda^2} = \frac{Z_0}{rk_0 A}\frac{1}{n^4 B^4}(\frac{\partial^2 \gamma}{\partial \lambda^2} nB - \gamma(\frac{\partial^2 n}{\partial \lambda^2} B + 2\frac{\partial n}{\partial \lambda} C\delta r \frac{\partial \gamma}{\partial \lambda} + n(\delta r)^2(\frac{\partial \gamma}{\partial \lambda})^2 B + n\delta r C \frac{\partial^2 \gamma}{\partial \lambda^2}))n^2 B^2 -$$
$$(\frac{\partial \gamma}{\partial \lambda} nB - \gamma(\frac{\partial n}{\partial \lambda} B + nC\delta r \frac{\partial \gamma}{\partial \lambda}))(2n\frac{\partial n}{\partial \lambda} B^2 + 2n^2 BC\delta r \frac{\partial \gamma}{\partial \lambda})$$

(C.4)

$$\frac{\partial^2 Z_B}{\partial \beta \partial \lambda} = (\delta r B \delta r \frac{\partial \gamma}{\partial \lambda}\frac{\partial \gamma}{\partial \beta} E + C(\frac{\partial^2 \gamma}{\partial \beta \partial \lambda} E + \frac{\partial \gamma}{\partial \lambda}\frac{\partial \gamma}{\partial \beta}\frac{\delta r}{2}\frac{1}{D^2})) + \frac{\delta r}{2}((C\delta r \frac{\partial \gamma}{\partial \lambda}\frac{\partial \gamma}{\partial \beta} + B\frac{\partial^2 \gamma}{\partial \beta \partial \lambda})D^2 - B\frac{\partial \gamma}{\partial \beta}\delta r D\sinh(\gamma\frac{\delta r}{2})\frac{\partial \gamma}{\partial \lambda}))\frac{Z_P}{D^4} +$$
$$(C\delta r \frac{\partial \gamma}{\partial \beta} E + B\frac{\partial \gamma}{\partial \beta}\frac{\delta r}{2}\frac{1}{D^2})\frac{\partial Z_P}{\partial \lambda} + (C\delta r \frac{\partial \gamma}{\partial \lambda} E + B\frac{\partial \gamma}{\partial \lambda}\frac{\delta r}{2}\frac{1}{D^2})\frac{\partial Z_P}{\partial \beta} + BE\frac{\partial^2 Z_P}{\partial \beta \partial \lambda}$$

(C.5)

$$\frac{\partial^2 Z_B}{\partial \lambda^2} = (\delta r(B\delta r(\frac{\partial \gamma}{\partial \lambda})^2 E + cC(\frac{\partial^2 \gamma}{\partial \lambda^2} E + (\frac{\partial \gamma}{\partial \lambda})^2 \frac{\delta r}{2}\frac{1}{D^2})) + \frac{\delta r}{2}((C\delta r(\frac{\partial \gamma}{\partial \lambda})^2 + B\frac{\partial^2 \gamma}{\partial \lambda^2})D^2 -$$
$$B\frac{\partial \gamma}{\partial \lambda} D\sinh(\gamma\frac{\delta r}{2})\frac{\partial \gamma}{\partial \lambda}\delta r))\frac{Z_P}{D^4} + 2(C\delta r \frac{\partial \gamma}{\partial \lambda} E + B\frac{\partial \gamma}{\partial \lambda}\frac{\delta r}{2}\frac{1}{D^2})\frac{\partial Z_P}{\partial \lambda} + BE\frac{\partial^2 Z_P}{\partial \lambda^2}$$

(C.6)

Where

$$\frac{\partial^2 \gamma}{\partial \beta \partial \lambda} = (A - n^2 k_0^2 - \frac{2n\beta l k_0}{Ar^2})^{-\frac{3}{2}}(k_0^2 n\frac{\partial n}{\partial \lambda} + \frac{\beta l k_0}{Ar^2}\frac{\partial n}{\partial \lambda})(\beta - \frac{nlk_0(l^2 - \beta^2 r^2)}{A^2 r^4}) + (A - n^2 k_0^2 - \frac{2n\beta l k_0}{A})^{-\frac{1}{2}}\frac{lk_0(\beta^2 r^2 - l^2)}{A^2 r^4}\frac{\partial n}{\partial \lambda}$$

$$\frac{\partial^2 \gamma}{\partial \lambda^2} = \frac{1}{2}(\frac{1}{2}(A - n^2 k_0^2 - \frac{2n\beta l k_0}{A})^{-\frac{3}{2}}(\frac{\partial n}{\partial \lambda} k_0(2nk_0 + \frac{2\beta l}{A}))^2 - (A - n^2 k_0^2 - \frac{2n\beta l k_0}{A})^{-\frac{1}{2}}(2k_0((\frac{\partial n}{\partial \lambda})^2 + n\frac{\partial^2 n}{\partial \lambda^2}) + \frac{2\beta l k_0 \frac{\partial^2 n}{\partial \lambda^2}}{A}))$$